

**LATE TRANSITION METAL COMPLEXES
INCORPORATING HEMILABILE MIXED-DONOR
N-HETEROCYCLIC CARBENE LIGANDS**

by

HOWARD JONG

B.Sc., Simon Fraser University, 2003

A THESIS SUBMITTED IN PARTIAL FULFILLMENT
OF THE REQUIREMENTS FOR THE DEGREE OF

DOCTOR OF PHILOSOPHY

in

THE FACULTY OF GRADUATE STUDIES

(CHEMISTRY)

THE UNIVERSITY OF BRITISH COLUMBIA

(Vancouver)

April 2010

© Howard Jong 2010

ABSTRACT

The discovery of N-heterocyclic carbenes (NHC) has dramatically affected the world of catalysis. Their inherent properties that make them excellent auxiliary ligands for catalytic processes have countless laboratories worldwide probing and exploiting every notable feature they possess. However, while there is no shortage of attention in this field of research, there has been considerably less interest in NHCs with an ability chelate to metals via a mixed-donor ligand architecture. Thus, this thesis describes the synthesis and application of a ligand set comprised of bidentate mixed-donor NHC ligands.

The ligands prepared all contain a mesitylimidazol-2-ylidene core unit, but incorporate different donor-functionalized tethers. These mixed-donor NHC ligands are synthesized by using a strong base, such as $\text{KN}(\text{SiMe}_3)_2$, to deprotonate the imidazolium salt precursors. This strategy was used to effectively prepare 1-mesityl-3-(2-(mesitylamino)ethyl)imidazol-2-ylidene, $^{\text{Mes}}[\text{CNH}]$ and 1-mesityl-3-(2-aminoethyl)imidazol-2-ylidene, $^{\text{Mes}}[\text{CNH}_2]$.

$^{\text{Mes}}[\text{CNH}]$ was found to be a convenient proligand for the synthesis of various M-NHC (M = Rh, Ir, Ru, Pd, Ni, Fe, Ag, Li) compounds. These $^{\text{Mes}}[\text{CNH}]\text{-M}$ complexes demonstrated the hemilabile character of the $^{\text{Mes}}[\text{CNH}]$ ligand forming complexes that incorporated either a coordinated or uncoordinated amino tether. $^{\text{Mes}}[\text{CNH}]\text{M}(\text{diene})\text{Cl}$, $^{\text{Mes}}[\text{CN}]\text{M}(\text{diene})$ and $[\text{Mes}[\text{CNH}]\text{M}(\text{diene})]\text{BF}_4$ (M = Rh, Ir; diene = 1,5-cyclooctadiene, 2,5-norbornadiene) were synthesized and investigated for their ability to perform hydrogenation and hydrosilylation reactions with various substrates.

$^{\text{Mes}}[\text{CNH}]\text{Ru}(\text{=CHPh})(\text{PCy}_3)\text{Cl}_2$, $^{\text{Mes}}[\text{CNH}]\text{Ru}(\text{=CHPh})(\text{py})\text{Cl}_2$ (py = pyridine) and $^{\text{Mes}}[\text{CNH}]\text{Ru}(\text{=CHPh})(\text{PMe}_3)\text{Cl}_2$ were also synthesized and fully characterized. The activity of the former two Ru complexes was studied for their ability to catalyze ring-closing metathesis (RCM) and ring-opening metathesis polymerization (ROMP) reactions. In addition, the

phosphine dissociation rate of $^{\text{Mes}}[\text{CNH}]\text{Ru}(=\text{CHPh})(\text{PCy}_3)\text{Cl}_2$ was measured via magnetization transfer experiments and compared to other known Ru-benzylidene analogues.

In addition to the amino-tethered NHC proligands, a phosphine analogue $^{\text{Mes}}[\text{CP}]$ was prepared and its reactivity with late transition metal complexes was investigated. While the free NHC-phosphine species could not be isolated, deprotonation of both the iminium and phosphine protons followed by the addition of $[\text{M}(\text{COD})\text{Cl}]_2$ ($\text{M} = \text{Rh}, \text{Ir}$) yields $^{\text{Mes}}[\text{CP}]\text{M}(\text{COD})$, which incorporates a bidentate NHC-phosphide ligand. $^{\text{Mes}}[\text{CP}]\text{Ir}(\text{COD})$ was then investigated for its ability to perform hydrogenation and benchmarked to its $^{\text{Mes}}[\text{CN}]\text{Ir}(\text{COD})$ analogue.

TABLE OF CONTENTS

ABSTRACT	ii
TABLE OF CONTENTS.....	iv
LIST OF TABLES	vii
LIST OF FIGURES	ix
LIST OF SCHEMES.....	xiii
LIST OF ABBREVIATIONS.....	xv
ACKNOWLEDGEMENTS	xviii
CO-AUTHORSHIP STATEMENT.....	xix
CHAPTER ONE	1
1.1 Introdution to Carbenes.....	1
1.2 Bonding of Metal Coordinated Carbene Ligands	8
1.3 Late Transition Metal NHC Complexes in Catalysis	11
1.3.1 Ruthenium-NHC Complexes for Olefin Metathesis.....	12
1.3.2 Palladium-NHC Complexes for Cross-Coupling Reactions.....	15
1.3.3 Rhodium- and Iridium-NHC Complexes for Hydrogenation and Transfer Hydrogenation	17
1.3.4 Rhodium- and Iridium-NHC Complexes for Hydrosilylation	20
1.4 Scope of the Thesis	23
1.5 References.....	26

CHAPTER TWO	32
2.1 Introduction.....	32
2.2 Synthesis and Characterization of the ^{Mes} [CNH] Ligand.....	35
2.3 Synthesis and Characterization of Amino-Tethered NHC-Rhodium Compounds	37
2.4 Synthesis and Characterization of ^{Mes} [CNH]Ir(COD) Compounds	44
2.5 Catalytic Hydrogenation Investigation with Group 9 ^{Mes} [CNH] Precursors	46
2.6 Catalytic Hydrosilylation Reactions with Group 9 ^{Mes} [CNH] Precursors	48
2.7 Conclusions.....	51
2.8 Experimental Section	53
2.9 References.....	62
CHAPTER THREE	65
3.1 Introduction.....	65
3.2 Synthesis and Characterization of ^{Mes} [CNH]Ru(=CHPh)(PCy ₃)Cl ₂	66
3.3 Isomerization of ^{Mes} [CNH]Ru(=CHPh)(PCy ₃)Cl ₂ in Solution	69
3.4 RCM and ROMP Catalytic Reactions with ^{Mes} [CNH]Ru(=CHPh)(PCy ₃)Cl ₂	74
3.5 Measurement of Phosphine Exchange Rates via Magnetization Transfer.....	77
3.6 Investigating the Coordinative Propensity of the Amino Tether of ^{Mes} [CNH]Ru(=CHPh)(PCy ₃)Cl ₂	81
3.7 Synthesis, Characterization of ^{Mes} [CNH]Ru(=CHPh)(py)Cl ₂ and ^{Mes} [CNH]Ru(=CHPh)(PMe ₃)Cl ₂	82
3.8 RCM and ROMP Activity of ^{Mes} [CNH]Ru(=CHPh)(py)Cl ₂	87
3.9 Insight into Mechanism of ^{Mes} [CNH]Ru(=CHPh)(PCy ₃)Cl ₂ in Metathesis.....	88
3.10 Conclusions.....	90
3.11 Experimental Section	91
3.12 References.....	95

CHAPTER FOUR	98
4.1 Introduction.....	98
4.2 Synthesis and Reactivity of N-heterocyclic Carbenes with Silver(I)	99
4.3 Synthesis, Characterization of ^{Mes} [CNH] with Silver(I)	101
4.4 Transmetalation of ^{Mes} [CNH]-Ag Compounds with Palladium	103
4.5 Synthesis and Reactivity of N-heterocyclic Carbenes with Lithium	106
4.6 Synthesis, Characterization and Reactivity of ^{Mes} [CNH] with Lithium	108
4.7 Synthesis, Characterization and Reactivity of ^{Mes} [HCPH]Cl	112
4.8 Deprotonation Studies of ^{Mes} [HCPH]Cl.....	114
4.9 Synthesis and Reactivity of ^{Mes} [CP]M(COD) (M = Rh, Ir)	118
4.10 Synthesis, Characterization and Reactivity of ^{Mes} [CNH ₂]	126
4.11 Conclusions.....	128
4.12 Experimental Section.....	131
4.13 References.....	138
CHAPTER FIVE.....	142
5.1 Synopsis and Analysis	142
5.2 Future Work	147
5.3 Concluding Remarks.....	160
5.4 Experimental Section	161
5.5 References.....	164
APPENDIX A	166
A.1 X-ray Crystallographic Data	166
A.2 Details from the Magnetization Transfer Experiments.....	174
A.3 References.....	176

LIST OF TABLES

Table 2.1.	Consolidated table of bond lengths and angles for complexes 2.3 , 2.5 , 2.8 , 2.10 and 2.11 (M = Rh or Ir).....	43
Table 2.2.	Consolidated results from the hydrosilylation of phenylacetylene and dimethylphenylsilane by precursors 2.3 – 2.8 and 2.10 – 2.12	50
Table 3.1.	Selected bond lengths and angles for compounds 3.1 , 3.2 and 3.3 . Atom labels have been renamed for simplicity in comparative analysis.....	69
Table 3.2.	RCM results for 3.1 compared with reference catalysts under similar conditions.....	75
Table 3.3.	ROMP results for 3.1 compared with reference catalysts under similar conditions.....	76
Table 3.4.	Phosphine dissociation rate constants and activation parameters determined by magnetization transfer experiments for 3.1 – 3.4	80
Table 3.5.	Selected bond lengths and angles for complexes 3.5 – 3.7	84
Table 3.6.	Entries 1 – 4 show RCM results for 1 mol % of 3.5 . Entries 5 – 6 show ROMP data for 0.1 mol % of 3.5 . All reactions performed at 30 °C in CD ₂ Cl ₂	88
Table 4.1.	Selected bond lengths and angles for ^{Mes} [CNLi] ₂ , 4.4	111
Table 4.2.	Selected bond lengths and angles for complexes 4.7 and 4.8 compared to their congeners 2.5 and 2.11 respectively (M = Rh, Ir).....	120
Table 4.3.	Selected bond lengths and angles for complex 4.8a	122
Table 4.4.	Results from the hydrogenation test reactions of 4.8 and 2.11 using cyclohexene as the substrate. H ₂ pressure was applied at either 1 or 4 atm and the reaction was allowed to react for 18 hours in a Teflon-sealed glass reactor.....	126
Table A.1.	Crystallographic structural refinement information for ^{Mes} [CNH] (2.2), ^{Mes} [CNH]Rh(COD)Cl (2.3) and ^{Mes} [CN]Rh(COD) (2.5).....	167

Table A.2.	Crystallographic structural refinement information for $[\text{Mes}[\text{CNH}]\text{Rh}(\text{NBD})]\text{BF}_4$ (2.8), $[\text{Mes}[\text{CNH}]\text{Ir}(\text{COD})\text{Cl}]$ (2.10) and $[\text{Mes}[\text{CN}]\text{Ir}(\text{COD})]$ (2.11).....	168
Table A.3.	Crystallographic structural refinement information for $[\text{Mes}[\text{CNH}]\text{Ru}(=\text{CHPh})(\text{PCy}_3)\text{Cl}_2]$ (3.1), $[\text{Mes}[\text{CNH}]\text{Ru}(=\text{CHPh})(\text{py})\text{Cl}_2]$ (3.5) and $[\text{Mes}[\text{CNH}]\text{Ru}(=\text{CHPh})(\text{PMe}_3)\text{Cl}_2]$ (3.7).....	169
Table A.4.	Crystallographic structural refinement information for $[\text{Mes}[\text{CNH}]\text{AgCl}]$ (4.2), $[\text{Mes}[\text{CNH}]_2\text{PdCl}_2]$ (4.3) and $[\text{Mes}[\text{CNLi}]_2]$ (4.4).....	170
Table A.5.	Crystallographic structural refinement information for $[\text{Mes}[\text{CP}]\text{Rh}(\text{COD})]$ (4.7), $[\text{Mes}[\text{CP}]\text{Rh}(\text{COD})]$ (4.8) and 4.8a	171
Table A.6.	Crystallographic structural refinement information for $[\text{Mes}[\text{CN}]\text{Zr}(\text{NMe}_2)_3]$ (5.1), $[\text{Mes}[\text{CNH}]\text{Rh}(\text{PPh}_3)_2\text{Cl}]$ (5.3) and $[\text{Mes}[\text{CNH}]\text{FeBr}_2]$ (5.4).....	172
Table A.7.	Crystallographic structural refinement information for $[\text{Mes}[\text{CNH}]_2\text{NiCl}_2]$ (5.5).....	173
Table A.8.	The tabulated rate constants and T_1 values obtained from the variable temperature magnetization transfer experiments of 3.1 used for the Eyring plot.....	175

LIST OF FIGURES

Figure 1.1.	The push-pull electronic effects exhibited by phosphinosilylcarbene 1.5	3
Figure 1.2.	The schematic of the “push-push” π -donor and the “pull-pull” inductive electronic effects exhibited by N-heterocyclic carbene compounds.....	5
Figure 1.3.	The four different electron configurations possible for a basic six-electron divalent carbene compound.....	6
Figure 1.4.	(a) A classic example of a metal complex containing a Fischer-type carbene and (b) a bonding scheme of the donor-acceptor framework of the Fischer carbene with a metal.....	8
Figure 1.5.	(a) A classic example of a metal complex containing a Schrock-type carbene and (b) a bonding scheme of the covalent interaction of the Schrock carbene with a metal.....	10
Figure 2.1.	ORTEP view of 2.2 , with thermal ellipsoids depicted at 50 % probability. All hydrogen atoms have been omitted for clarity except for H3n, which was located in a difference map and refined isotropically.....	36
Figure 2.2.	ORTEP view of 2.3 , with thermal ellipsoids depicted at 50 % probability. All hydrogen atoms have been omitted for clarity except for H3n, which was located in a difference map and refined isotropically.....	39
Figure 2.3.	ORTEP view of 2.5 , with thermal ellipsoids depicted at 50 % probability. All hydrogen atoms have been omitted for clarity.....	40
Figure 2.4.	ORTEP view of 2.8 , with thermal ellipsoids depicted at 50 % probability. All hydrogens have been omitted for clarity except for H3n, which was located in a difference map and refined isotropically.....	42
Figure 2.5.	ORTEP view of 2.10 , with thermal ellipsoids depicted at 50 % probability. All hydrogens are removed for clarity except for H3n, which was located in a difference map and refined isotropically.....	45
Figure 2.6.	ORTEP view of 2.11 , with thermal ellipsoids depicted at 50 % probability. All hydrogens are removed for clarity.....	46

Figure 3.1.	ORTEP view of $^{\text{Mes}}[\text{CNH}]\text{Ru}(=\text{CHPh})(\text{PCy}_3)\text{Cl}_2$, 3.1 , with thermal ellipsoids at 50 % probability. All hydrogens were removed for clarity except H3n and H24, which were located in a difference map and refined isotropically.....	68
Figure 3.2.	The $^1\text{H}/^{31}\text{P}$ HMBC spectrum of 3.1 and 3.1a in CD_2Cl_2 . The inset is an expansion of the spectral region focused on the correlation between the benzyldiene proton and PCy_3	71
Figure 3.3.	Downfield inverse-gated 151 MHz ^{13}C NMR spectrum of 3.1 and 3.1a in CD_2Cl_2	73
Figure 3.4.	The Eyring plot of the phosphine exchange experiments for 3.1	79
Figure 3.5.	The RCM conversion of S1 catalyzed by 3.1 at 100 °C in d_{10} - <i>o</i> -xylene.....	81
Figure 3.6.	ORTEP view of $^{\text{Mes}}[\text{CNH}]\text{Ru}(=\text{CHPh})(\text{py})\text{Cl}_2$, 3.5 , with thermal ellipsoids at 50 % probability. All hydrogens were removed for clarity except H3n and H24, which were located and refined isotropically.....	83
Figure 3.7.	ORTEP view of $^{\text{Mes}}[\text{CNH}]\text{Ru}(=\text{CHPh})(\text{PMe}_3)\text{Cl}_2$, 3.7 , with thermal ellipsoids at 50 % probability. All hydrogens were removed for clarity except H3n and H24, which were located and refined isotropically.....	86
Figure 4.1.	An ORTEP drawing of $^{\text{Mes}}[\text{CNH}]\text{AgCl}$, 4.2 , with thermal ellipsoids drawn at 50 % probability. All hydrogens atoms, except H3n, were removed for clarity. H3n was located in a difference map and refined isotropically.....	103
Figure 4.2.	An ORTEP drawing of $^{\text{Mes}}[\text{CNH}]_2\text{PdCl}_2$, 4.3 , with thermal ellipsoids drawn at 50 % probability. All hydrogens atoms, except H3n, were removed for clarity. H3n was located in a difference map and refined isotropically. Half of the structure was generated by symmetry as the molecule resides on an inversion center.....	106
Figure 4.3.	An ORTEP drawing of $^{\text{Mes}}[\text{CNLi}]_2$, 4.4 , with thermal ellipsoids drawn at 50 % probability. Mesityl substituents coordinated to N1 and N1a were omitted for clarity (except for <i>ipso</i> -carbons). All hydrogens atoms were also removed for clarity.....	110

Figure 4.4.	The solid-state molecular structure of 4.4 reoriented to show alignment of mesityl substituents suggesting π -stacking interactions. All hydrogens were omitted for clarity.....	111
Figure 4.5.	The stacked 161 MHz ^{31}P NMR proton coupled spectrum depicting compounds 4.6a and 4.6b at $-20\text{ }^{\circ}\text{C}$ and $+60\text{ }^{\circ}\text{C}$ in d_8 -THF. The inset shows the expanded view of the phosphide triplet resonance.....	117
Figure 4.6.	ORTEP drawings of $^{\text{Mes}}[\text{CP}]\text{Rh}(\text{COD})$ (4.7) and $^{\text{Mes}}[\text{CP}]\text{Ir}(\text{COD})$ (4.8) with thermal ellipsoids drawn at 50 % probability. All hydrogens have been removed for clarity.....	119
Figure 4.7.	An ORTEP drawing of 4.8a with thermal ellipsoids drawn at 50 % probability. The mesityl group (except C_{ipso}) coordinated to N1 and all hydrogens (except H1ir) have been omitted for clarity. H1ir was located in a difference map and refined isotropically.....	122
Figure 5.1.	An ORTEP drawing of $^{\text{Mes}}[\text{CN}]\text{Zr}(\text{NMe}_2)_3$, 5.1 , with thermal ellipsoids drawn at 50% probability. All hydrogens atoms were removed for clarity.....	149
Figure 5.2.	An ORTEP drawing of one molecule of $^{\text{Mes}}[\text{CNH}]\text{Rh}(\text{PPh}_3)_2\text{Cl}$, 5.3 , in the asymmetric unit with thermal ellipsoids drawn at 50 % probability. All hydrogens atoms were removed for clarity, except for H3n that was located in a difference map and refined isotropically.....	152
Figure 5.3.	An ORTEP drawing of $^{\text{Mes}}[\text{CNH}]\text{FeBr}_2$, 5.4 , with thermal ellipsoids drawn at 50 % probability. All hydrogens atoms were removed for clarity, except for H3n that was located in a difference map and refined isotropically.....	155
Figure 5.4.	An ORTEP drawing of $^{\text{Mes}}[\text{CNH}]_2\text{NiCl}_2$, 5.5 , with thermal ellipsoids drawn at 50 % probability. All hydrogens atoms were removed for clarity, except for H3n that was located in a difference map and refined isotropically. The molecular structure was solved as a half unit and the full molecule was generated by inversion symmetry.....	157
Figure A.1.	A pulse sequence diagram of the magnetization transfer experiment used to measure the phosphine exchange rate of 3.1 and PCy_3	174

Figure A.2.	The stacked 162 MHz ^{31}P NMR spectra of the magnetization transfer experiment used to measure the phosphine exchange rate of 3.1 and PCy_3 in $\text{d}_{10}\text{-}o\text{-xylene}$ at 80 °C.....	174
Figure A.3.	A plot of the observed normalized integrals of the Ru- PCy_3 (3.1) and free PCy_3 resonances measured by the ^{31}P NMR magnetization transfer experiment at 95 °C. The observed data is fitted and overlaid with the calculated values generated by the CIFIT software.....	175

LIST OF SCHEMES

Scheme 1.1	2
Scheme 1.2	3
Scheme 1.3	9
Scheme 1.4	10
Scheme 2.1	33
Scheme 2.2	35
Scheme 2.3	37
Scheme 2.4	38
Scheme 2.5	40
Scheme 2.6	41
Scheme 2.7	44
Scheme 2.8	48
Scheme 2.9	49
Scheme 2.10	50
Scheme 2.11	51
Scheme 3.1	70
Scheme 3.2	77
Scheme 3.3	78
Scheme 3.4	82

Scheme 3.5	82
Scheme 3.6	89
Scheme 4.1	100
Scheme 4.2	104
Scheme 4.3	105
Scheme 4.4	107
Scheme 4.5	114
Scheme 4.6	116
Scheme 4.7	125
Scheme 4.8	128
Scheme 5.1	150
Scheme 5.2	153
Scheme 5.3	154
Scheme 5.4	156
Scheme 5.5	156
Scheme 5.6	159

LIST OF ABBREVIATIONS

Å	Angstrom
a, b, c	unit cell dimensions; lengths (Å)
α , β , γ	unit cell dimensions, angles (°)
atm	atmosphere
^{107}Ag	silver-107
^{109}Ag	silver-109
Ar	aryl
BARF	tetrakis[3,5-bis(trifluoromethyl)phenyl]borate
br	broad
^nBu	n-butyl group
^{13}C	carbon-13
Cy	cyclohexyl
calc	calculated
COD	1,5-cyclooctadiene
COE	cyclooctene
Δ	heat
d	doublet
dd	doublet of doublets
dt	doublet of triplets
DFT	density functional theory
DMSO	dimethyl sulfoxide
DME	dimethoxyethane
D_e	bond dissociation energy

d^n	numbers of <i>d</i> -electrons
d_n	n-deuterated
EI-MS	electron ionization/mass spectrometry
Et	ethyl group
eu	entropy units
ΔG^\ddagger	Gibbs energy of activation
ΔH^\ddagger	enthalpy of activation
^1H	proton
$\{^1\text{H}\}$	proton decoupled
hr(s)	hour(s)
HMBC	heteronuclear multiple bond correlation
HSQC	heteronuclear single quantum coherence
IAd	1,3-diadamantylimidazol-2-ylidene
ICy	1,3-bis(cyclohexyl)imidazol-2-ylidene
IMe	1,3-dimethylimidazol-2-ylidene
IMes	1,3-dimesitylimidazol-2-ylidene
IPr	1,3-bis(2,6-diisopropylphenyl)imidazol-2-ylidene
$^nJ_{AB}$	n-bond scalar coupling constant between nuclei A and B
kcal	kilocalories
^7Li	lithium-7
Mes	2,4,6-trimethylphenyl, or mesityl
<i>m</i>	<i>meta</i>
NBD	2,5-norbornadiene
NHC	N-heterocyclic carbene

NMR	nuclear magnetic resonance
<i>o</i>	<i>ortho</i>
ORTEP	Oakridge Thermal Ellipsoid Plot
OAc	acetate
OTf	trifluoromethanesulfonate, or triflate (CF ₃ SO ₃ ⁻)
^t OBu	<i>tert</i> -butoxide
<i>p</i>	<i>para</i>
³¹ P	phosphorus-31
{ ³¹ P}	phosphorus-31 decoupled
Ph	phenyl group
PhMe	toluene
ⁱ Pr	isopropyl group
py	pyridine
¹⁰³ Rh	rhodium-103
RCM	ring-closing metathesis
ROMP	ring-opening metathesis polymerization
rt	room temperature
s	singlet
SIMes	1,3-dimesityl-4,5-dihydroimidazol-2-ylidene
SIPr	1,3-bis(2,6-diisopropylphenyl)-4,5-dihydroimidazol-2-ylidene
t	triplet
THF	tetrahydrofuran
VT	variable temperature
<i>V</i>	unit cell volume (Å ³)
<i>Z</i>	number of asymmetric units in unit cell

ACKNOWLEDGEMENTS

First and foremost, I would like to acknowledge my supervisor, Professor Michael D. Fryzuk. While my time at UBC has been lengthy, he has remained patient and supportive. The time that I have spent under his supervision has taught me many things, which have greatly improved my knowledge of chemistry. The experience and knowledge that I've gained at UBC is invaluable and I have become a more intelligent person from this experience under the guidance of Professor Fryzuk.

I'd also like to extend my thanks to my parents George and Frieda Jong for being the parents that never stop giving. They provide support in any and every way possible and have helped me immensely financially. It has always been my aim in life to use my experience and achievements to demonstrate to them that their time and investment has returned substantial dividends by becoming a person they are proud to call their son.

I'd also like to thank the Fryzuk group members for their collaborations and making the working atmosphere enjoyable. In particular, I'd like to thank Bryan Shaw, Nathan Halcovitch and Kyle Parker for their assistance in proof-reading my thesis. I would also like to acknowledge Erin MacLachlan and Liam Spencer for being the role models that I could never live up to – they are truly two of the smartest and hardest working people I know. I also want to acknowledge Brian Patrick for his assistance with crystallography and performing solid-state miracles.

To all my other friends and family, I am sincerely thankful that I have your support in everything I do – loyalty is true friendship and it is not something that I take lightly. As such, I will always watch your back as you have mine.

Last but not least, I'd like to acknowledge Lindy Chan who has been the backbone of my sanity and provided the foundations for me to become a better man. She has been, and always will be, the one person that I cannot live without.

CO-AUTHORSHIP STATEMENT

Chapters two, three, four and five were conducted in collaboration with Professor Michael D. Fryzuk, the research supervisor for the thesis, who assisted with the development of the related work. Chapter two was also assisted by Dr. Brian O. Patrick who assisted with the X-ray structural information. All experimental research, data analysis and manuscript preparation were performed by the author of the thesis.

CHAPTER ONE

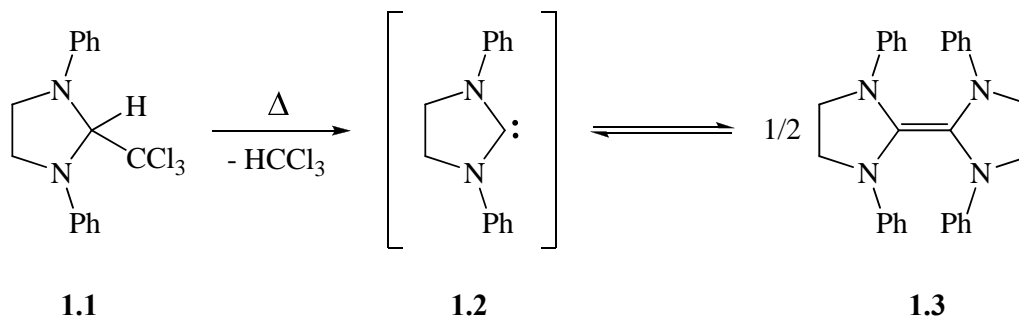
N-Heterocyclic Carbenes: An Overview

1.1 Introduction to Carbenes

Carbenes are broadly defined as divalent carbon compounds of the general formula :CR_2 . The research of carbenes began as a chemical curiosity over five decades ago with pioneering work done by Doering and Hoffmann.¹ While the isolation of free carbenes remained elusive, Fischer *et al.* was able to indirectly incorporate them into organometallic systems in 1964.² During this period, free carbenes were regarded by chemists as highly reactive transient species in solution and referred to as “the missing class” of carbon compounds.³ Continual research of elusive carbene compounds led Wanzlick *et al.* to the discovery that the stability of carbenes could be dramatically improved by incorporating amino substituents. This prompted the attempted elimination of chloroform from 1,3-diphenyl-4,5-dihydroimidazol-2-ylidene (**1.1**) by thermolysis (Scheme 1.1) in an effort to generate the free carbene species (**1.2**).⁴ However, the reaction failed and no free carbene was detected, only the olefin (**1.3**) was isolated. Although the initial goal to isolate the free carbene was unsuccessful, the equilibrium that was suggested to

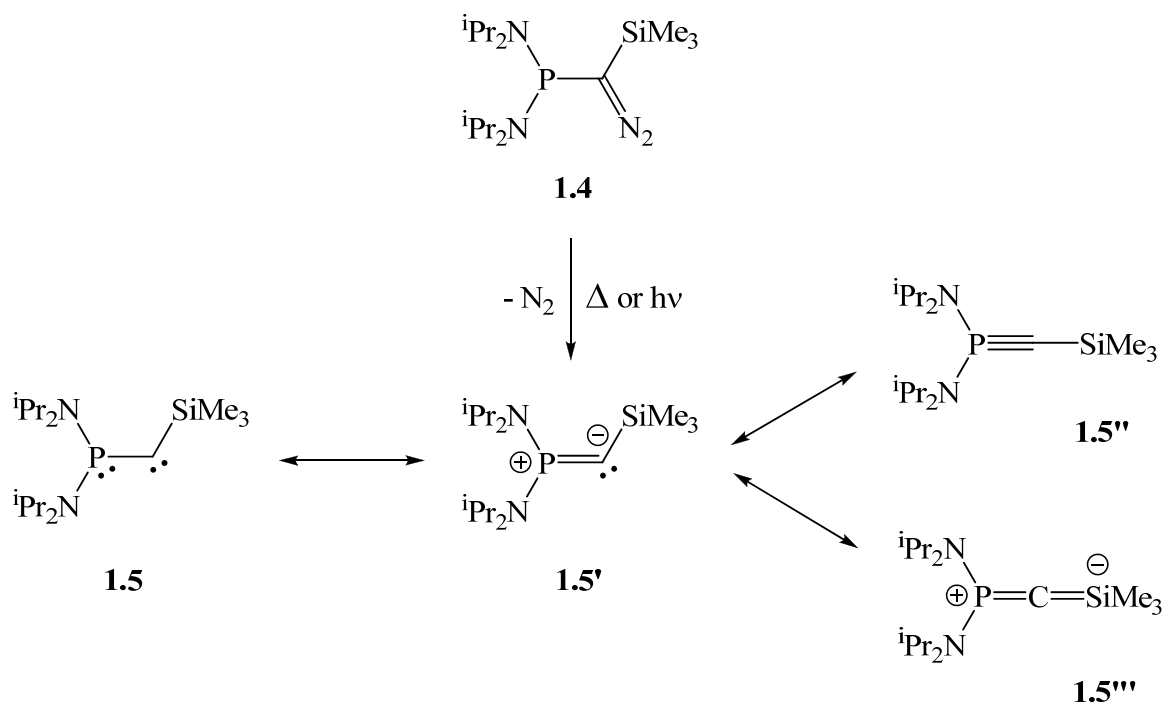
exist between **1.2** and **1.3**, which was substantiated years later,⁵ was vital for work in the field that followed.

Scheme 1.1



The first carbene was isolated in 1988 when Bertrand and co-workers formed the phosphinosilylcarbene **1.5** through the elimination of N₂ via thermolysis (250 °C), or photolysis (300 nm), from [bis(diisopropylamino)phosphino](trimethylsilyl)diazomethane (**1.4**) (Scheme 1.2). Compound **1.5** was isolated as a red oil and found to be stable for weeks at room temperature under an inert atmosphere.

Scheme 1.2



The phosphinosilylcarbene can form various resonance structures to aid its stability. The resonance system of **1.5** exhibits a “push-pull” mechanism that describes the ability for the carbene to facilitate as either a π -acceptor or a π -donor to its adjacent heteroatoms (Figure 1.1). However, while there is spectroscopic evidence of a partial double bond character that exists between P and C, it has been suggested that only weak interactions exist between the carbene lone pair and the low-lying σ^* -orbitals of P and Si to account for **1.5''** and **1.5'''**, thus they are generally considered secondary contributors to **1.5** and **1.5'**.^{6, 7}

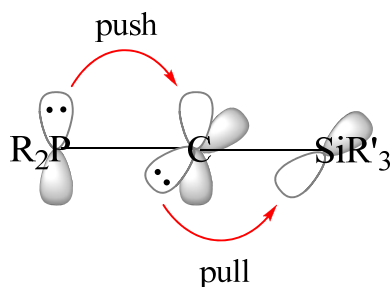
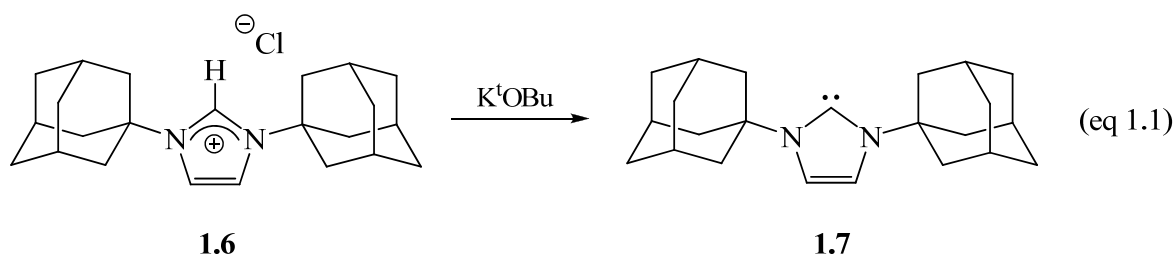


Figure 1.1. The push-pull electronic effects exhibited by phosphinosilylcarbene **1.5**.

Although the isolation of the first stable carbene was an enormous step forward in carbene chemistry, its popularity did not rapidly expand until after the isolation of the first stable crystalline carbene compound synthesized by Arduengo in 1991.⁸ This class of carbene is currently referred to as the N-heterocyclic carbene (NHC) – the free carbene that Wanzlick failed to isolate 20 years earlier. The deprotonation of 1,3-diadamantylimidazolium chloride (**1.6**) with a strong base cleanly generates the free NHC, 1,3-diadamantylimidazol-2-ylidene (IAd) (**1.7**), in good yield (eq 1.1), which was similar to the deprotonation scheme applied earlier by Wanzlick to trap NHCs.⁷



The isolation of crystalline **1.7** allowed for single crystal X-ray diffraction studies to be performed, which provided evidence to support some of the earlier hypotheses of the NHC electronic structure. The solid-state molecular structure of **1.7** displays an N—C_{carbene}—N angle (102.2(2) °) that is significantly smaller than the typical range of values observed for the corresponding angle in imidazolium salts (108.5 – 109.7 °) and is supportive of carbenes bearing π -donor substituents.⁸ This is in agreement with Wanzlick's original hypothesis that π -donation from the nitrogen lone pair in the imidazole ring would help stabilize the NHC.⁴ However, this “push-push” π - donor effect is also accompanied by a “pull-pull” inductive effect due the nitrogen atoms being more electronegative to create a synergic bonding scheme that optimizes electroneutrality of the carbene (Figure 1.2).⁹

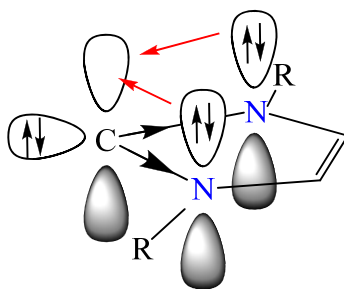


Figure 1.2. The schematic of the “push-push” π -donor and the “pull-pull” inductive electronic effects exhibited by N-heterocyclic carbene compounds.

Despite the electronic stability built into the NHC model, the principal rationale explaining why **1.7** is isolable and **1.2** is not is the size of the imidazole substituents. The adamantyl group of **1.7**, being substantially larger than the phenyl group in **1.2**, provides the steric bulk necessary for the kinetic stabilization of the free NHC as it prevents dimerization from occurring.¹⁰

To gain a better understanding of the contributing factors that determine whether a free NHC is isolable, the electronic structure of the NHC deserves to be discussed further. Carbenes are fundamentally divalent carbon compounds and the bent geometry of the central NHC carbon imposes sp^2 -hybridized frontier orbitals with an empty p_π -orbital positioned orthogonal to the sp^2 plane. This enables the two nonbonding electrons of the NHC to form one of four different possible electronic configurations (Figure 1.3). However, of the four possible arrangements, only the 3B_1 (i) and 1A_1 (ii) states are typically considered as (iii) and (iv) are higher energy states that are not observed.⁷

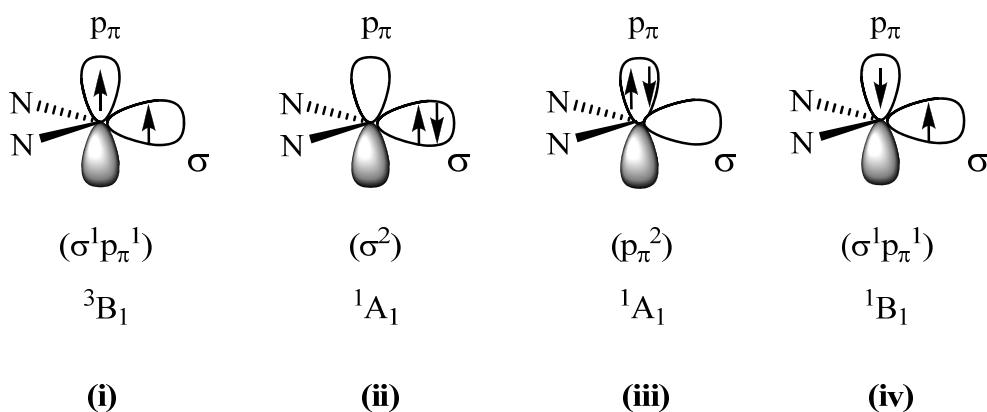
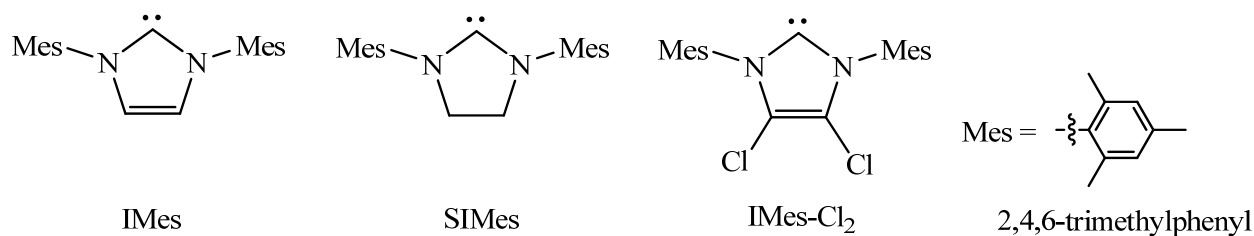


Figure 1.3. The four different electron configurations possible for a basic six-electron divalent carbene compound.

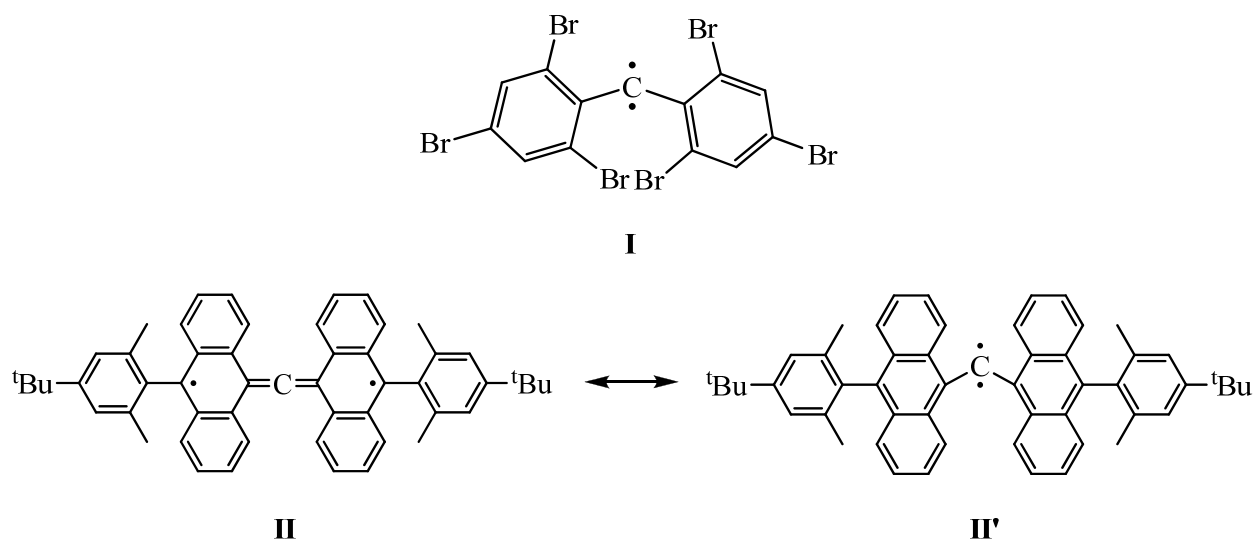
It is commonly accepted that the lowest energy state for a divalent carbon is its triplet state **(i)**, which is anomalous to the trend of all other elements in its periodic column preferring the singlet ground state.¹¹ For a methylene unit ($:\text{CH}_2$) with a triplet ground state, the gap to the higher energy singlet state is approximately 9 kcal/mol.¹² However, in the case of NHCs, the inductive effect of the σ -withdrawing amine groups lowers the energy of the singlet state such that it can become the preferred ground state. It is calculated that a singlet-triplet energy gap ($\Delta E_{\text{S-T}}$) of approximately 46 kcal/mol is necessary to invoke a stable singlet species.¹³ Since the $\Delta E_{\text{S-T}}$ for common NHCs such as IAd, IMes (1,3-dimesitylimidazol-2-ylidene) and SIMes (1,3-dimesityl-4,5-dihydroimidazol-2-ylidene) is in the range of 65 – 85 kcal/mol, this indicates a clear propensity for these NHCs to maintain a singlet ground state electron configuration.¹⁴ Modulating the $\Delta E_{\text{S-T}}$ can be managed by tuning the substituents of the imidazole backbone of the NHC unit, which affects the σ -withdrawing induction within the imidazole ring. The effect is dramatic when the backbone of IMes is substituted with electron withdrawing groups such as chlorines to form IMes- Cl_2 , which is found to be a free carbene so stable that not only does it resist dimerization, it is also tolerant of air and moisture on the bench top for two days without degradation.¹⁵



A comparison was made between IMes and SIMes to evaluate the effect of having an unsaturated NHC backbone relative to a saturated one. The study showed that the ΔE_{S-T} difference between them is approximately 10 kcal/mol in favor of IMes being the more stable of the two with ΔE_{S-T} gap near 80 kcal/mol.¹⁴ The increased stability of IMes is attributed to the partial aromatic character exhibited by the imidazole ring system that is absent in SIMes.¹⁶ The increased stability of IMes is also partially responsible for its reduced nucleophilicity compared to SIMes.¹⁷ The partial aromaticity exhibited by IMes is suggested to inhibit its π -accepting character when coordinated to electron-rich metal complexes opposed to SIMes that is slightly better at accepting π -backdonation from a metal center.¹⁸ Thus, the net result is SIMes being a slightly more strongly bound ligand to metal complexes than IMes, in general.

Until this point, only the isolation of stable singlet carbenes has been mentioned. However, there has also been interest in the synthesis of stable triplet carbene compounds. Due to their highly reactive nature, free triplet carbenes have been extremely challenging to isolate. The early groundwork was laid by Zimmerman and Paskovich *et al.* in the 1960s when they investigated hindered divalent carbon-diazo compounds as a source for generating triplet carbenes.¹⁹ While they were not able to isolate such a species, their work paved the way for Tomioka and co-workers to isolate the first stable triplet carbene (**I**) in solution at low temperature in 1995.²⁰ With its isolation, it became apparent that triplet carbene compounds needed to be treated similarly to compounds that contained free radicals. Further development progressed to the synthesis of di{9-[10-(2,6-dimethyl-4-tert-butylphenyl)-anthryl]}carbene (**II**) in 2003 by Tomioka *et al.*²¹ Compound **II** has been shown to be stable in solution at room

temperature for a week, which is among the most persistent triplet carbenes species known to date. Despite the monumental progress made in the field, triplet carbenes remain as chemical curiosities. Thus, these carbenes will not be discussed further as they are beyond the scope of this thesis. Reviews of triplet carbenes have been published that outline their development in more detail, should the reader find the area to be of interest.^{7, 22}



1.2 Bonding of Metal Coordinated Carbene Ligands

As a result of the discovery of the first metal complex with a bound carbene ligand in 1964 by Fischer *et al.*, this unique type of carbene now bears his name.² Fischer carbenes are defined as carbene ligands with at least one π -donating substituent that are coordinated to a low-valent transition metal. As a result, the carbene carbon is electrophilic with the bound metal bearing the majority of the electron density (Scheme 1.3).²³ The coordination of Fischer carbenes follows a donor-acceptor model where the carbene donates through its sp^2 -hybridized σ -orbital to a metal d-orbital and accepts backdonation from the metal via its empty p_π -orbital (Figure 1.4).

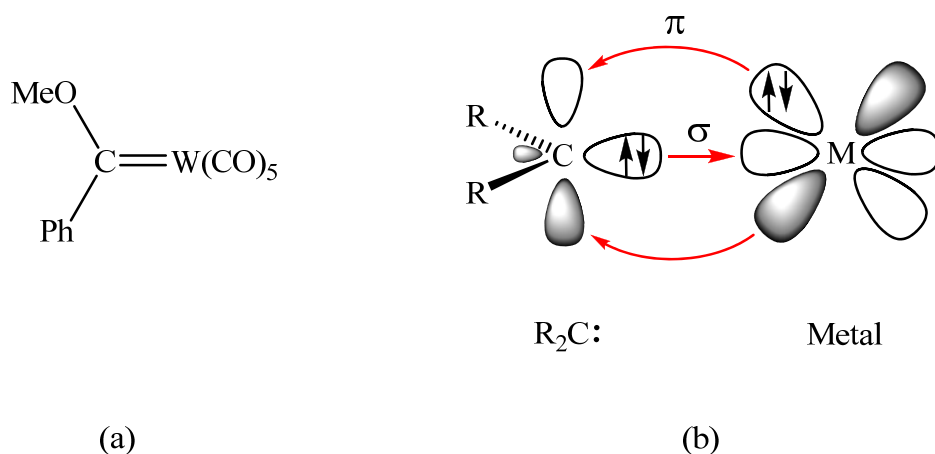
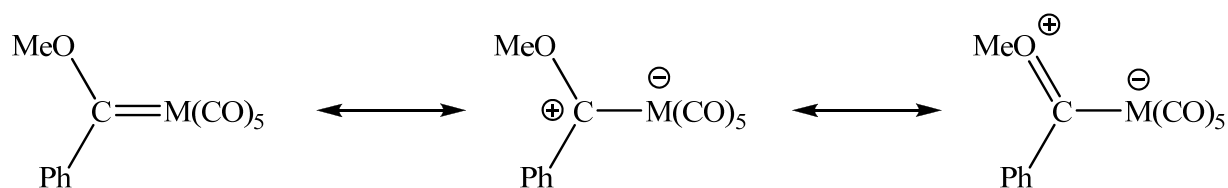


Figure 1.4. (a) A classic example of a metal complex containing a Fischer-type carbene and (b) a bonding scheme of the donor-acceptor framework of the Fischer carbene with a metal.

Scheme 1.3



Following the discovery of the Fischer carbene was a second type of metal coordinated carbene – the Schrock carbene. Schrock carbenes, also known as alkylidenes, were first synthesised in 1974.²⁴ The Schrock carbene was noticeably different from the Fischer-type as these ligands are typically found on high oxidation state metal complexes. Moreover, the Schrock carbenes did not contain π -donating substituents to delocalize electron density in the carbene p_{π} -orbital. The absence of the heteroatomic substituent also implies that the inductive effect is absent, which has been ascribed as a necessary feature to stabilize the singlet ground state carbene as per Fischer carbenes and NHCs. Thus, the bonding model of alkylidenes closely resembles that of C=C bonds in that a polarized covalent double bond with the metal center, bearing a triplet ground state (Figure 1.5), is normally considered. Moreover, the covalent

framework that forms a formal σ - and a π -bond results in the alkylidene carbon being nucleophilic (Scheme 1.4), which is the opposite of what is observed in Fischer carbenes.²⁵

Scheme 1.4

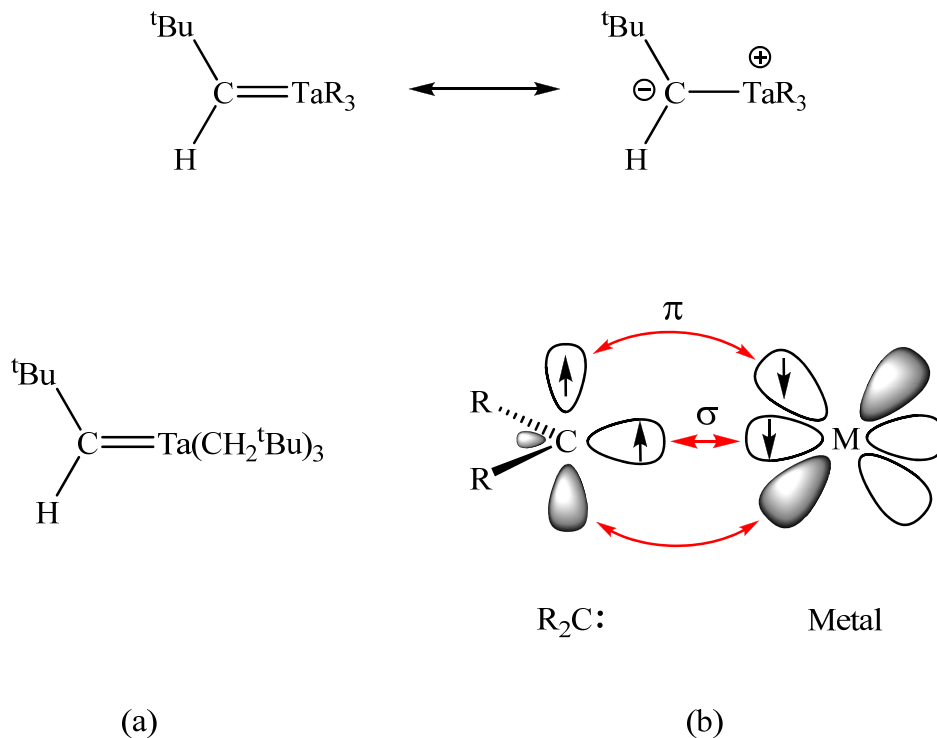


Figure 1.5. (a) A classic example of a metal complex containing a Schrock-type carbene and (b) a bonding scheme of the covalent interaction of the Schrock carbene with a metal.

At first glance, the bonding scheme of Fischer carbenes to metals is similar to that of NHCs since NHCs have two π -donating heteroatomic substituents. However, there is a substantial difference between the two ligand types. Fischer carbenes coordinate to metals synergically via a σ -donor and π -acceptor model while NHCs are primarily σ -donors with a weak π -acceptor character and do not depend on backdonation from the metal to form stable metal-NHC adducts.²⁶ Various main group-NHC adducts have been synthesized that showcase the pure σ -donor bonding character of NHCs.²⁷ However, despite forming only a single bond with the metal, the metal-NHC bond is very strong. It has been calculated that an NHC-AuCl

bond ($D_e = 82.8$ kcal/mol) surpasses the carbene-metal bond found in the Fischer carbene (HO)HC=W(CO)₅ complex ($D_e = 75.0$ kcal/mol), which has the π -backdonation contribution from the metal.²⁸ Nevertheless, it should be noted that although NHCs are considered to be predominantly σ -donors, they have shown to exhibit significant amounts of π -accepting character in very electron-rich systems.²⁹

The strong coordinating character of NHCs is advantageous as it makes them good auxiliary ligands for organometallic catalysts. This feature is also a trait that compares well with phosphines that have been shown to be excellent ligands for catalytic applications. In fact, it has been determined that NHCs are often stronger donors than phosphines.³⁰ NHCs have shown to possess several other advantages over their phosphine counterparts as NHCs are not prone to oxidation and, in general, form more thermally stable metal complexes.^{31, 32} These advantages, along with the ability to easily tune steric and electronic properties, make NHCs enticing alternatives to phosphine ligands. Perhaps the most compelling reasons for the growing interest in NHCs are their ability to replace phosphine ligands to generate late transition metal catalyst precursors that are more robust and versatile than their phosphine analogues.

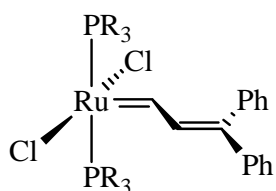
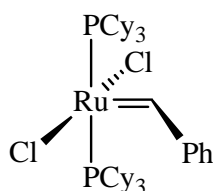
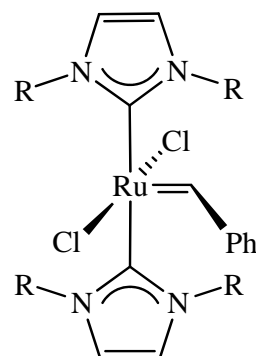
1.3 Late Transition Metal NHC Complexes in Catalysis

While NHCs have been found to be useful in a variety of catalytic applications that have traditionally been carried out using phosphine ligand systems,³³ there are standout cases where NHCs excel as auxiliary ligands. Specifically, NHC catalyst precursors have shown to be particularly effective for olefin metathesis and cross-coupling reactions. In addition, NHC-precursors have shown to be attractive alternatives for other applications such as hydrogenation, transfer hydrogenation and hydrosilylation where their effectiveness rivals those of benchmark phosphine-based systems.

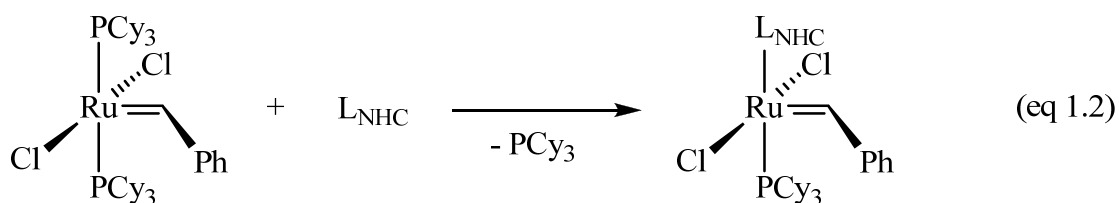
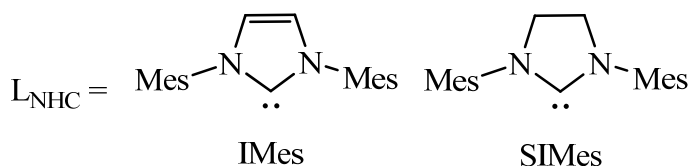
1.3.1 Ruthenium-NHC Complexes for Olefin Metathesis

In terms of impact, olefin metathesis is a prime example of where NHCs excel as ancillary ligands. While the development of highly active Ru catalyst precursors for olefin metathesis did not materialize overnight, the world of olefin metathesis was changed by the introduction of NHCs.

The first milestone in Ru olefin metathesis catalysis was achieved with the synthesis of the first single-component homogeneous Ru-alkylidene precursor (**1.8**) that was prepared by Grubbs and co-workers.³⁴ Although **1.8** did show good activity for ring-opening metathesis polymerization (ROMP) of highly strained cyclic olefins, its activity for simple olefins was poor. However, the catalyst activity of **1.8** was not its outstanding feature; it was its ability to perform olefin metathesis in both organic and protic solvents efficiently in addition to its tolerance of various functional groups that was impressive. The catalyst was improved a year later by the substitution of PPh₃ ligands with PCy₃ to generate **1.9**.³⁵ Yet, the next milestone was not reached until the synthesis of the benzylidene bisphosphine complex Ru(=CHPh)(PCy₃)₂Cl₂ (**1.10**), which is commonly referred to as Grubbs 1st generation catalyst.³⁶ Complex **1.10** was discovered as an efficient precursor for a wide array of olefin metathesis applications, and was also found to be air and moisture stable. Thus, it has become a benchmark compound for ring closing metathesis (RCM) and ring-opening metathesis polymerization (ROMP) reactions. The performance of **1.10** was attributed to the balance of its bulky, strong electron-donating PCy₃ ligands with its fast-initiating benzylidene moiety.³⁷

R = Ph (**1.8**)R = Cy (**1.9**)**1.10**R = ⁱPr (**1.11**)R = Cy (**1.12**)

During the time compound **1.10** was being developed, NHCs were gaining popularity. Thus, the timing was ideal for these phosphine alternative ligands to be experimented with established catalyst precursors like **1.10**. Herrmann and co-workers were the first to synthesize bis-NHC complexes of ruthenium (**1.11** – **1.12**), which were found to be very active, air-stable catalyst precursors.³⁸ However, their activities were not significantly improved from that of **1.10**. As researchers gained a better understanding of the olefin metathesis mechanism, which was originally proposed by Chauvin *et al.*,³⁹ it was realized that one of the ligands must dissociate from Ru to generate the active catalyst.⁴⁰ This model prompted the development of mixed phosphine-NHC Ru precursors as it has been recognized that NHCs are stronger σ -donors, bulkier, and much less labile than phosphine ligands.³⁰ During this development period, popular proligands such as IMes⁴¹ and SIMes⁴² were used to incorporate NHCs into the Ru-benzylidene system by the direct addition of one equivalent of the aforementioned NHCs to **1.10** displacing one unit of PCy₃ to yield (L_{NHC})Ru(=CHPh)(PCy₃)Cl₂ (L_{NHC} = IMes (**1.13**)^{43, 44}, SIMes (**1.14**)⁴⁵) (eq 1.2).

**1.10**

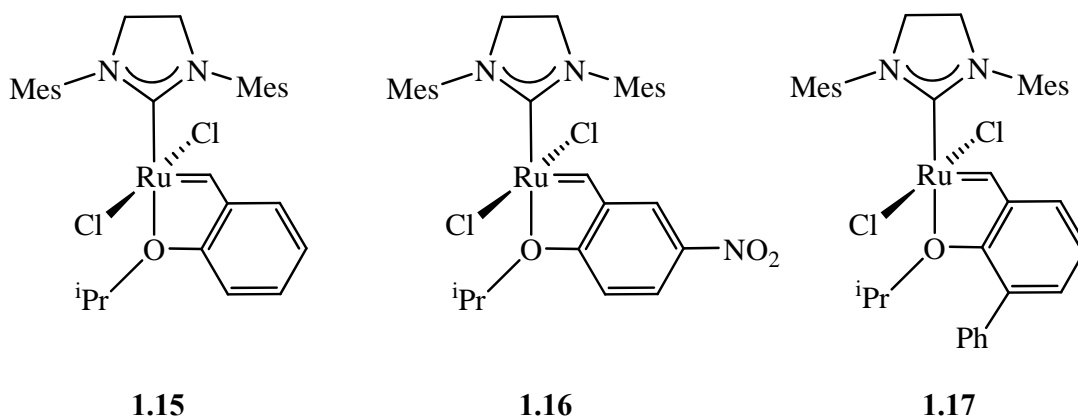
IMes

SIMes

1.13**1.14**

Complex **1.13** was found to be less active for RCM of diethyl diallylmalonate at room temperature. However, at slightly elevated temperatures (40 °C), **1.13** overtakes **1.10** in terms of activity, substrate yield and substrate breadth.⁴³ The increased performance as well as improved thermal stability are clearly attributed to the advantages associated with NHC ligands compared to their phosphine counterparts.⁴⁴ Although **1.13** demonstrated an improvement over **1.10**, its achievement has been largely overshadowed by the improved performance of **1.14** for RCM and ROMP reactions. Complex **1.14**, commonly referred to as Grubbs 2nd generation catalyst, epitomizes how incorporating NHCs into catalysts can transform the activity of systems that were previously dominated by phosphine ligands. The rationale for the improvement in activity of **1.14** relative to **1.13** points to an electronic effect as SIMes is a stronger donor than IMes, as sterically the difference between them is negligible. Precursor **1.14** has expanded the field of substrates available for RCM and ROMP transformations, as well as demonstrated exceptional activities even at very low catalyst loadings.^{45, 46} While **1.14** is not better than its Ru-PR₃ analogues for every substrate, it is recognized to be superior for the majority of the olefin metathesis reactions available for the synthesis of organic compounds. As such, both **1.10** and **1.14** are now commercially available and are used in synthetic laboratories worldwide.

Despite the popularity of complexes **1.10** and **1.14**, research has progressed in search of even more active Ru catalysts for olefin metathesis. The understanding of how these Ru catalysts operate has prompted modifications of the dissociating component of **1.14**. The intent was to produce a dissociating unit that did not have a strong propensity to re-associate with the active Ru catalyst, thereby maintaining a larger percentage of the active species in the catalytic cycle. This effect has been shown to be true when the dissociating PCy₃ of **1.14** is replaced by a less basic phosphine such as PPh₃.⁴⁷ Other examples of Ru catalyst precursors with increased catalyst longevity have been synthesized with the most notable being the Grubbs-Hoveyda catalyst **1.15**.⁴⁸ Since its inception, several other derivatives of Grubbs-Hoveyda system (**1.16**⁴⁹ – **1.17**⁵⁰) have been prepared, all of which have demonstrated exceptional olefin metathesis activity.



1.3.2 Palladium-NHC Complexes for Cross-Coupling Reactions

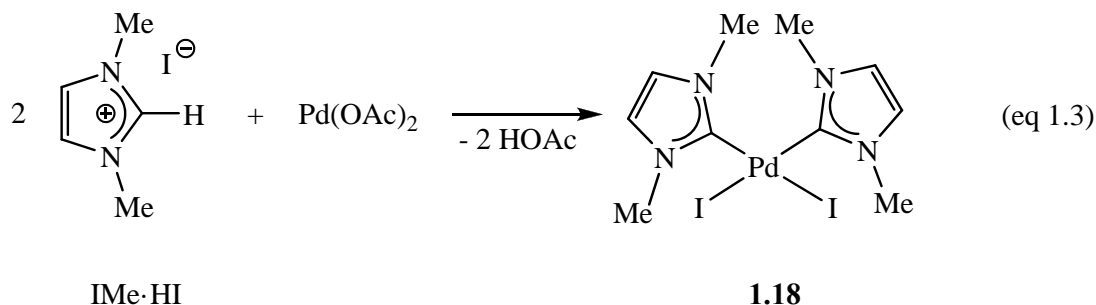
While the tale of Pd-NHC complexes for cross-coupling reactions is less elegant than that of Ru-NHC olefin metathesis systems, their influence on synthetic chemistry is no less profound. Since simple commercially available Pd systems, such as Pd(PPh₃)₄, are inherently effective cross-coupling precursors, a wide variety of active Pd derivatives have been developed.⁵¹ However, despite the assortment of Pd precursors available, the majority of the complexes incorporate tertiary phosphine ligands.⁵²

Since the discovery of NHCs, the realm of cross-coupling reactions has been overhauled by a new breed of highly active Pd-NHC catalyst precursors, especially for applications such as the Suzuki-Miyaura and Heck reactions.⁵³ The strong electron-donating ability of NHCs enhances the catalysts' ability to couple substrates that were previously unreactive with phosphine-based systems. Moreover, the size of the NHC ligands encourages rapid reductive elimination of the coupled products.⁵⁴ These features, in conjunction with improved thermal stability and oxidation resistance, make Pd-NHC catalysts very attractive.

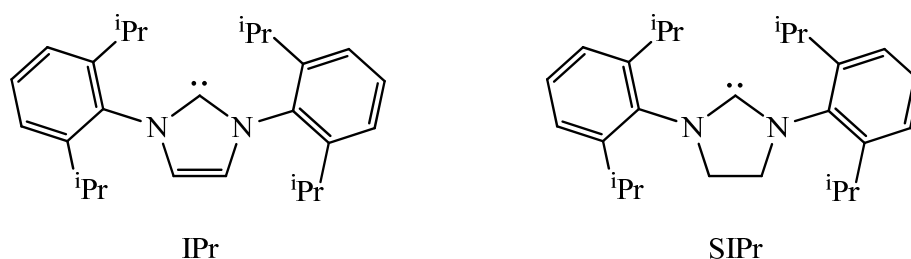
Although the synthesis of Pd(0)-NHC complexes would be ideal for catalysis as the compounds would already be primed for oxidative addition, there are surprisingly few examples of Pd(0)-NHC complexes isolated.⁵⁵ Pd(II)-NHC precursors are much more common as they are easy to handle and have good overall performance in cross-coupling reactions.

The first Pd(II)-NHC cross-coupling precursors were synthesized by Herrmann and co-workers in 1995.⁵⁶ The preparation of the Pd-NHC precursors was straightforward as the addition of an imidazolium salt ligand precursor to Pd(OAc)₂ yielded the desired Pd-NHC complex. This synthetic strategy was used for the preparation of Pd(IME)₂I₂ (IME = 1,3-dimethylimidazol-2-ylidene) (**1.18**). The synthesis was convenient as deprotonation of the imidazolium ligand precursor was not required since the acetate group on Pd acted as an internal base to drive the reaction. Complex **1.18** exhibited only moderate activity when used for the Heck reaction, but did show good thermal and hydrolytic stability. However, when IME·HI was deprotonated *in situ* with NaOAc and combined with a 0.5 equivalents of Pd₂(dba)₃, the Heck reactions that were previously performed with mediocre results were dramatically improved.⁵⁶ It was determined that the addition of the free IME to a Pd(0) complex to form the corresponding Pd(0)-IME species *in situ* was a way to bypass the induction period that **1.18** had to overcome before entering the catalytic cycle. Thus, the resultant Pd(0)-IME catalyst formed in solution was

immediately active and had greatly improved catalytic activity. This technique became very popular, which prompted nearly all Pd-NHC catalysts for cross-coupling applications to follow a similar protocol.⁵⁵



Further development of Pd-NHC systems showed that incorporating NHC ligands with bulky *ortho*-substituents, such as IPr (1,3-bis(2,6-diisopropylphenyl)imidazol-2-ylidene)⁵⁷ and SIPr (1,3-bis(2,6-diisopropylphenyl)-4,5-dihydroimidazol-2-ylidene),⁵⁸ yields superior activity. Furthermore, these Pd-NHC precursors had the broadest substrate range for various cross-coupling applications such as the Heck, Suzuki-Miyaura, Stille, Kumada and Buchwald-Hartwig reactions.^{54, 55} Thus, a variety of these bulky Pd-NHC precursors are now commercially available and used routinely for cross-coupling synthesis.



1.3.3 Rhodium- and Iridium-NHC Complexes for Hydrogenation and Transfer

Hydrogenation

It has been shown that NHCs are outstanding auxiliary ligands in catalytic systems for olefin metathesis and cross-coupling reactions. However, while NHCs continue to be effective

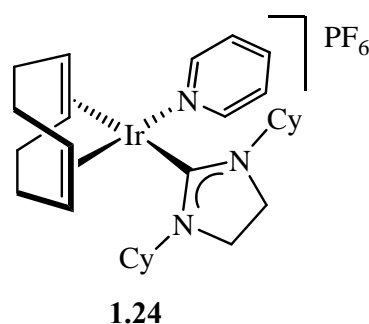
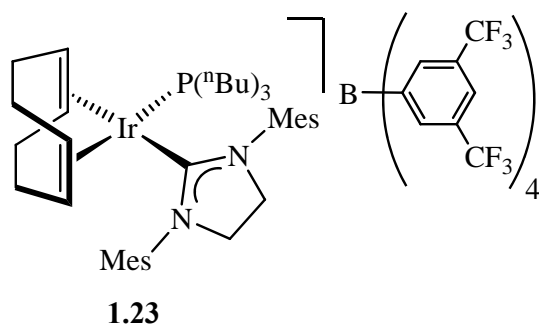
ancillary ligands for olefin hydrogenations they have not impacted the field with nearly the vigour as described in the previous sections.

Since the development of effective hydrogenation catalyst precursors such as Wilkinson's catalyst, $\text{Rh}(\text{PPh}_3)_3\text{Cl}$ (**1.19**),⁵⁹ and Crabtree's catalyst, $[\text{Ir}(\text{COD})(\text{py})\text{PCy}_3]\text{PF}_6$ (**1.20**),⁶⁰ it has been difficult to exceed the performance standards set by these systems. Simple replacement of a phosphine ligand with an NHC has only been shown to be competitive with its phosphine analogue, but not superior to it in terms of activity at room temperature conditions. This was found when $\text{Rh}(\text{PPh}_3)_2(\text{IMes})\text{Cl}$ (**1.21**) and $[\text{Ir}(\text{COD})(\text{py})(\text{SIMes})]\text{PF}_6$ (**1.22**) were synthesized and compared to benchmarks **1.19** and **1.20**, respectively, for the hydrogenation of olefins with 1 atm of H_2 pressure and 1 mol % catalyst loading.^{61, 62} Although the result is uninspiring, the precursors displayed improved thermal stability, which could also have been partially responsible for their average performance.^{61, 63} When the reactions are performed at slightly elevated temperatures (50 °C) and H_2 pressures (60 psi), the performance of **1.22** surpasses that of **1.20** as the latter complex is known to be thermally unstable.⁶² It has also been demonstrated that performance enhancements such as employing a phosphine sponge (CuCl) to aid catalyst initiation augments the activity of **1.21** in olefin hydrogenation reactions to a level that eclipses that of **1.19**, which has shown to be less sensitive to the additive.^{63, 64}



Despite NHCs often being described as phosphine alternatives, they can also serve as a constructive partner in catalytic systems as shown by Grubbs 2nd generation precursor.

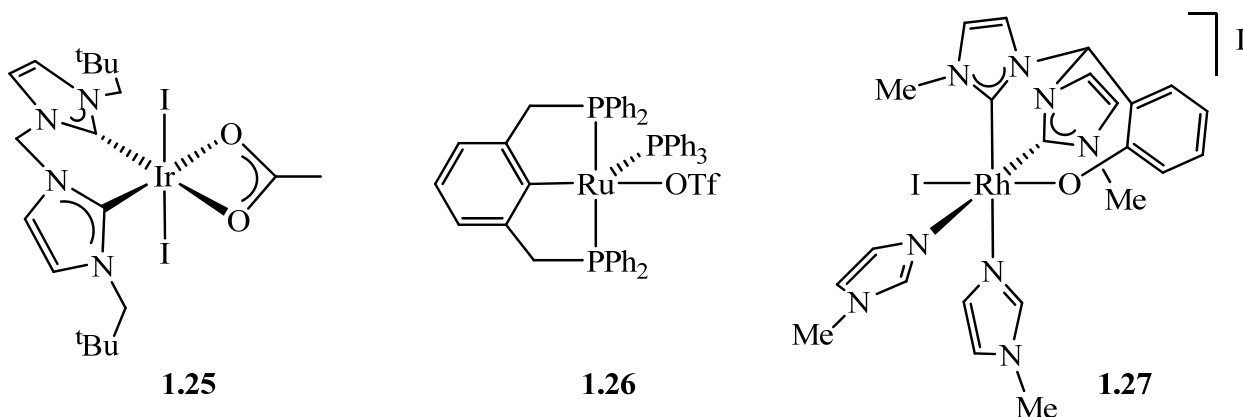
Modifying Crabtree's catalyst to an NHC-Ir(PR₃) motif instead of an NHC-Ir(py) arrangement improves catalytic activity at room temperature.⁶⁵ It has been shown that there is variation in catalyst performance associated with the steric bulk of the NHC ligand. Bulkier NHCs, such as IMes, have shown to be superior ancillary ligands for the hydrogenation of simple unhindered substrates when compared to smaller NHCs such as IMe. However, the reverse is true when more substituted olefins are the target substrates.⁶⁵ NHC-containing Crabtree derivatives can be refined further to yield the highly active [Ir(COD)(SIMes)P(ⁿBu)₃]BARF (BARF = tetrakis[3,5-bis(trifluoromethyl)phenyl]borate) (**1.23**) precursor that has improved catalyst longevity due to the incorporation of the stronger electron-donating NHC ligand and a non-coordinating counterion.⁶⁶



In addition to being active hydrogenation catalysts via an H₂ feedstock, cationic Ir-NHC complexes have also been found to be efficient transfer hydrogenation catalysts, which use a hydrogen transfer agent such as 2-propanol as the hydrogen source. Monodentate NHC derivatives of Crabtree's catalyst, such as [Ir(ICy)(COD)(py)]PF₆ (ICy = 1,3-bis(cyclohexyl)imidazol-2-ylidene) (**1.24**), have shown to be very active for the transfer hydrogenation of carbonyl-functionalized substrates, but less effective with simple olefins.⁶⁷

Despite the majority of highly active M-NHC (M = Rh, Ir) catalyst systems that are based on monodentate NHC ligands such as IMes or SIPr, recently developed chelating and pincer NHC ligands have been very effective auxiliary ligands of Rh and Ir precursors for transfer hydrogenation applications.^{68, 69} Chelating and pincer NHC ligands have the benefit of

generating more stable metal complexes and offer tunable properties such as steric bulk, bite angle as well as chirality.⁶⁹ The Ir(III)-pincer complex (**1.25**)⁷⁰ exhibits exceptional activity that rivals a Ru-phosphine system (**1.26**)⁷¹ that is regarded as one of the most active ketone transfer hydrogenation precursors known to date. In addition, **1.25** is air and moisture stable while being soluble in a variety of solvents, which makes it very easy to handle.⁷⁰ The Rh analogue of **1.25** has also been prepared and demonstrates very good activity for the transfer hydrogenation of ketones, but is less efficient than its Ir congener.⁷² However, a Rh complex (**1.27**) that incorporates a tripodal ligand with both a pincer NHC and a phenoxy tether has exhibited excellent activity for hydrogen-transfer reactions of ketones.⁷³

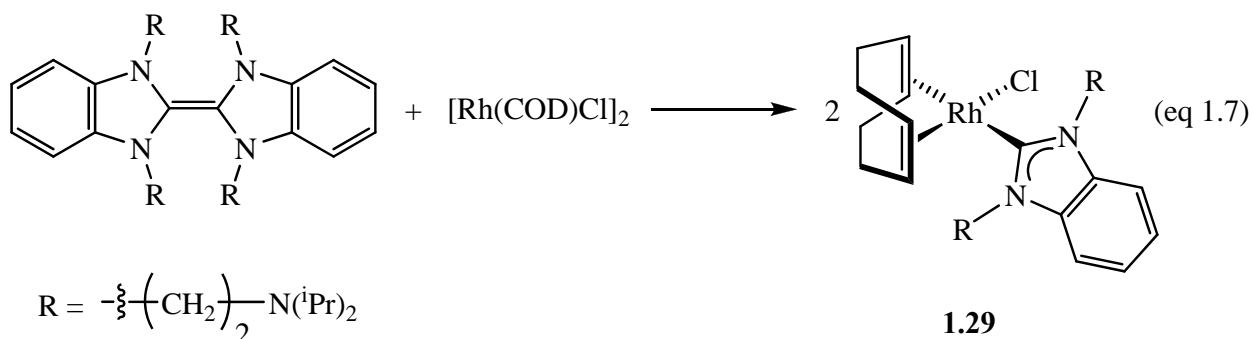
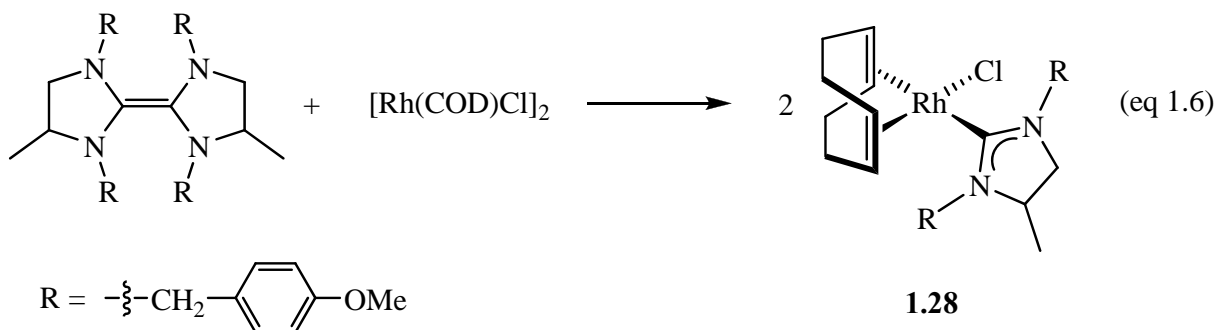


1.3.4 Rhodium- and Iridium-NHC Complexes for Hydrosilylation

Of the vast number of Rh-NHC catalyzed reactions that have been reported, hydrosilylation is one of the most actively researched.⁷⁴ Substrates such as ketones, imines, alkenes and alkynes are frequently probed. However, transformations of ketone and alkyne substrates are the most popular. Similar to transfer hydrogenation reactions, both monodentate and multidentate NHC ligands have produced good results in Rh-catalyzed hydrosilylation applications. However, while Ir was found to be more effective for hydrogen transfer reactions of ketones, they are generally less active than their Rh analogues as hydrosilylation catalysts.^{69, 75} Nonetheless, comparisons of hydrosilylation precursors should be made with the caveat that they

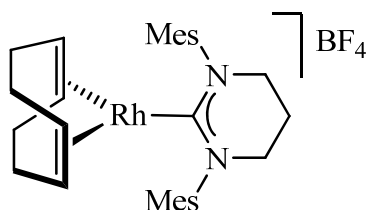
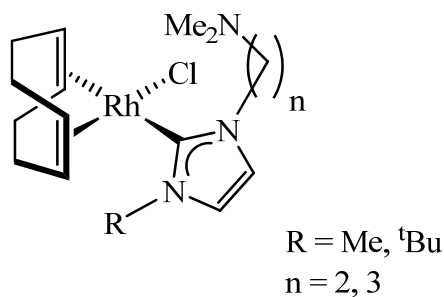
are very sensitive to solvent and experimental conditions, which affects catalyst activity and substrate selectivity.⁷⁶

Despite the growing interest in developing Rh-NHC precursors for hydrosilylation reactions, few examples have been reported that demonstrate significantly improved catalytic ability compared to Rh-phosphine complexes such as Wilkinson's catalyst (**1.19**). Nevertheless, monosubstituted NHC-derivatives of Wilkinson's catalyst, as well as NHC-Rh(COD)Cl variations, have both been found to be effective for the hydrosilylation of ketones.^{31, 77} Recently, more emphasis has been put on the development of effective monodentate Rh-NHC precursors that are based on the NHC-Rh(COD)Cl motif. Complexes **1.28** (eq 1.6) and **1.29** (eq 1.7) illustrate two NHC ligands that have been incorporated into that model where both compounds demonstrate good activity for the hydrosilylation of acetophenone with triethylsilane.⁷⁸



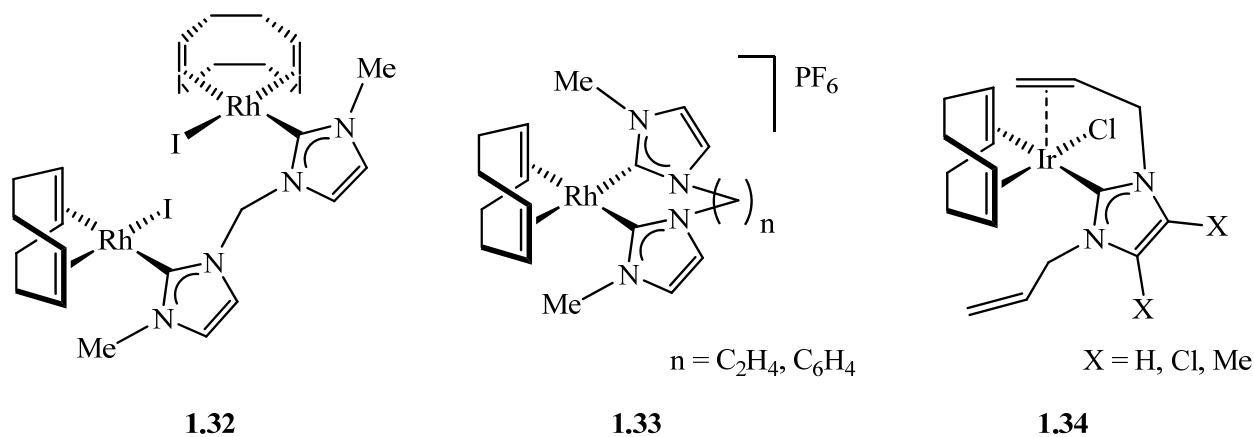
While most NHCs feature a five-membered heterocyclic ring, other unique NHCs have also proven to be productive for hydrosilylation catalysis. Complex **1.30** incorporates a six-

membered heterocyclic carbene, 1,3-dimesityl-3,4,5,6-tetrahydropyrimidin-2-ylidene, into a cationic Rh complex, which was found to have good activity for the hydrosilylation of various aryl ketones.⁷⁹ Moreover, **1.30** was able to achieve high selectivity for the addition of silanes to terminal alkynes.

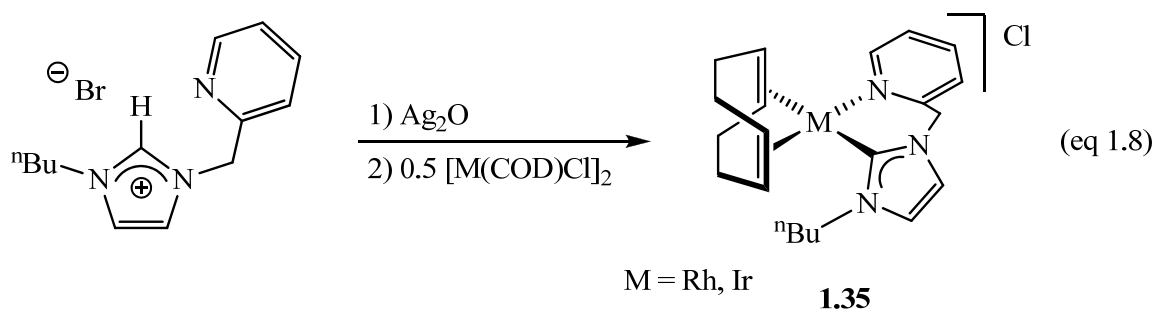
**1.30****1.31**

Hemilabile functionalized NHCs, such as the amino-tethered NHC ligand of **1.31**, have also demonstrated good selectivity and activity for the hydrogenation of various terminal alkynes.⁸⁰ It has been suggested that the hemilabile NHC ligand design may be advantageous for enhancing catalyst performance as NHCs have empirically been found to be effective as auxiliary ligands when combined with other ligands of lower electron density.³¹

The development of hydrosilylation precursors has also prompted the use of multidentate NHC ligands as an attractive alternative to monodentate NHC systems for hydrosilylation of terminal alkynes.^{68, 69, 81} Due to their chelating ability, they are able to adopt various coordination modes about the metal center. For example, bidentate NHCs can be used as a bridging component between two Rh(COD)I units to yield the bimetallic complex, **1.32**.⁸² Alternatively, they can be deployed more traditionally and chelated to a cationic Rh center to yield **1.33**.^{75, 83}



Despite iridium-based catalysts often lacking the activity of their rhodium counterparts, they can exhibit interesting properties. A unique alkenyl-functionalized NHC-Ir system (**1.34**) was developed by Mata *et al.* and displayed excellent selectivity for various alkyne substrates at low catalyst loadings. Complex **1.34** was also distinctive in its ability to vary the coordination mode of its alkenyl tethers to change its electronics and geometry.⁸⁴ Peris and co-workers designed a versatile pyridine-functionalized NHC ligand, which they were able to coordinate to M(COD) (M = Rh, Ir) in the absence of a base to generate **1.35** (eq 1.8). The unusual preparation of the M-NHC precursor yielded a cationic precursor that exhibited good activities for the hydrosilylation of terminal alkynes. However, while both Rh and Ir species were found to be active, the Ir analogue excelled at low catalyst loadings.⁸⁵



Although it is not yet proven that multidentate ligands have a performance edge over monodentate NHCs for hydrosilylation transformations, it has been demonstrated that the

hemilabile and chelating NHC architecture can be advantageous with their coordinative flexibility and tunable mixed-donor scaffold. These features have made multidentate NHCs suitable ancillary ligands for Rh and Ir hydrosilylation precursors as they exhibit very good activity and selectivity for alkyne substrates.

1.4 Scope of the Thesis

This introduction has highlighted the origin of carbene ligand synthesis and demonstrated how NHCs have progressed into an extremely useful class of ligands for catalytic applications. The bulk of the research has been on the development of monodentate NHC precursors as they have shown to be attractive alternatives to phosphine ligands. However, while there have been several reviews that outline the usefulness of chelating and pincer NHCs, the field is still relatively underexplored when compared to monodentate NHC ligands.^{68, 69, 81, 86} More specifically, the employment of mixed-donor and hemilabile NHC ligand systems is often overlooked as they have not yet made an impact on catalysis as observed with monodentate and pincer NHC ligand types. It is the intent of this thesis to explore the capabilities and expand the scope of mixed-donor hemilabile NHC-based complexes.

Chapter 2 describes the synthetic strategy, preparation and characterization of an amino-functionalized NHC proligand. The synthesis of Rh and Ir-NHC complexes is shown to yield an array of precursors that demonstrate the hemilabile character of the N-functionalized tether. The precursors are then tested for their ability to perform hydrogenation, transfer hydrogenation and hydrosilylation of a variety of substrates.

The work in Chapter 3 entails incorporating the hemilabile aminocarbene ligand into the Grubbs catalyst system and explores the effects of the tethering amino group on ring closing metathesis (RCM) and ring opening metathesis polymerization (ROMP) reactions of olefins.

Ligand dissociation kinetics are investigated and a correlation to its catalytic activity is assessed. Various derivatives of the Ru-NHC complex are also prepared and tested for their olefin metathesis activity.

Chapter 4 outlines the synthesis and characterization of several novel hemilabile mixed-donor NHC prolignands. The chemical properties of a primary aminocarbene and a phosphinocarbene are explored. Comparisons to the aminocarbene architecture developed in Chapter 2 are made and their specific properties are discussed. The reactivity of these analogues is also examined with Rh, Ir and Ru compounds. In addition, transmetallation agents are also prepared and used as an alternative synthetic strategy to synthesize late metal complexes.

The final chapter gives a synopsis of the work in this thesis and provides an analytical discussion of the accumulated results. Furthermore, several avenues of future research are explored and their potential impact in the field of NHC chemistry is discussed.

1.5 References

1. Doering, W. v. E.; Hoffmann, A. K., *J. Am. Chem. Soc.* **1954**, 76, 6162.
2. Fischer, E. O.; Maasbol, A., *Angew. Chem. Int. Ed.* **1964**, 3, 580.
3. Arduengo, A. J.; Bertrand, G., *Chem. Rev.* **2009**, 109, 3209.
4. Wanzlick, H. W., *Angew. Chem. Int. Ed.* **1962**, 1, 75.
5. Denk, M. K.; Hatano, K.; Ma, M., *Tetrahedron Lett.* **1999**, 40, 2057.
6. Soleilhavoup, M.; Baceiredo, A.; Treutler, O.; Ahlrichs, R.; Nieger, M.; Bertrand, G., *J. Am. Chem. Soc.* **1992**, 114, 10959.; Dixon, D. A.; Dobbs, K. D.; Arduengo, A. J.; Bertrand, G., *J. Am. Chem. Soc.* **1991**, 113, 8782.; Romer, B.; Gatev, G. G.; Zhong, M.; Brauman, J. I., *J. Am. Chem. Soc.* **1998**, 120, 2919.; Kato, T.; Gornitzka, H.; Baceiredo, A.; Savin, A.; Bertrand, G., *J. Am. Chem. Soc.* **2000**, 122, 998.
7. Bourissou, D.; Guerret, O.; Gabbal, F. P.; Bertrand, G., *Chem. Rev.* **2000**, 100, 39.
8. Arduengo, A. J.; Harlow, R. L.; Kline, M., *J. Am. Chem. Soc.* **1991**, 113, 361.
9. Pauling, L., *J. Chem. Soc., Chem. Commun.* **1980**, 688.
10. Diez-Gonzalez, S.; Nolan, S. P., *Coord. Chem. Rev.* **2007**, 251, 874.
11. Bundhun, A.; Ramasami, P.; Schaefer III, H. F., *J. Phys. Chem. A* **2009**, 113, 8080.; Apeloig, Y.; Pauncz, R.; Karni, M.; West, R.; Steiner, W.; Chapman, D., *Organometallics* **2003**, 22, 3250.
12. Mckeller, A. R. W.; Bunker, P. R.; Sears, T. J.; Evenson, K. M.; Saykally, R. J.; langhoff, S. R., *J. Chem. Phys.* **1983**.
13. Hoffmann, R., *J. Am. Chem. Soc.* **1968**, 90, 1475.
14. Heinemann, C.; Thiel, W., *Chem. Phys. Lett.* **1994**, 217, 11.
15. Arduengo, A. J.; Davidson, F.; Dias, H. V. R.; Goerlich, J. R.; Khasnis, D.; Marshall, W. J.; Prakasha, T. K., *J. Am. Chem. Soc.* **1997**, 119, 12742.

16. Heinemann, C.; Muller, T.; Apeloig, Y.; Schwartz, H., *J. Am. Chem. Soc.* **1996**, *118*, 2023.; Boehme, C.; Frenking, G., *J. Am. Chem. Soc.* **1996**, *118*, 2039.
17. Hiller, A. C.; Sommer, W. J.; Young, B. S.; Peterson, J. L.; Cavallo, L.; Nolan, S. P., *Organometallics* **2003**, *22*, 4322.
18. Fantasia, S.; Peterson, J. L.; Jacobson, H.; Cavallo, L.; Nolan, S. P., *Organometallics* **2007**, *26*, 5880.; Kelly III, R. A.; Clavier, H.; Guidice, S.; Scott, N. M.; Stevens, E. D.; Bordner, J.; Smardjiev, I.; Hoff, C. D.; Cavallo, L.; Nolan, S. P., *Organometallics* **2008**, *27*, 202.
19. Zimmerman, H. E.; Paskovich, D. H., *J. Am. Chem. Soc.* **1964**, *86*, 2149.
20. Tomioka, H.; Watanabe, T.; Hirai, K.; Furukawa, K.; Takui, T.; Itoh, K., *J. Am. Chem. Soc.* **1995**, *117*, 6376.
21. Iwamoto, E.; Hirai, K.; Tomioka, H., *J. Am. Chem. Soc.* **2003**, *125*, 14664.
22. Tomioka, H., *Acc. Chem. Res.* **1997**, *30*, 315.
23. Taylor, T. E.; Hall, M. B., *J. Am. Chem. Soc.* **1984**, *106*, 1576.
24. Schrock, R. R., *J. Am. Chem. Soc.* **1974**, *96*, 6796.
25. de Fremont, P.; Marion, N.; Nolan, S. P., *Coord. Chem. Rev.* **2009**, *253*, 862.
26. Green, J. C.; Scurr, R. G.; Arnold, P. L.; Cloke, F. G. N., *Chem. Commun.* **1997**, 1963.; Penka, E. F.; Schlapfer, C. W.; Atanasov, M.; Albrecht, M.; Daul, C., *J. Organomet. Chem.* **2007**, *692*, 5709.
27. Arduengo, A. J.; Dias, H. V. R.; Calabrese, J. C.; Davidson, F., *J. Am. Chem. Soc.* **1992**, *114*, 9724.; Li, X.-W.; Su, J.; Robinson, G. H., *Chem. Commun.* **1996**, 2683.; Nakai, H.; Tang, Y.; Gantzel, P.; Meyer, K., *Chem. Commun.* **2003**, *24*.; Boesveld, W. M.; Gehrhus, B.; Hitchcock, P. B.; Lappert, M. F.; Schleyer, P. v. R., *Chem. Commun.* **1999**, 755.
28. Boehme, C.; Frenking, G., *Organometallics* **1998**, *17*, 5801.

29. Jacobson, H.; Correa, A.; Poater, A.; Costabile, C.; Cavallo, L., *Coord. Chem. Rev.* **2009**, 253, 687.; Getty, K.; Delgado-Jaime, M. U.; Kennepohl, P., *J. Am. Chem. Soc.* **2007**, 129, 15774
30. Lee, M.-T.; Hu, C.-H., *Organometallics* **2004**, 23, 976.; Huang, J.; Schanz, H.-J.; Stevens, E. D.; Nolan, S. P., *Organometallics* **1999**, 18, 5375.
31. Herrmann, W. A.; Kocher, C., *Angew. Chem. Int. Ed.* **1997**, 36, 2162.
32. Regitz, M., *Angew. Chem. Int. Ed.* **1996**, 35, 725.; Jafarpour, L.; Nolan, S. P., *Adv. Organomet. Chem.* **2000**, 46, 181.
33. Herrmann, W. A., *Angew. Chem. Int. Ed.* **2002**, 41, 1290.
34. Nguyen, S. T.; Johnson, L. K.; Grubbs, R. H.; Ziller, J. W., *J. Am. Chem. Soc.* **1992**, 114, 3974.
35. Nguyen, S. T.; Grubbs, R. H.; Ziller, J. W., *J. Am. Chem. Soc.* **1993**, 115, 9858.
36. Schwab, P.; Grubbs, R. H.; Ziller, J. W., *J. Am. Chem. Soc.* **1996**, 118, 100.
37. Trnka, T. M.; Grubbs, R. H., *Acc. Chem. Res.* **2001**, 34, 18.
38. Weskamp, T.; Schattenmann, W. C.; Spiegler, M.; Herrmann, W. A., *Angew. Chem., Int. Ed.* **1998**, 37, 2490.
39. Herisson, J.-L.; Chauvin, Y., *Makromol. Chem.* **1971**, 141, 161 ; Katz, T. J.; McGinnis, J., *J. Am. Chem. Soc.* **1977**, 99, 1903.
40. Dias, E. L.; Nguyen, S. T.; Grubbs, R. H., *J. Am. Chem. Soc.* **1997**, 119, 3887.
41. Arduengo, A. J.; Dias, H. V. R.; Harlow, R. L.; Kline, M., *J. Am. Chem. Soc.* **1992**, 114, 5530.
42. Arduengo, A. J.; Goerlich, J. R.; Marshall, W. J., *J. Am. Chem. Soc.* **1995**, 117, 11027.
43. Scholl, M.; Trnka, T. M.; Morgan, J. P.; Grubbs, R. H., *Tetrahedron Lett.* **1999**, 40, 2247.

44. Huang, J.; Stevens, E. D.; Nolan, S. P.; Petersen, J. L., *J. Am. Chem. Soc.* **1999**, *121*, 2674.
45. Scholl, M.; Ding, S.; Lee, C. W.; Grubbs, R. H., *Org. Lett.* **1999**, *1*, 953.
46. Bielawski, C. W.; Grubbs, R. H., *Angew. Chem., Int. Ed.* **2000**, *39*, 2903.; Chatterjee, A. K.; Grubbs, R. H., *Org. Lett.* **1999**, *1*, 1751.; Chatterjee, A. K.; Morgan, J. P.; Scholl, M.; Grubbs, R. H., *J. Am. Chem. Soc.* **2000**, *122*, 3783.; Stragies, R.; Voigtmann, U.; Blechert, S., *Tetrahedron Lett.* **2000**, *41*, 5465; Smulik, J. A.; Diver, S. T., *Org. Lett.* **2000**, *2*, 2271.
47. Sanford, M. S.; Love, J. A.; Grubbs, R. H., *J. Am. Chem. Soc.* **2001**, *123*, 6543.
48. Garber, S. B.; Kingsbury, J. S.; Gray, B. L.; Hoveyda, A. H., *J. Am. Chem. Soc.* **2000**, *122*, 8168.; Gressler, S.; Randal, S.; Blechert, S., *Tetrahedron Lett.* **2000**, *41*, 9973.
49. Grela, K.; Harutyunyan, S.; Michrowska, A., *Angew. Chem. Int. Ed.* **2002**, *41*, 4038.
50. Wakamatsu, H.; Blechert, S., *Angew. Chem. Int. Ed.* **2002**, *41*, 2403.
51. Miyaura, N.; Suzuki, A., *Chem. Rev.* **1995**, *95*, 2457 ; Yamamura, M.; Moritani, I.; Murahashi, S.-I., *J. Organomet. Chem.* **1975**, *91*, C39.; Sekiya, A.; Ishikawa, N., *J. Organomet. Chem.* **1976**, *118*, 349.; Stille, J. K., *Angew. Chem. Int. Ed.* **1986**, *25*, 508 ; Wolfe, J., P.; Wagaw, S.; Marcoux, J.-F.; Buchwald, S. L., *Acc. Chem. Res.* **1998**, *31*, 805.; Dieck, H. A.; Heck, R. F., *J. Am. Chem. Soc.* **1974**, *96*, 1133.
52. Herrmann, W. A.; Ofele, K.; v. Preysing, D.; Schneider, S. K., *J. Organomet. Chem.* **2003**, *687*, 229.
53. Marion, N.; Nolan, S. P., *Acc. Chem. Res.* **2008**, *41*, 1440.
54. Kantchev, E. A. B.; O'Brien, C. J.; Organ, M. G., *Angew. Chem. Int. Ed.* **2007**, *46*, 2768.
55. Viciu, M.; Nolan, S. P., *Top. Organomet. Chem.* **2005**, *14*, 241.

56. Herrmann, W. A.; Elison, M.; Fischer, J.; Kocher, C.; Artus, G. R. J., *Angew. Chem. Int. Ed.* **1995**, *34*, 2371.
57. Huang, J.; Nolan, S. P., *J. Am. Chem. Soc.* **1999**, *121*, 9889.
58. Arduengo, A. J. US patent **5 077 414**. 1991.
59. Osborn, J. A.; Jardine, F. H.; Wilkinson, G., *J. Chem. Soc. A* **1966**, 1711.
60. Crabtree, R. H.; Morris, G. E., *J. Organomet. Chem.* **1977**, *135*, 395.
61. Grasa, G. A.; Moore, Z.; Martin, K. F.; Stevens, E. D.; Nolan, S. P.; Paquet, V.; Lebel, H., *J. Organomet. Chem.* **2002**, *658*, 126.
62. Lee, H. M.; Jian, T.; Stevens, E. D.; Nolan, S. P., *Organometallics* **2001**, *20*, 1255.
63. Allen, D. P.; Crudden, C. M.; Calhoun, L. A.; Wang, R., *J. Organomet. Chem.* **2004**, *689*, 3203.
64. Allen, D. P.; Crudden, C. M.; Calhoun, L. A.; Wang, R.; Decken, A., *J. Organomet. Chem.* **2005**, *690*, 5736.
65. Vazquez-Serrano, L. D.; Owens, B. T.; Buriak, J. M., *Chem. Commun.* **2002**, 2518.
66. Vazquez-Serrano, L. D.; Owens, B. T.; Buriak, J. M., *Inorg. Chim. Acta* **2006**, *359*, 2786.
67. Hiller, A. C.; Lee, H. M.; Stevens, E. D.; Nolan, S. P., *Organometallics* **2001**, *20*, 4246.
68. Mata, J. A.; Poyatos, M.; Peris, E., *Coord. Chem. Rev.* **2007**, *251*, 841.
69. Corberan, R.; Mas-Marza, E.; Peris, E., *Eur. J. Inorg. Chem.* **2009**, *13*, 1700.
70. Albrecht, M.; Miecznikowski, J. R.; Samuel, A.; Faller, J. W.; Crabtree, R. H., *Organometallics* **2002**, *21*, 3596.
71. Dani, P.; Karlen, T.; Gossage, R. A.; Gladiali, S.; Van Koten, G., *Angew. Chem., Int. Ed.* **2000**, *39*, 743.
72. Albrecht, M.; Crabtree, R. H.; Mata, J.; Peris, E., *Chem. Commun.* **2002**, 32.
73. Mas-Marza, E.; Poyatos, M.; Sanau, M.; Peris, E., *Organometallics* **2004**, *23*, 323.

74. Diez-Gonzalez, S.; Marion, N.; Nolan, S. P., *Chem. Rev.* **2009**, *109*, 3612.
75. Viciano, M.; Mas-Marza, E.; Sanau, M.; Peris, E., *Organometallics* **2006**, *25*, 3063.
76. Takeuchi, R.; Nitta, S.; Watanabe, D., *J. Org. Chem.* **1995**, *60*, 3045 ; Takeuchi, R.; Tanouchi, N., *J. Chem. Soc. Perkin Trans. I* **1994**, 2909.
77. Hill, J. E.; Nile, T. A., *J. Organomet. Chem.* **1977**, *137*, 293.
78. Yigit, M.; Ozdemir, I.; Cetinkaya, B.; Cetinkaya, E., *J. Mol. Catal. A: Chem.* **2005**, *241*, 88.; Ozdemir, I.; Yigit, M.; Yigit, B.; Cetinkaya, B.; Cetinkaya, E., *J. Coord. Chem.* **2007**, *60*, 2377.
79. Imlinger, N.; Wurst, K.; Buchmeiser, M. R., *J. Organomet. Chem.* **2005**.
80. Jimenez, M. V.; Perez-Torrente, J. J.; Bartolome, M. I.; Gierz, V.; Lahoz, F. J.; Oro, L. A., *Organometallics* **2008**, *27*, 224.
81. Normand, A. T.; Cavell, K. J., *Eur. J. Inorg. Chem.* **2008**, *18*, 2781.
82. Mas-Marza, E.; Poyatos, M.; Sanau, M.; Peris, E., *Inorg. Chem.* **2004**, *43*, 2213.
83. Poyatos, M.; Mas-Marza, E.; Mata, J. A.; Sanau, M.; Peris, E., *Eur. J. Inorg. Chem.* **2003**, 1215.
84. Zanardi, A.; Peris, E.; Mata, J. A., *New J. Chem.* **2008**, *32*, 120.
85. Mas-Marza, E.; Sanau, M.; Peris, E., *Inorg. Chem.* **2005**, *44*, 9961.
86. Peris, E.; Crabtree, R. H., *Coord. Chem. Rev.* **2004**, *248*, 2239.

CHAPTER TWO

Amine-Tethered Complexes of N-Heterocyclic Carbene Complexes of Rhodium and Iridium

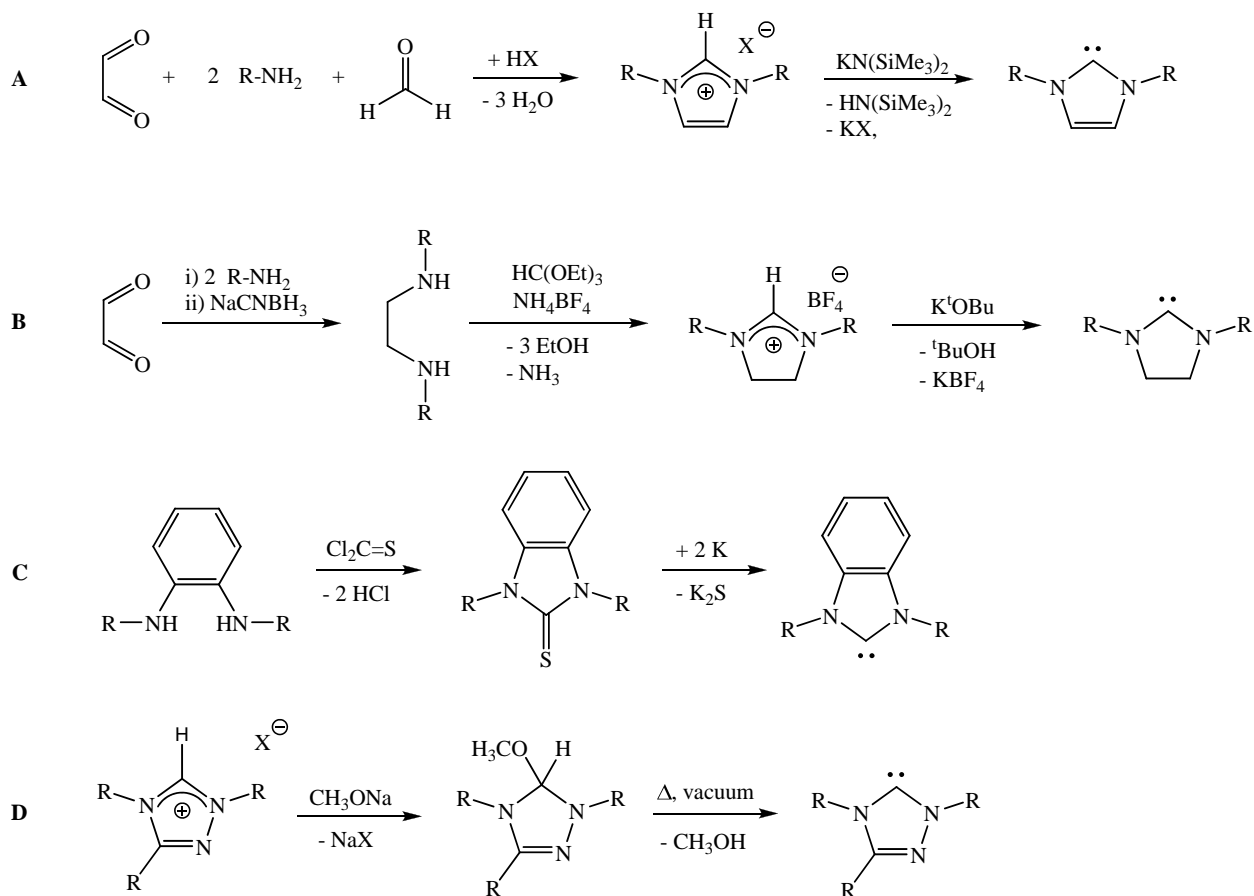
2.1 *Introduction*

In the previous chapter, the properties and benefits of carbenes in synthetic chemistry are broadly described. Comparisons were also made between the chemical characteristics of NHC and phosphine ligands. However, details on the synthetic strategies associated with the preparation of NHCs were not discussed. NHCs require either construction or elaboration of a heterocyclic ring involving nitrogen atoms, thus their syntheses are strategically quite different from those used to prepare phosphine ligands. For example, condensation processes are commonly employed in the assembly of imidazoles, which are used as a building block for heterocyclic precursors. In simple cases, imidazolium salts can be generated by reacting a commercially available monosubstituted imidazole with an alkyl halide. Scheme 2.1 demonstrates several methods by which NHCs can be synthesized.

A version of this chapter has been published.

Jong, H.; Patrick, B.O.; Fryzuk, M.D. (2008) Amine-Tethered N-Heterocyclic Carbene Complexes of Rhodium(I). *Can. J. Chem.* 86:803-810.

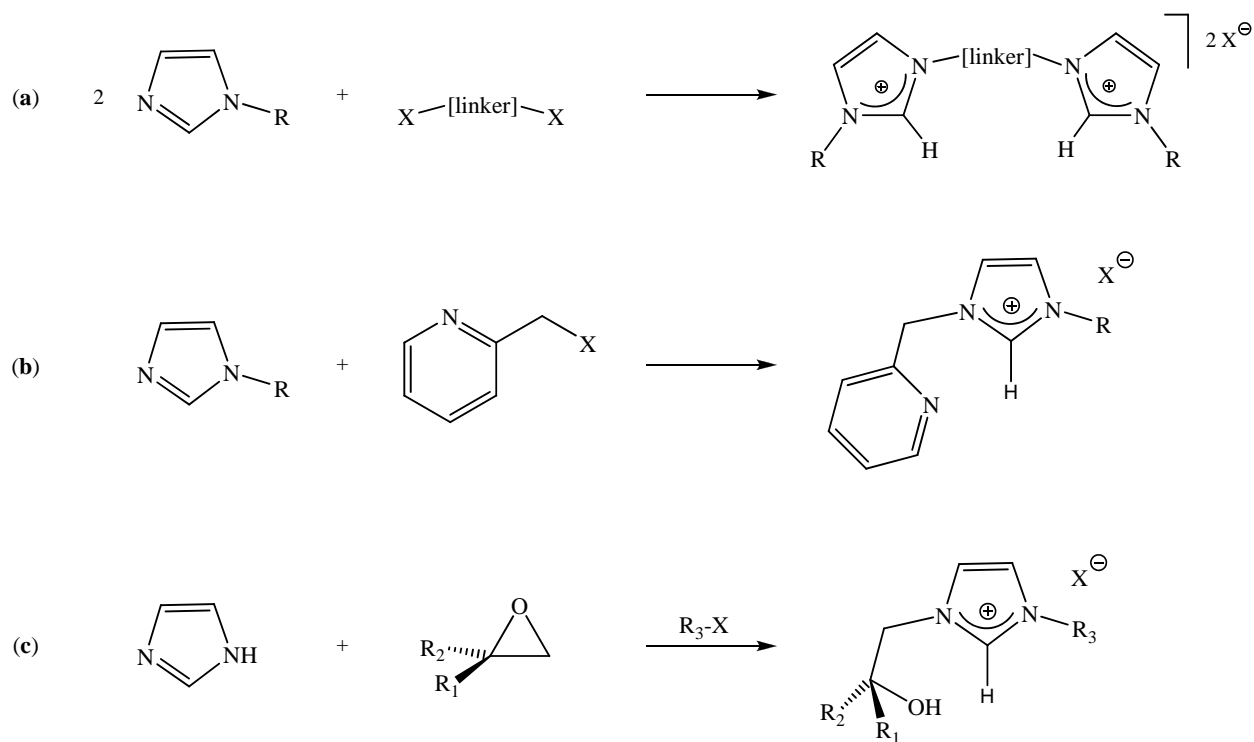
Scheme 2.1



In method **A**, the one-pot synthesis to generate the imidazolium salt is a convenient and efficient way to produce an air-stable starting material that requires only deprotonation with a strong base such as potassium hexamethyldisilazide ($\text{KN}(\text{SiMe}_3)_2$) to yield the free N-heterocyclic carbene.¹ The caveat, however, is that bulky R groups are typically necessary to prevent NHC dimerization as observed by Wanzlick.² To preserve the saturated backbone of the heterocycle, a step-wise approach must be taken as shown in **B**. The dihydroimidazolium salt can then be deprotonated in a similar fashion to **A**.³ The synthesis of the benzannulated NHC of **C** becomes slightly more complicated but the desulfurization of the cyclic thiourea derivative demonstrates the different paths available to produce NHCs.⁴ Vacuum thermolysis of triazoles in **D** is another interesting approach to generate more exotic NHC ligands.⁵

While the breadth of different monodentate NHC ligand-based complexes is wide, examples of metal complexes incorporating chelating NHC ligands are considerably more rare. Most common chelating NHC-metal complexes are the pincer-type ligands containing two NHC units employed to coordinate the metal centre, which has proven to be useful in a variety of catalytic applications such as hydrosilylation and cross-coupling reactions.⁶ NHC pincers can be constructed in a relatively straightforward manner by combining the substituted imidazole with a dihalo linker that is typically aliphatic or aromatic as shown by **(a)** in Scheme 2.2. Deprotonation of these bis-imidazolium species can typically be performed with weak bases (e.g. NaOAc, NEt₃, Cs₂CO₃) instead of stronger alternatives like KN(SiMe₃)₂ and NaH, which can also be used but tends to result in lower yields. The bidentate pincer ligands are also less stable than monodentate NHCs, in general, and have in certain cases been found to oxidatively add its centrally disposed C—H bond to a late metal.⁷ The method of combining a functionalized alkyl halide with a substituted imidazole was also applicable for **(b)** to produce a pyridine-linked imidazolium salt. The imidazolium salt from **(b)** has been found to be effective for direct addition to a basic metal center,⁸ or complexed to silver and used as a transmetallation agent.⁹ In **(c)**, a novel approach of ring-opening an epoxide followed by sequential addition of imidazole and an alkyl halide affords the protonated alcohol functionalized imidazolium proligand. Deprotonation is possible via addition of Ag₂O or 2 equivalents of lithium hexamethyldisilazide (LiN(SiMe₃)₂) to produce an alkoxy-NHC species in high yield useful for transmetallation applications.¹⁰

Scheme 2.2



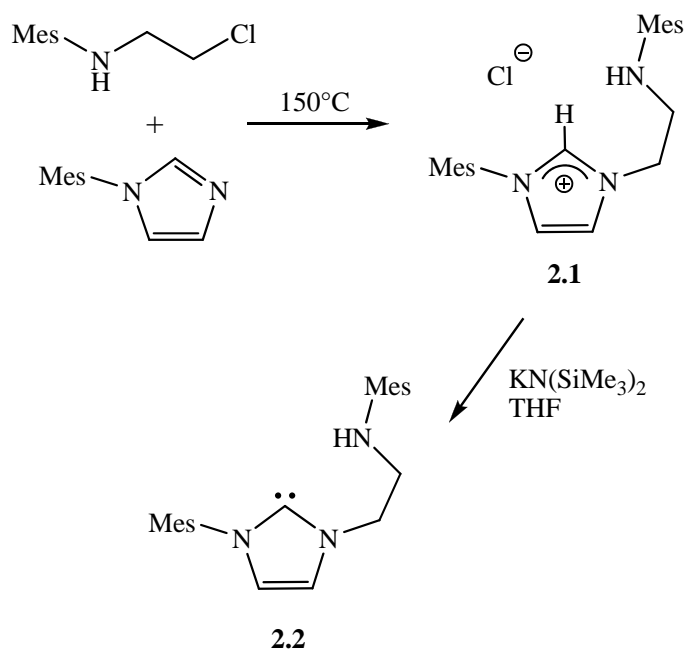
Despite rapid growth in research in the carbene arena, bidentate NHC ligands are still largely overlooked amongst the carbene community. This chapter will focus on the synthesis of a hemilabile mixed-donor NHC ligand, denoted $^{\text{Mes}}[\text{CNH}]$ and its applicability in coordination chemistry. The catalytic potential of $^{\text{Mes}}[\text{CNH}]$ with rhodium and iridium diene derivatives will also be discussed.

2.2 Synthesis and Characterization of the $^{\text{Mes}}[\text{CNH}]$ Ligand

Prior work performed within the Fryzuk group resulted in the preparation of a tridentate NHC ligand with flanking amino tethers by melting an imidazole with the appropriate 2-chloroethyl-N-arylamine.¹¹ A similar approach can be used to generate a bidentate analog in good yield; the reaction of neat mesitylimidazole with 2-chloroethyl-N-mesitylamine in a sealed vessel at 150 °C generates 1-mesityl-3-(2-(mesitylamino)ethyl)imidazolium chloride (**2.1**), which we denote as $^{\text{Mes}}[\text{HCNH}]\text{Cl}$. Deprotonation of **2.1** with $\text{KN}(\text{SiMe}_3)_2$ results in the

formation of the free carbene 1-mesityl-3-(2-(mesitylamino)ethyl)imidazol-2-ylidene (**2.2**), or $^{\text{Mes}}[\text{CNH}]$ (Scheme 2.3). A similar approach to generate tertiary amine side-arm donors has recently been reported.¹² Successful conversion to compound **2.2** can be clearly observed in the ^1H NMR spectrum as the iminium proton resonance at δ 10.7 of **2.1** disappears and a new ^{13}C NMR signal is observed at δ 215.6, due to the carbene carbon.¹³ Slowly evaporating a concentrated solution of **2.2** in toluene yields crystals suitable for X-ray diffraction analysis. Figure 2.1 shows the solid-state molecular structure of **2.2**.

Scheme 2.3



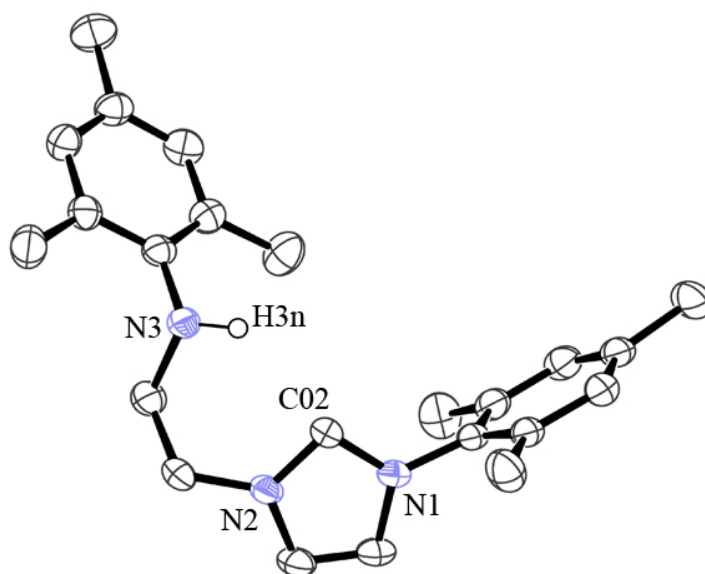


Figure 2.1. ORTEP view of **2.2**, with thermal ellipsoids depicted at 50 % probability. All hydrogen atoms have been omitted for clarity except for H3n, which was located in a difference map and refined isotropically.

The NHC unit incorporates an amino tether that can bind either as an amine or as an amido donor, after deprotonation. Such a bidentate coordination motif could augment the thermal stability of the resultant metal Rh and Ir complexes with respect to monodentate NHC-bound derivatives.¹⁴

2.3 *Synthesis and Characterization of Amino-Tethered NHC-Rhodium Compounds*

Incorporation of the NHC **2.2** to rhodium(I) can be accomplished by the addition of ^{Mes}[CNH] to 0.5 equiv of [Rh(diene)Cl]₂ (diene = 1,5-cyclooctadiene (COD), or 2,5-norbornadiene (NBD)) in a solution of THF at room temperature over a period of 8 h. Both complexes **2.3** – **2.4** are isolated as air-stable yellow powders in good yield (Scheme 2.4). The resultant NHC-Rh-diene complexes were characterized by ¹H and ¹³C NMR spectroscopy; for example, a weak doublet (*J*_{CRh} = 58 Hz) near δ 184 in the ¹³C NMR spectrum can be assigned to

the NHC carbene carbon and confirms the presence of the Rh-carbene bond for each of the diene derivatives.¹⁵

Scheme 2.4

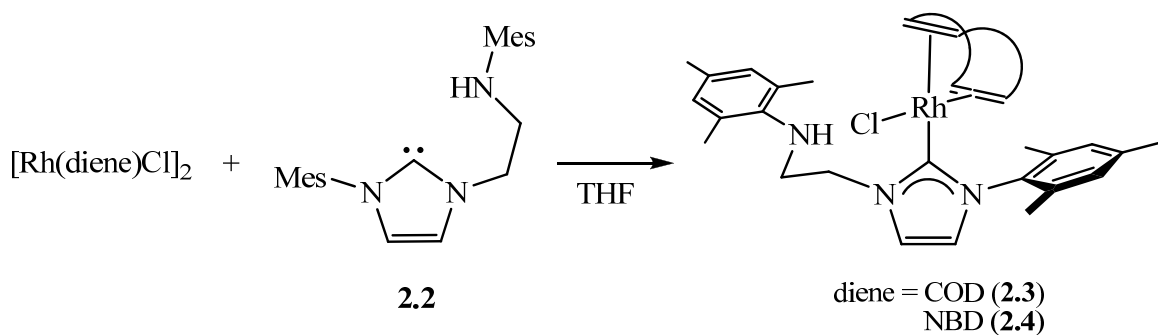


Figure 2.2 depicts the solid-state molecular structure of **2.3**; selected bond distances and angles are given in Table 2.1. The structure shows a mildly distorted square planar geometry about the rhodium(I) center, and the rhodium-carbene distance (Rh1-C02) of 2.039(2) Å is well within the range reported for similar Rh(I) derivatives.¹² The Rh-COD bond distances (calculated from the distance between the metal to the centroid of the olefinic fragment) are inequivalent with respect to its coordination being in either *cis* or *trans* positions relative to the C02 of the carbene carbon (*cis* = 1.99(1), *trans* = 2.07(1) Å). This inequivalence in bond length is expected and corroborates the *trans* disposed C=C fragment being less activated and less strongly bound to the rhodium center as is shown in the C=C bond distances of the COD (*trans*: 1.375(3) Å, *cis* 1.394(3) Å) fragment due to the strong *trans* influence imparted by the NHC ligand.

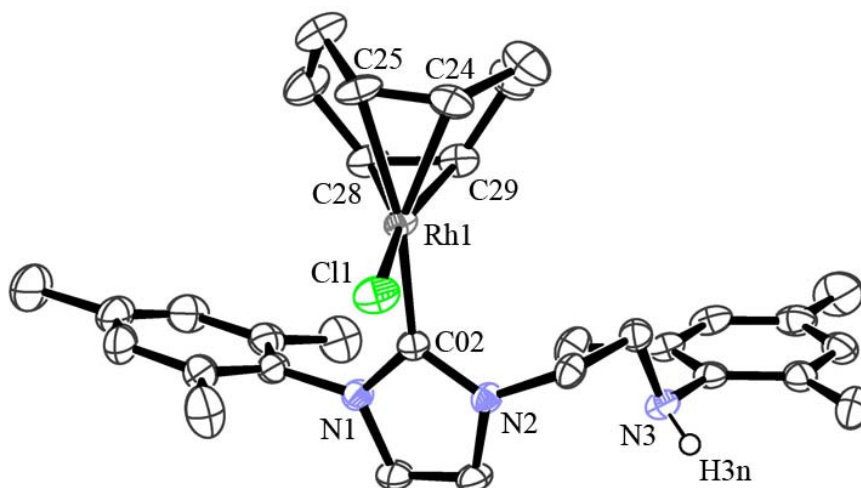


Figure 2.2. ORTEP view of **2.3**, with thermal ellipsoids depicted at 50 % probability. All hydrogen atoms have been omitted for clarity except for H3n, which was located in a difference map and refined isotropically.

To coordinate the pendent amine arm to rhodium, $\text{KN}(\text{SiMe}_3)_2$ can be added to compounds **2.3** and **2.4**. Alternatively, the bidentate amido carbene-rhodium complexes, **2.5** and **2.6**, can be synthesized in very good yield in one step by deprotonating imidazolium salt **2.1** with 2.2 equiv of $\text{KN}(\text{SiMe}_3)_2$ followed by an *in situ* reaction with 0.5 equiv of a rhodium-diene dimer at reduced temperatures. Complexes **2.5** and **2.6** maintain a slightly distorted square planar geometry and are characterized by a weak doublet resonance ($J_{\text{CRh}} = 56 \text{ Hz}$) at approximately δ 180 in the ^{13}C NMR spectrum (Rh-carbene carbon).

Interestingly, the single crystal X-ray structure of **2.5** (Figure 2.3) shows a nearly identical Rh1-C02 bond distance of $2.037(3) \text{ \AA}$ compared to that of **2.3** ($2.039(2) \text{ \AA}$); other selected bond distances and angles are given in Table 2.1; crystallographic data are given in Appendix A. The Rh-olefin distances (to the centroid of the C=C bond) for **2.5** are $2.01(1)$ and $2.09(1) \text{ \AA}$ respectively for the *cis* and *trans* orientations. These values compare to **2.3** (*cis*:

1.99(1), *trans*: 2.07(1) Å), which suggests that COD coordination may be slightly stronger for the chloro complex **2.3** as compared to the amido derivative **2.5**.

Scheme 2.5

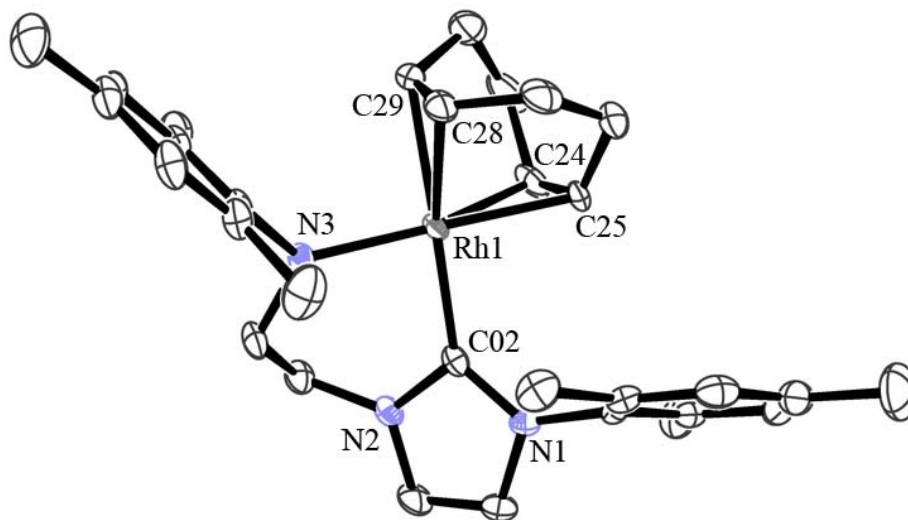
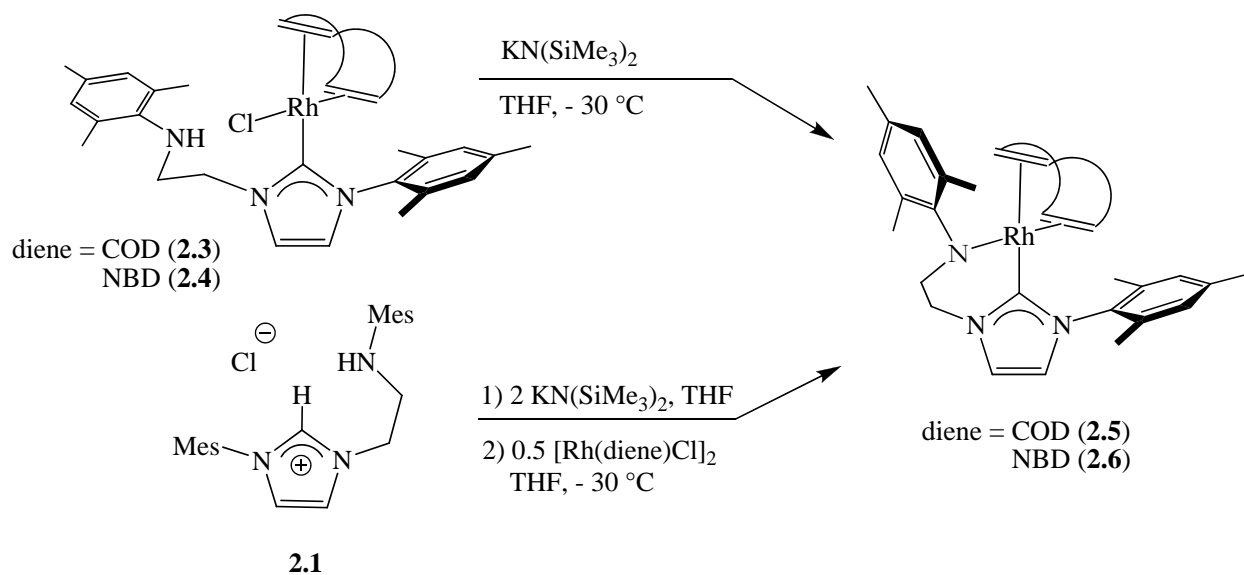
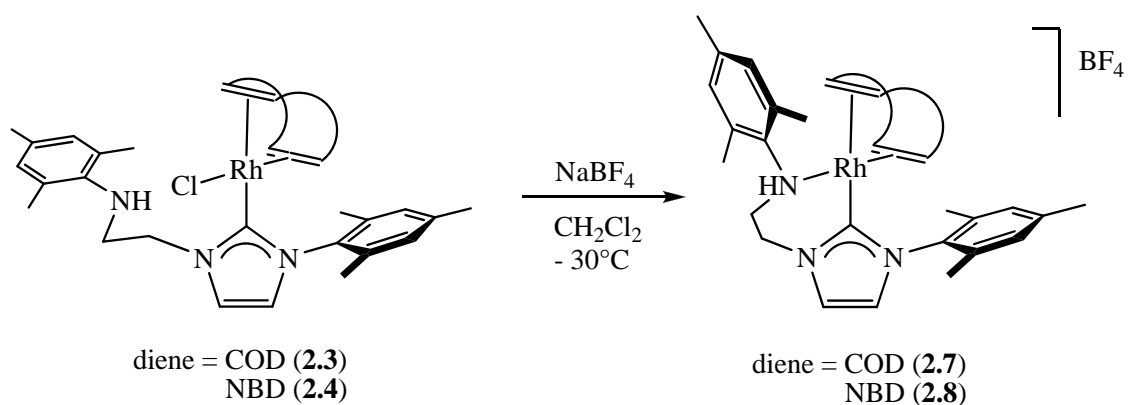


Figure 2.3. ORTEP view of **2.5**, with thermal ellipsoids depicted at 50 % probability. All hydrogen atoms have been omitted for clarity.

Cationic analogues can be synthesized with the addition of a halide extraction agent such as sodium tetrafluoroborate to **2.3** or **2.4** to cleanly yield the corresponding compounds **2.7** and **2.8** (Scheme 2.6). The ^1H NMR spectrum shows a slight upfield shift of the methylene protons on the ethyl spacer of **2.3** (δ 4.83, 3.48) as compared to **2.7** (δ 4.76, 3.47), where the upfield shift is larger for the NBD pair: compare **2.4**: δ 4.93, 3.64 for **2.4** versus δ 4.65, 3.25 for **2.8**. The N-H resonance in the ^1H NMR spectrum does shift downfield slightly upon coordination; for example, in **2.3** the uncoordinated N-H resonance is found at δ 3.18 whereas upon coordination in **2.7**, this resonance shifts to δ 3.26.

Scheme 2.6



The single crystal X-ray diffraction structure depicts **2.8** (Figure 2.4) with a distorted square planar geometry. Bond distances from the rhodium center to the *cis* and *trans* coordinated olefinic fragments of the norbornadiene ligand were found to be 1.99(1) and 2.08(1) Å respectively (measured to the center of the C=C centroid), which is typical of Rh-NBD complexes.¹⁶ These values also are akin to those of **2.3** and **2.5**, which suggests that the norbornadiene unit is similarly bound to the rhodium center as the cyclooctadiene unit; other bond distances and angles are given in Table 2.1.

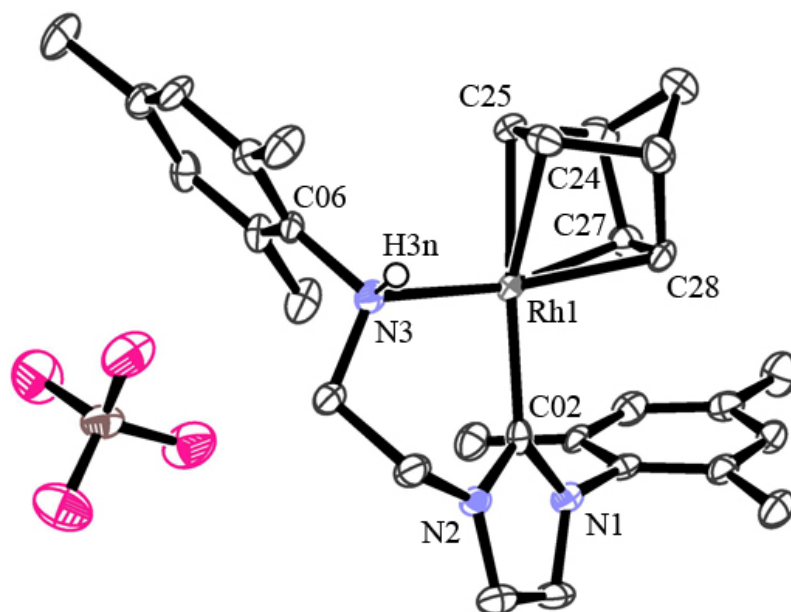


Figure 2.4. ORTEP view of **2.8**, with thermal ellipsoids depicted at 50 % probability. All hydrogens have been omitted for clarity except for H3n, which was located in a difference map and refined isotropically.

Upon inspection of the ^{13}C NMR data of the COD and NBD derivatives, one observes that all of the complexes exhibit very similar chemical shifts for the metal-carbene carbon, in a range from approx. δ 174 to 185, with the cationic derivative **2.8** being most upfield shifted to δ 174.6. Thus, there does not seem to be much change in the Rh-NHC interaction as a function of the amine tether being coordinated or dangling.

Table 2.1. Consolidated table of bond lengths and angles for complexes **2.3**, **2.5**, **2.8**, **2.10** and **2.11** (M = Rh or Ir).

	2.3	2.5	2.8	2.10	2.11
Bond Lengths (Å)					
M-C02	2.039(2)	2.037(3)	2.043(4)	2.034(3)	2.041(3)
M-(Cl1/N3) ^c	2.390(1)	2.048(3)	2.184(3)	2.365(1)	2.012(3)
M-(C=C) _{cis} ^{ab}	1.99(1)	2.01(1)	1.99(1)	1.95(1)	2.07(1)
M-(C=C) _{trans} ^{ab}	2.07(1)	2.09(1)	2.08(1)	2.45(1)	2.65(1)
Bond Angles (°)					
C02-M-(Cl1/N3) ^c	89.8(1)	88.0(1)	91.1(1)	90.1(1)	87.5(1)
C02-M-(C=C) _{cis} ^{ad}	93.6(2)	94.1(2)	100.5(2)	93.8(2)	94.5(2)
C02-M-(C=C) _{trans} ^{ad}	161.7(2)	161.9(2)	161.8(2)	161.3(2)	161.4(2)
Cl1-M-(C=C) _{cis} ^{ad}	89.2(2)	93.4(2)	95.4(2)	89.2(2)	93.2(2)
Cl(1)-M-(C=C) _{trans} ^{ad}	160.4(2)	160.8(2)	155.8(2)	159.9(2)	160.2(2)
(C=C) _{cis} -M-(C=C) _{trans} ^{ad}	87.8(2)	86.3(2)	72.7(2)	87.4(2)	85.9(2)

^a The *cis/trans* designation refers to position of olefin relative to the carbene carbon C(02).

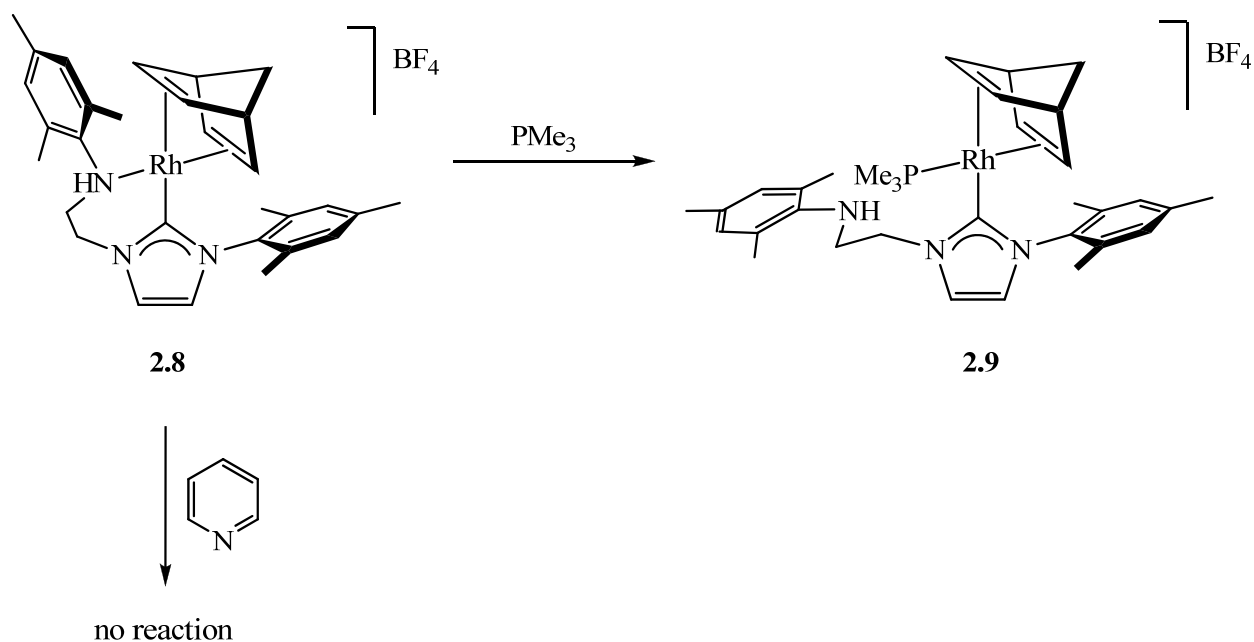
^b The distance measured is calculated from the metal to the center of the C=C centroid.

^c Bond distances and angles reflect substitution of -Cl1 with -N3 only, but their relative positions are identical.

^d The measured angles are calculated as an average of the two coordinated C=C carbons.

The reaction of the cationic complex **2.8** with pyridine and PMe₃ was examined to investigate the relative binding ability of the tethered amine. It was found that addition of excess pyridine did not result in decoordination of the amine arm on **2.8**, while addition of PMe₃ did result in the formation of the phosphine adduct **2.9** (Scheme 2.7).

Scheme 2.7



2.4 Synthesis and Characterization of $^{\text{Mes}}[\text{CNH}]\text{Ir}(\text{COD})$ Compounds

To generate the iridium analogues of complexes **2.3**, **2.5** and **2.7**, no amendments to the synthetic procedures are necessary except for the substitution of $[\text{Rh}(\text{COD})\text{Cl}]_2$ starting material with $[\text{Ir}(\text{COD})\text{Cl}]_2$. Resultant compounds $^{\text{Mes}}[\text{CNH}]\text{Ir}(\text{COD})\text{Cl}$, $^{\text{Mes}}[\text{CN}]\text{Ir}(\text{COD})$, $^{\text{Mes}}[\text{CNH}]\text{Ir}(\text{COD})\text{BF}_4$ are denoted as **2.10**, **2.11** and **2.12** respectively. The solid-state molecular structures of **2.10** and **2.11** were obtained and are depicted in Figures 2.5 and 2.6.

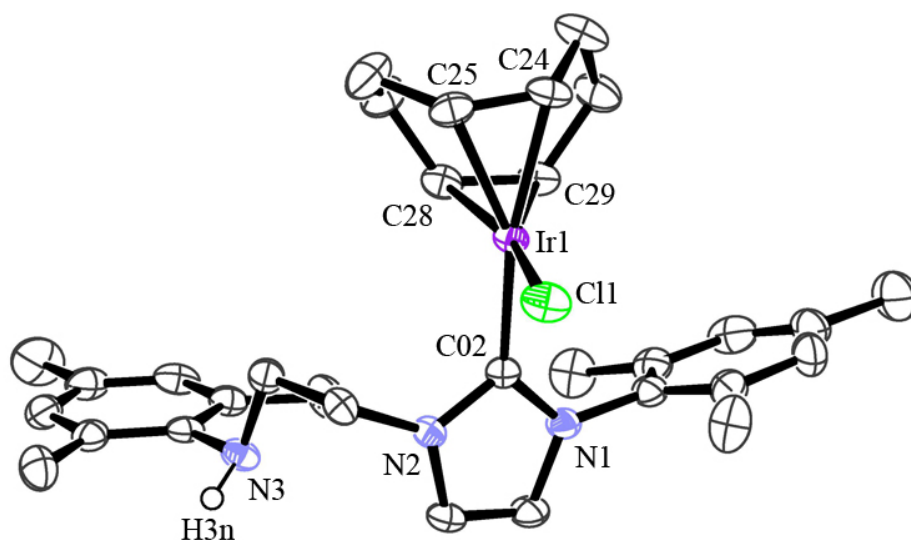


Figure 2.5. ORTEP view of **2.10**, with thermal ellipsoids depicted at 50 % probability. All hydrogens are removed for clarity except for H3n, which was located in a difference map and refined isotropically.

From single crystal X-ray diffraction data, it was revealed that structurally the Ir analogues were not significantly different from the Rh counterparts as the bond lengths and angles about the metal center were very similar. The only outstanding feature was the elongated *trans*-disposed Ir-COD bond length that was on average approximately 0.5 Å longer than the Rh variants. The longer olefin-Ir bond could be attributed to better overlap of the Ir-NHC frontier orbitals due to the increased bond covalency, thereby increasing the *trans* influence on COD and weakening the Ir-COD coordination. Despite the difference in the *trans* olefin position, reactivity comparisons could be made directly as results were solely ascribed to the substitution of the metal center. Table 2.1 contains a consolidated selection of bond lengths and angles of the synthesized Rh and Ir complexes.

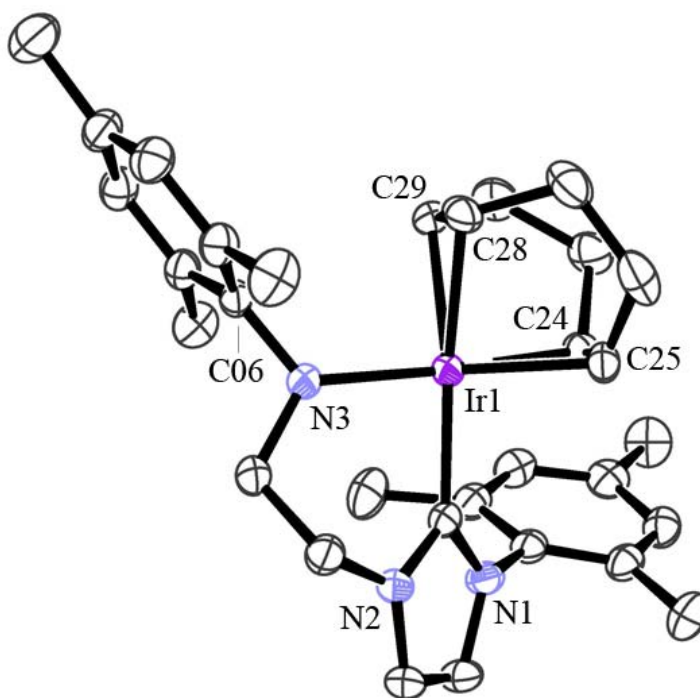


Figure 2.6. ORTEP view of **2.11**, with thermal ellipsoids depicted at 50 % probability. All hydrogens are removed for clarity.

2.5 Catalytic Hydrogenation Investigation with Group 9^{Mes}[CNH] Precursors

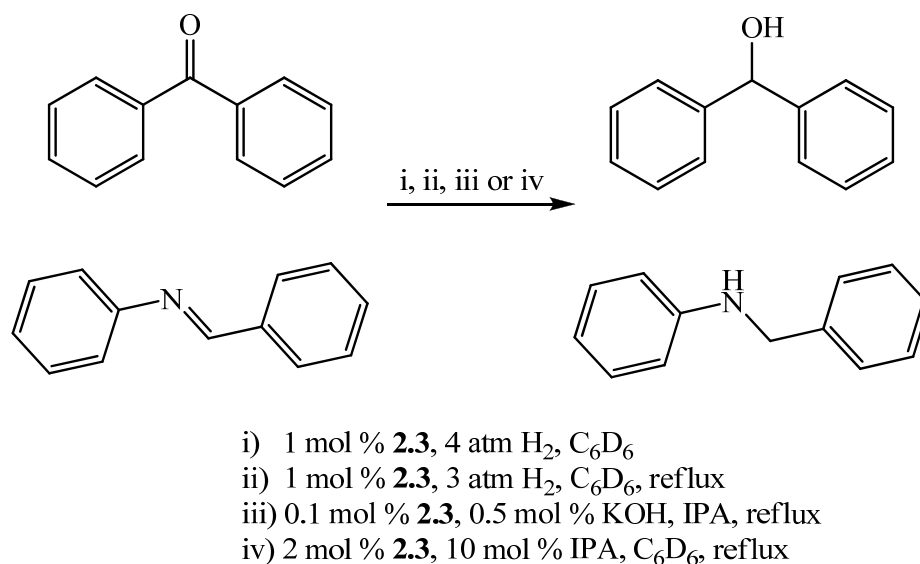
Hydrogenation test reactions were performed with complexes **2.3** – **2.8** using simple cyclic alkenes as substrates; cyclohexene (**C1**) and 1-methyl-cyclohexene (**C2**) were selected as they have been used frequently as benchmark substrates to test hydrogenation activity of later metal catalysts.¹⁷ Catalyst loading of 5 mol % was utilized and hydrogen pressure was deployed either at 1 or 4 atm. Reactions carried out under 1 atm hydrogen pressure were performed in sealable J. Young NMR tubes and monitored via ¹H NMR spectroscopy. Reactions carried out under 4 atm of hydrogen pressure were performed in thick-walled, Teflon-sealed glass reactors; samples were allowed to equilibrate to 1 atm H₂ pressure before NMR scale samples could be taken to observe reaction progress.

The results showed that these NHC-Rh(diene) precursors had long latency periods and subpar activity overall relative to other known NHC-Rh(diene) complexes in literature. None of the Rh precursors were able to surpass 70 % conversion of **C1** under 1 atm H₂ pressure after 12 hrs except for **2.3**. Under 4 atm of H₂ conversions appeared to improve, though the results were often accompanied by catalyst decomposition. As expected, the Rh precursors were less effective for hydrogenating the substituted cyclohexene **C2** substrate as they were not able to convert beyond 40 % after 72 hrs under 4 atm of H₂ with the exception of complexes **2.5** and **2.6**. Interestingly, these complexes recorded conversions greater than 90 %; however, catalyst decomposition was again apparent. It was determined that the induction period of our catalyst precursors **2.3** – **2.8** was long and the formation of metallic rhodium during the reaction made the hydrogenation results unclear.

To alleviate the problem of catalyst decomposition observed with the rhodium compounds, the corresponding reactions were performed with Ir analogues. Under similar experimental conditions, the formation of metallic iridium was not observed. However, complexes **2.10** – **2.12** significantly underperformed their Rh congeners at 4 atm of H₂ and recorded almost negligible activity with 1 atm H₂ pressure. The precursors were simply too stable with latency periods too long to be useful in catalytic processes.

The difficulties that arose from the pressurized hydrogenation catalysis led to investigations of other methods such as transfer hydrogenation of polar substrates. Transfer hydrogenation reactions with ketone and imine substrates were attempted with **2.3** due to its robustness and tolerance of air and moisture. Various common literature methods¹⁸ were attempted on benchmark test substrates such as benzophenone and N-benzylideneaniline (Scheme 2.8).

Scheme 2.8

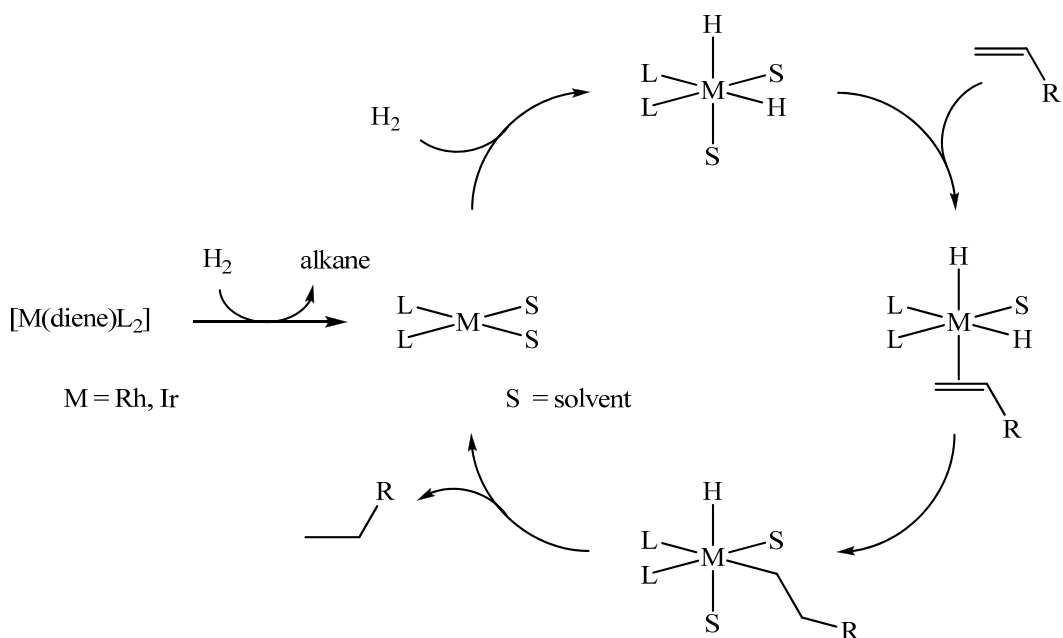


Of the four routes attempted, none of them exhibited any catalytic activity as observed in the ¹H NMR spectrum despite being allowed to run for an extended period of time (> 12 hrs).

Thus, it appeared that the precursor **2.3** was stable and reluctant to become activated in solution.

Efforts to determine the reactivity of the precursor complexes **2.3** – **2.12** were attempted by reaction with 1 atm H₂ in the absence of a substrate. Unfortunately, the results paralleled the catalytic runs in that these complexes remained largely unchanged on the basis of NMR spectroscopy. In addition, attempts to detect small amounts of hydride species, which should show resonances upfield of δ 0, were unsuccessful contrary to characteristic behavior of active Rh and Ir precursors.^{19, 20} Thus, it is conceivable that without the formation of metal-hydride intermediates, the coordinated olefins cannot be hydrogenated to form the active catalyst, which is commonly accepted as a necessary process in olefin-bound precursors.²¹ Scheme 2.9 describes a general hydrogenation mechanism for metal-olefin catalyst precursors.

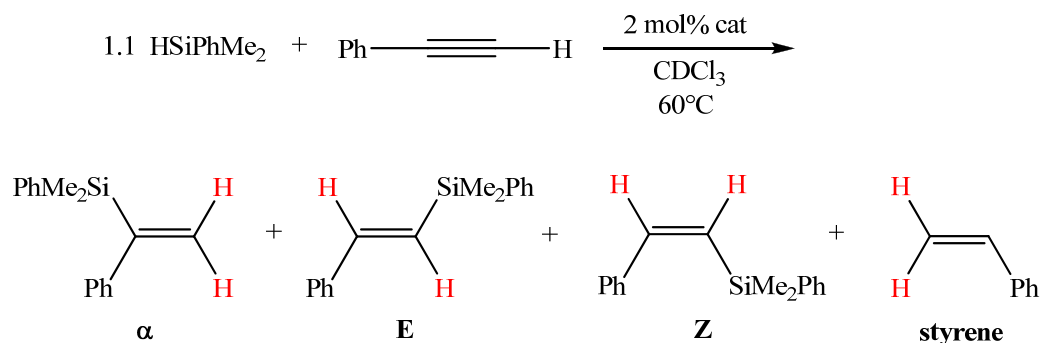
Scheme 2.9



2.6 Catalytic Hydrosilylation Reactions with Group 9^{Mes}[CNH] Precursors

Despite the lack of success from the hydrogenation studies, precursors **2.3** – **2.8** and **2.10** – **2.12** were investigated for their ability to catalyze the hydrosilylation of phenylacetylene with dimethylphenylsilane as described by Scheme 2.10. The substrates were selected based on their use as benchmark substrates to model activity for hydrosilylation catalysis. However, the detection and analysis of the product output was complicated by the generation of multiple isomers. Dimethylphenylsilane was added in slight excess to render phenylacetylene as the limiting reagent so its diagnostic methine resonance at δ 3.06 can be monitored by ^1H NMR. As the reaction progressed, signals corresponding to three different isomers (α , E and Z) emerged in the ^1H NMR spectrum and their integrals were recorded. Table 2.2 details the product ratios for these catalytic experiments. Scheme 2.11 depicts a generalized version of the Chalk-Harrod mechanism of the hydrosilylation of alkynes and formation of the various product isomers.²²

Scheme 2.10

**Table 2.2.** Consolidated results from the hydrosilylation of phenylacetylene and dimethylphenylsilane by precursors **2.3** – **2.8** and **2.10** – **2.12**.

Compound	ID #	<i>t</i> (hrs)	Conversion (%) ^a			
			α	<i>E</i>	<i>Z</i>	sty ^b
^{Mes} [CNH]Rh(COD)Cl	2.3	48	6	67	21	6
^{Mes} [CN]Rh(COD)	2.5	15	8	51	26	6
[^{Mes} [CNH]Rh(COD)]BF ₄	2.7	17	7	72	21	0
^{Mes} [CNH]Rh(NBD)Cl	2.4	4.5	6	57	30	5
^{Mes} [CN]Rh(NBD)	2.6	4	7	43	49	1
[^{Mes} [CNH]Rh(NBD)]BF ₄	2.8	6.5	7	43	50	0
^{Mes} [CNH]Ir(COD)Cl	2.10	4	3	9	87	0
^{Mes} [CN]Ir(COD)	2.11	4.5	4	8	83	5
[^{Mes} [CNH]Ir(COD)]BF ₄	2.12	8.5	6	7	79	8

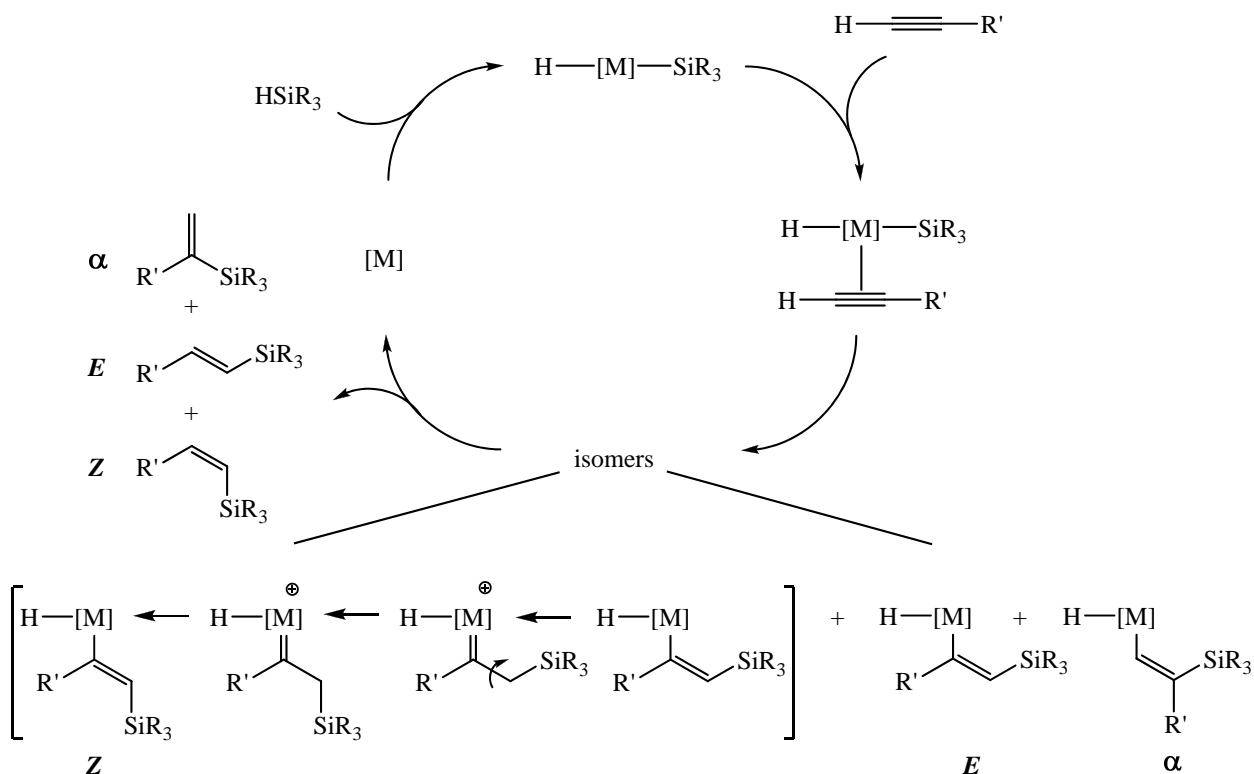
^a Product conversions were determined by ¹H NMR and measured relative to the acetylene proton resonance. Conversions of **2.3** - **2.8** represent an average of several runs and **2.10** - **2.12** were single run results.

^b Only styrene monomer was observed; polystyrene signals at δ 7 - 6 and 2.5 - 0 were absent.

The results from the hydrosilylation investigations were more promising than those from the hydrogenation study as all catalysts were able to achieve near quantitative conversions of the substrates, despite long reaction times in certain cases (using catalysts **2.3**, **2.5** and **2.7** in particular) and the emergence of styrene as an impurity in small quantities. Polystyrene was the expected by-product of the hydrosilylation process, yet no trace of polymerization was detected

in the ^1H NMR spectrum. From inspection, the relative ratios of isomeric selectivity provided no clear insight into how the different coordination modes of the tethered amine affected the hydrosilylation mechanism. As a generalization, it appeared that the $\text{Rh}(\text{COD})$ derivatives (**2.3**, **2.5** and **2.7**) had a slight bias towards producing the *E* isomer over the *Z* when compared to $\text{Rh}(\text{NBD})$ versions (**2.4**, **2.6** and **2.8**). However, the $\text{Rh}(\text{COD})$ catalysts were also significantly slower to achieve completion with reaction times more than double those of all others tested. Interestingly, the Ir analogues clearly demonstrated a preference for producing the *Z* isomer (opposite effect of Rh), yet there was no indication that the different coordinating modes of the tethered amino-arm affected the hydrosilylated product distribution.

Scheme 2.11



2.7 Conclusions

The ability of an amine-tethered NHC to coordinate to Rh and Ir diene complexes in either a monodentate or bidentate mode has been investigated. The synthetic protocols to

generate each class of compound are straightforward and illustrate the versatility of this ligand in its binding aptitudes. Given the variable complexes accessible, we examined their ability to act as catalyst precursors for the hydrogenation of cyclic alkenes. Unfortunately, regardless of the bonding mode and form of the tether (i.e. amine vs. amide), none of these complexes were especially active in hydrogenation. In addition, the neutral amine tethered NHC complex (**2.3**) was tested for its ability to act as transfer hydrogenation catalyst, but was found to be inactive with ketone- and imine-functionalized substrates. It appears that the diene ligands are too firmly bound to any of these complexes, regardless of the tether binding mode, so that neither substrates nor H_2 activation can occur in a facile manner under typical experimental conditions. However, the results from the hydrosilylation study showed more promise with quantitative conversions of the substrates, albeit with long reaction times. The coordinative nature of the pendent arm was determined to not be influential in the distribution of the resultant isomers, whereas, a change of metal center did affect the selectivity. The following chapters will further investigate the incorporation these versatile amine-tethered NHCs into other late transition metal systems.

2.8 *Experimental Section*

General Considerations. Unless otherwise specified, all experimental procedures were performed in a dry, oxygen-free nitrogen or argon atmosphere by Schlenk or glovebox techniques. 2-chloro-N-mesitylacetamide,²³ 2-chloroethyl-N-mesitylamine,²⁴ mesitylimidazole,²⁵ $[\text{Rh}(\text{COD})\text{Cl}]_2$,²⁶ $[\text{Rh}(\text{NBD})\text{Cl}]_2$,²⁷ and $[\text{Rh}(\text{COE})_2\text{Cl}]_2$ ²⁸ were prepared from literature methods. H_2 gas was passed through an activated 3 Å molecular sieve column before being introduced to the reaction vessel for hydrogenation studies. Dimethylphenylsilane and phenylacetylene were dried over 4 Å molecular sieves and then distilled under nitrogen and degassed via three freeze-pump-thaw cycles. All other chemicals were purchased commercially and used as received. Methylene chloride was dried by refluxing over CaH_2 overnight under nitrogen and collected by distillation. Anhydrous toluene, hexanes, pentane and tetrahydrofuran were purchased from Aldrich, sparged with nitrogen, and passed through columns containing activated alumina and Ridox catalyst. Deuterated benzene (C_6D_6) was purified via three freeze-pump-thaw cycles and then refluxed overnight in a sealed vessel, which contained sodium/potassium alloy, and vacuum transferred into a glass, Teflon-sealed vessel. Deuterated methylene chloride (CD_2Cl_2) was purified in a similar manner using CaH_2 as the drying agent. ^1H and ^{13}C NMR spectra were obtained by a Bruker AVANCE 300 or 400 MHz spectrometer. Elemental analysis and mass spectrometry (EI/MS) were performed at the Department of Chemistry at the University of British Columbia.

Mes[HCNH]Cl (2.1). A glass reactor fitted with a Kontes valve was charged with 3.00 g (55.2 mmol) of 2-chloroethyl-N-mesitylamine and 2.83 g (55.2 mmol) of mesitylimidazole, and the resultant mixture heated to 150 °C in an oil bath for 1.5 h. The reaction was allowed to cool to room temperature and the hard, air-stable, brown solid was filtered and washed with THF to produce the desired cream-colored solid. Yield: 5.10 g (90 %). ^1H NMR (CD_2Cl_2 , 400 MHz): δ

2.04, (s, 6H, -ArCH₃), 2.09 (s, 3H, -ArCH₃), 2.16 (s, 3H, -ArCH₃), 2.32 (s, 6H, -ArCH₃), 3.23 (t, 2H, *J* = 5.0 Hz, -N_{Ar}CH₂), 4.99 (t, 2H, *J* = 5.0 Hz, -N_{imid}CH₂), 6.72 (s, 2H, -ArH), 6.99 (s, 2H, -ArH), 7.12 (s, 1H, -imidH), 8.12 (s, 1H, -imidH), 10.7 (s, 1H -NCHN). ¹³C NMR (CD₂Cl₂, 100 MHz): δ 17.9, 18.5 (-*o*-ArCH₃), 20.8, 21.3 (-*p*-ArCH₃), 48.1 (-N_{Ar}CH₂), 50.1 (-N_{imid}CH₂), 122.8, 124.2 (-imidC), 129.6, 130.2(-ArC), 131.5, 131.9, 132.6, 134.9 (-ArC_{ipso}), 140.3 (-NCHN) 141.6, 142.8 (-ArC_{ipso}). EI-MS: 347 [M⁺]. Anal. Calc. For C₂₃H₃₀N₃Cl: C, 71.95; H, 7.88; N, 10.94. Found: C, 71.87; H, 7.62; N, 11.30 %.

^{Mes}[CNH] (**2.2**). A flask with 3.12 g (15.6 mmol) of KN(SiMe₂)₂ dissolved in 20 mL of THF was added to a 20 mL THF suspension containing 5.00 g (13.0 mmol) of **2.1** at room temperature. The mixture was stirred for 1.5 h and dried *in vacuo* to leave a beige powder. Colorless needle crystals suitable for X-ray diffraction were grown by slow evaporation from a solution of toluene. Yield: 4.10 g (91 %). ¹H NMR (C₆D₆, 400 MHz): δ 2.08 (s, 6H, -ArCH₃), 2.14 (s, 3H, -ArCH₃), 2.18 (s, 3H, -ArCH₃), 2.23 (s, 6H, -ArCH₃), 3.29 (m, 2H, -N_{Ar}CH₂), 3.91 (m, 2H, -N_{imid}CH₂), 4.24 (t, 1H, *J* = 7.1 Hz, -NH), 6.38 (d, 1H, *J* = 1.5 Hz, -imidH), 6.45 (d, 1H, *J* = 1.5 Hz, -imidH), 6.78 (s, 2H, -ArH), 6.80 (s, 2H, -ArH). ¹³C NMR (C₆D₆, 100 MHz): δ 18.5, 19.29, 21.1, 21.3 (-ArCH₃), 49.6 (-N_{Ar}CH₂), 51.9 (-N_{imid}CH₂), 120.0, 120.9 (-imidC), 129.5, 130.2 (-ArC), 130.6, 131.4, 135.7, 137.6, 139.6, 144.6 (-ArC_{ipso}), 215.6 (-NCN). EI-MS: 347 [M⁺]. Anal. Calc. For C₂₃H₂₉N₃·2/5C₄H₈O: C, 78.51; H, 8.62; N, 11.17. Found: C, 78.26; H, 8.50; N, 11.55 %.

^{Mes}[CNH]Rh(COD)Cl (**2.3**). A flask with 2.82 g (8.12 mmol) of ^{Mes}[CNH] was dissolved in 10 mL of THF and added dropwise to a stirring transparent yellow solution of 2.00 g (4.06 mmol) of [Rh(COD)Cl]₂ in 10 mL of THF. The reaction was stirred overnight at room temperature and the solvent was removed which resulted in the desired yellow powder. Yellow crystals suitable

for X-ray analysis were grown by slow evaporation in methylene chloride. Yield: 2.12 g (88 %).

^1H NMR (C_6D_6 , 400 MHz): δ 1.50 – 1.80 (m, -COD), 1.69 (s, 3H, -ArCH₃), 1.90 – 2.30 (m, -COD), 2.15 (s, 3H, -ArCH₃), 2.19 (s, 3H, -ArCH₃), 2.23 (s, 6H, -ArCH₃), 2.67 (s, 3H, -ArCH₃), 3.18 (br, 1H, -NH), 3.35 (m, -COD), 3.47 (t, 2H, $J = 6.2$ Hz, -N_{Ar}CH₂), 4.83 (t, 2H, $J = 6.2$ Hz, -N_{imid}CH₂), 5.26 (m, 1H, -COD), 5.36 (m, 1H, -COD), 6.00 (d, 1H, $J = 1.5$ Hz, -imidH), 6.46 (d, 1H, $J = 1.5$ Hz, -imidH), 6.70 (s, 2H, ArH), 6.81 (s, 4H, ArH), 6.86 (s, 2H, ArH). ^{13}C NMR (C_6D_6 , 100 MHz): δ 18.1, 19.0, 20.6, 21.1, 21.4 (-ArCH₃), 28.9, 29.8, 32.6, 34.7 (-COD), 49.0 (-N_{Ar}CH₂), 52.4 (-N_{imid}CH₂), 67.5, 67.3 (d, $J_{\text{CRh}} = 14$ Hz, -RhC_{COD}), 97.8, 98.6 (d, $J_{\text{CRh}} = 7$ Hz, -RhC_{COD}), 121.7, 122.9 (-imidC), 130.2, 130.7 (-ArC), 131.9, 134.7, 137.2, 138.3, 139.0, 143.9 (-ArC_{ipso}), 184.2 (d, $J_{\text{CRh}} = 52$ Hz, RhC_{NCN}). EI-MS: 593 [M^+]. Anal. Calc. For $\text{C}_{31}\text{H}_{41}\text{N}_3\text{ClRh}$: C, 62.68; H, 6.96; N, 7.07. Found: C, 62.61; H, 7.30; N, 7.32 %.

$^{\text{Mes}}[\text{CNH}]\text{Rh}(\text{NBD})\text{Cl}$ (2.4). Synthetic procedure as described for **2.3** using 1.126 g (3.239 mmol) of **2.2**, 746 mg (1.618 mmol) of $[\text{Rh}(\text{NBD})\text{Cl}]_2$. Yield: 1.47 g (80 %). ^1H NMR (CD_2Cl_2 , 400 MHz): δ 1.14 (s, 2H, -NBD), 2.02 (s, 6H, -ArCH₃), 2.22 (s, 3H, -ArCH₃), 2.28 (s, 6H, -ArCH₃), 2.41 (s, 3H, -ArCH₃), 3.40 (s, 2H, -NBD), 3.46 (s, 2H, -NBD), 3.64 (m, 2H, -N_{Ar}CH₂), 4.93 (m, 2H, -N_{imid}CH₂), 6.73 (d, 1H, $J = 1.6$ Hz, -imidH), 6.83 (s, 2H, -ArH), 7.05 (s, 2H, -ArH), 7.13 (d, 1H, $J = 1.6$ Hz, -imidH). ^{13}C NMR (CD_2Cl_2 , 100 MHz): δ 18.5, 18.8 (-ArCH₃), 20.86, 21.48 (-NBD), 49.51 (-N_{Ar}CH₂), 51.27 (d, $J = 3$ Hz, -RhC_{NBD}), 52.12, (-N_{imid}CH₂), 63.43 (d, $J_{\text{CRh}} = 5$ Hz, -RhC_{NBD}), 122.2, 123.1 (-imidC), 129.5, 129.9(-ArC), 130.8, 132.3, 136.1, 136.7, 139.5, 143.4 (-ArC_{ipso}), 183.9 (d, $J_{\text{CRh}} = 58$ Hz, RhC_{NCN}). EI-MS: 577 [M^+]. Anal. Calc. For $\text{C}_{30}\text{H}_{37}\text{N}_3\text{ClRh}$: C, 62.34; H, 6.45; N, 7.27. Found: C, 62.56; H, 6.83; N, 7.59 %.

$^{\text{Mes}}[\text{CN}]\text{Rh}(\text{COD})$ (2.5). A vial containing 300 mg (0.7813 mmol) of **2.1** was suspended in 5 mL of THF. To this mixture, 343 mg (1.719 mmol) of $\text{KN}(\text{SiMe}_3)_2$ dissolved in 2 mL of THF

was added dropwise at room temperature. The yellow-brown solution was stirred for 1 h and the cooled to $-30\text{ }^{\circ}\text{C}$. 193 mg (0.3914 mmol) of $[\text{Rh}(\text{COD})\text{Cl}]_2$ was dissolved in 10 mL of THF and was added dropwise at $-30\text{ }^{\circ}\text{C}$. The solution was warmed to room temperature and stirred for 1 additional hour that resulted in an orange-brown mixture. The THF was removed under vacuum and the product was extracted with toluene and filtered through Celite. Under reduced pressure, the toluene was removed and the product was washed with hexanes to give a golden orange powder. Cooling a concentrated toluene solution to $-30\text{ }^{\circ}\text{C}$ produced orange crystals suitable for X-ray analysis. Yield: 393 mg (90 %). ^1H NMR (C_6D_6 , 400 MHz): δ 1.55 – 1.88 (m, -COD), 2.05 – 2.25 (m, -COD), 2.10 (s, 3H, -ArCH₃), 2.21 (s, 6H, -ArCH₃), 2.32 (s, 3H, -ArCH₃), 2.71 (s, 6H, -ArCH₃), 2.99 (m, 2H, -N_{Ar}CH₂), 3.04 (m, 2H, -COD), 3.85 (m, 2H, -COD), 4.12 (m, 2H, -N_{imid}CH₂), 5.91 (d, 1H, $J = 1.7\text{ Hz}$, -imidH), 6.10 (d, 1H, $J = 1.7\text{ Hz}$, -imidH), 6.74 (s, 2H, ArH), 7.13 (s, 2H, ArH). ^{13}C NMR (C_6D_6 , 100 MHz): δ 18.93, 20.10, 21.32, 21.53 (-ArCH₃), 30.45, 34.05 (-COD), 54.14 (-N_{Ar}CH₂), 57.35 (-N_{imid}CH₂), 64.35 (d, $J_{\text{CRh}} = 11\text{ Hz}$, -RhC_{COD}), 94.54 (d, $J_{\text{CRh}} = 8\text{ Hz}$, -RhC_{COD}), 120.4, 122.0 (-imidC), 129.5, 129.9 (-ArC), 130.4, 135.9, 136.4, 138.3, 138.6, 157.9 (-ArC_{ipso}), 180.8 (d, $J_{\text{CRh}} = 56\text{ Hz}$, -RhC_{NCN}). EI-MS: 557 [M^+]. Anal. Calc. For $\text{C}_{31}\text{H}_{40}\text{N}_3\text{Rh}$: C, 66.78; H, 7.23; N, 7.54. Found: C, 66.46; H, 7.23; N, 7.40 %.

^{Mes}[CN]Rh(NBD) (2.6). Synthetic procedure as described for **2.5** using 300 mg (0.7813 mmol) of **2.1**, 343 mg (1.719 mmol) of $\text{KN}(\text{SiMe}_3)_2$ and 164 mg (0.3557 mmol) of $[\text{Rh}(\text{NBD})\text{Cl}]_2$. Yield: 143 mg (74 %). ^1H NMR (C_6D_6 , 400 MHz): δ 1.03 (b, 1H, -NBD), 1.09 (b, 1H, -NBD), 2.04 (s, 3H, -ArCH₃), 2.10 (s, 6H, -ArCH₃), 2.30 (s, 3H, -ArCH₃), 2.39 (b, 2H, -NBD), 2.77 (s, 6H, -ArCH₃), 3.17 (m, 2H, -N_{Ar}CH₂), 3.38 (m, 2H, -N_{imid}CH₂), 3.77 (br, 4H, -NBD), 5.85 (br, 1H, -imidH), 6.11 (br, 1H, -imidH), 6.70 (s, 2H, ArH), 7.07 (s, 2H, ArH). ^{13}C NMR (C_6D_6 , 100 MHz): δ 18.4, 20.2 (-ArCH₃), 21.4, 21.6 (-ArCH₃), 40.0, 40.1 (-NBD), 50.5 (-N_{imid}CH₂), 53.2, (-N_{imid}CH₂), 56.7 (-NBD), 63.3 (d, $J_{\text{CRh}} = 4\text{ Hz}$, -RhC_{NBD}), 74.1 (d, $J_{\text{CRh}} = 7\text{ Hz}$, -RhC_{NBD}), 120.6,

120.8 (-imidC), 129.1, 129.4 (-ArC), 130.4, 136.2, 136.3, 137.4, 138.8, 156.9 (-ArC_{ipso}), 178.3 (d, $J_{\text{CRh}} = 61$ Hz, -RhC_{N₃}). EI-MS: 539 [M^+]. Anal. Calc. For $\text{C}_{30}\text{H}_{36}\text{N}_3\text{Rh}\cdot 2/3\text{CH}_2\text{Cl}_2$: C, 61.47; H, 6.45; N, 7.01. Found: C, 61.73; H, 6.42; N, 7.07 %.

[^{Mes}[CNH]Rh(COD)]BF₄ (2.7). A vial with 1.00 g (1.68 mmol) of **2.3** was dissolved in 10 mL of CH₂Cl₂ and cooled to -30 °C. 222 mg (2 mmol) of NaBF₄ was ground and was slowly introduced to the solution at -30 °C. The mixture was warmed to room temperature and stirred overnight. The reaction was carefully monitored for the first 2 h to control the effervescing solution. Once complete, the mixture was filtered through Celite and the solvent was removed under reduced pressure to leave the desired yellow product. Yield: 867 mg (80 %). **5:** ¹H NMR (CD₂Cl₂, 400 MHz): δ 1.40 – 2.40 (m, -COD), 1.84 (s, 3H, -ArCH₃), 2.20 (s, 3H, -ArCH₃), 2.21 (s, 6H, -ArCH₃), 2.37 (s, 3H, -ArCH₃), 2.39 (s, 3H, -ArCH₃), 3.00 (m, 1H, -COD), 3.26 (br, 1H, -NH), 3.46 (m, 2H, -N_{Ar}CH₂), 3.60 (m, 1H, -COD), 4.69 (m, 1H, COD), 4.77 (m, 2H, -N_{imid}CH₂), 5.14 (m, 1H, -COD), 6.80 (s, 2H, -ArH), 6.81 (s, 1H, -ArH), 6.94 (s, 1H, -imidH), 7.10 (s, 1H, -imidH), 7.16 (s, 1H, -ArH). ¹³C NMR (CD₂Cl₂, 100 MHz): δ 18.11, 18.69, 20.01, 20.85, 21.37 (-ArCH₃), 28.50, 29.69, 31.99, 34.61 (-COD), 49.13 (-N_{Ar}CH₂), 52.46 (-N_{imid}CH₂), 68.6 (d, $J_{\text{CRh}} = 15$ Hz, -RhC_{COD}), 97.25, 97.33 (d, $J_{\text{CRh}} = 3$ Hz, -RhC_{COD}), 121.8, 123.8 (-imidC), 128.8, 129.9 (-ArCN_{Ar}), 130.0 (-ArCN_{imid}), 130.7 (-ArCN_{Ar}), 132.2, 135.0, 136.8, 137.5 (-ArCN_{imid}), 139.3, 143.4 (-ArC_{ipso}), 183.1 (d, $J_{\text{CRh}} = 51$ Hz, -RhC_{N₃}). EI-MS: 557 [$\text{M}^+ - \text{BF}_4$]. Anal. Calc. For $\text{C}_{31}\text{H}_{41}\text{N}_3\text{BF}_4\text{Rh}\cdot 1/5\text{C}_5\text{H}_{12}$: C, 58.25 H, 6.63 N, 6.37. Found: C, 58.63 H, 6.94 N, 6.44 %.

[^{Mes}[CNH]Rh(NBD)]BF₄ (2.8). Synthetic procedure as described for compound **2.7** using 214 mg (0.3702 mmol) of **2.4**, 51 mg (0.4645 mmol) of NaBF₄. Slow evaporation in a concentrated solution of CH₂Cl₂ produced yellow X-ray grade platelets. Yield: 189 mg (81 %). ¹H NMR (CD₂Cl₂, 400 MHz): δ 1.10 (br, 2H, -NBD), 2.04, (s, 6H, -ArCH₃), 2.23, (s, 3H, -ArCH₃), 2.37,

(s, 3H, -ArCH₃), 2.54, (s, 6H, -ArCH₃), 3.24, (br, 4H, -NBD), 3.50 (m, 2H, -N_{Ar}CH₂), 4.38 (s, 1H, -NH), 4.92 (m, 2H, -N_{imid}CH₂), 6.73 (s, 2H, *J* = 1.8 Hz, -imidH), 6.88 (s, 2H, -ArH), 7.01 (s, 2H, -ArH), 7.15 (d, 1H, *J* = 1 Hz, -imidH). ¹³C NMR (CD₂Cl₂, 100 MHz): δ 17.95, 19.04 (-*o*-ArCH₃), 20.59, 21.15 (-*p*-ArCH₃), 49.65 (-N_{Ar}CH₂), 51.11 (-N_{imid}CH₂), 51.47 (d, *J*_{CRh} = 1.8 Hz, -RhC_{NBD}), 64.06 (d, *J*_{CRh} = 5.1 Hz, -RhC_{NBD}), 122.6, 122.9 (-imidC), 129.6, 130.2, 130.6, 135.6, 139.8, 140.8 (-ArC), 174.6 (d, *J*_{CRh} = 59 Hz, -RhC_{NCN}). EI-MS: 539 [M⁺ - BF₄]. Anal. Calc. For C₃₀H₃₇N₃BF₄Rh·1/3C₆H₁₄: C, 58.37; H, 6.43; N, 6.38. Found: C, 58.18; H, 6.03; N, 6.03 %.

[^{Mes}[CNH]Rh(NBD)PMe₃]BF₄ (**2.9**). A vial with 32 mg (0.421 mmol) of PMe₃ was mixed with 3 mL of benzene and added dropwise to an orange suspension containing 218 mg (0.346 mmol) of **2.8** in 5 mL of benzene. Immediately after the addition, the solution becomes transparent to which becomes a suspended orange mixture after 5 min. The reaction was allowed to stir for 30 min before the solution was concentrated under rotary evaporation. The addition of pentane resulted in the precipitation of an orange powder, which was collected and dried under vacuum. Yield: 212 mg (87 %). ¹H NMR (CD₂Cl₂, 400 MHz): δ 1.27, (d, 2H, *J* = 7.4 Hz, -NBD), 1.43 (br, 9H, -P(CH₃)₃), 1.51 (s, 3H, -ArCH₃), 1.79 (s, 3H, -ArCH₃), 2.20 (s, 3H, -ArCH₃), 2.22 (s, 6H, -ArCH₃), 2.44 (s, 3H, -ArCH₃), 2.98 (br, 2H, -NBD), 3.32 (m, 2H, -N_{Ar}CH₂), 3.46, 3.50 (br, 2H, -NBD), 3.63 (m, 1H, -N_{imid}CH₂), 4.16 (br, 1H, -NBD), 4.67 (br, 1H, -NBD), 4.91 (m, 1H, -N_{imid}CH₂), 6.80 (d, 1H, -imidH), 6.85 (s, 2H, -ArH), 7.14 (s, 2H, -ArH), 7.50 (d, 1H, -imidH). ¹³C NMR (CD₂Cl₂, 100 MHz): δ 18.22 (-*o*-ArCH₃), 19.0 (-ArCH₃), 20.8 (m, -P(CH₃)₃), 21.9 (-*p*-ArCH₃), 42.2, 46.2 (-NBD), 49.9 (-N_{Ar}CH₂), 51.7 (-N_{imid}CH₂), 53.4 (-NBD), 61.7 (d, *J*_{CRh} = 3 Hz, -RhC_{NBD}) 66.1 (d, *J*_{CRh} = 5 Hz, -RhC_{NBD}), 67.5 (d, *J*_{CRh} = 4 Hz, -RhC_{NBD}) 77.4 (d, *J*_{CRh} = 6 Hz, -RhC_{NBD}), 123.1, 125.3 (-imidC), 130.5, 130.8, 133.4, 136.4, 140.8, 143.2 (-ArC), 183.8 (d, *J*_{CRh} = 58 Hz -RhC_{NCN}). ³¹P{¹H} NMR (CD₂Cl₂, 162 MHz): δ -12.91 (d, *J*_{PRh} = 122 Hz,

$P(CH_3)_3$). EI-MS: 539 [$M^+ - PMe_3, BF_4$]. Anal. Calc. For $C_{33}H_{46}N_3BF_4PRh \cdot 1/2C_6H_{14}$: C, 57.77; H, 7.14; N, 5.61. Found: C, 57.83; H, 6.89; N, 5.59 %.

$^{Mes} [CNH]Ir(COD)Cl$ (2.10). Synthetic procedure as described for compound **2.3** using 220 mg (0.6348 mmol) of **2.2** and 200 mg (0.2978 mmol) of $[Ir(COD)Cl]_2$. Slow evaporation from a concentrated solution of benzene yielded yellow crystals suitable for single crystal X-ray diffraction. Yield: 186 mg (91 %). 1H NMR (C_6D_6 , 400 MHz): δ 1.36 – 1.72 (m, -COD), 1.76 (s, 3H, -ArCH₃), 1.80 – 2.09 (m, -COD), 2.13 (s, 3H, -ArCH₃), 2.18 (s, 3H, -ArCH₃), 2.20 (s, 6H, -ArCH₃), 2.55 (s, 3H, -ArCH₃), 2.95 (br, 1H, -NH), 3.14 (t, 2H, -N_{Ar}CH₂), 3.38 (m, 2H, -COD), 4.51 (m, 1H, -COD), 4.72 (m, 1H, -COD), 4.94 (m, 2H, -N_{imid}CH₂), 5.97 (d, 1H, $J = 1.8$ Hz, -imidH), 6.44 (d, 1H, $J = 1.8$ Hz, -imidH), 6.70 (s, 1H, ArH), 6.78 (sh, 1H, ArH), 6.79 (s, 2H, ArH). ^{13}C NMR (CD_2Cl_2 , 100 MHz): δ 18.2, 18.6, 19.8, 20.9, 21.4(-ArCH₃), 29.2, 30.1, 32.9, 35.0 (-COD), 49.0 (-N_{Ar}CH₂), 51.6, 52.1 (-COD), 52.6 (-N_{imid}CH₂), 83.3, 83.4 (-COD), 121.9, 123.5 (-imidC), 128.7, 129.8, 129.9, 130.7 (-ArC), 132.4, 135.0, 136.6, 137.2, 139.3, 143.3 (-ArC_{ipso}), 180.7 (-IrC_NCN). EI-MS: 683 [M^+].

$^{Mes} [CN]Ir(COD)$ (2.11). Synthetic procedure as described for compound **2.5** using 116 mg (0.3021 mmol) of **2.1**, 140 mg (0.7018 mmol) of $KN(SiMe_3)_2$ and 92 mg (0.1370 mmol) of $[Ir(COD)Cl]_2$. Slow evaporation from a concentrated solution of hexanes yielded orange crystals suitable for single crystal X-ray diffraction. Yield: 72 mg (77 %). 1H NMR (C_6D_6 , 400 MHz): δ 1.32 – 1.80 (m, -COD), 1.95 – 2.29 (m, -COD), 2.10 (s, 3H, -ArCH₃), 2.21 (s, 6H, -ArCH₃), 2.33 (s, 3H, -ArCH₃), 2.59 (m, 2H, COD), 2.68 (s, 6H, -ArCH₃), 3.01 (m, 2H, -N_{Ar}CH₂), 3.65 (m, 2H, COD), 3.82 (m, 2H, -N_{imid}CH₂), 5.90 (d, 1H, $J = 1.4$ Hz, -imidH), 6.02 (d, 1H, $J = 1.4$ Hz, -imidH), 6.37 (s, 2H, ArH), 7.11 (s, 2H, ArH). ^{13}C NMR (C_6D_6 , 100 MHz): 18.9, 19.8, 21.4 (-ArCH₃), 31.4, 34.8, 45.4 (-COD), 54.4 (-N_{Ar}CH₂), 57.4 (-N_{imid}CH₂), 80.4 (-COD), 120.1, 122.3

(-imidC), 129.5, 129.8 (-ArC), 131.7, 135.7, 136.0, 138.5, 138.6, 156.2 (-ArC_{ipso}), 173.4 (-IrC_{N₃CN}). EI-MS: 647 [M⁺]. Anal. Calc. For C₃₁H₄₀N₃Ir: C, 57.56; H, 6.23; N, 6.50. Found: C, 56.98; H, 6.80; N, 6.33 %.

[^{Mes}[CNH]Ir(COD)]BF₄ (**2.12**). Synthetic procedure as described for compound **2.7** using 100 mg (0.1463 mmol) of **2.10** and 19 mg (0.1756 mmol) of NaBF₄. Yield: 72 mg (67 %). ¹H NMR (CD₂Cl₂, 400 MHz): δ 1.24 – 2.15 (m, -COD), 1.92 (s, 3H, -ArCH₃), 2.21 (s, 3H, -ArCH₃), 2.22 (s, 6H, -ArCH₃), 2.29 (s, 3H, -ArCH₃), 2.36 (s, 3H, -ArCH₃), 2.75 (s, 1H, -NH), 3.10, 3.18 (m, 2H, -COD), 3.51 (m, 2H, -N_{Ar}CH₂), 4.33 (m, 2H, -N_{imid}CH₂), 4.59 (m, 1H, -COD), 4.97 (m, 1H, COD), 6.81 (s, 2H, -ArH), 6.82 (sh, 1H, -imidH), 6.94 (s, 1H, -ArH), 7.04 (s, 1H, -ArH), 7.19 (d, *J* = 2.3 Hz, 1H, -imidH). ¹³C NMR (CD₂Cl₂, 100 MHz): δ 18.2, 18.7, 19.8, 21.4 (-ArCH₃), 29.3, 30.1, 33.0, 35.1 (-COD), 49.1 (-N_{Ar}CH₂), 51.62 (-COD), 52.1 (-N_{imid}CH₂), 52.6 (-COD), 83.3, 83.45 (-COD), 121.9, 123.5 (-imidC), 128.7, 129.8, 129.9, 130.8 (-ArC), 132.3, 135.0, 136.6, 137.3, 139.3, 143.3 (-ArC_{ipso}), 180.8 (IrC_{N₃CN}). EI-MS: 645 [M⁺ – BF₄].

Hydrogenation Procedures. The reactions were performed in thick-walled Teflon-sealed glass vessel, where the vessels were charged with 0.10 mL of substrate, 5 mol % catalyst, 5 mL of methylene chloride and pressurized with either 1 atm or 4 atm of hydrogen gas. The reactions with cyclohexene as the substrate were truncated at *t* = 15 min, 1 hr, 4 hrs and 12 hrs where an sample was taken from the vessel to determine conversion via ¹H NMR spectroscopy. From our preliminary results, significant conversions to hydrogenated substrates were not observed prior to the 4 and 12 hr mark using 4 and 1 atm of H₂ pressure respectively. When employing 1-methylcyclohexene as the substrate, it was found that the conversions were appreciably lower and the transformations occurred much more slowly. Select reactions were run with 1 atm of H₂ pressure for 12 hrs resulted in conversions no greater than 20 %. 4 atm reactions were performed with samples extracted and analyzed at *t* = 12 hrs, 72 hrs and 1.5 weeks.

Hydrosilylation Procedures. In a sealable J. Young NMR tube 0.009 mmol of catalyst was dissolved in 0.60 mL of CDCl_3 to which 0.077 mL (0.502 mmol) of dimethylphenylsilane and 0.05 mL (0.455 mmol) of phenylacetylene were added. The mixture was then heated to and maintained at 60 °C in an oil bath. The reaction progress was monitored by ^1H NMR observing the vinylic proton signals of the product isomers as a function of the silane and methine ^1H resonances from the substrates.

2.9 References

1. Arduengo, A. J., III Preparation of 1,3-disubstituted imidazolium salts. 91-US880 9114678, 19910214., 1991.
2. Wanzlick, H. W., *Angew. Chem. Int. Ed.* **1962**, *1*, 75.
3. Scholl, M.; Ding, S.; Lee, C. W.; Grubbs, R. H., *Org. Lett.* **1999**, *1*, 953.
4. Hahn, F. E.; Wittenbecher, L.; Van, D. L.; Frohlich, R., *Angew. Chem. Int. Ed.* **2000**, *39*, 541.
5. Enders, D.; Breuer, K.; Raabe, G.; Runsink, J.; Teles, J. H.; Melder, J.-P.; Ebel, K.; Brode, S., *Angew. Chem. Int. Ed.* **1995**, *34*, 1021.
6. Peris, E.; Crabtree, R. H., *Coord. Chem. Rev.* **2004**, *248*, 2239.
7. Mata, J. A.; Poyatos, M.; Peris, E., *Coord. Chem. Rev.* **2007**, *251*, 841.
8. Tulloch, A. A. D.; Danopoulos, A. A.; Kleinhenz, S.; Light, M. E.; Hursthouse, M. B.; Eastham, G., *Organometallics* **2001**, *20*, 2027.
9. McGuinness, D. S.; Cavell, K. J., *Organometallics* **2000**, *19*, 741.
10. Arnold, P. L.; Rodden, M.; Davis, K. M.; Scarisbrick, A. C.; Blake, A. J.; Wilson, C., *Chem. Commun.* **2004**, 1612; Arnold, P. L.; Scarisbrick, A. C.; Blake, A. J.; Wilson, C., *Chem. Commun.* **2001**, 2340.
11. Spencer, L. P.; Fryzuk, M. D., *J. Organomet. Chem.* **2005**, *690*, 5788.
12. Jimenez, M. V.; Perez-Torrente, J. J.; Bartolome, M. I.; Gierz, V.; Lahoz, F. J.; Oro, L. A., *Organometallics* **2008**, *27*, 224.
13. Arduengo, A. J., III; Harlow, R. L.; Kline, M., *J. Am. Chem. Soc.* **1991**, *113*, 361.
14. Mas-Marza, E.; Poyatos, M.; Sanau, M.; Peris, E., *Inorg. Chem.* **2004**, *43*, 2213; Poyatos, M.; Mas-Marza, E.; Mata, J. A.; Sanau, M.; Peris, E., *Eur. J. Inorg. Chem.* **2003**, 1215;

- Cesar, V.; Bellemin-Laponnaz, S.; Wadepohl, H.; Gade, L. H., *Chem. Eur. J.* **2005**, *11*, 2862.
15. Seayad, A. M.; Selvakumar, K.; Ahmed, M.; Beller, M., *Tetrahedron Lett.* **2003**, *44*, 1679.
 16. Yu, X.-Y.; Patrick, B. O.; James, B. R., *Organometallics* **2006**, *25*, 2359; Stradiotto, M.; Cipot, J.; McDonald, R., *J. Am. Chem. Soc.* **2003**, *125*, 5618; Sjoevall, S.; Johansson, M.; Andersson, C., *Organometallics* **1999**, *18*, 2198.
 17. Vazquez-Serrano, L. D.; Owens, B. T.; Buriak, J. M., *Chem. Commun.* **2002**, 2518; Crabtree, R., *Acc. Chem. Res.* **1979**, *12*, 331.
 18. Albrecht, M.; Crabtree, R. H.; Mata, J.; Peris, E., *Chem. Commun.* **2002**, 32; Burling, S.; Whittlesey, M. K.; Williams, J. M. J., *Adv. Synth. Catal.* **2005**, *347*, 591; Danopoulos, A. A.; Winston, S.; Motherwell, W. B., *Chem. Commun.* **2002**, 1376; Miecznikowski, J. R.; Crabtree, R. H., *Organometallics* **2004**, *23*, 629.
 19. Parent, J. S.; McManus, N. T.; Rempel, G. L., *Ind. Eng. Chem. Res.* **1996**, *35*, 4417; O'Connor, C.; Wilkinson, G., *J. Chem. Soc. A* **1968**, *11*, 2665; Osborn, J. A.; Jardine, F. H.; Young, J. F.; Wilkinson, G., *J. Chem. Soc. A* **1966**, *12*, 1711.
 20. Fairlie, D. P.; Bosnich, B., *Organometallics* **1988**, *7*, 936; Holliday, B. J.; Ulmann, P. A.; Mirkin, C. A.; Stern, C. L.; Zakharov, L. N.; Rheingold, A. L., *Organometallics* **2004**, *23*, 1671.
 21. Schrock, R. R.; Osborn, J. A., *J. Am. Chem. Soc.* **1976**, *98*, 4450; Crabtree, R. H., *Acc. Chem. Res.* **1979**, *12*, 331.
 22. Chalk, A. J.; Harrod, J. F., *J. Am. Chem. Soc.* **1965**, *87*, 16; Duckett, S. B.; Perutz, R. N., *Organometallics* **1992**, *11*, 90; Tanke, R. S.; Crabtree, R. H., *J. Am. Chem. Soc.* **1990**, *112*, 7984.

23. Reilly, T. J., *J. Chem. Educ.* **1999**, 76, 1557.
24. Bird, R.; Knipe, A. C.; Stirling, C. J. M., *J. Chem. Soc., Perkin Trans. 2* **1973**, 9, 1215.
25. Arduengo, A. J.; Gentry, F. P.; Taverkere, P. K.; Simmons, H. E. Process for manufacture of imidazoles. 6177575, January 23, 2001, 2001.
26. Chatt, J.; Venanzi, L. M., *J. Chem. Soc.* **1957**, 4735.
27. Abel, E. W.; Bennett, M. A.; Wilkinson, G., *J. Chem. Soc.* **1959**, 3178.
28. van der Ent, A.; Onderdelinden, A. L., *Inorg. Synth.* **1990**, 28, 92.

CHAPTER THREE

Coordinative and Catalytic Properties of Ruthenium(II) Complexes Containing a Hemilabile Amino-Functionalized N-Heterocyclic Carbene

3.1 Introduction

In the search for more efficient catalysts, ancillary ligand modifications on a proven catalyst precursor are useful to try to augment catalyst activity. This is certainly evident in the evolution of ruthenium-based metathesis catalysts for which improved versions have been discovered by changing one of the phosphine ligands to N-heterocyclic carbene (NHC) ligands.¹ The discovery that the lability and reassociative behavior of the *trans* ligand to the NHC is a key design feature was made by a number of different groups to significantly improve catalyst activity.¹⁻³ However, little focus has been put into studying the effects of having a chelating NHC ligand coordinated to these ruthenium-based systems.

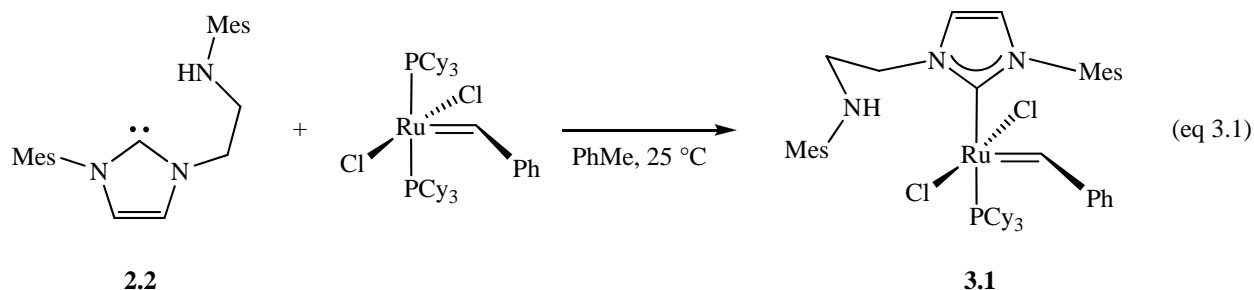
A version of this chapter will be submitted for publication.

Jong, H.; Fryzuk, M.D. (2010) Coordination Chemistry of a Hemilabile Amino-Tethered N-Heterocyclic Carbene on Ruthenium(II).

Our approach to ligand modifications relevant to this system is the incorporation of a hemilabile amino arm into the NHC to examine its effect in the stabilization of unsaturated intermediates. In this chapter the behavior of a tethered amino NHC ligand will be examined and shown that its effect is unfortunately mostly deleterious to catalysis. However, there are some intriguing effects on the coordination chemistry of these ruthenium benzylidene complexes that are explored herein that can be used to rationalize the observed catalytic behavior.

3.2 *Synthesis and Characterization of ^{Mes}[CNH]Ru(=CHPh)(PCy₃)Cl₂*

Analogues of Grubbs catalyst are relatively straightforward to synthesize as substitution of the phosphine units can proceed without complications when strongly σ -donating Lewis bases are added. Chapter 2 described the synthesis of a bidentate NHC ligand containing a mesitylamino tether, ^{Mes}[CNH], **2.2**.⁴ The addition of a single equivalent of **2.2** to Grubbs 1st generation bis-phosphine catalyst⁵ in a solution of toluene at room temperature generates the expected ^{Mes}[CNH]Ru(=CHPh)(PCy₃)Cl₂, **3.1**, product in good yield (eq 3.1).



This reaction is convenient as the starting compounds are tolerant of solvents such as CH₂Cl₂ and THF in addition to toluene and benzene. Moreover, the reaction time can be modulated with temperature as room temperature reactions are completed overnight whereas the equivalent result can be achieved by heating the mixture to 80 °C for 4 hours. Complex **3.1** is also fairly tolerant of air and moisture; however, it is best stored and handled under a dry inert atmosphere.

The formation of **3.1** can be followed as a function of time by withdrawing aliquots from the crude reaction mixture and monitoring the ^{31}P NMR spectrum to observe the resonances at δ 35.4 and 11.3 intensify (representing **3.1** and free PCy_3 , respectively) as the signal at δ 36.6 from Grubbs 1st generation catalyst recedes. A diagnostic doublet at δ 187.8 in the ^{13}C NMR spectrum with a coupling constant of $^2J_{\text{CP}} = 81$ Hz is assigned to the carbene coordinated to the Ru center and coupled to PCy_3 . However, a small amount of a side product was detected in concentrated samples and is discussed in the next section.

Magenta crystals of **3.1** suitable for single crystal X-ray diffraction studies can be obtained by slowly evaporating a concentrated solution of methylene chloride. Figure 3.1 depicts the solid-state molecular structure of $^{\text{Mes}}[\text{CNH}]\text{Ru}(=\text{CHPh})(\text{PCy}_3)\text{Cl}_2$. The geometry of **3.1** in the solid state is consistent with comparable analogues bearing slightly distorted square pyramidal geometry with the benzyldiene unit (C24) at the apical position. Table 3.1 outlines selected bond lengths and angles of **3.1** with its most similar structural counterparts, Grubbs 2nd generation catalyst **3.2**^{2, 6} and the IMes congener **3.3** developed simultaneously in the Nolan and Grubbs laboratories.⁷

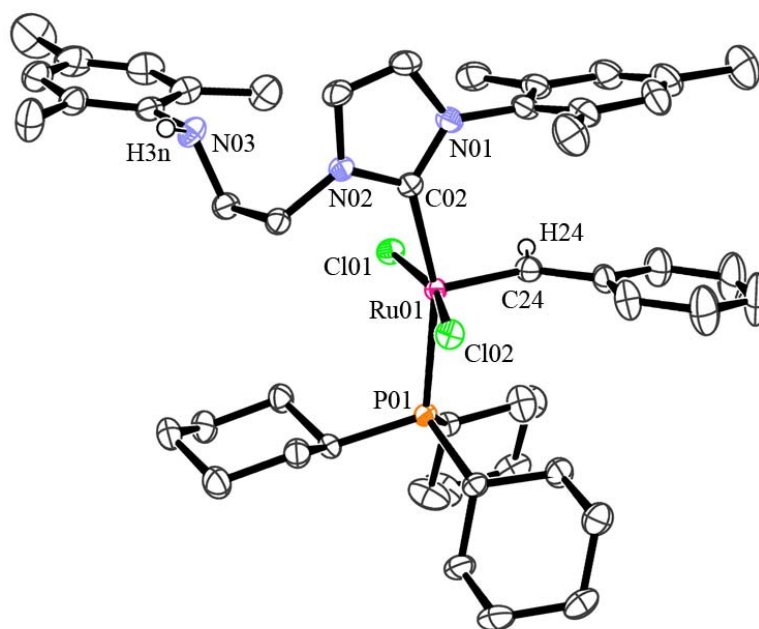
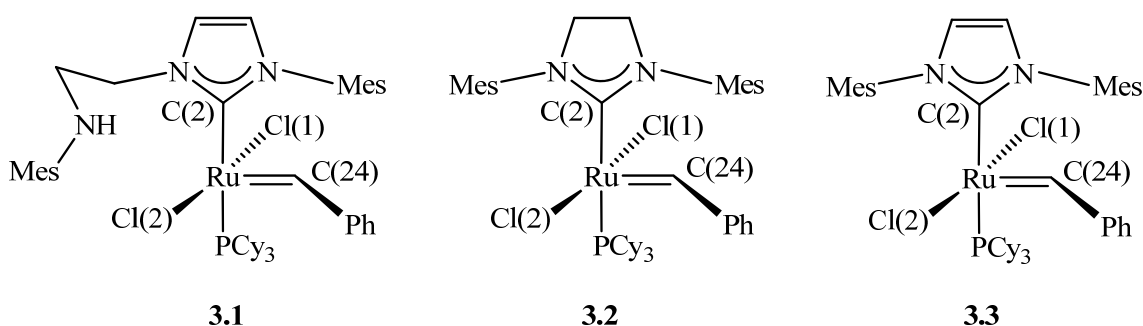


Figure 3.1. ORTEP view of $^{\text{Mes}}[\text{CNH}]\text{Ru}(=\text{CHPh})(\text{PCy}_3)\text{Cl}_2$, **3.1**, with thermal ellipsoids at 50 % probability. All hydrogens were removed for clarity except H3n and H24, which were located in a difference map and refined isotropically.

From inspection of the core bond lengths and angles of **3.1**, **3.2** and **3.3**, it is clear that there are negligible structural differences (Table 3.1). For example, the Ru(01)-C(02) bond length of 2.076(2) Å for compound **3.1** resides in between the values of 2.069(11) and 2.084(9) Å for **3.2** and **3.3**, respectively. The Ru(01)-C(24) benzylidene bond length of **3.1** was found to be virtually identical to that of **3.2** at 1.836(2) Å. The Ru(01)-P(01) bond length of 2.4386(6) Å for **3.1** was found to be slightly longer than that of **3.2** at 2.419(3) Å and that of **3.3** at 2.404(3) Å. Similarly, the bond angles for species **3.1** – **3.3** were comparable and varied only within a few degrees of each other.

Table 3.1. Selected bond lengths and angles for compounds **3.1**, **3.2** and **3.3**. Atom labels have been renamed for simplicity in comparative analysis.

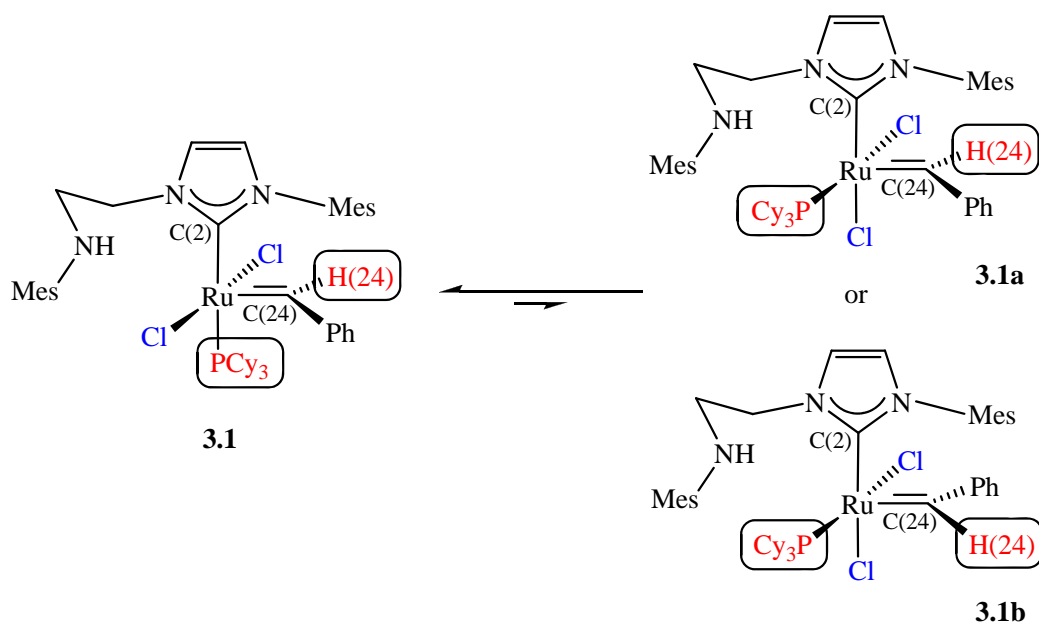


	3.1	3.2	3.3
Bond Lengths (Å)			
Ru-C(2)	2.076(2)	2.069(11)	2.084(9)
Ru-C(24)	1.836(2)	1.835(2)	1.841(11)
Ru-Cl(1)	2.4138(6)	2.393(3)	2.382(3)
Ru-Cl(2)	2.3959(6)	2.383(3)	2.392(2)
Ru-P	2.4386(6)	2.419(3)	2.404(3)
Bond Angles (°)			
C(24)-Ru-C(2)	97.99(10)	99.2(5)	98.7(4)
Cl(1)-Ru-C(24)	89.88(8)	87.1(5)	90.0(3)
Cl(2)-Ru-C(24)	105.01(8)	104.3(5)	102.9(3)
C(2)-Ru-Cl(1)	87.09(6)	86.9(3)	83.0(3)
Cl(1)-Ru-P	90.04(2)	89.86(9)	89.86(9)
Cl(1)-Ru-Cl(2)	165.06(2)	168.62(12)	166.96(9)
C(24)-Ru-P	99.61(8)	97.1(4)	93.5(3)
C(2)-Ru-P	162.31(7)	163.2(3)	167.1(3)

3.3 Isomerization of $^{Mes}[CNH]Ru(=CHPh)(PCy_3)Cl_2$ in Solution

When concentrated samples of **3.1** are probed by NMR spectroscopy, a second species can be detected in trace quantities with chemical shifts that are similar to those of **3.1**. The presence of the second species is likely an isomer, which is denoted **3.1a**. Complex **3.1a** is most easily identified by its benzylidene resonance (denoted H(24a)) at δ 20.08 in the 1H NMR spectrum that represents approximately a 1:7 ratio of the benzylidene signal of **3.1** at δ 19.19.

However, the H(24a) resonance is a $^3J_{\text{H(24a)-P}} = 12.9$ Hz doublet opposed to the singlet that represents **3.1**. The ^{31}P NMR spectrum confirms the presence of two phosphine species in solution with signals at δ 35.4 and 22.8 for **3.1** and **3.1a**, respectively, in approximately the same 7:1 integral ratio as observed in the ^1H NMR spectrum. Performing a $^1\text{H}\{^{31}\text{P}\}$ NMR experiment on the sample shows the δ 20.08 doublet collapse into a singlet, which gives evidence that H(24a) is coupled to the Ru-bound PCy_3 in solution at room temperature. Further evidence of the correlation was provided by the $^1\text{H}/^{31}\text{P}$ heteronuclear multiple bond correlation (HMBC) experiment to demonstrate the three-bond correlation between H(24a) and PCy_3 . No correlation was observed for H(24) with PCy_3 on **3.1**, which corroborates the H(24) singlet resonance in the ^1H NMR spectrum. Both phosphines showed correlation with cyclohexyl protons, which supports the presence of two Ru- PCy_3 species in solution. Figure 3.2 depicts the $^1\text{H}/^{31}\text{P}$ long-range correlation spectrum and Scheme 3.1 describes the proposed isomeric behavior.

Scheme 3.1[§]

[§] Neither complex **3.1a** or **3.1b** were isolated and its labeling scheme is intended only for consistency and simplicity with respect to comparisons with **3.1**.

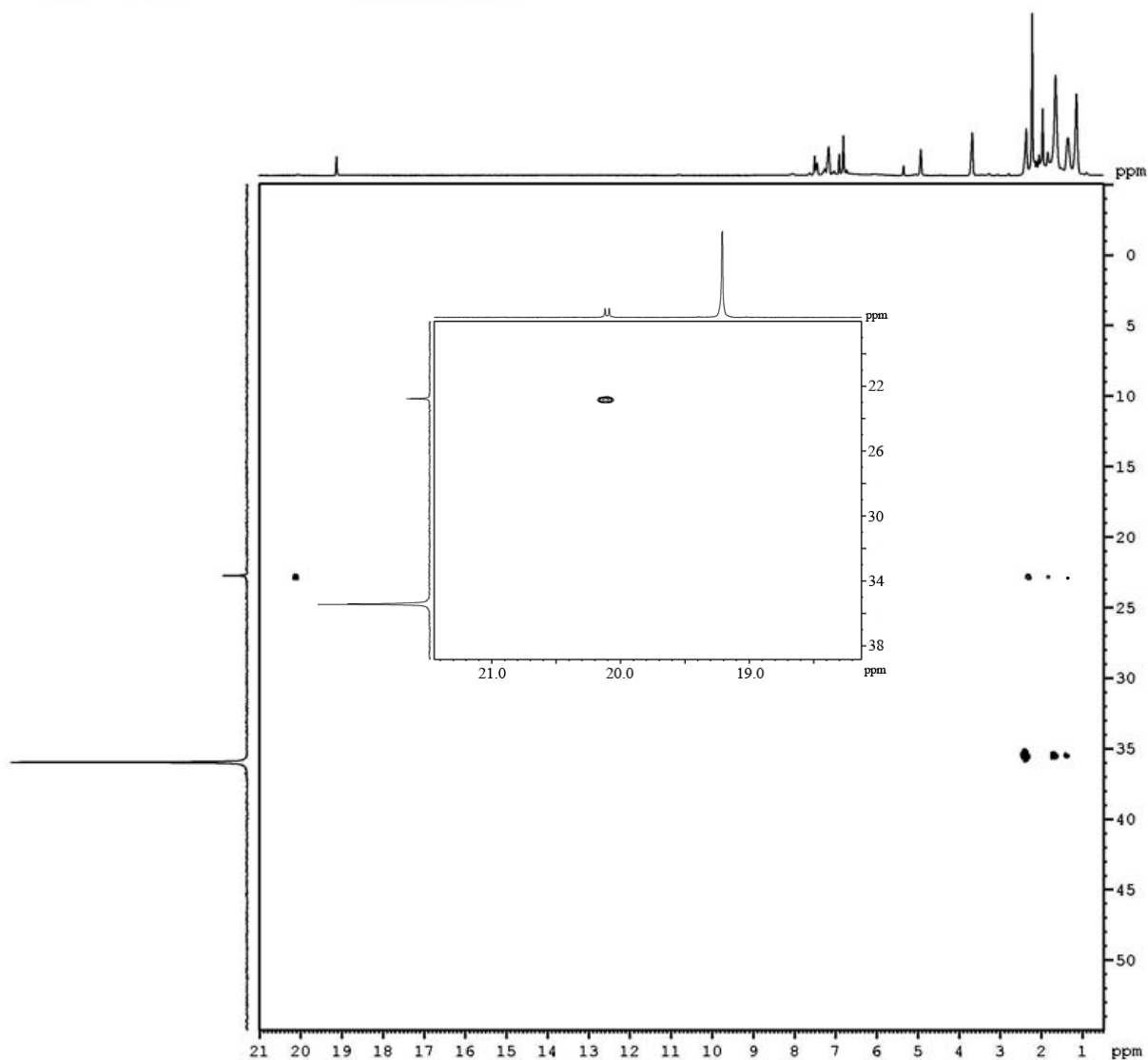


Figure 3.2. The $^1\text{H}/^{31}\text{P}$ HMBC spectrum of **3.1** and **3.1a** in CD_2Cl_2 . The inset is an expansion of the spectral region focused on the correlation between the benzylidene proton and PCy_3 .

The most likely structure of **3.1a** appears to be the result of a rearrangement of the *trans* disposed C(2)-Ru- PCy_3 unit of **3.1** to generate the *cis* positioned C(2a)-Ru- PCy_3 unit of **3.1a**. The new arrangement positions the PCy_3 ligand in **3.1a** in the plane of the benzylidene fragment and *anti* to H(24a) so that long-range coupling is more favorable. Analogous Ru compounds prepared by Fürstner and coworkers also show phosphine ligands oriented in the plane of the benzylidene unit (and *cis* to the NHC) and exhibits similar P—H coupling behavior. However,

inspection of the solid-state molecular structure of the Fürstner system reveals that their benzyldiene proton (H24) is oriented *syn* to PCy₃.⁸ Thus, a *syn* isomer is also possible for **3.1** and is denoted **3.1b** (Scheme 3.1). While identity of the minor isomer is equally probable to be either **3.1a** or **3.1b**, the remainder of the discussion will refer to **3.1a** as the minor (*cis*-oriented) product for simplicity and clarity.

The lack of P—H correlation between H(24) and PCy₃ in **3.1** is likely the result of PCy₃ being oriented orthogonal to the benzyldiene plane so that coupling is weak and unresolved in the ¹H NMR. An inverse-gated ¹³C NMR experiment was run on a 600 MHz spectrometer to meet signal sensitivity requirements and to provide quantitative integrations that further bolstered the presence of the two isomers in solution at room temperature. The doublet resonance at δ 306.0 (²J_{C(24)-P} = 12 Hz) was found in approximately a 1:7 ratio to the doublet at δ 294.5 (²J_{C(24)-P} = 7 Hz) representing complexes **3.1a** and **3.1**, respectively. A similar pattern was also found for the C(2)-P resonances at δ 187.8 (²J_{C(2)-P} = 81 Hz) and δ 182.7 (²J_{C(2)-P} = 104 Hz) for compounds **3.1** and **3.1a**, respectively, in a 7:1 ratio. The ¹³C NMR spectrum of the downfield resonances is shown in Figure 3.3.

Despite the presence of the both isomers in solution at room temperature, it was unclear whether or not the isomers were in equilibrium. Multiple syntheses of complex **3.1** with various batches of starting materials resulted in similar proportions of both isomers consistently. Variable temperature ¹H and ³¹P NMR experiments were performed with temperature ranges from 25 to -90 °C in CD₂Cl₂ and 25 to 100 °C in d₁₀-*o*-xylene to determine if it was possible to extract thermodynamic information to confirm the equilibrium. It was expected that the proportion of **3.1a** relative to **3.1** would change as the temperature decreased (and vice versa at higher temperatures), which would support the presence of an equilibrium. While the ratio of **3.1a** to **3.1** decreased to approximately 1:14 at -90 °C, the progression throughout the

temperature range was not smooth, as signal-to-noise ratios for the **3.1a** resonances became an issue, thus it was not possible to extract reliable quantitative thermodynamic information from the NMR experiments. Higher temperature experiments were not useful as phosphine dissociation became more prominent as temperature was increased, thus the presence of **3.1a** diminished with increasing temperature and eventually became immeasurable.

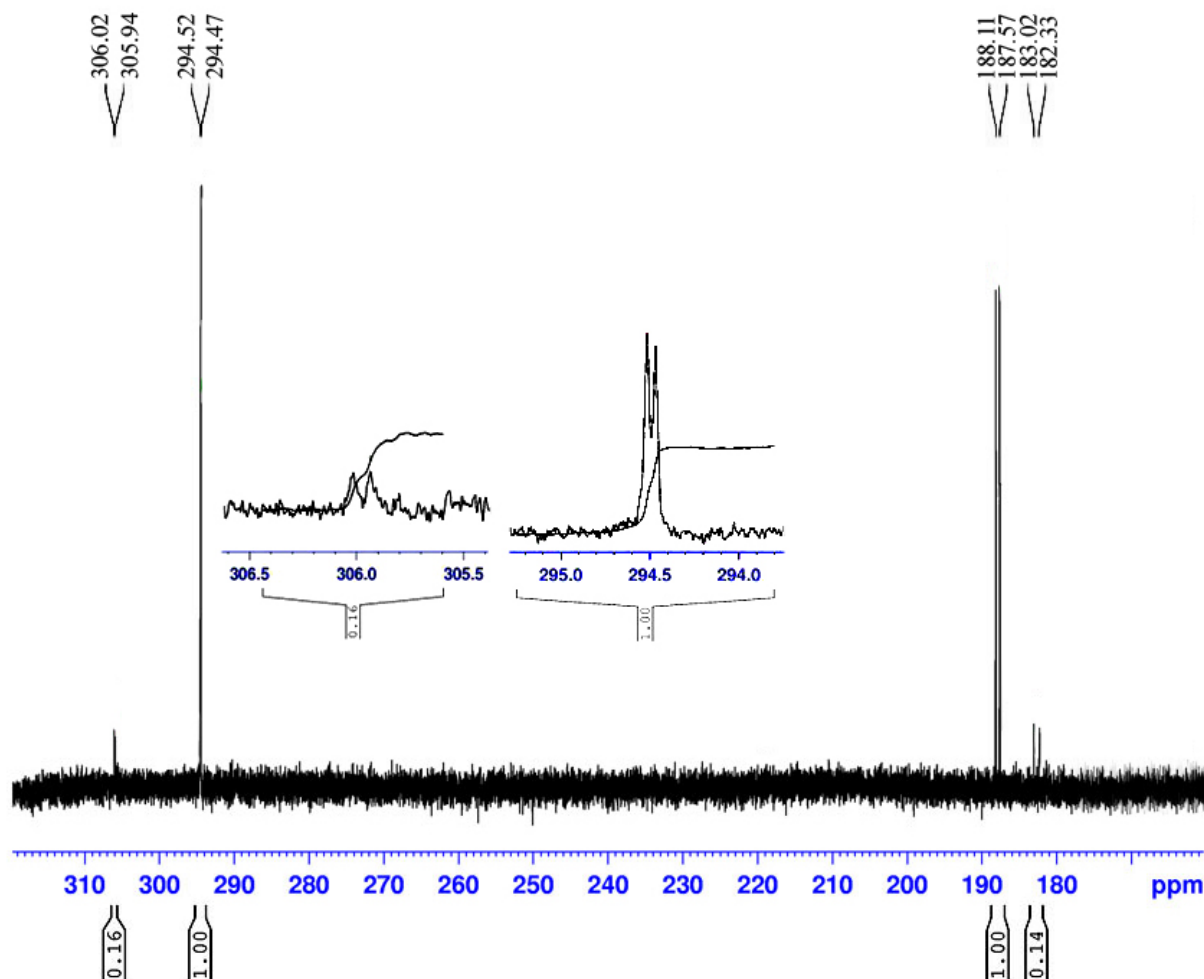


Figure 3.3. Downfield inverse-gated 151 MHz ^{13}C NMR spectrum of **3.1** and **3.1a** in CD_2Cl_2 .

A rationale for the formation of **3.1a** could likely be steric in nature as there have been no reports of this type of isomerization occurring with similar systems containing larger NHC ligands, such as SIMes or IMes, and bulky phosphines like PCy_3 as in complexes **3.2** and **3.3**, respectively. The flexible and less sterically encumbering tether of the $^{\text{Mes}}[\text{CNH}]$ ligand in **3.1**

would enable isomerization of the PCy₃ unit to a position that would presumably not be possible with bulkier NHC flanking substituents. The Ru complexes isolated by Fürstner and coworkers as well as other systems that contain less bulky NHC substituents are also known to exhibit *cis/trans* rearrangement.^{8,9} While the identity of the minor isomer is most likely as proposed in Scheme 3.1, the Grubbs group has suggested that the minor product could also be a rotamer that arises from rotation about the Ru—C(2) and Ru—C(24) bonds.¹⁰ Since rotation about these Ru-carbene bonds are known, a rotameric species of **3.1** cannot be discounted.^{11, 12} Despite the presence of **3.1a**, the catalytic activity of **3.1** was explored. The results demonstrate that the existence of **3.1a** in solution is largely inconsequential as it has been suggested that a *cis*-isomer, such as **3.1a**, would reconvert back to the *trans*-isomer (**3.1**) during catalysis, particularly at higher temperatures.⁸

3.4 RCM and ROMP Catalytic Reactions with ^{Mes}[CNH]Ru(=CHPh)(PCy₃)Cl₂

Catalytic ring-closing metathesis (RCM) and ring-opening metathesis polymerization (ROMP) reactions of **3.1** were investigated and benchmarked with both Grubbs 1st and 2nd generation catalysts to determine the effects of incorporating the ^{Mes}[CNH] ligand. The olefin substrates selected for RCM were diethyl diallylmalonate (**S1**) and 1,6-heptadien-4-ol (**S2**). Diethyl diallylmalonate is commonly used as the benchmark RCM substrate whereas 1,6-heptadien-4-ol was chosen for its selectivity towards being effectively metathesized by Grubbs 2nd generation catalyst while remaining inert to Grubbs 1st generation catalyst.² This preferential character of **S2**'s reactivity enabled an investigation of the effect of having an NHC unit in **3.1**. 1,5-cyclooctadiene (**S3**) was selected for the ROMP study as its results with various catalysts are well documented and easily employed as a benchmark substrate.

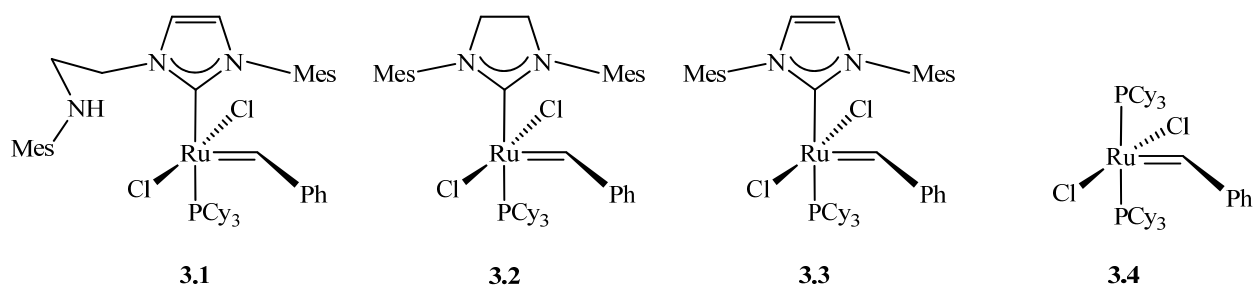


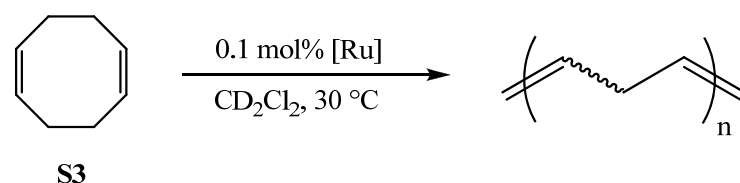
Table 3.2. RCM results for **3.1** compared with reference catalysts¹³ under similar conditions.

<p style="text-align: center;">S1</p>		<p style="text-align: center;">S2</p>	
Catalyst	<i>t</i> (min)	Conversion (%) ^a	
		S1	S2
3.1	30	25	
3.1	18 (hrs)	50	
3.1	24 (hrs)	-	no reaction
3.2	30	96	
3.2	40	> 98	
3.2^b	10	-	> 98
3.3	30	74	
3.3	80	> 95	
3.3	N/A	-	-
3.4	30	66	
3.4	76	> 74	
3.4^b	24 (hrs)	-	no reaction

^a Conversions measured by ¹H NMR

^b Values obtained from literature²

Table 3.3. ROMP results for **3.1** compared with reference catalysts¹³ under similar conditions.



Catalyst	<i>t</i> (min)	Conversion (%) ^a
3.1	4 (hrs)	> 75
3.2	6	> 99
3.3	80	> 99
3.4	90	> 40

^a Conversions measured by ¹H NMR

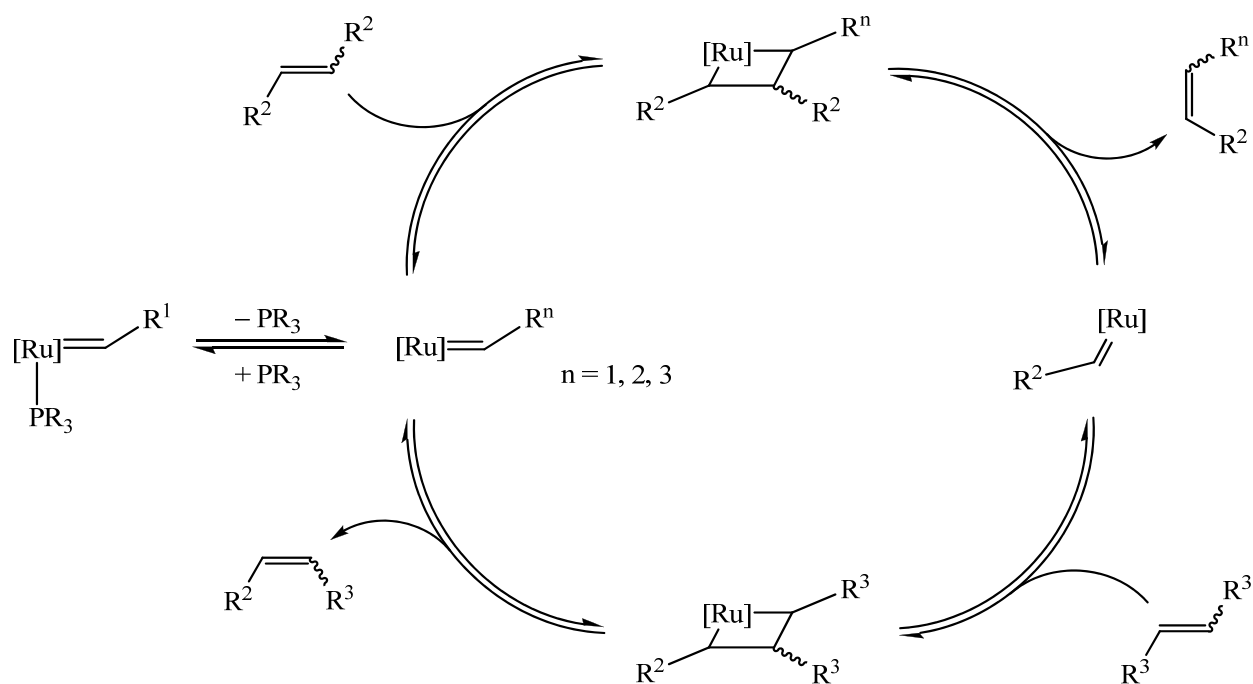
RCM reactions were performed with 1 mol % of catalyst in CD₂Cl₂ and run at 30 °C with conversion monitored by ¹H NMR. Investigation of the RCM experiments using ^{Mes}[CNH]Ru(=CHPh)(PCy₃)Cl₂ to catalyze **S1** and **S2** gave disappointing results. It was found that precursor **3.1** was completely inactive towards **S2** even at slightly elevated temperatures (40 °C), increased catalyst loadings (5 mol %), and long reaction times. Interestingly, the activity of **3.1** with **S1** also exhibited poor conversions and long reactivity times compared with Grubbs 1st (**3.4**) and 2nd (**3.2**) generation catalysts. Selected results from the RCM test reactions are summarized in Table 3.2 with the corresponding reference catalysts.¹³

It is clear that the change from having SIMes incorporated as in catalyst **3.2**, instead of the unsaturated IMes as in **3.3**, produced far superior results in terms of activity when performing RCM and ROMP reactions. However, the relative underperformance of **3.1** (as outlined in Table 3.2 and Table 3.3) cannot solely be attributed to the electronic differences between the saturated and unsaturated backbone of the NHC ligand, thus it was pertinent to probe what else was inhibiting the metathesis process.

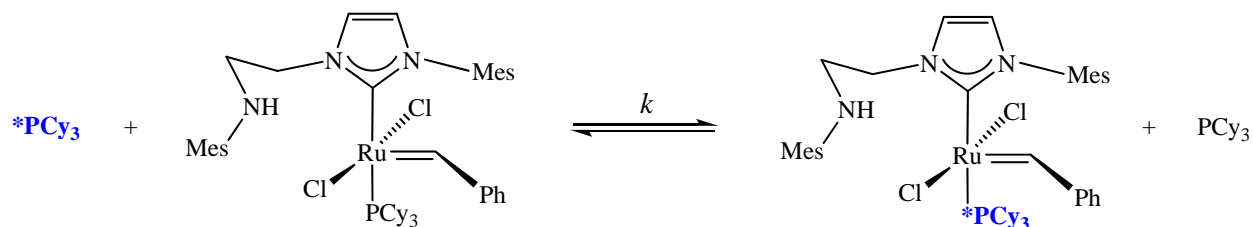
3.5 Measurement of Phosphine Exchange Rates via Magnetization Transfer

Having already shown that there are insignificant structural differences between **3.1** and its analogues, it was necessary to investigate how else the presence of the ^{Mes}[CNH] ligand could negatively impact the metathesis mechanism. It is commonly accepted that the active Ru catalyst is generated via the dissociation of the tricyclohexylphosphine (PCy₃) ligand,¹⁴ which directly correlates to the rate of catalyst initiation. Although the overall activity of the catalyst is dependent on other factors as well, the dissociation step is critical as it dictates the rate of entry of the precursor into the catalytic cycle.⁶ Scheme 3.2 outlines the generally accepted mechanism for the olefin metathesis process with Ru precursors.^{15, 16} Thus, it was essential that we determine and compare the rate of phosphine dissociation of **3.1** to known systems to better comprehend factors that may be responsible for its subpar catalytic activity.

Scheme 3.2



Scheme 3.3



Measuring the phosphine exchange rate between two identical species in solution can be used as a model to probe the dissociation rate of the phosphine ligand from the Ru precursor. Since phosphine exchange is a relatively slow process (as demonstrated by other similar Ru examples), ³¹P NMR spectroscopy can be used to probe the rate of phosphine exchange as described by Scheme 3.3. Using an analogous model to the original phosphine exchange study devised by Grubbs *et al.*¹⁷ for direct comparison, magnetization transfer (MT) studies were used to measure the rate constants (*k*) of **3.1** for the phosphine exchange process outlined in Scheme 3.3. The samples were prepared in solutions of d₁₀-*o*-xylene for improved solubility and a higher boiling point compared to d₈-toluene. The MT experiments were conducted by selectively inverting the free phosphine resonance via a shaped pulse and the ³¹P NMR spectra were obtained with various mixing times (21 experiments ranging from 0.000003 to 30 s). The time dependent magnetization data was analyzed and fitted with CIFIT¹⁸ software to determine the phosphine exchange rates of **3.1**. Figure 3.4 shows the Eyring plot from the MT phosphine exchange experiments of **3.1**.

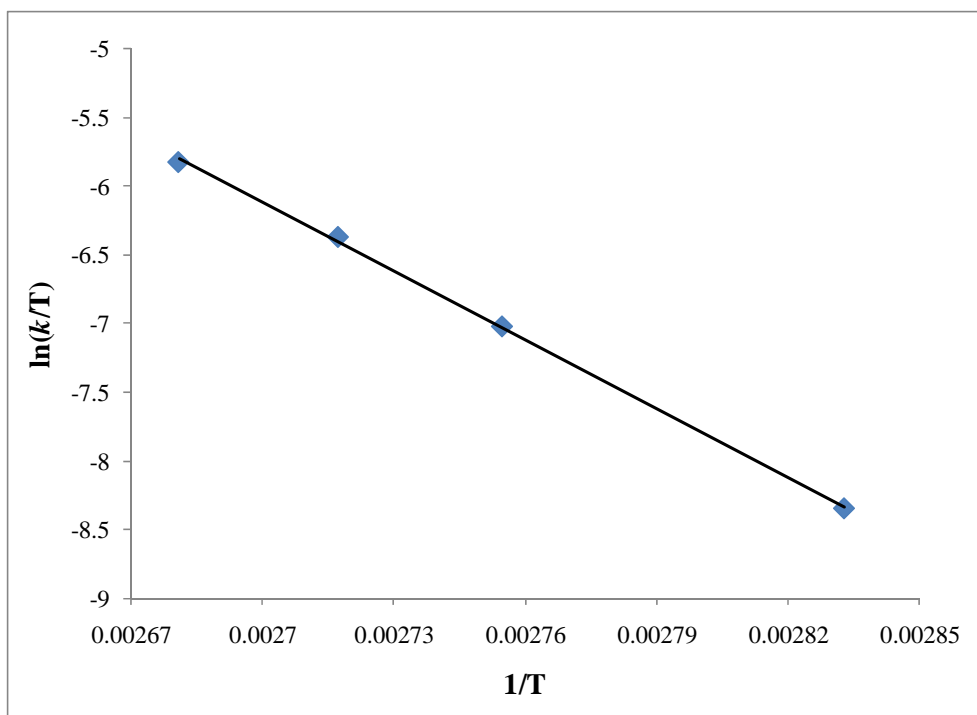


Figure 3.4. The Eyring plot of the phosphine exchange experiments for **3.1**.

Analyzing the rate of phosphine exchange for reference catalysts **3.2** – **3.4**, it was found that they all exhibit a similar sensitivity to temperature variation. However, it was interesting to see that when the phosphine exchange rates of **3.1** were compared to the reference catalysts, the exchange rates for **3.1** were much more sensitive to temperature changes. The increased temperature sensitivity could be attributed to the higher entropy of activation (ΔS^\ddagger) of **3.1** when compared with compounds **3.2** – **3.4**, which all had comparable ΔS^\ddagger values within experimental error. Possible rationalization of the higher ΔS^\ddagger value of **3.1** could be that in solution it is a fluxional, weakly coordinating, tethered amino complex, which is not observed in the solid-state. Thus, upon activation, both PCy_3 and the amino tether dissociate from Ru and produce a higher ΔS^\ddagger value than complexes **3.2** – **3.4** that do not incorporate a hemilabile amino arm. There is little empirical evidence from variable-temperature (VT) NMR spectroscopy to support the rapidly exchanging coordination/dissociation process of the amino tether of **3.1** in solution. However,

the mechanism appears to be the most likely rationale to account for the larger ΔS^\ddagger relative to its reference complexes. Despite a larger ΔS^\ddagger value being favorable for precursor activation, the value of ΔH^\ddagger of **3.1** is also higher, thus results in a ΔG^\ddagger value that is similar to its reference compounds at room temperature.

Extrapolation of the Eyring plots can be used as an estimation of initiation kinetics for the precursors.¹⁶ Extrapolation to an experimental temperature of 40 °C shows more realistic variance in initiation rates. Under normal conditions, it can be assumed that the phosphine dissociation rate of **3.1** was similar in magnitude to both **3.2** and **3.3** (its closest structural congeners). The rate differences between them are further abated as the reaction temperature increases, yet in terms of overall activity they differed significantly.

Table 3.4. Phosphine dissociation rate constants and activation parameters determined by magnetization transfer experiments for **3.1** – **3.4**.

Catalyst	40°C ^a	k (s ⁻¹)		ΔH^\ddagger	ΔS^\ddagger	ΔG^\ddagger (25°C)
		80°C	100°C	(kcal/mol)	(eu)	(kcal/mol)
3.1	$(1.8 \pm 0.4) \times 10^{-4}$	0.083 ± 0.004	1.09 ± 0.05	33 ± 1	30 ± 2	24 ± 1
3.2 ^b	$(8.8 \pm 0.2) \times 10^{-4}$	0.13 ± 0.01	1.02 ± 0.02	27 ± 2	13 ± 6	23.0 ± 0.4
3.3 ^b	$(2.8 \pm 0.2) \times 10^{-4}$	0.03 ± 0.01	0.23 ± 0.2	25 ± 4	6 ± 11	24 ± 1
3.4 ^b	$(1.18 \pm 0.02) \times 10^{-1}$	9.6 ± 0.2^a	63.0 ± 0.8	23.6 ± 0.5	12 ± 2	19.88 ± 0.06

^a Values extrapolated from Eyring plots

^b Data obtained from ref 14

Complex **3.1** was the only example that was not able to metathesize the substrate to completion even with prolonged reaction times. RCM reactions involving **3.1** and **S1** at 100 °C in d₁₀-*o*-xylene showed improved activity, but overall conversion greater than 70 % would require in excess of 30 hours to achieve as outlined in Figure 3.5. The outcome ultimately implies that it is unlikely that the phosphine dissociation rate of **3.1** is the primary cause of the inefficient RCM process.

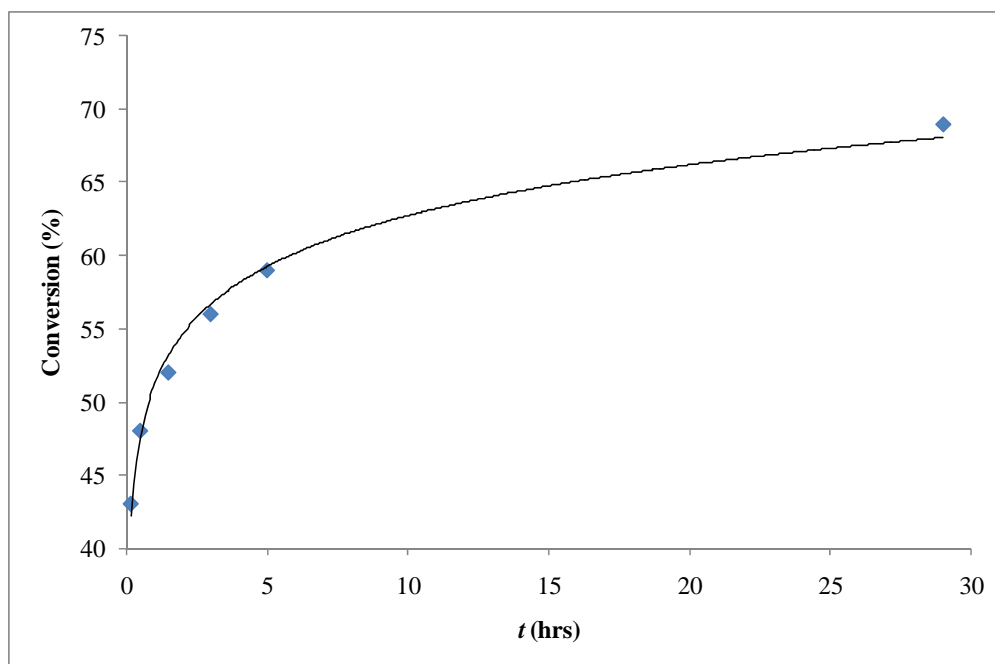


Figure 3.5. The RCM conversion of **S1** catalyzed by **3.1** at 100 °C in d_{10} -*o*-xylene.

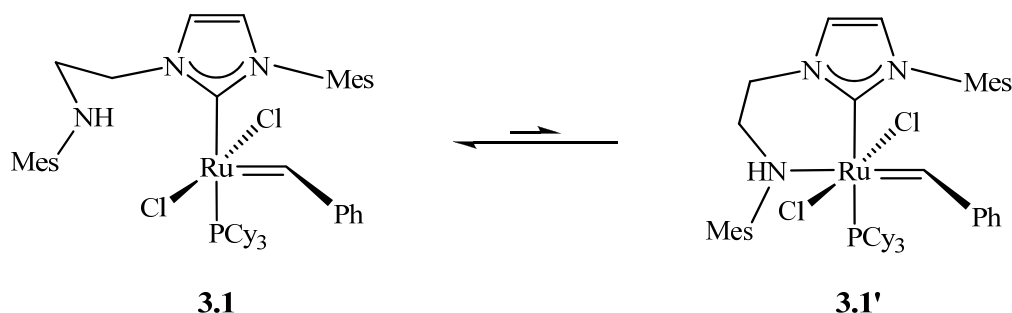
3.6 Investigating the Coordinative Propensity of the Amino Tether of



Another avenue that may be a hindrance to RCM and ROMP catalysis is the participation of the pendant amine in $^{Mes}[CNH]Ru(=CHPh)(PCy_3)Cl_2$. Considering the square-pyramidal geometry of **3.1**, the exposed face of the pyramid may be vulnerable to attack from the amino tether (Scheme 3.4), thus forming an 18-electron complex that is potentially inactive to metathesis. While the coordination of the pendant amine could be rapid and fluxional, a bound tether would impose an additional dissociative barrier on the precursor, thereby hindering the initiation of the active 14-electron catalyst. It has been shown that ethylene build-up (in a closed system) generated as a by-product in metathesis may be responsible for forming an 18-electron species that can interfere, or even shut down catalysis.⁶ Therefore, interaction of the amino tether

from **3.1** may behave similarly to a bound ethylene species impeding metathesis of the substrates. However, the likelihood of this process to occur depends on whether or not steric congestion around Ru becomes an issue due to the bulkiness of the mesitylamino substituent and the cyclohexylphosphine group.

Scheme 3.4

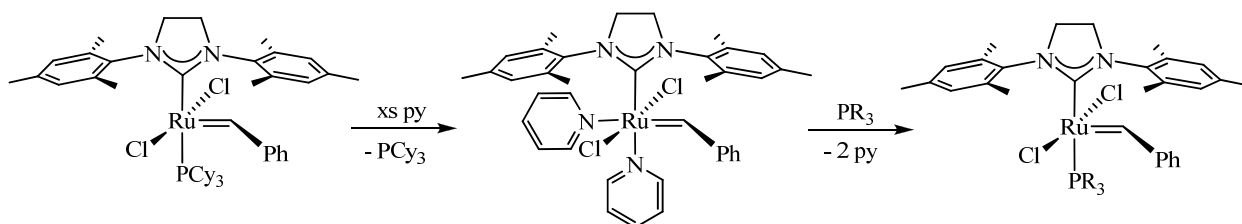


3.7 Synthesis, Characterization of $^{\text{Mes}}[\text{CNH}]\text{Ru}(=\text{CHPh})(\text{py})\text{Cl}_2$ and

$^{\text{Mes}}[\text{CNH}]\text{Ru}(=\text{CHPh})(\text{PMe}_3)\text{Cl}_2$

Comparative metathesis reactions with Ru precursors that contained different phosphine dissociating ligands could provide further insight into how the amino tether could interrupt the catalytic cycle. A common approach to synthesizing these analogues is to proceed through a mediating complex. The addition of pyridine to Ru precursors is known to displace the coordinated phosphine group to generate an octahedral bis-pyridine species that can be easily isolated and is reactive towards other phosphine ligands to yield Ru-PR₃ derivatives,¹⁹ as outlined in Scheme 3.5.

Scheme 3.5



When a similar approach was taken with complex **3.1** to synthesize its pyridine derivative, the result was not the anticipated bis-pyridine species. Rather it was a mono-bound pyridine product with the pendant amino arm of the ^{Mes}[CNH] ligand coordinated to the Ru center. This resultant 18-electron complex, ^{Mes}[CNH]Ru(=CHPh)(py)Cl₂ (**3.5**) is, to the best of our knowledge, the first example of a Grubbs catalyst derivative incorporating a bidentate amino-NHC ligand. Compound **3.5** features a green color that is similar to the bis-pyridine-Ru complex, **3.6**.¹⁹ Single crystals suitable for X-ray diffraction studies for **3.5** can be grown via slow evaporation from a concentrated solution of toluene. The solid-state molecular structure is represented in Figure 3.6.

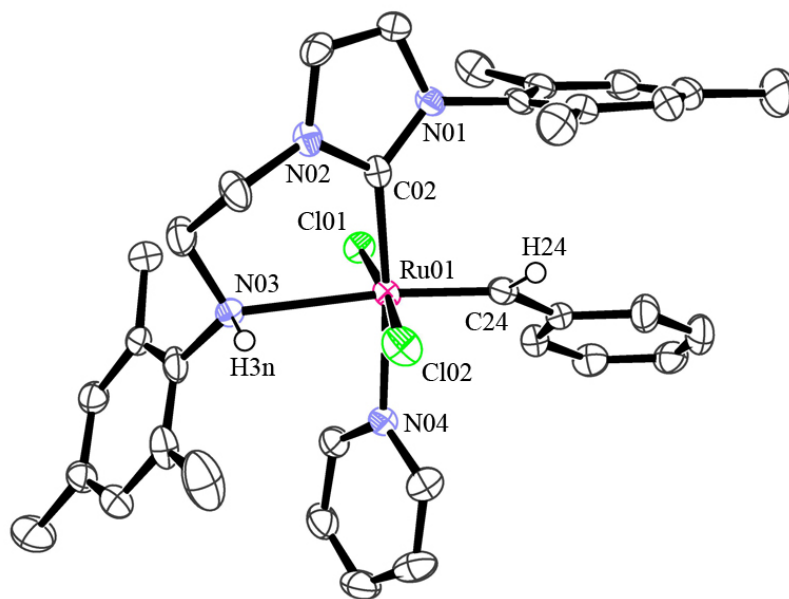
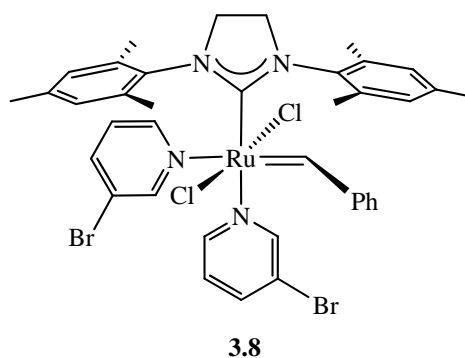
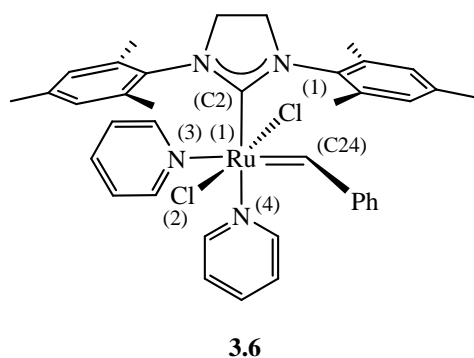


Figure 3.6. ORTEP view of ^{Mes}[CNH]Ru(=CHPh)(py)Cl₂, **3.5**, with thermal ellipsoids at 50 % probability. All hydrogens were removed for clarity except H3n and H24, which were located and refined isotropically.

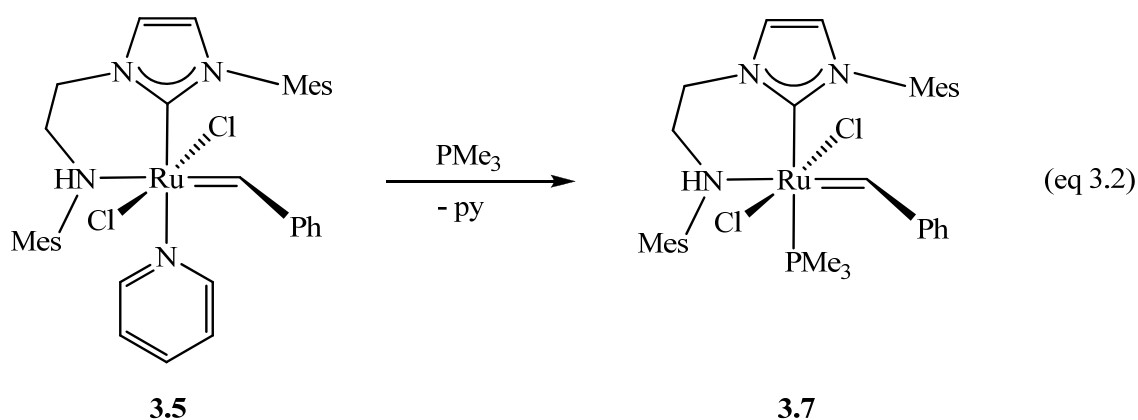
Table 3.5. Selected bond lengths and angles for complexes **3.5** – **3.7**.

	3.5	3.6	3.7
Bond Length (Å)			
Ru01-C02	2.037(2)	2.033(4)	2.092(2)
Ru01-N04	2.173(2)	2.203(3)	2.390(1)
Ru01-C24	1.849(2)	1.873(4)	1.860(2)
Ru01-N03	2.516(5)	2.372(4)	2.579(2)
Ru01-Cl01	2.3849(7)	2.400(1)	2.4136(4)
Ru01-Cl02	2.4165(7)	2.423(1)	2.4097(4)
Bond Angles (°)			
C02-Ru01-C24	94.1(1)	93.6(2)	92.51(7)
C02-Ru01-N04	173.51(8)	176.4(1)	176.99(5)
C02-Ru01-N03	88.7(1)	102.9(1)	86.29(6)
C02-Ru01-Cl01	92.45(7)	93.8(1)	89.05(5)
C02-Ru01-Cl02	87.36(7)	84.4(1)	89.98(5)
C24-Ru01-N04	91.62(9)	87.1(2)	88.16(5)
C24-Ru01-N03	170.8(2)	161.2(1)	177.59(6)
C24-Ru01-Cl01	97.54(8)	100.6(1)	100.33(5)
C24-Ru01-Cl02	88.08(8)	84.8(1)	87.60(5)
Cl01-Ru01-Cl02	174.37(2)	174.5(1)	172.04(2)



The geometry of $^{\text{Mes}}[\text{CNH}]\text{Ru}(=\text{CHPh})(\text{py})\text{Cl}_2$ is octahedral with bond lengths and angles that are consistent with analogous Ru complexes.²⁰ Comparisons of **3.5** can be made with **3.6** to highlight slight differences between them. The Ru(01)-N(04) distance of 2.173(2) Å in **3.5** was found to be marginally shorter than the 2.203(3) Å of **3.6**. However, the Ru(01)-N(03) distance of 2.516(5) Å in **3.5** is significantly longer than the 2.372(2) Å bond in **3.6**. This may provide insight into the coordinative strength of the bound pendant amine in **3.5** as it was determined that

the bound N(03) positioned pyridine in **3.6** was loosely coordinated and was volatile under vacuum,¹⁹ a result that was substantiated by its elongated Ru-N bond length.



Despite the potentially weakly coordinating amino tether of **3.5**, further reactivity with bulkier phosphines such as triphenylphosphine was not possible. However, addition of a smaller phosphine like trimethylphosphine to **3.5** yielded ^{Mes}[CNH]Ru(=CHPh)(PMe₃)Cl₂ (**3.7**) as shown in eq 3.2. Complex **3.7** had a resonance at δ -14.3 and was absent of the free PMe₃ resonance at δ - 62 in the ³¹P NMR spectrum. The lack of resonances attributed to the pyridine unit and the observation of a PMe₃ doublet at δ 0.78 (²J_{HP} = 8.8 Hz) in the ¹H NMR spectrum corroborated the ligand substitution. A solid-state molecular structure of **3.7** was obtained and shown in Figure 3.7.

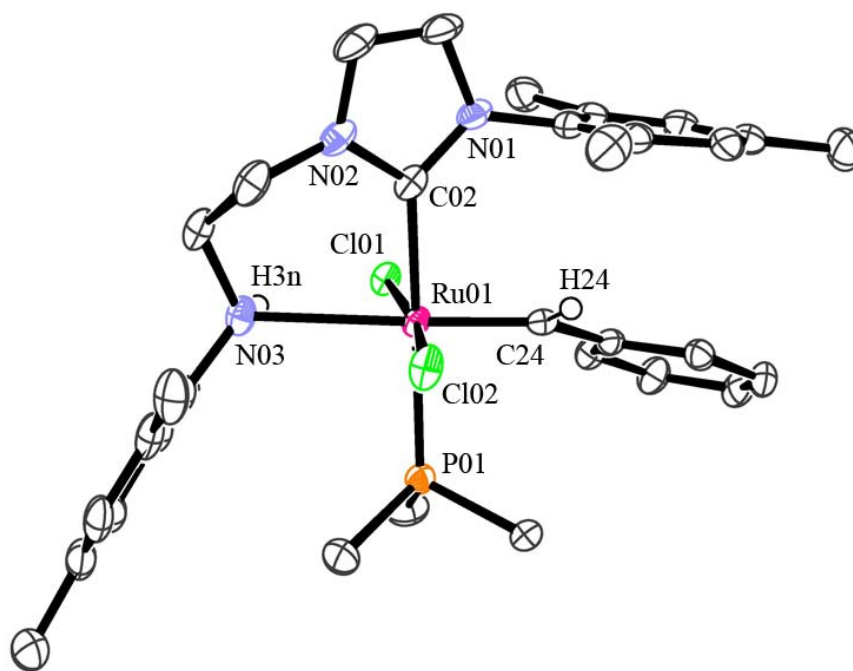


Figure 3.7. ORTEP view of $^{\text{Mes}}[\text{CNH}]\text{Ru}(=\text{CHPh})(\text{PMe}_3)\text{Cl}_2$, **3.7**, with thermal ellipsoids at 50 % probability. All hydrogens were removed for clarity except H3n and H24, which were located and refined isotropically.

Structurally, **3.7** possesses similar characteristics to **3.5**. The two were differentiated most significantly by the C(02)-Ru(01) bond length of 2.092(2) Å that was more comparable to **3.1**. The Ru-N(03) bond length of 2.579(2) Å was also found to be slightly longer than **3.5** at 2.516(5) Å. Having isolated a second example demonstrating the coordinative ability of the amino unit of the $^{\text{Mes}}[\text{CNH}]$ ligand, the assumption that the tethered arm of **3.1** was disruptive in the catalytic cycle of olefin metathesis becomes more convincing. The propensity of coordination of the amino arm (Scheme 3.4) appears to be highly dependent on the steric bulk of its flanking ligand. The difference in size of pyridine and PMe_3 relative to PCy_3 is clearly the determining factor as it enables the amino tether spatial freedom to coordinate easily. It is unclear at this point whether coordination of the amino unit is favored given the orientation and bulk of the PCy_3 ligand. However, it is highly likely that coordination occurs once PCy_3 has

dissociated from the metal center. From the magnetization transfer experiments of **3.1**, it appeared that the propensity to bind the pendant amine did not significantly affect the rate of phosphine dissociation.

Attempts to regenerate **3.1** via the addition of PCy₃ would be expected to fail as the cone angle of PCy₃ (170 °) is larger than that of PPh₃ (145 °).²¹ Yet **3.1** can indeed be regenerated by the addition of PCy₃ to complex **3.5**, but only to a maximum yield of 29 % after 24 hours as indicated by ³¹P NMR. The result implied that the electronic properties of the phosphine ligands took precedent over steric bulk in these substitution examples as the increased electron-donating property of PCy₃ was sufficient to displace the coordinated pyridine on **3.5** (albeit in low yield) despite its larger physical size relative to PPh₃. The result differed greatly from those of **3.6**, which had demonstrated its coordinated pyridine ligands were substitutionally labile to PCy₃, PPh₃ and even electron-deficient phosphines such as P(*p*-CF₃C₆H₄)₃. The innate resistance of **3.5** to react with PPh₃ led to investigation of its ability to undergo RCM and ROMP catalysis as it had previously been shown that bis-pyridine complexes such as **3.6** and **3.8** were efficient metathesis precursors.^{19, 22}

3.8 RCM and ROMP Activity of ^{Mes}[CNH]Ru(=CHPh)(py)Cl₂

RCM conversions of substrates **S1** and **S2** were 10 and 4 %, respectively after 45 min when **3.5** was used as a catalyst. The results clearly demonstrated that **3.5** underperformed **3.1** with **S1** under similar experimental conditions. However, it was interesting to see that although conversion was low, compound **3.5** was able to perform RCM on **S2** where complex **3.1** was completely resistant. Over an extended reaction period, the transformation of **S1** with **3.5** did not improve beyond 10 % where the conversion of **S2** increased to 30 % after 12 hours at 30 °C. The pyridine derivative **3.5** also fared poorly against **3.1** in parallel ROMP reactions with **S3** yielding 30 and 57 %, respectively, after corresponding reaction times of 4 and 12 hours. The results from

the RCM and ROMP tests indicated that the activity of precursor **3.5** was inferior to its benchmarks despite besting **3.1** in the RCM conversion of **S2**. It appeared that the initiation process of **3.5** to transition from the 18-electron state to the active 14-electron catalyst was likely a primary reason for it being a substandard metathesis agent as 18-electron Ru precursors have been linked to poor catalytic activity in prior studies.⁶ The isolation of **3.5** and its apparent low metathesis activity lead to the inference that coordination of the tethered amine in **3.1**, either prior to or during the catalytic cycle, was likely to be a principal cause for the lacklustre RCM and ROMP activity observed relative to its benchmark precursors.

Table 3.6. Entries 1 – 4 show RCM results for 1 mol % of **3.5**. Entries 5 – 6 show ROMP data for 0.1 mol % of **3.5**. All reactions performed at 30 °C in CD₂Cl₂.

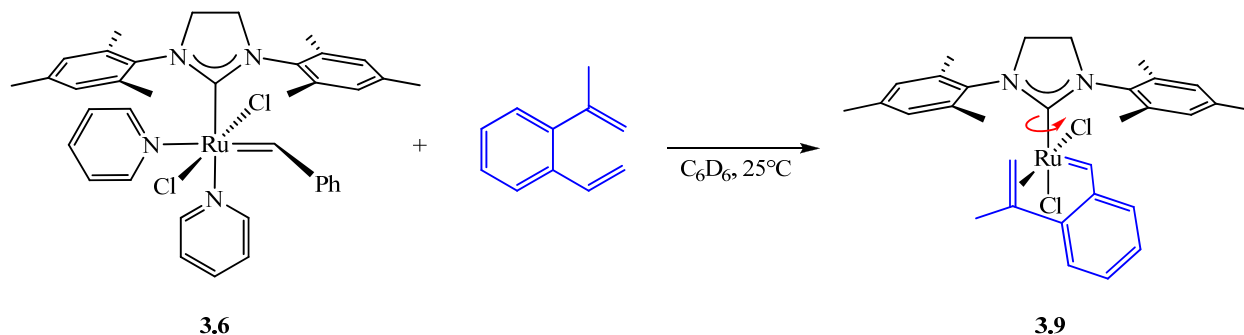
Entry	Substrate	Conversion (%)	<i>t</i> (hrs)
1	S1	10	0.75
2	S1	10	12
3	S2	4	0.75
4	S2	30	12
5	S3	30	4
6	S3	57	12

3.9 *Insight into Mechanism of^{Mes}[CNH]Ru(=CHPh)(PCy₃)Cl₂ in Metathesis*

Although the potential likelihood of the pendant amine on **3.1** coordinating with the Ru center and perturbing the catalytic process was high, its implications are expected to be more complex. Recent in depth reports investigating the mechanism of the metathesis process of Grubbs-type catalysts have revealed that isomerization of the substituents likely occurs in order to facilitate lower energy pathways for the metathesis to proceed efficiently.^{12, 23} The mechanistic studies effectively simulated the metathesis process at the point of coordination. An intermediate species was trapped to gain insight into how the complexes' behaved under experimental

conditions. The employment of divinylbenzene, or a substituted variation, was used to mimic two incoming olefinic substrates. However, with the substrates being linked by a rigid benzyl backbone, it was possible to probe the metallocyclic intermediate with NMR spectroscopy. The results from the NMR experiments, and the isolation of a solid-state molecular structure of intermediate **3.9**, exposed an isomer of the initial catalyst where the *trans*-disposed chloride ligands had become *cis* to one another. The isomerization process was concurrently accompanied by a *cis* alignment of the two vinyl substituents of the divinylbenzene substrate. To structurally facilitate the *cis*-disposed motif of the substrate, the NHC ligand had rotated about its vertically bound axis. Scheme 3.6 outlines the development.

Scheme 3.6



If the metathesis mechanism ensues through the isomerized intermediate **3.9**, the coordination of the tethered amino group of **3.1** would significantly encumber the catalyst's ability to isomerize. Therefore, it can be concluded that the inclusion of chelating NHC ligands should be regarded more as a liability rather than an upgrade when designing novel Grubbs-type Ru precursors. However, if the coordination of the tether was to be used intentionally as a stereo-directing feature,²⁴ it should be anchored to the metal center opposed to having hemilabile character as exemplified by the pendant amino arm of **3.1**, **3.5** and **3.7**.

3.10 Conclusions

In summary, three novel derivatives of Grubbs catalyst containing an amino-NHC ligand were synthesized and fully characterized. With **3.9** demonstrating the ability of these Ru-NHC systems to isomerize, the proposed accompaniment of **3.1** by **3.1a** in solution becomes much more plausible. However, the fluxional nature of the chloro and phosphine ligands in **3.1** does not appear to materially affect the phosphine dissociation process. It was also shown that the coordinative potential of the tethered amino group of **3.1** was likely disruptive in the catalytic process of RCM and ROMP reactions involving substrates **S1** – **S3**. The isolation and poor activity of **3.5** led to the inference that the hemilabile amino arm was responsible for the catalytic impediment. Its coordination yielded an 18-electron Ru complex that proved to be an additional activation barrier that was counterproductive to the generation of the active 14-electron catalytic species. Although an amino form of **3.1** was never detected spectroscopically, it is reasonable to assume that the amino tether could coordinate either prior to, or after, dissociation of the PCy₃ ligand during the catalytic initiation process, which would be an additional hurdle negatively affecting RCM and ROMP activity. The isolation of **3.7** reinforced the assumption that the tethered amino arm of **3.1** would coordinate to Ru if given the spatial freedom by its flanking ligands. To date, there are few reports that involve chelating NHC ligand based Ru precursors used for RCM and ROMP applications. However, this could be an area of growing interest as the development of Ru precursors for stereo-specific applications becomes more popular. Avenues to manipulate the hemilabile nature of **2.2** will be explored in the following chapters.

3.11 Experimental Section

General Considerations. Unless otherwise specified, all experimental procedures were performed in a dry, oxygen-free nitrogen or argon atmosphere by Schlenk or glovebox techniques. Compound **2.2** was synthesized as previously described.⁴ 1,5-cyclooctadiene was dried over activated 4 Å molecular sieves and distilled into Teflon-sealed glass vessel. Grubbs 1st generation catalyst Ru(=CHPh)(PCy₃)Cl₂ (**3.4**) and all other chemicals were purchased commercially and used as received. Anhydrous toluene, hexanes and pentane were purchased from Aldrich, sparged with nitrogen, and passed through columns containing activated alumina and Ridox catalyst. Methylene chloride and tetrahydrofuran were purified similarly, except without treatment with Ridox catalyst. Deuterated benzene (C₆D₆) was purified via refluxing under nitrogen with CaH₂ then vacuum transferred in to a Teflon-sealed glass vessel containing 4 Å molecular sieves. Gases were removed by three freeze-pump-thaw cycles. Deuterated methylene chloride (CD₂Cl₂) was purified in a similar manner as C₆D₆. ¹H, ¹³C and ³¹P NMR spectra were obtained by a Bruker AVANCE 300, 400 or 600 MHz spectrometer. Elemental analysis and mass spectrometry (EI/MS) were performed at the Department of Chemistry at the University of British Columbia.

Mes[CNH]Ru(=CHPh)Cl₂PCy₃ (3.1). A 5 mL toluene solution containing 507 mg (1.458 mmol) was added slowly to 1.0 g (1.215 mmol) of Ru(=CHPh)(PCy₃)Cl₂ dissolved in 10 mL of toluene. The resultant mixture was allowed to stir overnight. The solution was concentrated under vacuum and hexanes was added to precipitate the magenta product, which was collected on a glass frit and washed with hexanes. Yield: 930 mg (86 %). ¹H NMR (400 MHz, CD₂Cl₂) δ: 1.14 (br, -PCy₃), 1.36 (m, -PCy₃), 1.65 (br, -PCy₃), 1.95 (br, 6H, -ArCH₃), 2.22 (br, 9H, -ArCH₃), 2.40 – 2.32 (br, 6H, -ArCH₃, -PCy₃), 3.60 (br, 1H, -NH), 3.69 (m, 2H, -N_{Mes}CH₂), 4.94 (m, 2H, -N_{imid}CH₂), 6.80 (s, 2H, -MesH), 6.88 (d, 1H, *J* = 1.7 Hz, -imidH), 7.32 – 7.07 (m, 6H, -MesH, -

ArH), 7.43 (m, 1H, -ArH), 7.47 (d, 1H, $J = 1.7$ Hz, -imidH), 19.19 (s, 1H, -RuCHPh). ^{13}C NMR (151 MHz, CD_2Cl_2) δ : 18.50, 18.73, 20.86, 21.26, 21.70 (-ArCH₃), 27.23 (-PCy₃), 28.38 (d, $^2J_{\text{CP}} = 9.7$ Hz, -PCy₃), 30.06 (-PCy₃), 32.05 (d, $^1J_{\text{CP}} = 16$ Hz, -PCy₃), 48.96 (-N_{Mes}CH₂), 51.49, (-N_{imid}CH₂), 122.7, 124.1 (d, $^4J_{\text{CP}} = 2$ Hz, -imidC), 125.8, 129.5, 129.8 (-*m*-Ar_{Mes}C), 128.5, 128.7, 129.1 (-ArC), 129.4, 131.1, 132.2, 136.6, 136.8, 139.1, 143.6 (-Ar_{Mes}C_{ipso}), 151.8 (-ArC_{ipso}), 187.8 (d, $^2J_{\text{CP}} = 81$ Hz, -RuC_{NCN}), 294.5 (d, $^2J_{\text{CP}} = 7$ Hz, -Ru=CHPh). ^{31}P NMR (162 MHz, CD_2Cl_2) δ : 35.4 (s, Ru-PCy₃). Anal. Calcd for C₄₈H₆₈N₃Cl₂PRu: C, 64.78; H, 7.70; N, 4.72. Found: C, 65.00; H, 7.49; N, 4.67.

Mes₃[CNH]Ru(=CHPh)Cl₂(py) (3.5). To 100 mg (0.1123 mmol) of **3.1** dissolved in 10 mL of toluene was added 1 mL of pyridine dropwise to the stirring solution. A color change from maroon to green is observed upon stirring for 10 min. The reaction was allowed to stir for 30 min total at which the solution was concentrated and pentane was added to afford a green suspension that was cooled to -30 °C before filtration. The green product was dried under vacuum. X-ray suitable crystals can be grown via slow evaporation from a concentrated sample in methylene chloride. Yield: 50 mg (73 %). ^1H NMR (400 MHz, CD_2Cl_2) δ : 2.04 (s, 3H, -ArCH₃), 2.06 (s, 3H, -ArCH₃), 2.28 (s, 6H, -ArCH₃), 2.42 (s, 6H, -ArCH₃), 3.61 (m, 2H, -N_{Mes}CH₂), 4.74 (m, 2H, -N_{imid}CH₂), 6.02 (t, 2H, $J = 7.1$ Hz, -*m*-pyH), 6.17 (s, 1H, -imidH), 6.42 (s, 1H, -imidH), 6.46 (br, 1H, -*p*-pyH), 6.51 (s, 2H, -MesH), 6.57 (s, 2H, -MesH), 6.95 (t, 2H, $J = 7.1$ Hz, -*m*-PhH), 7.23 (sh, 1H, -*p*-PhH), 7.30 (br, 1H, -NH), 8.16 (d, 2H, $J = 7.1$ Hz, -*o*-PhH), 8.50 (d, 2H, $J = 6.1$ Hz, -*o*-pyH), 19.8 (s, 1H, -RuCHPh). ^{13}C NMR (151 MHz, CD_2Cl_2) δ : 19.34, 20.81, 21.34, 21.53 (-ArCH₃), 51.19 (-N_{Mes}CH₂), 52.93 (-N_{imid}CH₂), 122.5 (-*m*-pyC), 123.2, 124.0 (-imidC), 127.8, 129.6, 129.7, 130.5, 131.5, 131.6 (-ArC), 132.5 (-ArC_{ipso}), 135.4 (-*p*-pyC), 137.5, 137.7, 138.6, 145.1, 153.3 (-ArC_{ipso}), 153.8 (-*o*-pyC), 185.1 (-RuC_{NCN}), 320.0 (-RuCHPh). Anal. Calcd for C₃₀H₄₀N₄Cl₂Ru: C, 61.04; H, 5.85; N, 8.14. Found: C, 61.21; H, 5.96; N, 8.47.

$\text{Mes}[\text{CNH}]\text{Ru}(=\text{CHPh})\text{Cl}_2(\text{PMe}_3)$ (**3.7**). To a 10 mL toluene solution containing 110 mg (0.1597 mmol) of $\text{Mes}[\text{CNH}]\text{Ru}(=\text{CHPh})(\text{py})\text{Cl}_2$ was added 0.02 mL (0.1940 mmol) of PMe_3 at room temperature. The green mixture was allowed to stir for 1 hr and tested for completion periodically via unlocked ^{31}P NMR. The solution was then concentrated and hexanes was added to afford a dark green suspension. The suspension was chilled to $-35\text{ }^\circ\text{C}$ before being filtered. The green product was collected and washed with hexanes followed by drying under vacuum. X-ray suitable crystals can be grown via slow evaporation from a concentrated toluene solution. Yield: 74 mg (68 %). ^1H NMR (400 MHz, C_6D_6) δ : 0.78 (d, 9H, $^2J_{\text{HP}} = 8.8\text{ Hz}$, $-\text{PCH}_3$), 1.91 (s, 3H, $-\text{ArCH}_3$), 2.15 (s, 9H, $-\text{ArCH}_3$), 2.6 (s, 6H, $-\text{ArCH}_3$), 3.39 (m, 2H, $-\text{N}_{\text{Mes}}\text{CH}_2$), 4.64 (m, 2H, $-\text{N}_{\text{imid}}\text{CH}_2$), 6.17 (s, 1H, $-\text{imidH}$), 6.21 (br, 1H, $-\text{NH}$), 6.35 (br, 3H, imidH , $-\text{MesH}$), 6.78 (s, 2H, $-\text{MesH}$), 7.02 (t, 2H, $-\text{m-PhH}$), 7.24 (t, 1H, $-\text{p-PhH}$), 8.29 (d, 2H, $J = 7.5\text{ Hz}$, $-\text{o-PhH}$), 20.0 (s, 1H, $-\text{RuCHPh}$). ^{13}C NMR (151 MHz, CD_2Cl_2) δ : 11.0 (d, $^1J_{\text{CP}} = 25\text{ Hz}$, $-\text{P}(\text{CH}_3)_3$), 16.1, 17.7, 18.1, 18.4 ($-\text{ArCH}_3$), 48.4 ($-\text{N}_{\text{Mes}}\text{CH}_2$), 50.03 ($-\text{N}_{\text{imid}}\text{CH}_2$), 122.9, 123.1 (d, $^4J_{\text{CP}} = 3\text{ Hz}$, imidC), 128.7, 128.8, 129.5, 129.6, 130.6 ($-\text{ArC}$), 131.7, 132.0, 132.1, 136.9, 137.9, 138.5, 147.0, 154.3 ($-\text{ArC}_{\text{ipso}}$), 189.7 (d, $^2J_{\text{CP}} = 100\text{ Hz}$, $-\text{RuC}_{\text{NCN}}$), 311.0 (d, $^2J_{\text{CP}} = 127$, $-\text{Ru}=\text{CHPh}$). ^{31}P NMR (162 MHz, C_6D_6) δ : -14.2 (s, $-\text{Ru-PMe}_3$). Anal. Calcd for $\text{C}_{33}\text{H}_{44}\text{N}_3\text{Cl}_2\text{PRu}$: C, 57.81; H, 6.47; N, 6.13. Found: C, 58.22; H, 5.95; N, 6.12.

Magnetization Transfer. A sealable J. Young NMR tube was charged with 17.0 mg (0.0191 mmol) of complex **3.1**, 8.0 mg (0.0287 mmol) of PCy_3 and 0.6 mL of d_{10} -*o*-xylene. The suspension was then allowed to thermally equilibrate at the experimental temperature at which point the contents will have completely dissolved (minimum temperature of $80\text{ }^\circ\text{C}$ required). The free PCy_3 resonance was selectively inverted via a 180 ° Gaussian 1.1000 shaped pulse with a duration of p22:50 ms at power level sp2. 21 progressive mixing times ranging from 0.000003 to 30 s were run and a subsequent non-selective 90 ° pulse was applied to record the FID. ^1H

decoupling with WALTZ-16 was applied during the 90 ° pulse. Signal integrals of both the coordinated and free PCy₃ were analyzed with the CIFIT software to obtain phosphine exchange rate constants. Standard T₁ recovery experiments were performed at each temperature and analyzed with the CIFIT program. The pulse sequence, sample plots of the fitted data and the values collected for the construction of the Eyring plot of **3.1** can be found in the Appendix A. Eyring plot data for compounds **3.2**, **3.3** and **3.4** were attained from their original source.¹⁶

General Procedures for RCM of S1. To a Teflon sealed J. Young NMR tube was added 1.650 μmol of Ru catalyst, 0.040 mL (0.1650 mmol) of diethyl diallylmalonate and 0.60 mL of CD₂Cl₂. The sample was then heated to 30 °C and conversion was determined by ¹H NMR using the ratio of methylene signals of the product relative to the substrate. Conversions of highly active catalysts are measured by equilibrating the sample containing the dissolved catalyst to 30 °C in the NMR probe before injection of the substrate via syringe.

General Procedures for RCM of S2. Procedures are as described for RCM of **S1** using 0.021 mL (0.1650 mmol) of 1,6-heptadien-4-ol, 8.250 μmol of Ru catalyst and 0.62 mL of CD₂Cl₂.

General Procedures for ROMP of S3. Procedures are as described for RCM of **S1** using 0.020 mL (0.1650 mmol) of 1,5-cyclooctadiene, 0.10 mL of 1.65 mM solution (0.1650 μmol) of Ru catalyst in CD₂Cl₂ and 0.52 mL of CD₂Cl₂.

3.12 References

1. Samojlowicz, C.; Bieniek, M.; Grela, K., *Chem. Rev.* **2009**, *109*, 3708.
2. Scholl, M.; Ding, S.; Lee, C. W.; Grubbs, R. H., *Org. Lett.* **1999**, *1*, 953.
3. Garber, S. B.; Kingsbury, J. S.; Gray, B. L.; Hoveyda, A. H., *J. Am. Chem. Soc.* **2000**, *122*, 8168; Grela, K.; Harutyunyan, S.; Michrowska, A., *Angew. Chem., Int. Ed.* **2002**, *41*, 4038; Gessler, S.; Randl, S.; Blechert, S., *Tetrahedron Lett.* **2000**, *41*, 9973; Wakamatsu, H.; Blechert, S., *Angew. Chem., Int. Ed.* **2002**, *41*, 2403.
4. Jong, H.; Patrick, B. O.; Fryzuk, M. D., *Can. J. Chem.* **2008**, *86*, 803.
5. Schwab, P.; Grubbs, R. H.; Ziller, J. W., *J. Am. Chem. Soc.* **1996**, *118*, 100.
6. Love, J. A.; Sanford, M. S.; Day, M. W.; Grubbs, R. H., *J. Am. Chem. Soc.* **2003**, *125*, 10103.
7. Huang, J.; Stevens, E. D.; Nolan, S. P.; Petersen, J. L., *J. Am. Chem. Soc.* **1999**, *121*, 2674; Scholl, M.; Trnka, T. M.; Morgan, J. P.; Grubbs, R. H., *Tetrahedron Lett.* **1999**, *40*, 2247.
8. Pruhs, S.; Lehmann, C. W.; Furstner, A., *Organometallics* **2004**, *23*, 280.
9. Benitez, D.; Goddard, W. A., *J. Am. Chem. Soc.* **2005**, *127*, 12218; Barbasiewicz, M.; Szadkowska, A.; Bujok, R.; Grela, K., *Organometallics* **2006**, *25*, 3599; Diesendruck, C. E.; Tzur, E.; Ben-Asuly, A.; Goldberg, I.; Straub, B. F.; Lemcoff, N. G., *Inorg. Chem.* **2009**, ASAP; Diesendruck, C. E.; Tzur, E.; Ben-Asuly, A.; Goldberg, I.; Straub, B. F.; Lemcoff, N. G., *Inorg. Chem.* **2009**, *48*, 10819.
10. Keitz, B. K.; Grubbs, R. H., *Organometallics* **2010**, *29*, 403.
11. Grisi, F.; Costabile, C.; Gallo, E.; Mariconda, A.; Tedesco, C.; Longo, P., *Organometallics* **2008**, *27*, 4649; Anderson, D. R.; Hickstein, D. D.; O'Leary, D. J.; Grubbs, R. H., *J. Am. Chem. Soc.* **2006**, *129*, 8386; Stewart, I. C.; Benitez, D.; O'Leary,

- D. J.; Tkathouk, E.; Day, M. W.; Goddard III, W. A.; Grubbs, R. H., *J. Am. Chem. Soc.* **2009**, *131*, 1931; Fournier, P.-A.; Savoie, J.; Stenne, B.; Bedard, M.; Grandbois, A.; Collins, S. K., *Chem. Eur. J.* **2008**, *14*, 8690.
12. Anderson, D. R.; O'Leary, D. J.; Grubbs, R. H., *Chem. Eur. J.* **2008**, *14*, 7536
 13. Ritter, T.; Hejl, A.; Wenzel, A. G.; Funk, T. W.; Grubbs, R. H., *Organometallics* **2006**, *25*, 5740.
 14. Dias, E. L.; Nguyen, S. T.; Grubbs, R. H., *J. Am. Chem. Soc.* **1997**, *119*, 3887; Ulman, M.; Grubbs, R. H., *Organometallics* **1998**, *17*, 2484; Vyboishchikov, S. F.; Buhl, M.; Thiel, W., *Chem. Eur. J.* **2002**, *8*, 3962.
 15. Herisson, J.-L.; Chauvin, Y., *Makromol. Chem.* **1971**, *141*, 161; Katz, T. J.; McGinnis, J., *J. Am. Chem. Soc.* **1975**, *97*, 1592; Grubbs, R. H.; Burk, P. L.; Carr, D. D., *J. Am. Chem. Soc.* **1975**, *97*, 3265; Katz, T. J.; Rothchild, R., *J. Am. Chem. Soc.* **1976**, *98*, 2519; Grubbs, R. H.; Carr, D. D.; Hoppin, C.; Burk, P. L., *J. Am. Chem. Soc.* **1976**, *98*, 3478.
 16. Sanford, M. S.; Love, J. A.; Grubbs, R. H., *J. Am. Chem. Soc.* **2001**, *123*, 6543.
 17. Sanford, M. S.; Ulman, M.; Grubbs, R. H., *J. Am. Chem. Soc.* **2001**, *123*, 749.
 18. Bain, A. D.; Kramer, J. A., *J. Magn. Reson.* **1996**, *118A*, 21.
 19. Sanford, M. S.; Love, J. A.; Grubbs, R. H., *Organometallics* **2001**, *20*, 5314.
 20. Abdur-Rashid, K.; Guo, R.; Lough, A. J.; Morris, R. H.; Song, D., *Adv. Synth. Catal.* **2005**, *347*, 571; Occhipinti, G.; Bjorsvik, H.-R.; Tornroos, K. W.; Jensen, V. R., *Organometallics* **2007**, *26*, 5803.
 21. Tolman, C. A., *Chem. Rev.* **1977**, *77*, 313.
 22. Love, J. A.; Morgan, J. P.; Trnka, T. M.; Grubbs, R. H., *Angew. Chem., Int. Ed.* **2002**, *41*, 4035.

23. Stewart, I. C.; Benitez, D.; O'Leary, D. J.; Tkatchouk, E.; Day, M. W.; Goddard III, W. A.; Grubbs, R. H., *J. Am. Chem. Soc.* **2009**, *131*, 1931.
24. Van Veldhuizen, J. J.; Garber, S. B.; Kingsbury, J. S.; Hoveyda, A. H., *J. Am. Chem. Soc.* **2002**, *124*, 4954; Hoveyda, A. H.; Gillingham, D. G.; Van Veldhuizen, J. J.; Kataoka, O.; Garber, S. B.; Kingsbury, J. S.; Harrity, J. P. A., *Org. Biomol. Chem.* **2004**, *2*, 8.

CHAPTER FOUR

Ligand Modifications: Derivatives, Congeners and Metallation of ^{Mes}[CNH]

4.1 Introduction

It has been demonstrated in the previous chapters that the ^{Mes}[CNH] proligand (**2.2**) behaves predictably as a stable, free carbene species that can be handled and used similarly to other common NHCs such as IMes. Despite it being ineffective as an auxiliary ligand for catalytic processes investigated thus far, compound **2.2** can be useful for exploring the coordination chemistry of a variety of transition elements. While the hemilabile, mixed-donor character of **2.2** can still be considered an asset, it was necessary to investigate adjustments that could be made to potentially improve its role as an auxiliary ligand in organometallic reactions. It is well known that making small ligand modifications can often have a significant impact on subsequent complex reactivity. In this chapter several ligand modifications are described and the reactivity of these proligands with various transition metals is discussed.

A version of this chapter will be submitted for publication.

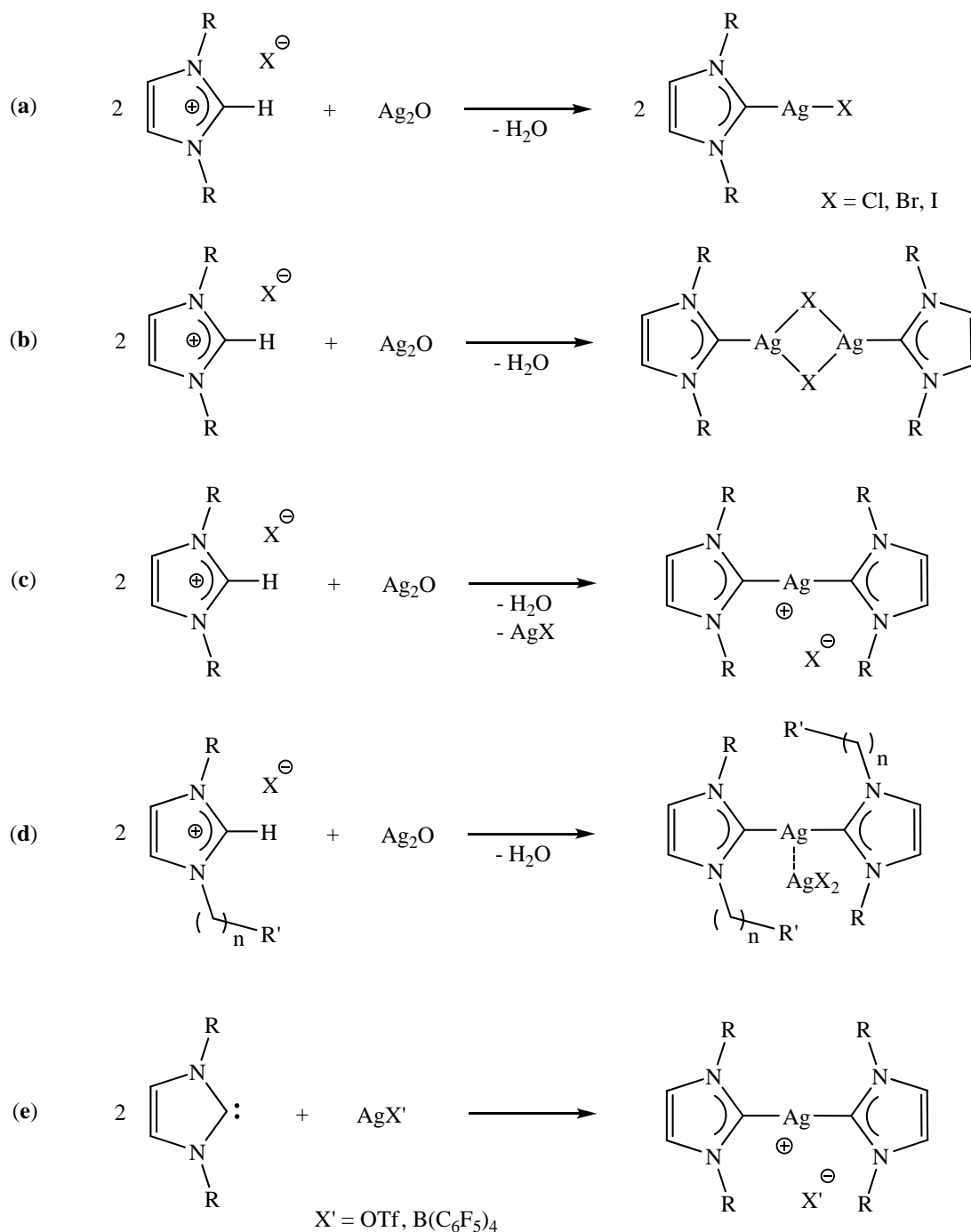
Jong, H.; Fryzuk, M.D. (2010) The Synthesis and Reactivity of Rhodium and Iridium Complexes Containing an N-Heterocyclic Carbene-Phosphide Ligand

4.2 *Synthesis and Reactivity of N-heterocyclic Carbenes with Silver(I)*

One way to enhance the usefulness of the imidazolium salt ligand as a precursor is to convert it into a form suitable for coordination to a metal complex. This approach has been used extensively with NHCs by preparing silver adducts that can be readily used as metallating agents.¹ This method has proved to be successful in the past as an entry point to synthesize NHC complexes when the free NHC proligand was either difficult to handle or not isolable.

The most common approach is to react silver(I) oxide with an imidazolium salt to produce the respective Ag-NHC complex. This method is convenient as it can typically be performed on the bench-top in air. However, the reaction often yields various Ag-NHC products depending on the characteristics of the NHC ligand. Scheme 4.1 describes some of the more common outcomes of the reaction of Ag₂O with imidazolium precursors. From the reaction of two equivalents of an imidazolium salt with Ag₂O, water is eliminated to yield the corresponding NHC-silver(I) complex as shown by (a) in Scheme 4.1. In certain cases, bridging halide compounds have also been observed in the solid state as in (b). Imidazolium salts that do not have halide counter-ions typically react with Ag₂O to form the bis-carbene silver complex as shown by (c). Alternatively, when the N-functionalized substituents of the imidazolium salt are different, it has been observed that [(NHC)₂Ag][AgX₂] ion-pair compounds can be formed; this is generally more applicable when one of the substituents is a flexible tether as depicted in (d). Direct addition of two equivalents of NHC to a solution containing a silver(I) salt that incorporates a weakly coordinating counterion, such as triflate or pentafluoroborate, typically proceeds smoothly to give a bis(carbene) silver(I) cation as shown in (e). However, while it is possible to synthesize Ag-NHC complexes starting with the free carbene, it is much more common to use the imidazolium salt precursor to react directly with Ag₂O.

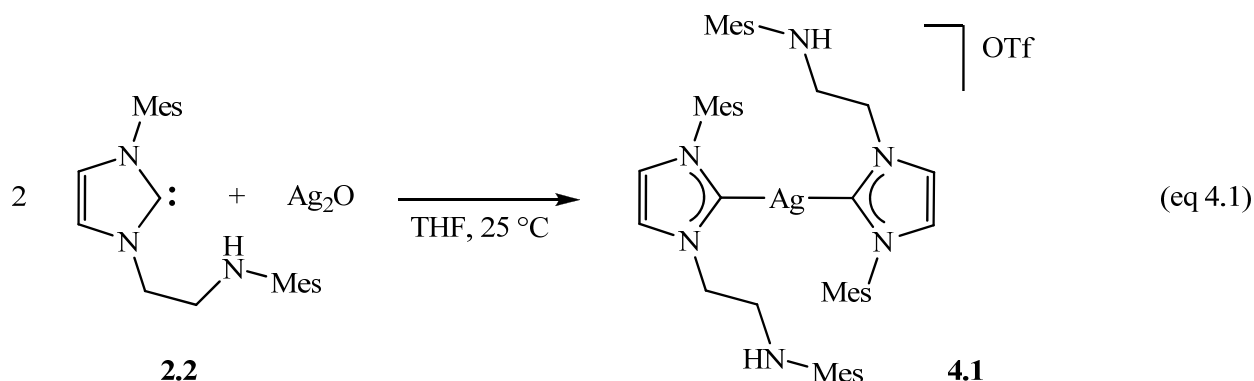
Scheme 4.1



These Ag-NHC compounds can be used as transmetallation agents to incorporate one or more NHC ligands into the desired metal complex. Group 8, 9 and 10 complexes are the most common metallation targets that utilize this method.

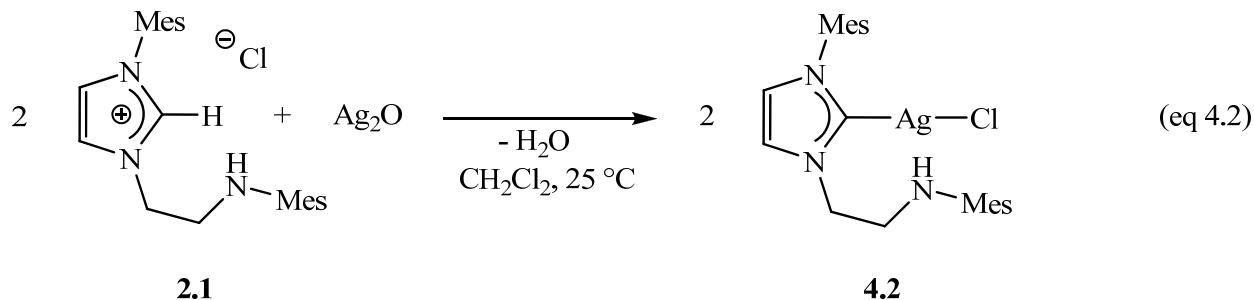
4.3 Synthesis, Characterization of ^{Mes}[CNH] with Silver(I)

Following procedures similar to those found in the literature for synthesizing Ag-NHC complexes, two equivalents of compound **2.2** can be added to a solution of silver(I) triflate dissolved in THF to generate the expected (^{Mes}[CNH]₂Ag)OTf complex (**4.1** in eq 4.1). This synthesis is performed in the absence of light and is complete in 30 minutes to yield a pale grey powder.



The most easily distinguishable feature in the ¹H NMR spectrum of **4.1** is the downfield shift of the two imidazole backbone protons to δ 7.40 and 6.94 from δ 6.38 and 6.45, respectively, exhibited by the free carbene, **2.2**. The distinct, well-resolved, *J* = 1.7 Hz doublet resonances that are observed for the imidazole backbone protons of **2.2** are also lost in the ¹H NMR spectrum of **4.1** with the coupling pattern of the imidazole protons complicated by coupling to the two *I* = ½, spin-active ¹⁰⁷Ag and ¹⁰⁹Ag nuclei. The ¹³C NMR spectrum shows the incorporation of silver as the centrally disposed carbene carbon of **4.1** displays strong coupling to the two spin-active silver nuclei with two downfield doublet resonances at δ 181.7 with *J*_{C¹⁰⁷Ag} = 181 Hz and *J*_{C¹⁰⁹Ag} = 208 Hz, which is consistent with the literature values observed for Ag-NHC coupling constants.² The imidazole backbone carbons also exhibit weak coupling to the ¹⁰⁷Ag and ¹⁰⁹Ag nuclei as resonances are observed at δ 122.9 and 123.6 with coupling constants of ³*J*_{CAg} = 5 Hz are observed in the ¹³C NMR spectrum.

When two equivalents of imidazolium salt **2.1** are added to Ag_2O , $^{\text{Mes}}[\text{CNH}]\text{AgCl}$ (**4.2**) is produced by reaction (a) in Scheme 4.1. This reaction is slow at room temperature and takes approximately one week to go to completion (eq 4.2).



Complex **4.2** is not easily characterized by NMR spectroscopy as the diagnostic silver-carbene coupling pattern is absent in the ^{13}C NMR spectrum. However, this phenomenon has been observed in other Ag-NHC complexes, but usually in the form of the dinuclear Ag system as shown from (d) in Scheme 4.1.^{3,4} The absence of an imidazolium proton resonance at δ 10.7 in the ^1H NMR spectrum rules out the presence of unreacted **2.1**. The ^{13}C NMR spectrum also does not indicate the presence of free carbene **2.2** as its diagnostic resonance at δ 216 is not observed. Fortunately, colorless crystals of **4.2**, which were grown from a concentrated solution in dichloromethane at low temperatures, could be analyzed by single crystal X-ray crystallography. Figure 4.1 shows the solid-state molecular structure of **4.2**. The geometry of **4.2** about the silver(I) center is linear as expected with the C02-Ag-Cl01 angle being $176.2(7)^\circ$. Complex **4.2** also exhibits a C02—Ag01 bond length of $2.076(2) \text{ \AA}$, which lies within the range of other comparable Ag-NHC complexes.⁴

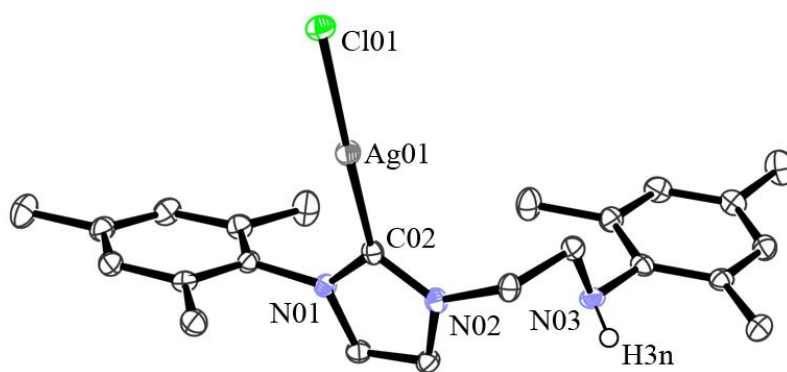


Figure 4.1. An ORTEP drawing of $^{\text{Mes}}[\text{CNH}]\text{AgCl}$, **4.2**, with thermal ellipsoids drawn at 50 % probability. All hydrogens atoms, except H3n, were removed for clarity. H3n was located in a difference map and refined isotropically.

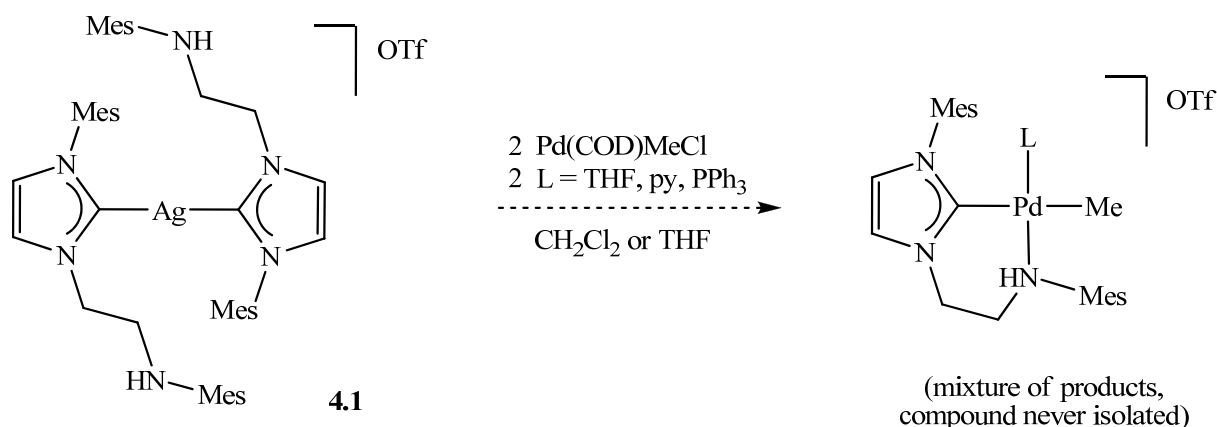
4.4 Transmetalation of $^{\text{Mes}}[\text{CNH}]\text{-Ag}$ Compounds with Palladium

Employing Ag-NHC complexes for transmetalation with palladium halides is common for the synthesis of neutral Pd catalysts used for the Heck reaction.¹ However, there has been considerably fewer reports of cationic Pd precursors that are effective for this process. Recently there has been several examples of Pd complexes that employ tridentate and pincer NHC ligands that can perform Heck reactions with good activity.⁵ Thus, it is of interest to explore further possibilities of cationic Pd complexes that incorporate chelating NHC ligands such as $^{\text{Mes}}[\text{CNH}]$.

The synthetic strategy produces a Pd complex that incorporates a methyl substituent in addition to the chelating NHC ligand as NHC-PdMe complexes in literature have demonstrated excellent activity for C—C coupling reactions.^{5,6} Thus, it was anticipated that the reaction of $[\text{Mes}][\text{CNH}]_2\text{Ag}]\text{OTf}$ (**4.1**) with Pd(COD)MeCl (COD = 1,5-cyclooctadiene) in the presence of a coordinating neutral third ligand such as tetrahydrofuran (THF), pyridine (py) or triphenylphosphine (PPh₃) would generate the desired $[\text{Mes}[\text{CNH}]\text{Pd}(\text{L})\text{Me}]\text{OTf}$ complex (L =

THF, py or PPh_3). However, despite multiple attempts under various conditions, the reaction yielded a mixture of products that could not be identified by NMR spectroscopy (Scheme 4.2).

Scheme 4.2

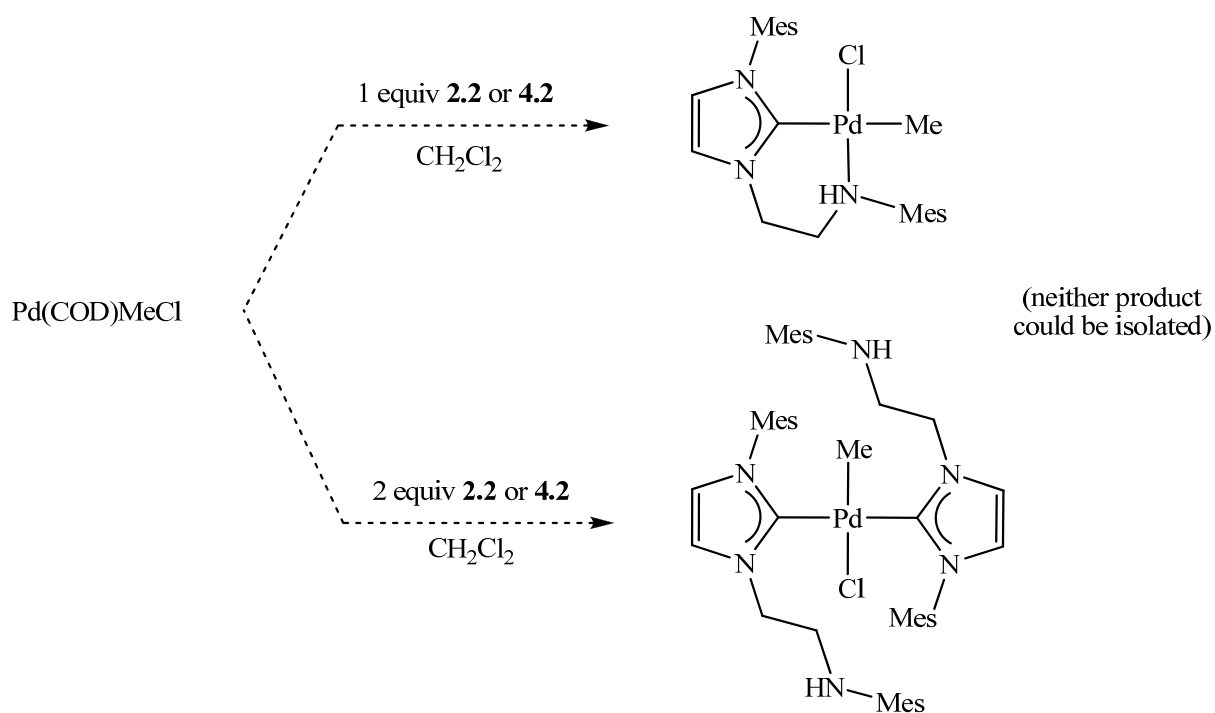


Cavell and coworkers have shown that pyridyl-functionalized NHC ligands are extremely effective auxiliary ligands for synthesizing highly active neutral Pd catalysts for C—C coupling reactions.⁷ Since the primary ligands employed in these catalysts are mixed-donor NHCs, it was desirable to see whether catalyst activity would extend to other hemilabile N-functionalized NHC ligand auxiliaries.

The reaction of one or two equivalents of free carbene $^{\text{Mes}}[\text{CNH}]$ with Pd(COD)MeCl would be another approach to prepare $^{\text{Mes}}[\text{CNH}]\text{PdMeCl}$ and $^{\text{Mes}}[\text{CNH}]_2\text{PdMeCl}$, respectively. However, the direct addition of **2.2** to Pd(COD)MeCl also results in an intractable mixture of products. The use of $^{\text{Mes}}[\text{CNH}]\text{AgCl}$ (**4.2**) as a transmetallating agent was also examined and found to be unsuccessful in generating a single isolable product when either one or two equivalents of **4.2** was added to Pd(COD)MeCl (Scheme 4.3). From the crude reaction mixture, crystals of $^{\text{Mes}}[\text{CNH}]_2\text{PdCl}_2$ (**4.3**) suitable for single crystal X-ray diffraction can be obtained in low yield by slowly concentrating the saturated CH_2Cl_2 /hexanes mixture. Figure 4.2 depicts the

solid-state molecular structure of **4.3**. The expected square planar geometry is observed with the C02-Pd01-Cl01 angle being $89.83(9)^\circ$ and a Pd01—C02 bond length of $2.018(3) \text{ \AA}$ that is typical of Pd-NHC complexes.⁸ Since complex **4.3** sits on an inversion center, the other half of the ORTEP depiction of $^{\text{Mes}}[\text{CNH}]\text{PdCl}$ was generated by symmetry. Surprisingly, complex **4.3** could not be isolated cleanly by the addition of two equivalents of **4.2** or **2.2** to $\text{Pd}(\text{COD})\text{Cl}_2$; both methods resulted in a mixture of products.

Scheme 4.3



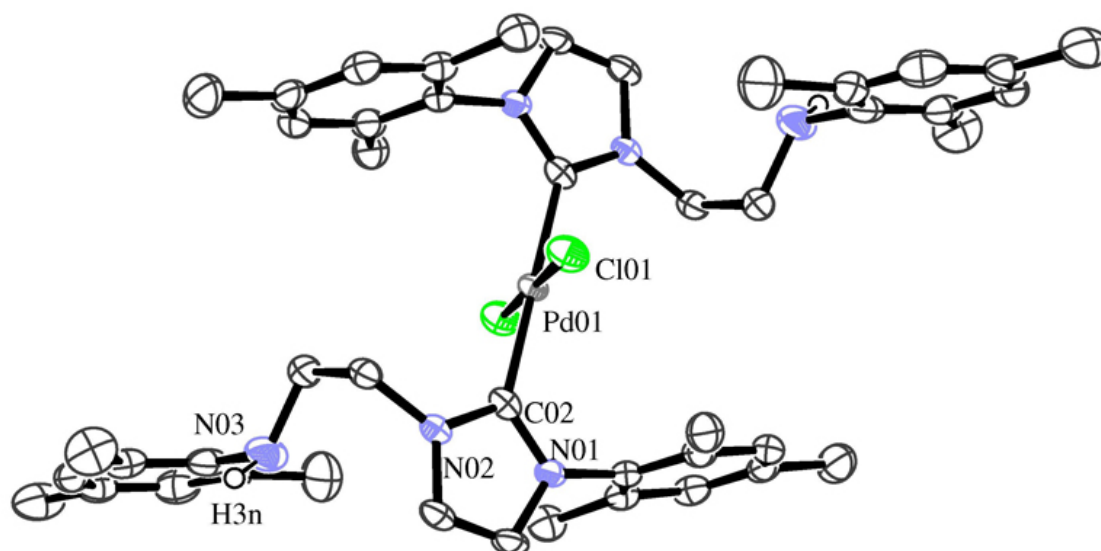


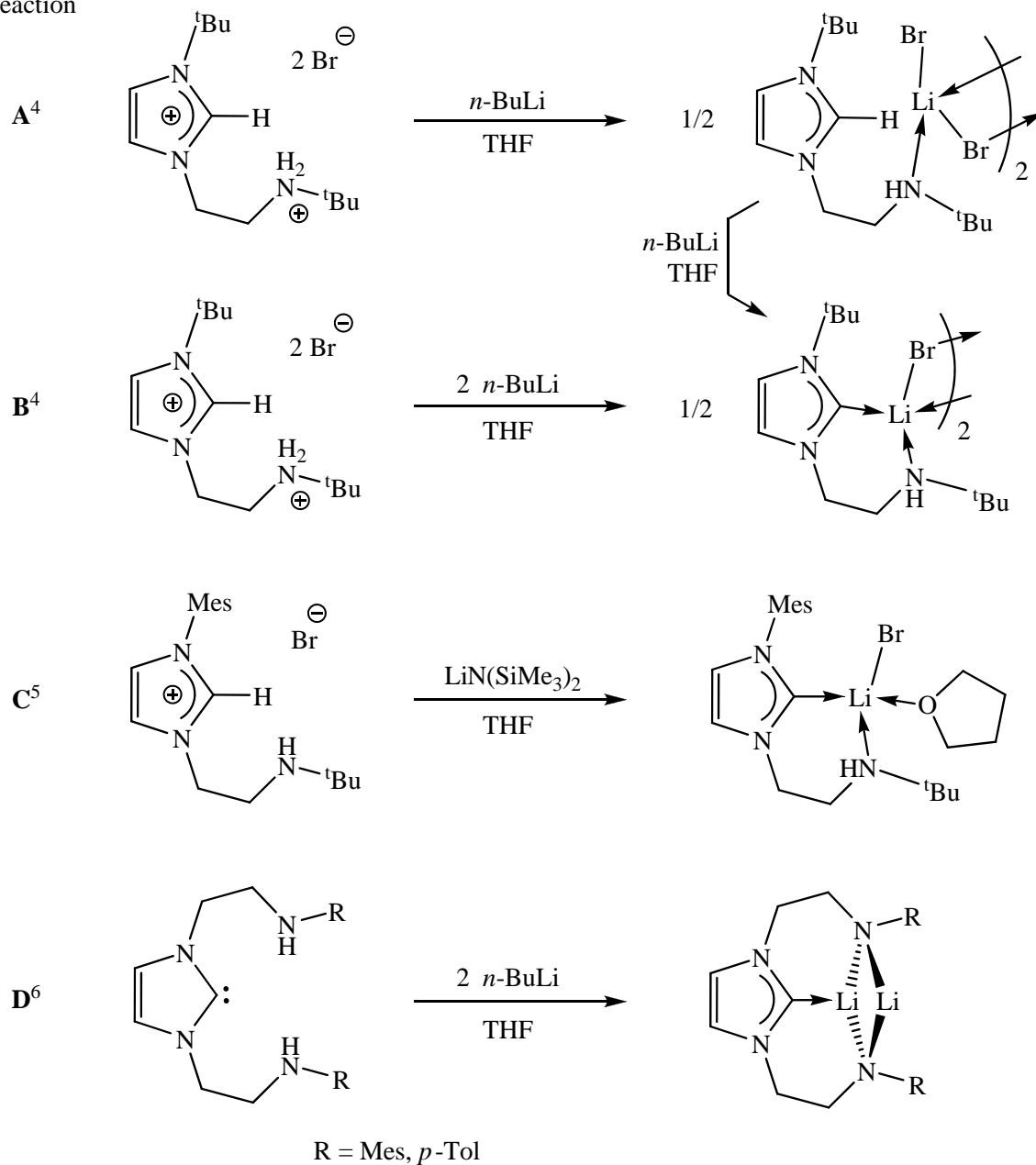
Figure 4.2. An ORTEP drawing of $^{\text{Mes}}[\text{CNH}]_2\text{PdCl}_2$, **4.3**, with thermal ellipsoids at drawn 50 % probability. All hydrogens atoms, except H3n, were removed for clarity. H3n was located in a difference map and refined isotropically. Half of the structure was generated by symmetry as the molecule resides on an inversion center.

4.5 Synthesis and Reactivity of *N*-heterocyclic Carbenes with Lithium

While silver-NHC complexes can be versatile transmetallating agents, the use of Li-NHC salt metathesis agents is considerably less common. $\text{LiN}(\text{SiMe}_3)_2$ and *n*-BuLi are often used to deprotonate NHCs, and occasionally they can form useful Li-NHC complexes. Typically, Li-NHC compounds are used for metallation with early transition metal or electrophilic halide complexes.⁹⁻¹¹ Recently, it has been shown that Li-NHC complexes can be useful for metallation with late metal halide compounds as well.¹² Scheme 4.4 depicts several examples used to prepare chelating Li-NHC complexes.

Scheme 4.4

Reaction



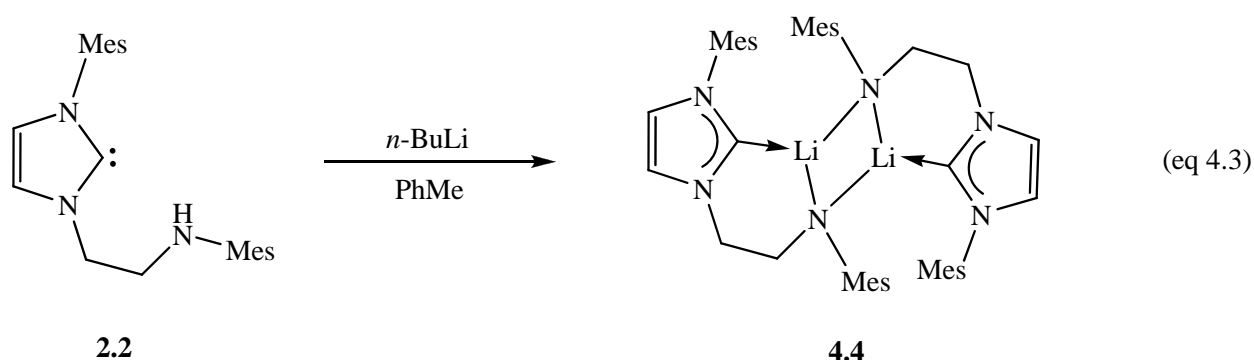
As shown in **A**, *n*-BuLi can be added to deprotonate the dicationic tethered imidazolium salt to generate a dimeric Li complex that bridges through the bromide atoms with the imidazolium unit left to dangle as shown by **A** in Scheme 4.4.⁹ However, if two equivalents of *n*-BuLi are added to this dicationic tethered imidazolium salt, a dimeric Li-NHC complex with a

coordinated amino tether that bridged through Li and a halide forms as described by **B**.

Alternatively, the product from **B** can be synthesized by further addition of *n*-BuLi to the product of **A**.⁹ Deprotonation of a typical mixed-donor imidazolium salt with two equivalents of LiN(SiMe₃)₂ results in a Li-NHC complex that contains a coordinated amido tether as described by **C**.¹⁰ Deprotonation of a tridentate diamine that contains a free NHC by *n*-BuLi has also been shown to form Li-NHC complexes, as shown in **D**.¹¹ These methods provide access to metathesis agents that are generally more effective for metallating electrophilic metal halides than Ag-NHC compounds.

4.6 Synthesis, Characterization and Reactivity of ^{Mes}[CNH] with Lithium

The free amino carbene **2.2** can be deprotonated by *n*-BuLi to generate a rare Li-NHC complex that is dimeric in solution linked by bridging amido substituents as described by eq 4.3. The Li-NHC dimer is denoted ^{Mes}[CNLi]₂ (**4.4**). Complex **4.4** is, to the best of our knowledge, the first Li-NHC dimer that features a bidentate NHC ligand that bridges through non-halide substituents. The synthesis is high yielding and proceeds cleanly at room temperature in two hours.



Compound **4.4** displays a broad singlet at δ 2.71 in the ⁷Li NMR spectrum. The ¹H NMR spectrum of **4.4** indicates a symmetric structure in solution and is absent of the diagnostic amine N—H resonance of **2.2** at δ 4.23. ¹³C NMR spectroscopy reveals a broad, weak resonance at δ

198.4 attributed to the Li-NHC carbene carbon of **4.4**. The ^{13}C NMR spectrum also shows a downfield shift of the N—C_{ipso} carbon of the amino tether to δ 158.0 from δ 144.6 (of **2.2**) as assigned by $^1\text{H}/^{13}\text{C}$ HSQC and HMBC correlation spectroscopy.

To test if complex **4.4** is dimeric in solution, ^1H , ^{13}C and ^7Li NMR analysis were performed with the assistance of $^1\text{H}/^{13}\text{C}$ HSQC and HMBC correlation experiments in $\text{d}_8\text{-THF}$. However, the results did not show evidence of a solvent-stabilized monomer in solution. A similar conclusion was reached when a drop of THF was added to a sample of **4.4** in C_6D_6 , which did not indicate the formation of a Li-THF adduct. Although it can be difficult to identify THF adducts of lithium amides in solution without the assistance of ^6Li and ^{15}N labelled NMR experiments, literature reports indicate that aggregate Li structures are usually maintained, but can coordinate ethereal solvents as an aggregate.¹³

Crystals of **4.4** suitable for single crystal X-ray diffraction analysis can be grown by slow evaporation of a concentrated sample in C_6H_6 . The solid-state molecular structure is depicted in Figure 4.2. Complex **4.4** features a planar rhombic Li—N core that contains Li—N bond lengths in the range of 1.986(4) – 2.004(4) Å. The amido-mesityl substituents deviate from the central Li—N plane at an angle of approximately 120.6 °, while the imidazole rings lie out of the plane at an average of 146.9 °. The structure of **4.4** has C_i symmetry in the solid-state and exhibits a short Li1—C2 (and Li2—C2a) bond length of 2.119(4) Å, which is among the shortest lithium-carbene bonds found in literature.^{9, 14-16} The Li—C_{carbene} bond of **4.4** is shorter than a comparable Li-alkoxide NHC complex that features a bond length of 2.135 Å¹⁵, and as short as the Li—C_{carbene} bond length of an amino-NHC ligated LiBr·THF adduct at 2.125(7) Å (product of **C** in Scheme 4.4).¹⁰ However, the Li—C_{carbene} bond length of **4.4** is slightly longer than that of the lithium-NHC pincer complex synthesized by Hoffman *et al.* that is reported to have the shortest Li—C_{carbene} bond length to date at 2.089(10) Å.¹⁶

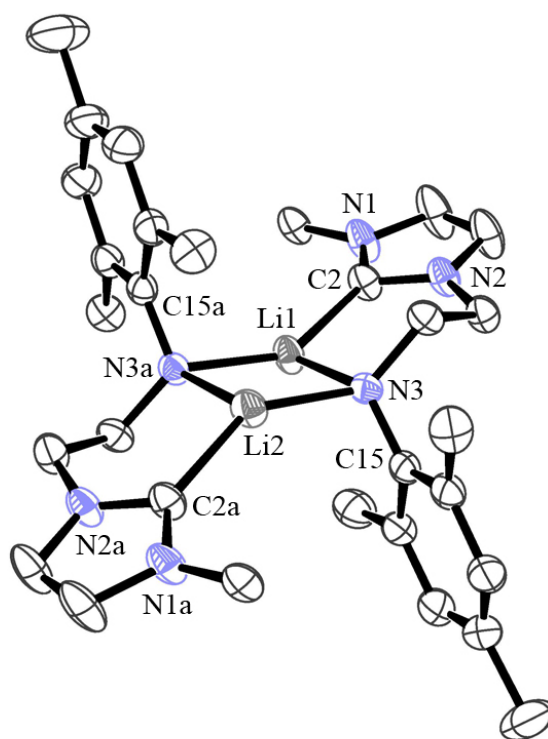


Figure 4.3. An ORTEP drawing of $^{\text{Mes}}[\text{CNLi}]_2$, **4.4**, with thermal ellipsoids drawn at 50 % probability. Mesityl substituents coordinated to N1 and N1a were omitted for clarity (except for *ipso*-carbons). All hydrogens atoms were also removed for clarity.

Orienting the solid-state molecular structure of **4.4** to look down at the (Li—N)₂ plane (Figure 4.3) reveals the possibility of π – π interactions between the mesityl substituents. Inspection of the distances between the mesityl substituents shows the closest point between the two layers being 4.105 Å (C17···C7a) and 5.290 Å (C4···C20a) at its widest divergence. While the π – π interactions between the mesityl groups may be limited at these distances,^{17, 18} the observation of the aromatic groups leaning towards one another indicates that the preferred structural geometry attempts to maximize the π -stacking effect as opposed to the mesityl groups diverging from one another to minimize steric repulsion. The mesityl substituents attempt to align facially in a staggered conformation, which has been shown as the preferred alignment to

optimize π -stacking interactions.¹⁷ However, the rigidity of the Li-NHC core prevents the mesityl substituents from aligning more effectively with one another.

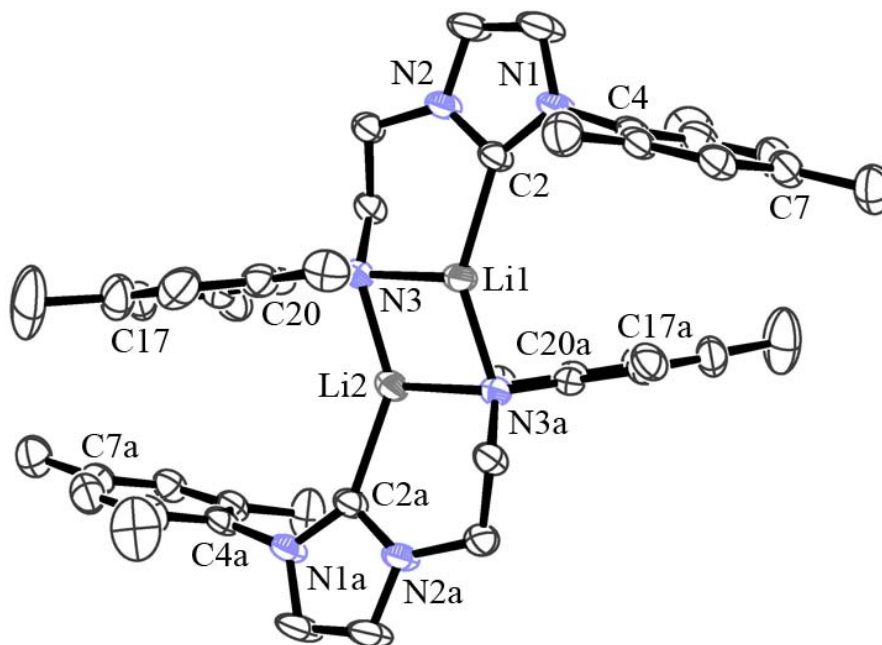


Figure 4.4. The solid-state molecular structure of **4.4** reoriented to show alignment of mesityl substituents suggesting π -stacking interactions. All hydrogens were omitted for clarity.

Table 4.1. Selected bond lengths and angles for ^{Mes}[CNLi]₂, **4.4**.

Bond Lengths (Å)			
Li1-C2	2.119(4)	Li1-N3a	1.997(4)
Li1-N3	2.004(4)	N3-C15	1.408(3)
Bond Angles (°)			
C2 (oop)	148.3(3)	N3a-Li1-N3	104.6(2)
C15 (oop)	118.1(3)	N3a-Li1-C2	145.5(2)
C15-N3-Li1	129.6(2)	N3-Li1-C2	101.7(2)
Li2-N3-Li1	75.3(2)		

oop = out of plane^a

^a The plane is defined by bridging planar rhombus encompassed by Li1-N3-Li2-N3a.

There are reports from the Fryzuk group that demonstrate chelating mixed-donor NHC ligands can participate in interesting coordination chemistry with early transition metals.¹⁹ Thus,

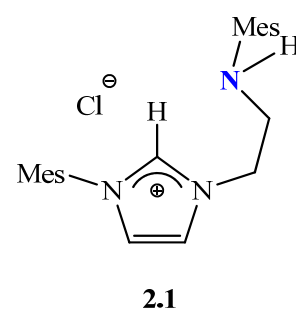
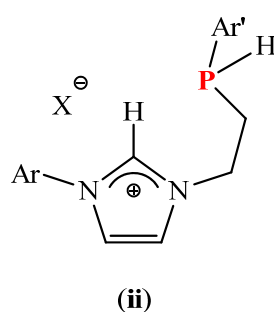
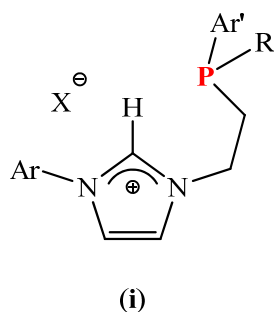
exploring the reactivity of $^{\text{Mes}}[\text{CNH}]$ and $^{\text{Mes}}[\text{CNLi}]_2$ with Group 4 metal complexes was attractive. Unfortunately, transmetallation of **4.4** with Zr and Ti complexes to incorporate the $^{\text{Mes}}[\text{CN}]$ ligand was not straightforward and resulted in mixtures of products that eluded characterization. It was more convenient to use aminolysis of $\text{Zr}(\text{NMe}_2)_4$ with **2.2** to generate a penta-coordinate $^{\text{Mes}}[\text{CN}]\text{Zr}(\text{NMe}_2)_3$ complex that will be discussed in more detail in the following chapter.

The reaction of **4.4** with $[\text{Rh}(\text{COD})\text{Cl}]_2$ resulted in an inseparable mixture of products, whereas the addition of free NHC **2.2** to Rh- and Ir-diene complexes generated an array of discrete complexes as described in Chapter 2. Although the isolation and characterization of a Li-NHC complex like **4.4** was rare, its usefulness as a transmetallation agent was limited. Thus, it was necessary to explore other congeners of $^{\text{Mes}}[\text{CNH}]$ that could be used as a substitute. The reactivity of the new $^{\text{Mes}}[\text{CNH}]$ analogues could then be compared to those of **2.2**, which would act as a benchmark.

4.7 *Synthesis, Characterization and Reactivity of $^{\text{Mes}}[\text{HCPH}]\text{Cl}$*

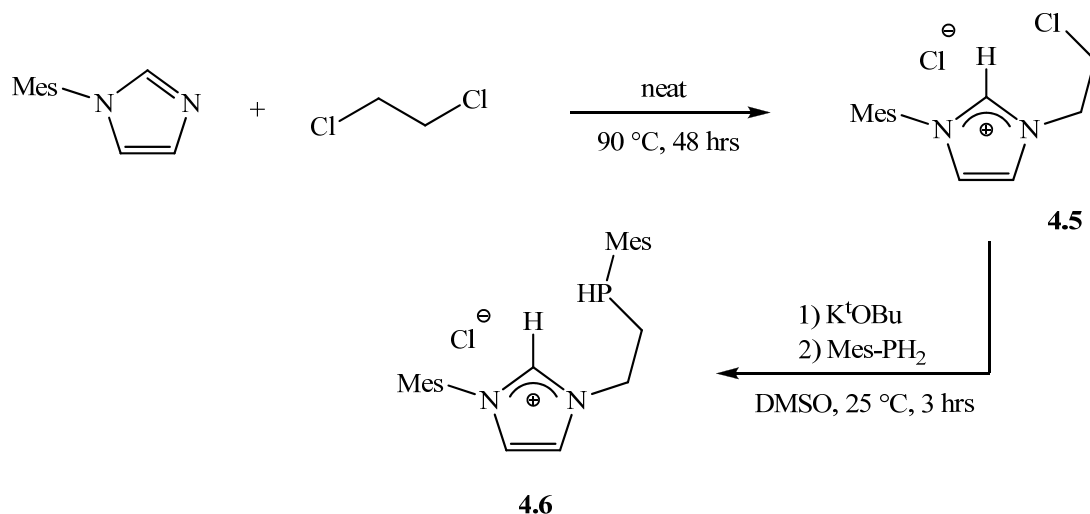
As discussed in earlier chapters, the N-mesitylamino tether of $^{\text{Mes}}[\text{CNH}]$ appeared to be a labile donor as it was found to be non-coordinating in many complexes. Since phosphines are considered soft donors and amines are categorized as hard donors, the preparation of an analogous mesitylphosphine tether for this carbene system would be a better match for softer metal complexes, particularly those of Rh and Ir.

Bidentate imidazolium salts with a tertiary phosphine tether (**i**) are known in the literature and their reactivity with later transition metal complexes has been studied by various groups.²⁰ However, to the best of our knowledge, the synthesis of a congener with a secondary phosphine tether such as (**ii**) is unknown.



To construct a compound of type (ii), the initial building block, 1-mesityl-3-(chloroethyl)imidazolium chloride, **4.5**, was synthesized by heating mesityl imidazole with neat 1,2-dichloroethane to 90 °C for 48 hours. Compound **4.5** can be easily identified in the ^1H NMR spectrum as the imidazole protons shift downfield to δ 10.2, 8.42 and 7.10 from δ 7.56, 7.10 and 7.07, respectively, observed for the mesityl imidazole starting material. The addition of potassium *tert*-butoxide and mesitylphosphine to **4.5** in a solution of DMSO afforded the desired imidazolium salt with a mesitylphosphino tether, denoted **4.6**, which is completely analogous to **2.1**. Complex **4.6** exhibits a doublet resonance at δ - 97.4 ($J_{\text{PH}} = 222$ Hz) in the proton coupled ^{31}P NMR spectrum compared to mesitylphosphine that exhibits a $J_{\text{PH}} = 203$ Hz triplet resonance at δ - 153.4. In the ^1H NMR spectrum, the phosphine proton shows a doublet of triplets coupling pattern is observed at δ 4.42 ($J_{\text{HP}} = 222$ and $^3J_{\text{HH}} = 7.7$ Hz) that is attributed to the coupling to ^{31}P and the CH_2 group of the tether. The methylene proton signals from the ethylene spacer also show coupling to phosphorus with coupling constants of $^2J_{\text{HP}} = 125$ and $^3J_{\text{HP}} = 108$ Hz. The ^{13}C NMR spectrum displays the central iminium carbon resonance at δ 139.7. Coupling of the ethylene carbons to the ^{31}P nucleus can be clearly resolved in the ^{13}C NMR spectrum with the J_{CP} coupling values of 18 and 9 Hz, for carbons one (δ 23.1) and two (δ 49.9) bonds away from the ^{31}P nucleus, respectively. The assignment of the NMR spectra was assisted by performing $^1\text{H}/^{13}\text{C}$ HSQC and HMBC correlation experiments.

Scheme 4.5

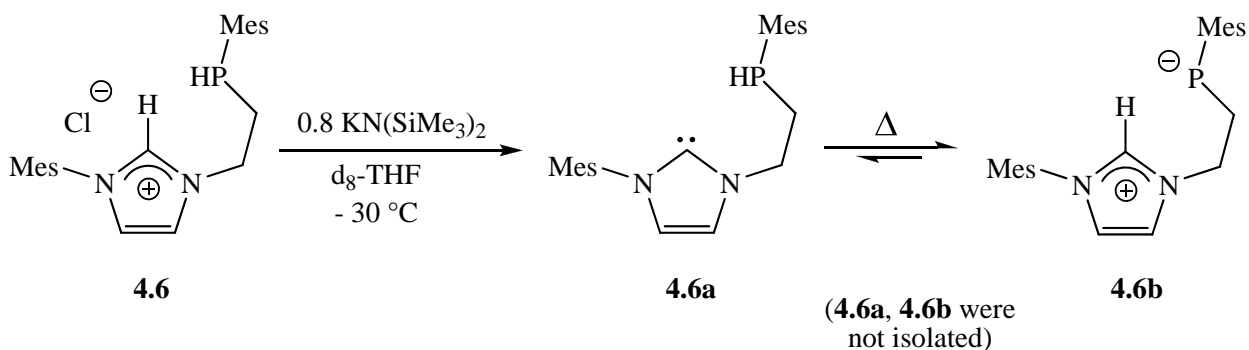


4.8 Deprotonation Studies of ^{Mes}[HCPH]Cl

Having synthesized the mixed-donor imidazolium salt with a secondary phosphine tether, it was of interest to deprotonate **4.6** to generate the free NHC species so comparisons with **2.2** could be made. However, attempts to selectively deprotonate the central iminium proton of **4.6** were not as straightforward as in the case with **2.1**. A variety of bases (KN(SiMe₃)₂, NaN(SiMe₃)₂, K^tOBu, *n*-BuLi, NaH, CsCO₃, and NaOAc) were tested and all resulted in a mixture of unidentifiable products. It was anticipated that the acidity of the phosphino proton would likely be greater than an analogous amino proton.²¹ Literature reports indicate that *N*-methylaniline exhibits a pK_a value of 29.5 in DMSO, while the analogous methylphenylphosphine is calculated to have a pK_a value of 26.7.²² Since the pK_a value of the iminium proton is in the region of 20 – 24,²³ it was expected to be sufficiently acidic such that selective deprotonation with one equivalent of an appropriately strong base would leave the P—H unit intact. However, despite various combinations of reaction conditions and bases, the free NHC species of **4.6** could not be isolated.

To investigate the nature of the deprotonation behavior of **4.6**, variable temperature NMR spectroscopy was performed. Compound **4.6** was dissolved in d_8 -THF and 0.8 equivalents of $\text{KN}(\text{SiMe}_3)_2$ was added at $-30\text{ }^\circ\text{C}$ before being introduced to the NMR spectrometer probe equilibrated at $-30\text{ }^\circ\text{C}$. Sequential ^1H and ^{31}P NMR experiments were performed at $10\text{ }^\circ\text{C}$ increments until $60\text{ }^\circ\text{C}$ was reached (Scheme 4.6). The purpose of adding less than one stoichiometric equivalent was to use the integrals of the iminium and imidazole protons of **4.6** to determine the extent of deprotonation effectiveness. At reduced temperatures, **4.6** was found to be deprotonated selectively at the iminium position to yield **4.6a** as evidenced by the absence of the iminium proton at $\delta\text{ }11.0$ in the ^1H NMR spectrum. The ^{31}P NMR proton coupled spectrum confirmed the existence of the P—H unit with the $J_{\text{PH}} = 222\text{ Hz}$ doublet resonance at $\delta -97$ being preserved. The ^1H and ^{31}P NMR spectra of **4.6a** remained unchanged at $0\text{ }^\circ\text{C}$ for 45 minutes. However, as the temperature increased another resonance at $\delta -240$ (denoted **4.6b**) emerged in the ^{31}P proton coupled NMR spectrum while the doublet resonance at $\delta -97$ receded. The resonance of **4.6b** was observed as a $^2J_{\text{PH}} = 15\text{ Hz}$ triplet resulting from the coupling of the phosphide nucleus to the adjacent methylene protons of the ethylene spacer. Complex **4.6b** was expected to be zwitterionic, but in equilibrium with **4.6a**. At $60\text{ }^\circ\text{C}$ the ratio of **4.6a** to **4.6b** was approximately 1:4 in the ^{31}P proton coupled NMR spectrum demonstrating the presence of both species. However, the iminium proton of **4.6b** was never observed in the ^1H NMR spectrum throughout the variable temperature NMR study. This observation could suggest the formation of a P(CH)N heterocyclic species instead of **4.6b**. However, a P—CH doublet resonance was not observed in the ^1H or ^{31}P NMR spectra that would indicate the formation of a P(CH)N system.²⁴ The absence of the iminium proton resonance of **4.6b** could be attributed to rapid exchange between **4.6a** and **4.6b**, thereby not observable on the NMR timescale. Figure 4.4 illustrates the proton coupled ^{31}P NMR spectra at -20 and $+60\text{ }^\circ\text{C}$.

Scheme 4.6



Analyzing the variable temperature NMR data from the deprotonation reaction of complex **4.6** led to the assumption that isolation of **4.6a** could be possible if the workup was performed at temperatures below 0 °C. However, repeating the deprotonation reaction of **4.6** (Scheme 4.6) at – 78 °C and executing the workup at – 4 °C generated a product in low yield that was impure and not easily characterized. The ^{31}P NMR proton-coupled spectrum showed the mixture did contain a complex that exhibited the desired doublet resonance at $\delta - 97$ and the ^1H NMR spectrum showed no traces of the iminium signal from **4.6**. However, the desired free NHC complex **4.6a** was not the major product by inspection of the ^1H NMR spectrum.

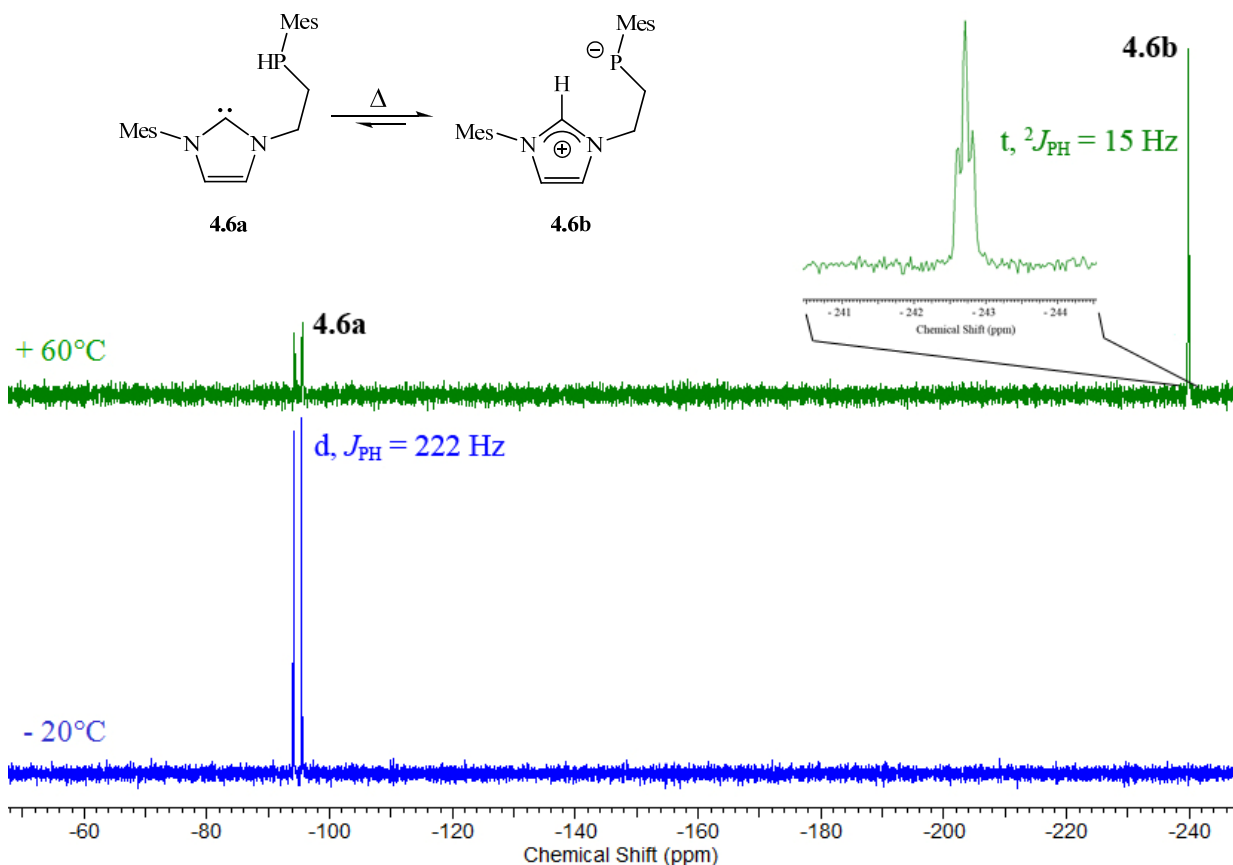


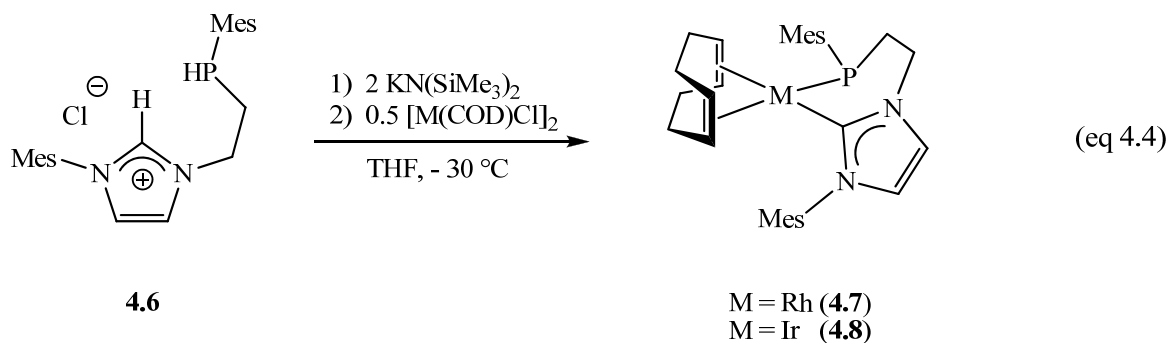
Figure 4.5. The stacked 161 MHz ^{31}P NMR proton coupled spectrum depicting compounds **4.6a** and **4.6b** at -20°C and $+60^\circ\text{C}$ in d_8 -THF. The inset shows the expanded view of the phosphide triplet resonance.

Another approach to the synthesis of compound **4.6a** was to deprotonate **4.6** *in situ* at low temperatures and trap **4.6a** by binding it to a metal center. Again, an efficient synthetic strategy remained elusive as neither the addition of $\text{Rh}(\text{PPh}_3)_3\text{Cl}$, or 0.5 equivalents of $[\text{Rh}(\text{COD})\text{Cl}]_2$, to a solution containing a deprotonated sample of **4.6** at -78°C yielded a discrete isolable species. The reaction of **4.6** with either Ag_2O or $n\text{-BuLi}$ to generate a transmetallating agent was also unsuccessful. Since it was difficult to isolate **4.6a** selectively due to problems during workup, the substitution of mesitylphosphine of **4.6** with a different phosphine that would have a higher pK_a value, such as an alkyl phosphine, could prove to be more effective. However, repeating the synthesis of **4.6** and replacing Mes-PH_2 with Cy-PH_2 ($\text{Cy} = \text{C}_6\text{H}_{11}$) was problematic and low

yielding. Thus, the strategy to deprotonate both the iminium as well as the phosphine proton of **4.6** became an attractive alternative.

4.9 Synthesis and Reactivity of $^{\text{Mes}}[\text{CP}]\text{M}(\text{COD})$ ($\text{M} = \text{Rh}, \text{Ir}$)

The addition of two equivalents of $\text{KN}(\text{SiMe}_3)_2$ to **4.6** followed by the introduction of 0.5 equivalents of $[\text{Rh}(\text{COD})\text{Cl}]_2$ at $-30\text{ }^\circ\text{C}$ yields the NHC-phosphine rhodium complex, $^{\text{Mes}}[\text{CP}]\text{Rh}(\text{COD})$ (**4.7** in eq 4.4). After addition of the rhodium-diene, the workup can be performed at room temperature to yield an air and moisture sensitive dark green powder. The ^{31}P NMR spectrum of compound **4.7** reveals a diagnostic $J_{\text{PRh}} = 73\text{ Hz}$ doublet resonance at $\delta\ 9.1$, due to phosphorus coupling to the ^{103}Rh nucleus. The carbene carbon of **4.7** appears as a doublet of doublets at $\delta\ 186.5$ ($J_{\text{CRh}} = 54\text{ Hz}$ and $^2J_{\text{CP}} = 17\text{ Hz}$) due to the coupling to both ^{103}Rh and ^{31}P in the ^{13}C NMR spectrum. The analogous reaction strategy (eq 4.5) can be applied to trap **4.6b** with 0.5 equivalents of $[\text{Ir}(\text{COD})\text{Cl}]_2$ to yield $^{\text{Mes}}[\text{CP}]\text{Ir}(\text{COD})$ (**4.8**). Complex **4.8** exhibits a diagnostic signal in the ^{31}P NMR spectrum at $\delta - 0.5$. In the ^{13}C NMR spectrum, the Ir-carbene resonance is observed as a $^2J_{\text{CP}} = 11\text{ Hz}$ doublet at $\delta\ 177.9$ as the carbene carbon couples to the ^{31}P nucleus. Complexes **4.7** and **4.8** are, to the best of our knowledge, the first Rh and Ir complexes containing a chelating NHC-phosphide ligand.



Since ^{103}Rh is a spin-active nucleus, it can be used for NMR solution diagnostics. During the synthesis of **4.7**, there was evidence that a second phosphine species is present in solution as the ^{31}P NMR spectrum of the reaction mixture exhibits two additional phosphorus resonances. The $J_{\text{PRh}} = 74$ Hz doublet resonance at δ 9.0 represents the major product and is assigned to complex **4.7**. The secondary product (**4.7a**) exhibits a $J_{\text{PRh}} = 111$ Hz triplet resonance at δ - 14.4, which could result from coupling of the phosphide tether to another ^{103}Rh nucleus. The ratio of **4.7** to **4.7a** was approximately 4:1 in the crude mixture. However, upon workup and recrystallization from a toluene/hexanes solution, pure **4.7** is isolated in moderate yield (59 %). This workup is also effective for the isolation of **4.8**. Crystals of **4.7** and **4.8** suitable for X-ray diffraction analysis can be obtained by slowly concentrating a benzene/hexanes solution. Figure 4.5 depicts the solid-state molecular structure of both **4.7** and **4.8**. Selected bond lengths and angles are listed in Table 4.2.

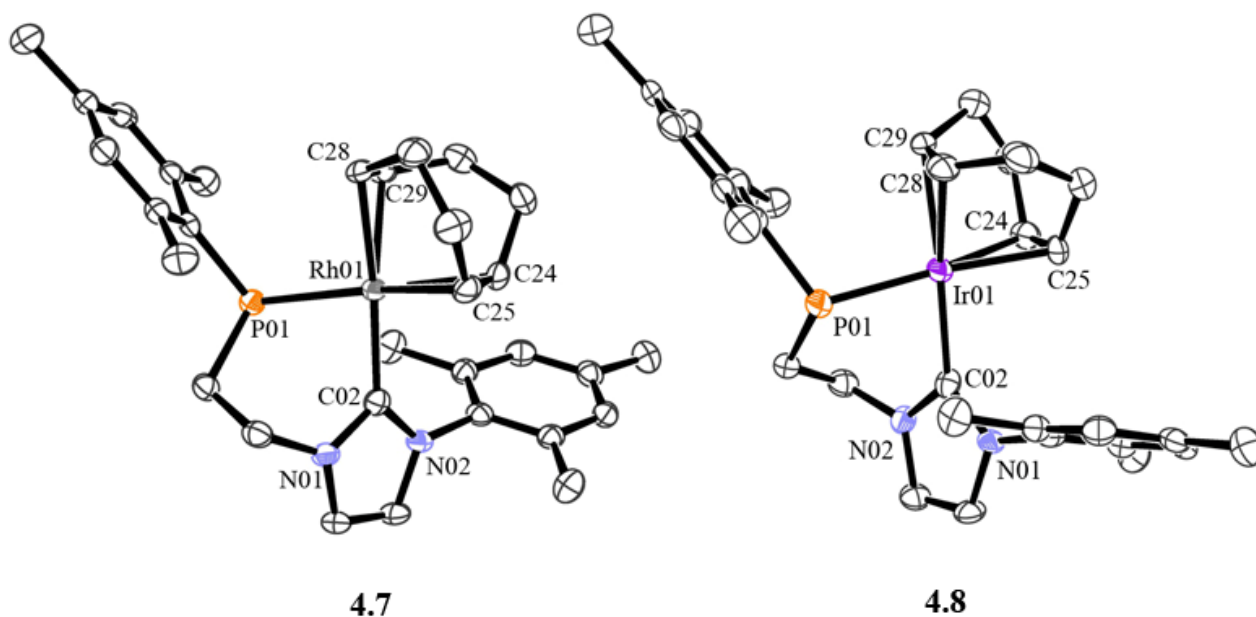


Figure 4.6. ORTEP drawings of $^{\text{Mes}}[\text{CP}]\text{Rh}(\text{COD})$ (**4.7**) and $^{\text{Mes}}[\text{CP}]\text{Ir}(\text{COD})$ (**4.8**) with thermal ellipsoids drawn at 50 % probability. All hydrogens have been removed for clarity.

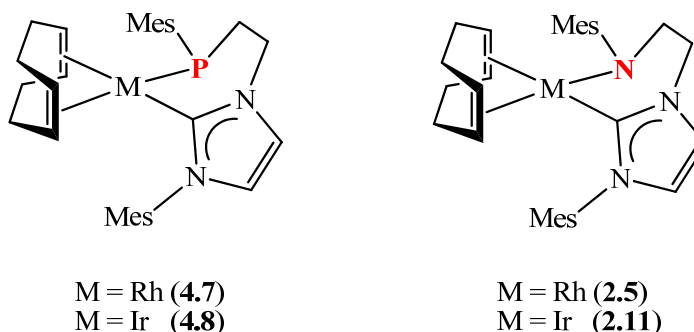


Table 4.2. Selected bond lengths and angles for complexes **4.7** and **4.8** compared to their congeners **2.5** and **2.11** respectively (M = Rh, Ir).

	4.7	2.5^a	4.8	2.11^a
Bond Lengths (Å)				
M01-C02	2.035(3)	2.037(3)	2.033(4)	2.041(3)
M01-(C24/C25) _{cent} ^b	2.07(1)	2.01(1)	2.04(1)	1.99(1)
M01-(C28/29) _{cent} ^b	2.08(1)	2.09(1)	2.06(1)	2.06(1)
M01-(P01/N03) ^c	2.355(1)	2.048(3)	2.342(1)	2.012(3)
Bond Angles (°)				
C02-M01-(C24/C25) _{avg} ^d	95.8(2)	93.9(2)	95.2(2)	94.5(2)
C02-M01-(C28/C29) _{avg} ^d	161.7(2)	161.8(2)	161.4(2)	161.4(2)
C02-M01-(P01/N03) ^c	82.4(1)	88.0(1)	83.2(1)	87.5(1)
M01-(P01/N03)-C05 ^c	107.4(1)	124.8(2)	107.8(1)	124.9(2)
M01-(P01/N03)-C06 ^c	111.8(1)	125.4(2)	112.9(1)	124.8(2)
C05-(P01/N03)-C06 ^c	102.5(1)	109.7(3)	103.1(2)	110.3(3)

^a Complexes **2.5** = ^{Mes}[CN]Rh(COD) and **2.11** = ^{Mes}[CN]Ir(COD) are reported in Chapter 2.

^b Distances were measured from either Rh or Ir to the center of the C=C centroid.

^c Bond distances and angles reflect substitution of -P01 with -N03 only, but their relative positions are identical.

^d The measured angles are calculated as an average of the two coordinated C=C carbons.

Complex **4.8** is structurally very similar to **4.7** and exhibits the same square planar geometry and nearly identical M—C02 bond lengths. Although there is little to differentiate between the Rh and Ir compounds in the solid-state, there appears to be a noticeable difference when compared to their analogues that incorporate the ^{Mes}[CN] ligand instead. The most noticeable difference between **4.7** and **4.8** compared to ^{Mes}[CN]Rh(COD) (**2.5**) and

$^{\text{Mes}}[\text{CN}]\text{Ir}(\text{COD})$ (**2.11**), respectively, is the longer M—COD (M = Rh and Ir) bond *trans* disposed to the heteroatomic donor of the tether. Complexes **4.7** and **4.8** have a stronger phosphido donor that induces a more significant *trans* influence on the opposing metal-olefin bond than **2.5** and **2.11**, respectively, that employs an amino donor. The stronger *trans* influence induced by the phosphido donor lengthens the M—COD bond and presumably weakens the bond strength. The weaker coordination of COD to Rh or Ir may be advantageous for hydrogenation studies as it was shown in Chapter 2 that compounds **2.5** and **2.11** were not effective hydrogenation catalyst precursors partly due to a tightly bound COD ligand.

While the Rh byproduct detected by ^{31}P NMR spectroscopy was not isolated, evidence that helped uncover its identity was fortuitously discovered during the synthesis of the iridium analogue **4.8**. Compound **4.8** lacks the diagnostic advantage of the ^{103}Rh nucleus for solution analysis of byproducts. However, the crystallization process of **4.8** yields two different products from a THF/hexanes solution. The first to crystallize from solution, in very low yield, are yellow platelets that are characterized as a mesityl C—H activated Ir complex, which incorporates a phosphide tether bridging two different Ir complexes, one being $^{\text{Mes}}[\text{CP}^*]\text{Ir}(\text{COD})\text{H}$ ($^{\text{Mes}}[\text{CP}^*]$ = mesityl C—H activated phosphide ligand) and the other being an $\text{Ir}^{\text{I}}(\text{COD})\text{Cl}$ unit. Figure 4.6 shows the solid-state molecular structure of the bridging phosphido di-iridium complex, which is denoted **4.8a**. Compound **4.8a** can be described as a bimetallic complex consisting of an Ir^{III} and an Ir^{I} center. Similarly, a bridging Rh-phosphide species (**4.7a**) could be the byproduct detected in the ^{31}P NMR spectrum of **4.7**, as it would account for the triplet resonance observed due to coupling to two ^{103}Rh nuclei.

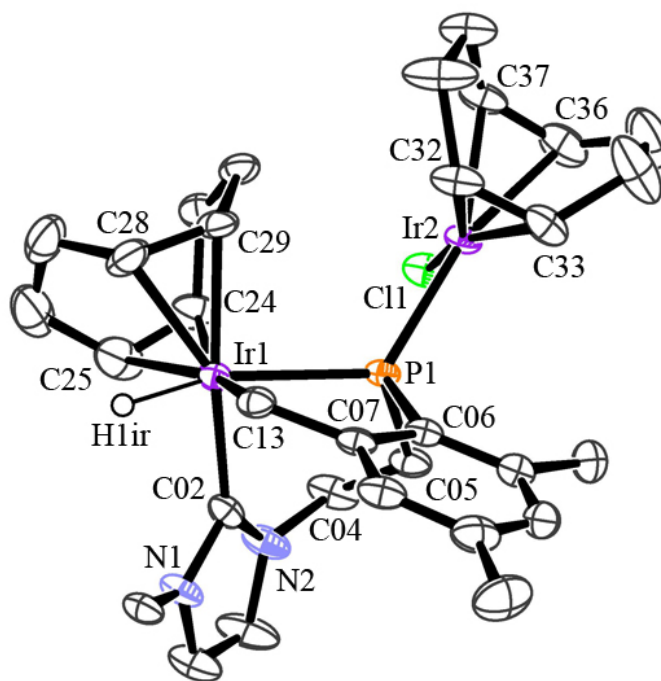


Figure 4.7. An ORTEP drawing of **4.8a** with thermal ellipsoids drawn at 50 % probability. The mesityl group (except C_{ipso}) coordinated to N1 and all hydrogens (except H1ir) have been omitted for clarity. H1ir was located in a difference map and refined isotropically.

Table 4.3. Selected bond lengths and angles for complex **4.8a**.

Bond Lengths (Å)			
Ir1-C02	2.038(5)	Ir1-H1ir	1.49(2)
Ir1-C13	2.105(5)	Ir2-(C32/C33) _{cent} ^a	1.99(1)
Ir1-(C24/C25) _{cent} ^a	2.16(1)	Ir2-(C36/C37) _{cent} ^a	2.04(1)
Ir1-(C28/29) _{cent} ^a	2.09(1)	Ir2-P1	2.348(1)
Ir1-P1	2.442(1)	Ir2-Cl1	2.385(1)
Bond Angles (°)			
C02-Ir1-C13	94.3(2)	C13-C07-C06	121.5(5)
C02-Ir1-(C24/C25) _{avg} ^b	93.3(3)	C07-C06-P1	115.7(4)
C02-Ir1-(C28/C29) _{avg} ^b	161.4(3)	C06-P1-C05	100.1(2)
C02-Ir1-P1	84.4(2)	C06-P1-Ir2	114.4(2)
C02-Ir1-H1ir	82(3)	C06-P1-Ir1	99.0(2)
C13-Ir1-P1	82.0(2)	H1ir-Ir1-P1	165(3)
C13-Ir1-H1ir	93(3)	P1-Ir2-Cl1	89.23(5)

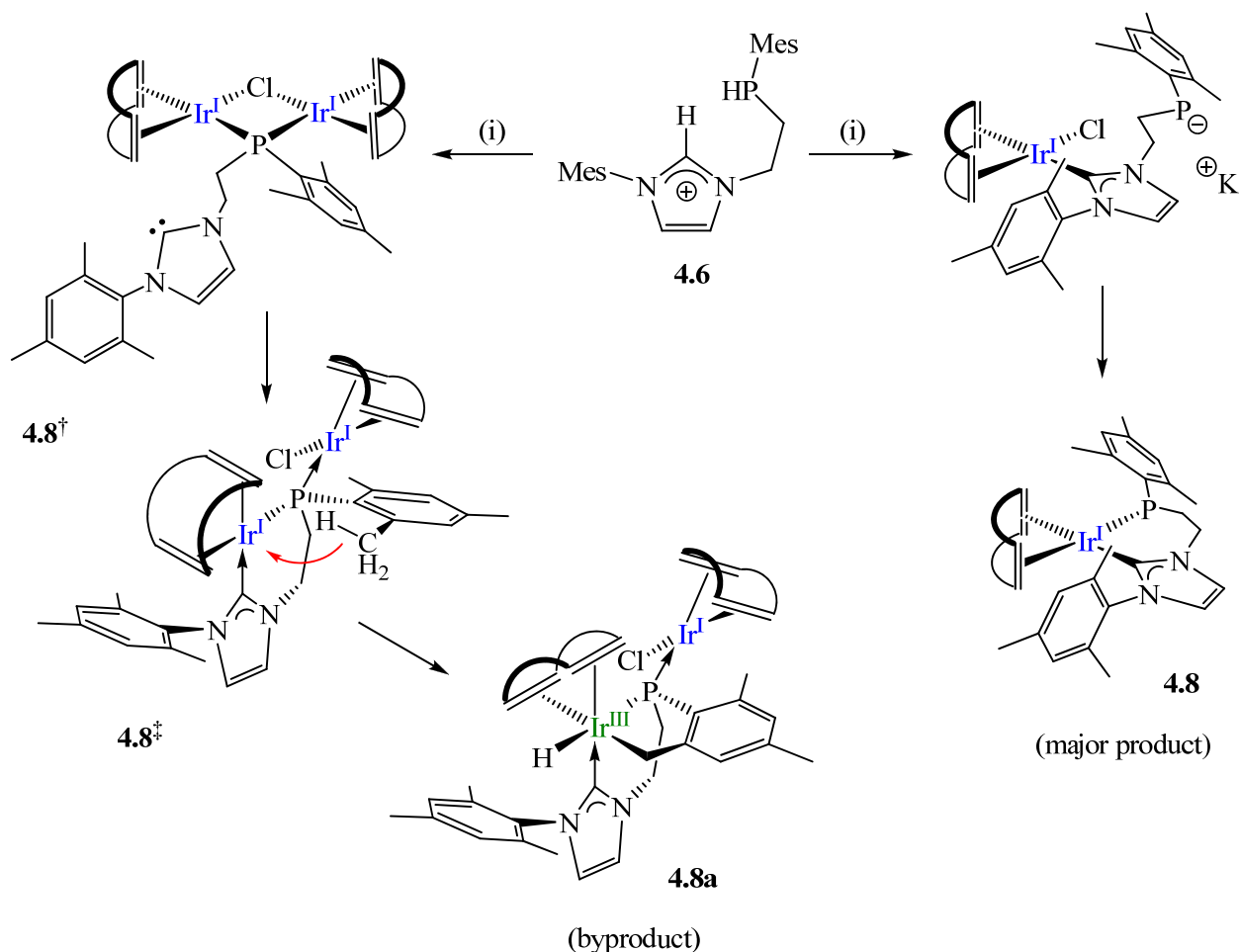
^a Distances are measured from Ir to the center of the C=C centroid.

^b The measured angles are calculated as an average of the two coordinated C=C carbons.

Complex **4.8a** exhibits a distorted octahedral geometry about the trivalent Ir1 center and predictably square planar about monovalent Ir2. The Ir1—C02 bond length of 2.038(5) Å is in the range expected for Ir-NHC complexes.^{25, 26} The iridium hydride was located in a difference map and refined isotropically, but was never observed in solution as the crystallization of **4.8a** was very low yielding and only observable in the solid-state; albeit consistently throughout multiple synthetic batches of **4.8**. The Ir1—H1ir bond length was found to be 1.49(2) Å, which is in agreement with other reported Ir—H complexes.²⁷ The Ir1—P1 bond length was found to be very long at 2.442(1) Å, while Ir2—P1 was 2.348(1) Å. Typically, Ir—P bond lengths are reported to be in the range of 2.20 – 2.36 Å.^{26, 28} Despite the Ir1—P1 interaction being a bridging component, the bond length to Ir1 was substantially longer than expected. However, the interaction between the Ir center and the coordinated COD also exhibited some irregularities in **4.8a**. Typically, the bond length between Ir—COD (measured from Ir to the center of the C=C centroid of the olefin) in similar systems demonstrate a longer bond length between Ir—COD that is positioned *trans* (Ir—(C28/C29)_{cent}) to the coordinated NHC, compared to the coordinated C=C bond *cis* disposed (Ir—(C24/C25)_{cent}) to the NHC ligand. Thus, the observed metal-olefin bond elongation would reaffirm the strong *trans* influence induced by the NHC ligand. This effect is clearly evident in other M(COD) (where M = Ir or Rh) systems that incorporate either the ^{Mes}[CN] or ^{Mes}[CP] ligand as shown in Table 4.2. However, this trend appears to be broken in the case of complex **4.8a** as the bond length of Ir1—(C28/C29)_{cent} = 2.09(1) Å compared with Ir1—(C24/C25)_{cent} = 2.16(1) Å that has the C=C unit positioned *cis* to the NHC, but *trans* to the C—H activated methyl group (C13). Coordinated alkyl ligands are not typically known to be strong σ -donors. However, the formation of the five-membered metallacycle (encompassing C13, P1 and Ir1) may be partially responsible for the abnormal bond lengths.

Since the two equivalents of $\text{KN}(\text{SiMe}_3)_2$ are added to **4.6** before $[\text{Ir}(\text{COD})\text{Cl}]_2$ is introduced into the mixture, the deprotonated $^{\text{Mes}}[\text{CP}]$ proligand can presumably react with Ir through two different mechanisms (Scheme 4.7). One pathway is the reaction of free NHC with Ir to break apart the dimer leaving the phosphide tether to dangle, which subsequently coordinates to Ir through salt metathesis generating **4.8** in moderate yield (69%). The other pathway could be the reaction of the phosphide tether with $[\text{Ir}(\text{COD})\text{Cl}]_2$ displacing one of the bridging chloride atoms to form an $[\text{Ir}^{\text{I}}(\text{COD})]_2(\mu\text{-Cl})(\mu\text{-P-NHC})$ dimer (**4.8**[†]). The dangling NHC group could subsequently bind to one of the $\text{Ir}(\text{COD})$ units leaving the phosphido fragment as the only bridging component (**4.8**[‡]). C—H activation could then follow via oxidative addition of the methyl C—H bond across $^{\text{Mes}}[\text{CP}]\text{Ir}^{\text{I}}(\text{COD})$ occurs to produce **4.8a** in very low yield. The two mechanisms seem plausible as further reactivity of pure **4.8** with $[\text{Ir}(\text{COD})\text{Cl}]_2$ is not observed.

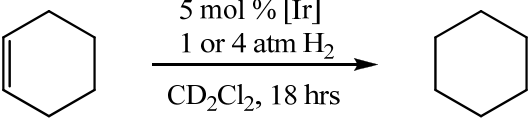
Scheme 4.7



(i) 2 $\text{KN}(\text{SiMe}_3)_2$, 0.5 $[\text{Ir}(\text{COD})\text{Cl}]_2$, THF, -30 °C
 (4.8⁺ and 4.8^{*} are unobserved intermediates)

Simple hydrogenation tests were performed with **4.8** using cyclohexene as the substrate and applying 1 and 4 atm of H_2 pressure. Although the results were improved from **2.11**, the overall activity was still disappointing relative to other known Ir-NHC catalysts. However, the improvement may have been partially attributed to the destabilization of the COD ligand in **4.8** due to the stronger *trans* influence induced by the phosphido tether. Despite the activity improvement made by the ligand modification of $^{\text{Mes}}[\text{CN}]$ to $^{\text{Mes}}[\text{CP}]$, the fundamental problem behind why these catalyst precursors are inefficient for hydrogenation reactions remains unresolved. Table 4.4 summarizes the hydrogenation results of **4.8** and **2.11**.

Table 4.4. Results from the hydrogenation test reactions of **4.8** and **2.11** using cyclohexene as the substrate. H₂ pressure was applied at either 1 or 4 atm and the reaction was allowed to react for 18 hours in a Teflon-sealed glass reactor.

		
Conversion (%) ^a		
Catalyst [Ir]	1 atm	4 atm
4.8	22	54
2.11 ^b	nil	23

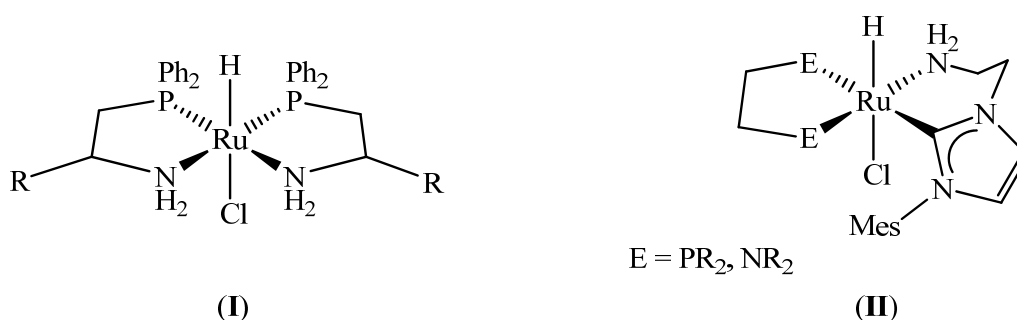
^a Conversions were measured in solution by ¹H NMR spectroscopy.

^b Complex **2.11** = ^{Mes}[CN]Ir(COD) as reported in Chapter 2.

4.10 Synthesis, Characterization and Reactivity of ^{Mes}[CNH₂]

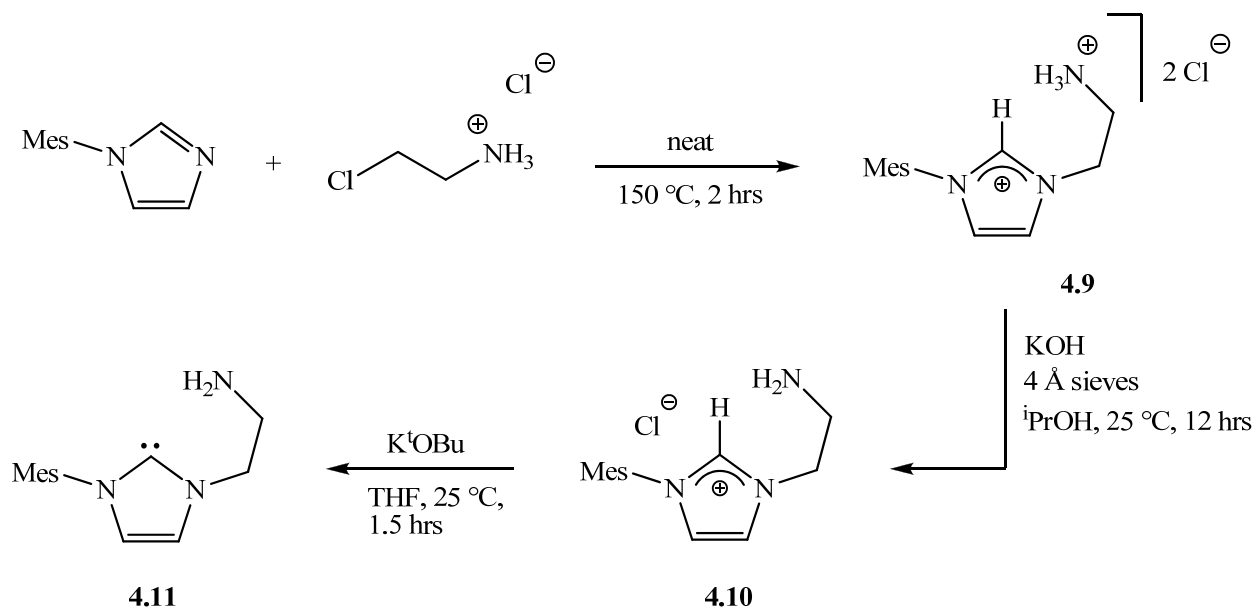
From the synthesis and reactivity studies of **4.6**, it was concluded that modifying of the ^{Mes}[CNH] ligand and substituting an amino tether by a phosphino tether was less productive than originally anticipated. Thus, it was hoped that modification of the amino substituent may yield a more positive result. As a starting point, it was necessary to have an objective that was appropriate for these NHC mixed-donor ligand systems. It was reported by Morris and coworkers that their chelating ligand systems were effective for bifunctional transfer hydrogenations catalysis when complexed to Ru.²⁹ One catalyst variation that was particularly interesting was a Ru catalyst that incorporated β-aminophosphine ligands (**I**). This type of Ru catalyst was useful for selective hydrogenation of substrates that incorporated polar functional groups such as ketones and imines, but unreactive towards olefins. The success of (**I**) was attributed to the electron donating strength of the phosphino group that increased the acidity of the ligand's amino protons that could be used as a proton source for the bifunctional transfer hydrogenation process.³⁰ Since it is commonly accepted that NHCs are stronger σ-donors than

phosphines, the synthesis of an NHC ligand that has an amino tether (**II**) similar to the beta-aminophosphine ligand system reported by Morris *et al.* was investigated.



To construct an NHC ligand similar to that suggested in complex **II**, mesitylimidazole can be heated to 150 °C neat with 2-chloroethylamine hydrochloride to generate a dicationic imidazolium salt, $^{Mes}[HCNH_3] \cdot 2Cl$, which is denoted **4.9**. Compound **4.9** can be identified in the 1H NMR spectrum by its diagnostic iminium proton resonance at δ 9.47. Deprotonation of **4.9** at the ammonium position can be performed by the addition of **4.9** to a solution of KOH in anhydrous 2-propanol in the presence of molecular sieves to generate the hydroscopic imidazolium salt $^{Mes}[HCNH_2]Cl$ (**4.10**). Complex **4.10** exhibits a downfield shift of the iminium resonance to δ 10.6 in the 1H NMR spectrum. Compound **4.10** can be deprotonated once more with K^tOBu to produce the air- and moisture-sensitive free carbene $^{Mes}[CNH_2]$ (**4.11**), in low yield. Successful synthesis of **4.11** can be determined by the disappearance of the iminium resonance at δ 10.6 from **4.10** in the 1H NMR spectrum in addition to the emergence of a downfield shifted resonance at δ 216.3 in the ^{13}C NMR spectrum assigned to the carbene carbon. It should be noted that **4.9** cannot be doubly deprotonated in one step to generate **4.11** due to the insolubility of **4.9** in solvents in which **4.11** is unreactive; **4.9** is only soluble in water and light alcohols, which are reactive with NHCs. Compound **4.11** is to the best of our knowledge the first NHC functionalized with a primary amino alkyl tether. Scheme 4.8 describes the synthetic route to **4.11**.

Scheme 4.8



Following the synthesis of the Ru catalyst previously mentioned (**I**), compound **4.11** was added to a solution of $\text{Ru}(\text{PPh}_3)_3\text{HCl}$ and heated at reflux overnight.³⁰ However, the reaction proceeded to yield a mixture of products that were unidentifiable by NMR spectroscopy. Various changes to the reaction conditions, solvents and reagents were attempted, but isolation of a pure $^{\text{Mes}}[\text{CNH}_2]\text{-Ru}$ complex remained elusive.

4.11 Conclusions

Several examples of metallation of the $^{\text{Mes}}[\text{CNH}]$ proligand were explored yielding silver(I) and lithium complexes of **2.2**. While it was intended that the synthesis of the $^{\text{Mes}}[\text{CNH}]\text{-Ag}$ complexes **4.1** and **4.2** would expand the synthetic arsenal to gain access of complexes that were unavailable by the direct addition of the free $^{\text{Mes}}[\text{CNH}]$ ligand, the end result fell short of expectations. Similarly, the synthesis of a rare lithiated NHC-amido dimer was found to be unable to transmetallate the $^{\text{Mes}}[\text{CN}]$ unit to early transition metals.

With the lack of success from transmetallation, ligand modifications were explored. A new analogue of $^{\text{Mes}}[\text{CNH}]$ was synthesized with changes made to the amino tether. $^{\text{Mes}}[\text{HCPH}]\text{Cl}$ was successfully isolated, but proved to be problematic during deprotonation reactions to produce the free carbene species **4.6a**. While it was observed by low temperature NMR analysis that compound **4.6** could be selectively deprotonated at the iminium position yielding the free NHC, it was not possible to isolate this species even at reduced temperatures. Rather, double deprotonation of the imidazolium salt **4.6** was necessary to coordinate the $^{\text{Mes}}[\text{CP}]$ ligand to a metal center. The double deprotonation strategy produced Rh and Ir complexes **4.7** and **4.8**. During the synthesis of **4.7** and **4.8**, it was found that the coordinated $^{\text{Mes}}[\text{CP}]$ ligand had the capacity to react further and form bimetallic phosphido bridged complexes. The di-iridium complex, **4.8a**, was isolated and characterized by single-crystal X-ray analysis. The propensity of forming the bridging species (**4.7a**) was also evident in solution as during the synthesis of **4.7** coupling of the phosphido tether to two Rh centers was observed in the ^{31}P NMR spectrum. However, compounds **4.7** and **4.8** can be purified by recrystallization, which enabled their reactivity to be investigated. Complexes **4.7** and **4.8** were characterized by X-ray diffraction crystallography and were found to be structurally very similar to each other as well as to their $^{\text{Mes}}[\text{CN}]$ ligated congeners **2.5** and **2.11**, respectively. Hydrogenation test reactions were performed with **4.8** and it was found to be superior to the $^{\text{Mes}}[\text{CN}]\text{Ir}(\text{COD})$ analogue, but still subpar in terms of overall activity compared to other known Ir-NHC catalysts.

The difficulty associated with the synthesis of the free NHC $^{\text{Mes}}[\text{CPH}]$ ligand encouraged further ligand modifications of $^{\text{Mes}}[\text{CNH}]$ to be made at the amino position instead of pursuing synthesis of other phosphine derivatives. The strategy was to synthesize a mixed-donor NHC-amino proligand intended for bifunctional transfer hydrogenation reactions as its chemical properties appeared to be favorable for such applications. However, it was found that although a

new free carbene proligand, $^{\text{Mes}}[\text{CNH}_2]$ could be synthesized, metallation to Ru complexes was problematic.

This chapter has demonstrated various possibilities available for modifying the mixed-donor NHC ligand, $^{\text{Mes}}[\text{CNH}]$, originally developed in Chapter 2, to yield a well-defined set of ligands. However, while the modifications have displayed interesting properties, the ability to apply the adapted ligands for the synthesis of useful organometallic complexes has been mostly inadequate. The following chapter will outline other possibilities available with this NHC ligand set with an emphasis on future reactivity studies.

4.12 *Experimental Section*

General Considerations. Unless otherwise specified, all experimental procedures were performed in a dry, oxygen-free nitrogen or argon atmosphere by Schlenk or glovebox techniques. Compounds **2.1** and **2.2** was synthesized as previously described in Chapter 2.³¹ All other chemicals were purchased commercially and used as received. Anhydrous toluene, hexanes and pentane were purchased from Aldrich, sparged with nitrogen, and passed through columns containing activated alumina and Radox catalyst. Methylene chloride and tetrahydrofuran were purified similarly, except without treatment from Radox catalyst. Deuterated benzene (C_6D_6), and methylene chloride (CD_2Cl_2) were purified via refluxing under nitrogen with CaH_2 then vacuum transferred in to a Kontes sealed glass vessel containing 4 Å molecular sieves. Gases were removed by three freeze-pump-thaw cycles. Deuterated chloroform ($CDCl_3$) was distilled under N_2 and collected over activated 4 Å molecular sieves into a Kontes sealed glass vessel followed by three freeze-pump-thaw degassing cycles. 1H , ^{13}C and ^{31}P NMR spectra were obtained by a Bruker AVANCE 300, 400 MHz spectrometer. Elemental analysis and mass spectrometry (EI/MS) were performed at the Department of Chemistry at the University of British Columbia.

($^{Mes}[CNH]_2Ag$)OTf (**4.1**). To 70.0 mg of AgOTf (0.2724 mmol) in 10 mL of THF, 200 mg (0.5755 mmol) of **2.2** dissolved in 10 mL of THF added dropwise at room temperature in the absence of light. The mixture was stirred for 30 min in the dark and then concentrated until a suspended consistency. The mixture was then cooled to $-35\text{ }^\circ\text{C}$ and filtered. The light grey powder was then washed with Et_2O and dried under vacuum. Yield: 80 mg (49 %). 1H NMR (CD_2Cl_2 , 400 MHz) δ : 1.77 (s, 6H, $-ArCH_3$), 2.01 (s, 6H, $-ArCH_3$), 2.23 (s, 3H, $-ArCH_3$), 2.24 (s, 3H, $-ArCH_3$), 2.88 (t, 1H, $J = 8.0\text{ Hz}$, $-N_{Ar}HCH_2$), 3.02 (m, 2H, $-N_{Ar}HCH_2$), 4.22 (t, 2H, $J = 5.3\text{ Hz}$, $-N_{imid}CH_2$), 6.79 (s, 2H, $-ArH$), 6.80 (s, 2H, $-ArH$), 6.94 (m, 1H, $-imidH$), 7.40 (m, 1H, $-imidH$). ^{13}C NMR (CD_2Cl_2 , 100 MHz) δ : 17.8, 18.3 ($-o-ArCH_3$), 20.9, 21.2 ($-p-ArCH_3$), 49.5 ($-$

$N_{\text{imid}}CH_2$), 53.1 ($-N_{\text{Ar}}CH_2$), 122.9 (d, $J_{\text{CAg}} = 5$ Hz, -imidC), 123.6 (d, $J_{\text{CAg}} = 5$ Hz, -imidC), 129.7, 129.9 (-ArC), 131.0 (-*o*-ArC_{ipso}), 132.9 (-*p*-ArC_{ipso}), 135.3 (-*o*-ArC_{ipso}), 136.0 (-ArC_{ipso}), 140.0 (-*p*-ArC_{ipso}), 142.6 (-ArC_{ipso}), 181.7 (dd, $J_{\text{C}^{107}\text{Ag}} = 181$ Hz, $J_{\text{C}^{109}\text{Ag}} = 208$ Hz, -AgC_NCN).

^{Mes}[CNH]AgCl (4.2). A flask containing 300 mg (0.7813 mmol) of **2.1**, 86 mg (0.3711 mmol) of Ag₂O and 50 mL of CH₂Cl₂ was stirred under N₂ for 1 week in the absence of light. The dark suspension becomes a light grey over the week. The suspension was then filtered through Celite (in air) into a flask containing MgSO₄. The MgSO₄ was filtered off and the colorless filtrate was removed under vacuum to leave a white solid. The white product was collected and washed with Et₂O and dried under vacuum. Yield: 76 mg (42 %). ¹H NMR (CDCl₃, 400 MHz) δ: 1.93 (s, 6H, -ArCH₃), 2.12 (s, 6H, -ArCH₃), 2.19 (s, 3H, -ArCH₃), 2.30 (s, 3H, -ArCH₃), 2.93 (t, 1H, $J = 7.9$ Hz, -N_{Ar}HCH₂), 3.32 (m, 2H, -N_{Ar}HCH₂), 4.39 (t, 2H, $J = 5.8$ Hz, -N_{imid}CH₂), 6.78 (s, 2H, -ArH), 6.91 (s, 2H, -ArH), 6.92 (sh, 1H, -imidH), 7.31 (d, 1H, $J = 1.5$ Hz, -imidH). ¹³C NMR (CDCl₃, 100 MHz) δ: 17.6, 18.9 (-*o*-ArCH₃), 20.5, 20.98 (-*p*-ArCH₃), 49.1 (-N_{Ar}CH₂), 52.7 (-N_{imid}CH₂), 122.1, 122.4 (-imidC), 129.4, 129.5 (-ArC), 130.2 (-*o*-ArC_{ipso}), 132.4 (-*p*-ArC_{ipso}), 134.6 (-*o*-ArC_{ipso}), 135.3 (-ArC_{ipso}), 139.5 (-*p*-ArC_{ipso}), 141.7 (-ArC_{ipso}). EI-MS: 491 [M⁺]. Anal. Calc. For C₂₃H₂₉N₃ClAg: C, 56.28; H, 5.96; N, 8.56. Found: C, 56.34; H, 5.90; N, 8.21 %.

^{Mes}[CNH]₂PdCl₂ (4.3). A 100 mg (0.1090 mmol) of **4.2** in 5 mL of CH₂Cl₂ was added to a stirring solution containing 26 mg (0.09808 mmol) of Pd(COD)MeCl in 5 mL of CH₂Cl₂. The mixture was allowed to stir for 2 hrs to yield a grey suspension. The suspension was filtered through a plug of Celite and concentrated under vacuum leaving a brown-grey residue. Hexanes were then added to the concentrate to precipitate a pale grey solid that was collected by filtration and dried under vacuum. The product isolated is a crude mixture of Pd compounds. Complex **4.3** can only be isolated as colorless crystals via slow evaporation of the crude solid from a 4:1

mixture of CH₂Cl₂/hexanes. The crystals isolated are suitable for X-ray diffraction analysis.

Yield: 5 mg (6 %).

Mes[CNLi]₂ (4.4). To 2.00 g (5.755 mmol) of compound **2.2** dissolved in 40 mL of toluene was added 4.0 mL (6.400 mmol) of 1.6 M *n*-BuLi solution in hexanes via syringe at room temperature. The brown solution becomes amber in color upon addition of the *n*-BuLi and the solution is stirred for 2 hrs. The solvent was then removed under vacuum and the product was triturated with hexanes. The resultant gold powder was then collected on a glass frit and washed with 3 x 5 mL aliquots of hexanes. Yield: 1.92 g (94 %). ¹H NMR (C₆D₆, 400 MHz) δ: 1.85 (s, 6H, -ArCH₃), 2.10 (s, 6H, -ArCH₃), 2.24 (s, 3H, -ArCH₃), 2.31 (s, 3H, -ArCH₃), 3.54 (t, 2H, *J* = 2.7 Hz, -N_{imid}CH₂), 3.83 (t, 2H, *J* = 2.7 Hz, -N_{Li}CH₂), 6.08 (d, 1H, *J* = 1.4 Hz, -imidH), 6.12 (d, 1H, *J* = 1.4 Hz, -imidH), 6.83 (s, 2H, -ArH), 6.85 (s, 2H, -ArH). ¹³C NMR (C₆D₆, 100 MHz) δ: 18.0, 21.2, 21.3, 21.4 (-ArCH₃), 54.0 (-N_{imid}CH₂), 54.3 (-N_{Li}CH₂), 119.7, 121.8 (-imidC), 124.5 (-ArC_{ipso}), 129.5, 130.4 (-ArC), 132.5, 135.8, 138.1, 138.6, 158.0 (-ArC_{ipso}), 198.5 (-LiC_NCN). ⁷Li NMR (C₆D₆, 156 MHz) δ: 2.71 (s, -N_{Li}C_NCN). EI-MS: 347 [1/2 (M⁺ – Li)]. Anal. Calc. For C₄₆H₅₆N₆Li₂: C, 78.16; H, 7.99; N, 11.89. Found: C, 75.96; H, 7.81; N, 11.40 %.

Mes[HCeCl]Cl (4.5). A 5.00 g (26.85 mmol) of mesityl imidazole dissolved in 20 mL of 1,2-dichloroethane was refluxed for 2 days. The mixture was then cooled to room temperature and concentrated under vacuum. 10 mL of Et₂O was then added to precipitate a white solid that was collected and washed with Et₂O, then dried under vacuum. Yield: 3.46 g (69 %). ¹H NMR (CDCl₃, 300 MHz) δ: 1.93 (s, 6H, -ArCH₃), 2.20 (s, 3H, -ArCH₃), 4.04 (t, 2H, *J* = 5.5 Hz, -ClCH₂), 5.00 (t, 2H, *J* = 5.5 Hz, -N_{imid}CH₂), 6.86 (s, 2H, -ArH), 7.10 (s, 1H, -imidH), 8.42 (s, 1H, -imidH), 10.17 (s, 1H, -NCHN). EI-MS: 249 [M⁺ – Cl]. Anal. Calc. For C₁₄H₁₈N₂Cl₂: C, 58.96; H, 6.36; N, 9.82. Found: C, 59.30; H, 7.94; N, 9.57 %.

Mes⁺[HCPH]Cl (4.6). To 1.79 g (0.0118 mol) of K^tOBu in 50 mL of degassed DMSO was added a solution of 4.14 g (0.0145 mol) of **4.5** in 50 mL of degassed DMSO and stirred for 10 min. Mesitylphosphine was then added to the solution via syringe to generate a pink solution and allowed to continue to stir for 2 hrs. DMSO was removed via distillation with dynamic vacuum and degassed MeOH was then added to precipitate a red powder. The MeOH was removed under vacuum and washed with 100 mL of degassed H₂O. The mixture was then extracted with 3 x 50 mL of CH₂Cl₂ and dried with MgSO₄. The solvent was removed under vacuum and Et₂O was added to the sticky pink residue to precipitate a powder. The product was collected by vacuum filtration and was washed repeatedly with Et₂O until the yellow byproduct disappeared. The pink powder was then dried under vacuum to yield a pale pink powder. Yield: 3.45 g (59 %). ¹H NMR (CD₂Cl₂, 400 MHz) δ: 2.07 (s, 3H, -ArCH₃), 2.08 (s, 3H, -ArCH₃), 2.24 (s, 3H, -ArCH₃), 2.34 (s, 3H, -ArCH₃), 2.44 (dm, 2H, ²J_{HP} = 124.9 Hz, -P_{Ar}CH₂), 2.46 (s, 6H, -ArCH₃), 4.42 (dt, 1H, J_{HP} = 221.5 Hz, ³J_{HH} = 7.7 Hz, -MesPHCH₂), 4.66 (dm, 2H, ³J_{HP} = 107.6 Hz, -N_{imid}CH₂), 6.90 (s, 1H, -ArH), 6.91 (s, 1H, -ArH), 7.03 (s, 2H, -ArH), 7.21 (t, J = 1.7 Hz, imidH), 7.76 (t, J = 1.7 Hz, imidH), 11.0 (t, 1H, J = 1.7 Hz, -NCHN). ¹³C NMR (CD₂Cl₂, 100 MHz) δ: 18.0, 21.3, 21.4 (-ArCH₃), 23.1 (d, J_{CP} = 18 Hz, -P_{Ar}CH₂), 23.5 (d, ³J_{CP} = 11 Hz, -o-ArCH₃), 49.9 (d, ²J_{CP} = 9 Hz, -N_{imid}CH₂), 123.1, 123.5 (-imidC), 128.0 (d, ²J_{CP} = 14 Hz, -o-ArC_{ipso}), 129.6, 129.7, 130.2 (-m-ArC), 131.5, 134.9, 139.2 (-ArC_{ipso}), 139.7 (-NCHN), 141.7 (-ArC_{ipso}), 142.5 (d, J_{CP} = 12 Hz, -ArC_{ipso}P). ³¹P NMR (CDCl₃, 162 MHz) δ: -97.4 (d, J_{PH} = 222 Hz, -MesPHEt). EI-MS: 365 [M⁺ - HCl]. Anal. Calc. For C₂₃H₃₀N₂PCl: C, 68.90; H, 7.54; N, 6.99. Found: C, 70.16; H, 7.64; N, 7.32 %.

Mes⁺[CP]Rh(COD) (4.7). To a vial containing 104 mg (0.2594 mmol) of **4.6** is dissolved in 5 mL of THF was added 114 mg (0.5715 mmol) of KN(SiMe₃)₂ in 2 mL of THF dropwise. The mixture becomes an amber suspension and was allowed to stir for 1 hr before 63 mg (0.1278

mmol) of $[\text{Rh}(\text{COD})\text{Cl}]_2$ in 10 mL of THF was added dropwise to the mixture. The resultant dark green solution was allowed to stir overnight at room temperature then concentrated to dryness under vacuum. The residue was extracted into C_6H_6 and filtered through a plug of Celite. The filtrate was concentrated under vacuum and pentane was added to precipitate a dark green powder. The product was collected by filtration followed by a pentane wash and dried under vacuum. Yield: 85 mg (59 %). ^1H NMR (C_6D_6 , 400 MHz) δ : 1.74 – 2.13 (br, -COD), 1.81 (br, 2H, $-\text{P}_{\text{Ar}}\text{CH}_2$), 2.10 (s, 3H, $-\text{ArCH}_3$), 2.24 (s, 3H, $-\text{ArCH}_3$), 2.27 (br, -COD), 2.95 (s, 6H, $-\text{ArCH}_3$), 3.90 (br, -COD), 4.11 (br, 2H, $-\text{N}_{\text{imid}}\text{CH}_2$), 5.98 (d, 1H, $J = 1.7$ Hz, -imidH), 6.23 (d, 1H, $J = 1.7$ Hz, -imidH), 6.73 (s, 2H, -ArH), 7.06 (s, 2H, -ArH). ^{13}C NMR (C_6D_6 , 100 MHz) δ : 19.8 (-COD), 21.3, 21.5 ($-\text{ArCH}_3$), 24.1 (d, $J_{\text{CP}} = 32$ Hz, $-\text{P}_{\text{Ar}}\text{CH}_2$), 26.0, 26.2 ($-\text{ArCH}_3$), 32.0 (-COD), 57.1 (d, $J_{\text{CP}} = 5$ Hz, $-\text{N}_{\text{imid}}\text{CH}_2$), 81.3, 87.4 (-COD), 120.6, 122.3 (-imidC), 129.3, 129.5 (-ArC), 135.2, 136.6, 138.0, 138.9 ($-\text{ArC}_{\text{ipso}}$), 143.1 (d, $^2J_{\text{CP}} = 11$ Hz, $-\text{ArC}_{\text{ipso}}$), 144.9 (d, $J_{\text{CP}} = 45$ Hz, $-\text{ArC}_{\text{ipso}}$), 186.5 (dd, $J_{\text{CRh}} = 54$ Hz, $^2J_{\text{CP}} = 17$ Hz, $-\text{RhC}_{\text{NCN}}$). ^{31}P NMR (C_6D_6 , 161 MHz) δ : 9.0 (d, $J_{\text{PRh}} = 74$ Hz, -MesPRh). EI-MS: 574 $[\text{M}^+]$. Anal. Calc. For $\text{C}_{31}\text{H}_{40}\text{N}_2\text{PRh}$: C, 64.80; H, 7.02; N, 4.88. Found: C, 64.50; H, 7.15; N, 4.75 %.

Mes[CP]Ir(COD) (4.8). The synthetic procedure was as described for **4.7** using 108 mg (0.2694 mmol) of **4.6**, 119 mg (0.5965 mmol) of $\text{KN}(\text{SiMe}_3)_2$ and 90 mg (0.1340 mmol) of $[\text{Ir}(\text{COD})\text{Cl}]_2$. The product is collected as an orange-brown solid. Yield: 110 mg (63 %). ^1H NMR (CDCl_3 , 400 MHz) δ : 1.65 (br,), 1.84 (br,), 1.92 – 2.16 (m, -COD), 2.09 (s, 3H, $-\text{ArCH}_3$), 2.23 (br, 6H, $-\text{ArCH}_3$), 2.28 (s, 3H, $-\text{ArCH}_3$), 2.96 (s, 6H, $-\text{ArCH}_3$), 3.28 (br,), 3.77 (br,), 4.00 (m, 2H, $-\text{N}_{\text{Mes}}\text{CH}_2$), 5.97 (d, 1H, $J = 1.8$ Hz, -imidH), 6.18 (d, 1H, $J = 1.8$ Hz, -imidH), 6.72 (s, 2H, -ArH), 7.08 (s, 2H, -ArH). ^{13}C NMR (C_6D_6 , 100 MHz) δ : 19.7 (-COD), 21.3, 21.4 ($-\text{ArCH}_3$), 23.0 (d, $J_{\text{CP}} = 25$ Hz, $-\text{P}_{\text{Ar}}\text{CH}_2$), 25.7, 25.8 ($-\text{ArCH}_3$), 32.3, 33.5 (-COD), 58.0 ($-\text{N}_{\text{imid}}\text{CH}_2$), 64.3, 75.0 (-COD), 120.6, 122.6 (-imidC), 129.3, 129.4 (-ArC), 136.0, 137.9, 139.0, 141.7, 142.0, 143.6 (-

ArC_{ipso}), 177.9 (d, $^2J_{CP} = 11$ Hz, -IrC_{NCN}). ^{31}P NMR (C₆D₆, 161 MHz) δ : - 0.5 (s, -MesPEt). EI-MS: 664 [M^+]. Anal. Calc. For C₃₁H₄₁N₃Ir: C, 56.09; H, 6.07; N, 4.22. Found: C, 56.07; H, 6.09; N, 4.36 %.

Mes[HCNH₃]·2Cl (4.9). A Schlenk was charged with 500 mg (2.685 mmol) of mesityl imidazole and 311 mg (2.681 mmol) of 2-chloroethylamine hydrochloride. The mixture was then heated to 150 °C neat for 2 hrs. The hard solid was collected by filtration and washed with anhydrous Et₂O under air. The hygroscopic off-white crude powder was then dried under vacuum and stored under N₂. Yield 700 mg (86 %). The crude product is 92 % pure but can be used as is for the synthesis of **4.10** as the 8 % impurity is unreacted 2-chloroethylamine hydrochloride that can be removed during workup. ^1H NMR (CD₃OD, 400 MHz) δ : 2.17 (s, 6H, -ArCH₃), 2.40 (s, 3H, -ArCH₃), 3.71 (m, 2H, -NH₃CH₂), 4.85 (m, 2H, -N_{imid}CH₂), 7.16 (s, 2H, -ArH), 7.84 (s, 1H, -imidH), 8.15 (s, 1H, -imidH), 9.47 (s, 1H, -NCHN). ^{13}C NMR (CD₃OD, 100 MHz) δ : 17.7, 21.3 (-ArCH₃), 40.0 (-NH₃CH₂), 48.2 (-N_{imid}CH₂), 124.9, 126.2 (-imidC), 130.9 (-ArC), 132.5, 136.0 (-ArC_{ipso}), 139.6 (-HCHN), 142.7 (-ArC_{ipso}). EI-MS: 229 [$\text{M}^+ - 2 \text{HCl}$]. Anal. Calc. For C₁₄H₂₁N₃Cl₂·2/25C₂H₇NCl₂: C, 52.84; H, 6.92; N, 13.75. Found: C, 59.93; H, 6.88; N, 13.53 %.

Mes[HCNH₂]Cl (4.10). A 50 mL Schlenk was charged with 75 mg (1.337 mmol) of dry KOH powder, 25 mL of anhydrous 2-propanol and activated 4 Å molecular sieves. 200 mg (0.6617 mmol) of **4.9** was then added under a stream of N₂ and the suspension was stirred overnight. The solvent was removed under vacuum and the product was then extracted with 2 x 20 mL of CH₂Cl₂ and filtered through a plug of Celite. The pale yellow filtrate was concentrated until viscous followed by addition of 10 mL of Et₂O to precipitate the off-white powder that was collected by filtration. The product was washed with 3 x 5 mL of Et₂O and dried under vacuum. Yield 85 mg (48 %). ^1H NMR (CD₂Cl₂, 400 MHz) δ : 1.50 (br, -NH₂), 2.08 (s, 6H, -ArCH₃), 2.34

(s, 3H, -ArCH₃), 3.17 (m, 2H, -NH₂CH₂), 4.68 (m, 2H, -N_{imid}CH₂), 7.03 (s, 2H, -ArH), 7.20 (s, 1H, -imidH), 8.00 (s, 1H, -imidH), 10.6 (s, 1H, -NCHN). ¹³C NMR (CD₂Cl₂, 100 MHz) δ: 17.9, 21.4 (-ArCH₃), 42.4 (-NH₂CH₂), 52.5 (-N_{imid}CH₂), 123.1, 123.8 (-imidC), 130.2 (-ArC), 131.5, 135.0 (-ArC_{ipso}), 139.8 (-NCHN), 141.6 (-ArC_{ipso}).

^{Mes}[CNH₂] (**4.11**). To a suspension of 100 mg (0.3763 mmol) **4.10** in 10 mL of THF was added a 5 mL solution of THF containing 47 mg (0.4189 mmol) of K^tOBu dropwise at room temperature. The mixture was stirred for 1.5 hours and the yellow suspension slowly abates to an orange solution. The solution was then filtered through a plug of Celite to remove the fine KCl precipitate and then concentrated until the solution became viscous. Hexanes was then added to precipitate an orange-brown solid. The suspension was then cooled to – 30 °C and collected by filtration. The rust-colored powder was then dried under vacuum. Yield 25 mg (29%). ¹H NMR (C₆D₆, 400 MHz) δ: 0.91 (br, 2H, -NH₂), 2.07 (s, 6H, -ArCH₃), 2.13 (s, 3H, -ArCH₃), 2.82 (br, 2H, -NH₂CH₂), 3.79 (t, 2H, *J* = 5.7 Hz, -N_{imid}CH₂), 6.37 (d, 1H, *J* = 1.5 Hz, -imidH), 6.50 (d, 1H, *J* = 1.5 Hz, -imidH), 6.77 (s, 2H, -ArH). ¹³C NMR (C₆D₆, 100 MHz) δ: 18.4, 21.3 (-ArCH₃), 44.2 (-NH₂CH₂), 54.8 (-N_{imid}CH₂), 119.6, 120.7 (-imidC), 129.4 (-ArC), 135.8, 137.5, 139.6 (-ArC_{ipso}), 216.3 (-NCN).

4.13 References

1. Lin, I. J. B.; Vasam, C.; Sekhar, *Coord. Chem. Rev.* **2007**, *251*, 642.
2. Wang, H. M. J.; Lin, I. J. B., *Organometallics* **1998**, *17*, 972.
3. Sentman, A. C.; Csihony, S.; Waymouth, R. M.; Hendrick, J. L., *J. Org. Chem.* **2004**, *70*, 2391.
4. de Fremont, P.; Scott, N. M.; Stevens, E. D.; Ramnial, T.; Lightbody, O. C.; Macdonald, C., L.B.; Clyburne, J. A. C.; Abernethy, C. D.; Nolan, S. P., *Organometallics* **2005**, *24*, 6301.
5. Magill, A. M.; McGuinness, D. S.; Cavell, K. J.; Britovsek, G. J. P.; Gibson, V. C.; White, A., J.P.; Williams, D. J.; White, A. H.; Skelton, B. W., *J. Organomet. Chem.* **2001**, *617-618*, 546.; Nielsen, D. J.; Cavell, K. J.; Skelton, B. W.; White, A. H., *Inorg. Chim. Acta* **2006**, *359*, 1855.
6. Lee, H. M.; Zeng, J. Y.; Hu, C.-H.; Lee, M.-T., *Inorg. Chem.* **2004**, *43*, 6822.
7. McGuinness, D. S.; Cavell, K. J., *Organometallics* **2000**, *19*, 741.
8. Herrmann, W. A.; Elison, M.; Fischer, J.; Koecher, C.; Artus, G. R. J., *Angew. Chem., Int. Ed.* **1995**, *34*, 2371.
9. Arnold, P. L.; Mungur, S. A.; Blake, A. J.; Wilson, C., *Angew. Chem., Int. Ed.* **2003**, *42*, 5981.
10. Shih, W.-C.; Wang, C.-H.; Chang, Y.-T.; Yap, G. P. A.; Ong, T.-G., *Organometallics* **2009**, *28*, 1060.
11. Spencer, L. P.; Beddie, C.; Hall, M. B.; Fryzuk, M. D., *J. Am. Chem. Soc.* **2006**, *128*, 12531.
12. Huang, Y.-P.; Tsai, C.-C.; Shih, W.-C.; Chang, Y.-C.; Lin, S.-T.; Yap, G. P. A.; Chao, I.; Ong, T.-G., *Organometallics* **2009**, *28*, 4316.

13. Bernstein, M. P.; Romesberg, F. E.; Fuller, D. J.; Harrison, A. T.; Collum, D. B.; Liu, Q. Y.; Williard, P. G., *J. Am. Chem. Soc.* **1992**, *114*, 5100.; DePue, J. S.; Collum, D. B., *J. Am. Chem. Soc.* **1988**, *110*, 5518.; Galiano-Roth, A. S.; Michaelides, E. M.; Collum, D. B., *J. Am. Chem. Soc.* **1988**, *110*, 2658.; Kallman, N.; Collum, D. B., *J. Am. Chem. Soc.* **1987**, *109*, 7466.; Lucht, B. L.; Collum, D. B., *J. Am. Chem. Soc.* **1994**, *116*, 6009.; Lucht, B. L.; Collum, D. B., *J. Am. Chem. Soc.* **1996**, *118*, 2217.; Remenar, J. F.; Lucht, B. L.; Collum, D. B., *J. Am. Chem. Soc.* **1997**, *119*, 5567.; Rutherford, J. L.; Collum, D. B., *J. Am. Chem. Soc.* **1999**, *121*, 10198.
14. Boche, G.; Hilf, C.; Harms, K.; Marsch, M.; Lohrenz, J. C. W., *Angew. Chem., Int. Ed.* **1995**, *34*, 487.; Wacker, A.; Pritzkow, H.; Siebert, W., *Eur. J. Inorg. Chem.* **1998**, 843.; Arduengo, A. J., III; Tamm, M.; Calabrese, J. C.; Davidson, F.; Marshall, W. J., *Chemistry Letters* **1999**, *21*, 1021.; Frankel, R.; Birg, C.; Kernbach, U.; Habereeder, T.; Noth, H.; Fehlhhammer, W. P., *Angew. Chem., Int. Ed.* **2001**, *40*, 1907.; Mungur, S. A.; Liddle, S. T.; Wilson, C.; Sarsfield, M. J.; Arnold, P. L., *Chem. Commun.* **2004**, 2738.; Arnold, P. L.; Rodden, M.; Wilson, C., *Chem. Commun.* **2005**, 1743.; Frankel, R.; Kniczek, J.; Ponikwar, W.; Noth, H.; Polborn, K.; Fehlhhammer, W. P., *Inorg. Chim. Acta* **2001**, *312*, 23.; Nieto, I.; Bontchev, R. P.; Smith, J. M., *Eur. J. Inorg. Chem.* **2008**, 2476.
15. Arnold, P. L.; Rodden, M.; Davis, K. M.; Scarisbrick, A. C.; Blake, A. J.; Wilson, C., *Chem. Commun.* **2004**, 1612.
16. Shishkov, I. V.; Rominger, F.; Hofmann, P., *Organometallics* **2009**, *28*, 3532.
17. Jorgensen, W. L.; Severance, D. L., *J. Am. Chem. Soc.* **1990**, *112*, 4768.
18. Hunter, C. A.; Sanders, J. K. M., *J. Am. Chem. Soc.* **1990**, *112*, 5525.; Sato, T.; Tsuneda, T.; Hirao, K., *J. Chem. Phys.* **2005**, *123*, 104307.

19. Spencer, L. P.; Winston, S.; Fryzuk, M. D., *Organometallics* **2004**, 23, 3372.; Spencer, L. P.; Fryzuk, M. D., *J. Organomet. Chem.* **2005**, 690, 5788.
20. Yang, C.; Lee, H. M.; Nolan, S. P., *Org. Lett.* **2001**, 3, 1511.; Danopoulos, A. A.; Winston, S.; Gelbrich, T.; Hursthouse, M. B.; Tooze, R. P., *Chem. Commun.* **2002**, 482.; Lee, H. M.; Chiu, P. L.; Zeng, J. Y., *Inorg. Chim. Acta* **2004**, 357, 4313.; Stylianides, N.; Danopoulos, A. A.; Tsoureas, N., *J. Organomet. Chem.* **2005**, 690, 5948.; Wolf, J.; Labande, A.; Daran, J.-C.; Poli, R., *J. Organomet. Chem.* **2006**, 691, 433.
21. Henderson, W. A.; Streuli, C. A., *J. Am. Chem. Soc.* **1960**, 82, 5791.
22. Li, J.-N.; Liu, L.; Fu, Y.; Guo, Q.-X., *Tetrahedron* **2006**, 62, 445.
23. Amyes, T. L.; Diver, S. T.; Richard, J. P.; Rivas, F. M.; Toth, K., *J. Am. Chem. Soc.* **2004**, 126, 4366.; Nair, V.; Bindu, S.; Sreekumar, V., *Angew. Chem. Int. Ed.* **2004**, 43, 5130
24. Achamlale, S.; Mabrouk, H.; Elachqar, A.; El Hallaoui, A.; El Hajji, S.; Alami, A.; Bellan, J.; Mazieres, M. R.; Wolf, J. G.; Pierrot, M., *Phosphorus, Sulfur Silicon Relat. Elem.* **2007**, 182, 357.; Boukallaba, K.; Elachqar, A.; El Hallaoui, A.; Alami, A.; El Hajji, S.; Labriti, B.; Atmani, A.; El Bali, B.; Lachkar, M.; Allouchi, H.; Martinez, J.; Rolland, V., *Phosphorus, Sulfur Silicon Relat. Elem.* **2007**, 182, 1045.; Boukallaba, K.; Elachqar, A.; El Hallaoui, A.; Alami, A.; El Hajji, S.; Labriti, B.; Martinez, J.; Rolland, V., *Phosphorus, Sulfur Silicon Relat. Elem.* **2006**, 181, 819.; Otero, A.; Carrillo-Hermosilla, F.; Terreros, P.; Exposito, T.; Rojas, S.; Fernandez-Baeza, J.; Antinolo, A.; Lopez-Solera, I., *Eur. J. Inorg. Chem.* **2003**, 3233.
25. Lee, H. M.; Jiang, T.; Stevens, E. D.; Nolan, S. P., *Organometallics* **2001**, 20, 1255.; Chianese, A. R.; Li, X.; Janzen, M. C.; Faller, J. W.; Crabtree, R. H., *Organometallics* **2003**, 22, 1663.; Chianese, A. R.; Kovacevic, A.; Zeglis, B. M.; Faller, J. W.; Crabtree,

- R. H., *Organometallics* **2004**, 23, 2461.; Albrecht, M.; Miecznikowski, J. R.; Samuel, A.; Faller, J. W.; Crabtree, R. H., *Organometallics* **2002**, 21, 3596.
26. Vazquez-Serrano, L. D.; Owens, B. T.; Buriak, J. M., *Chem. Commun.* **2002**, 2518.
27. Lee, D.-H.; Chen, J.; Faller, J. W.; Crabtree, R. H., *Chem. Commun.* **2001**, 213.; Whited, M. T.; Grubbs, R. H., *Organometallics* **2008**, 2, 5737.; Torres, O.; Martin, M.; Sola, E., *Organometallics* **2009**, 28, 863.
28. Grasa, G. A.; Moore, Z.; Martin, K. L.; Stevens, E. D.; Nolan, S. P.; Paquet, V.; Lebel, H., *J. Organomet. Chem.* **2002**, 658, 126.; Allen, D. P.; Crudden, C. M.; Calhoun, L. A.; Wang, R.; Decken, A., *J. Organomet. Chem.* **2005**, 690, 5736.; Roberts, D. A.; Steinmetz, G. R.; Breen, M. J.; Shulman, P. M.; Morrison, E. D.; Duttera, M. R.; DeBrosse, C. W.; Whittle, R. R.; Geoffroy, G. L., *Organometallics* **1983**, 2, 846.; Bottcher, H.-C.; Graf, M.; Merzweiler, K., *J. Organomet. Chem.* **1996**, 525, 191.; Ebsworth, E. A. B.; Gould, R. O.; McManus, N. T.; Rankin, D. W. H.; Walkinshaw, M. D.; Whitelock, J. D., *J. Organomet. Chem.* **1983**, 249, 227.; Targos, T. S.; Geoffroy, G. L.; Rheingold, A. L., *Organometallics* **1986**, 5, 12.
29. Clapham, S. E.; Hadzovic, A.; Morris, R. H., *Coord. Chem. Rev.* **2004**, 248, 2201.; Abdur-Rashid, K.; Clapham, S. E.; Hadzovic, A.; Harvey, J. N.; Lough, A. J.; Morris, R. H., *J. Am. Chem. Soc.* **2002**, 124, 15104.; Abdur-Rashid, K.; Lough, A. J.; Morris, R. H., *Organometallics* **2001**, 20, 1047.
30. Abdur-Rashid, K.; Guo, R.; Lough, A. J.; Morris, R. H.; Song, D., *Adv. Synth. Catal.* **2005**, 347, 571.
31. Jong, H.; Patrick, B. O.; Fryzuk, M. D., *Can. J. Chem.* **2008**, 86, 803.

CHAPTER FIVE

Conclusions and Future Direction

5.1 *Synopsis and Analysis*

This thesis has been based upon the development of a hemilabile ligand set that is comprised of a functionalized tether adjoined to an N-heterocyclic carbene (NHC) unit. With NHCs gaining popularity due to their synthetic flexibility and strong σ -donating character that resemble phosphine ligands, it was of particular interest to explore the reactivity and behavior of chelating mixed-donor NHC ligands in a variety of different coordination environments.

The synthesis and characterization of ^{Mes}[CNH] (**2.2**) was described in Chapter 2 and this became the basis of development for further ligand modifications that were later described in Chapter 4. Imidazolium salt precursor **2.1** was prepared by the reaction of mesitylimidazole with neat 2-(chloroethyl)mesitylamine at 150°C. Facile deprotonation of **2.1** with a strong base provided access to the aminocarbene **2.2** in good yield. Both the imidazolium salt and free carbene were useful entry points for the preparation of transition metal complexes. As such, Rh- and Ir-NHC complexes could be synthesized by the facile addition of **2.2** to [M(diene)Cl]₂ (M = Rh, Ir) compounds. The NHC-M(diene) complexes synthesized in Chapter 2 demonstrated a

variety of coordination modes possible with $^{\text{Mes}}[\text{CNH}]$. Compound **2.2** was used as a monodentate NHC ligand with a dangling amino tether as shown in the preparation of compounds **2.3**, **2.4** and **2.10**. Deprotonation of the dangling amino tether can be performed to generate the coordinated amido NHC derivatives **2.5**, **2.6** and **2.11**. However, if a halide extracting agent is used (e.g. NaBF_4) instead of a base with **2.3**, **2.4** or **2.10**, the non-coordinating amino arm can be coaxed to bind to the metal center to form a cationic metal complex as demonstrated by the synthesis of **2.7**, **2.8** and **2.12**. Despite the convenience of a synthetic strategy that can generate a family of NHC-M(diene) compounds with a variety of amido tether coordination modes, the complexes were found to be ineffective olefin hydrogenation catalysts. Data on the Rh variants was complicated by the presence of metallic rhodium that also contributed to the hydrogenation results. While the Ir congeners did not have the interference of catalyst decomposition, they were found to be too stable and slow to enter the catalytic cycle. The Rh and Ir precursors were tested as hydrosilylation catalysis and showed some positive results. However, while the activity was much improved from those observed for the olefin hydrogenations studies, they were still considered subpar relative to other known NHC-M ($\text{M} = \text{Rh}, \text{Ir}$) catalyst precursors.

Since the combination of $^{\text{Mes}}[\text{CNH}]$ and Group 9 metal complexes did not lead to effective precursors, the focus was shifted to investigate the reactivity of **2.2** with Ru compounds. It is well established that a Ru-benzylidene catalyst that contains an NHC group often outperforms its Ru-PR_3 analogue in parallel olefin metathesis reactions. This improvement in catalytic activity is best exemplified by the substitution of a PCy_3 ligand of Grubbs 1st generation catalyst with SIMes to yield the Grubbs 2nd generation system, which is widely considered to be superior in terms of olefin metathesis activity. While there have been numerous reports on ligand development for Ru-benzylidene catalysts, the majority of the work has been

focused on modifications made to the dissociating group. As there was significantly less work reported on modifying the NHC unit, the hemilabile aptitude of **2.2** was explored for Ru-benzylidene olefin metathesis catalysis.

The reaction of **2.2** with Grubbs 1st generation catalyst proceeds smoothly to give $^{\text{Mes}}[\text{CNH}]\text{Ru}(=\text{CHPh})(\text{PCy}_3)\text{Cl}_2$ (**3.1**), which has the amino side arm uncoordinated. The presence of the unbound amino arm had the potential to induce substrate control for ring-closing metathesis (RCM) and ring-opening metathesis polymerization (ROMP) reactions, or aid the stability of an active catalytic species. However, the results from the olefin metathesis reactions of **3.1** were disappointing. The source of the low activity of **3.1** was not due to a significant decrease in rate of phosphine dissociation relative to other well-known Ru-benzylidene precursors, which were evaluated by magnetization transfer (MT) experiments. However, the isolation of an 18-electron Ru-pyridine complex (**3.5**) showed that the coordination of the amino tether of $^{\text{Mes}}[\text{CNH}]$ negatively impacted RCM and ROMP activity. The RCM and ROMP test reactions of **3.5** revealed a substantial decrease in catalytic activity relative to **3.1**, which indicated that the formation of the 18-electron Ru complex was counterproductive to the initiation mechanism to generate the active 14-electron catalyst. Thus, it was plausible that the coordination of the amino tether of **3.1** was also responsible for its poor RCM and ROMP activity.

The hemilabile nature of **2.2** proved to be difficult to utilize effectively in catalysis. Thus, it was of interest to modify the ligand properties such that they were more suitable for specific reactions. One approach was to substitute the functionalized amino tether with a phosphine group as the increased electron donating potential of the phosphine unit may be more favorable for catalyst initiation. The preparation of phosphine analogue of **2.2** was accomplished by the addition of mesitylphosphine to 2-(chloroethyl)mesitylimidazolium chloride (**4.5**) in the presence

of a strong base to yield the desired precursor $^{\text{Mes}}[\text{HCPH}]\text{Cl}$ (**4.6**). However, the selective deprotonation of **4.6** at the iminium proton position was not straightforward. Low temperature NMR studies determined that selective deprotonation at the iminium position was possible, but as the temperature increased the compound appeared to exhibit proton exchange between the phosphine tether and the carbene carbon. Efforts to trap the $^{\text{Mes}}[\text{CPH}]$ ligand with Ag, Li and Rh complexes were not successful. Thus, the difficulty of isolating the free $^{\text{Mes}}[\text{CPH}]$ species led to a double deprotonation strategy of both the phosphino and iminium positions of **4.6**, followed by subsequent addition of $[\text{M}(\text{COD})\text{Cl}]_2$ ($\text{M} = \text{Rh}, \text{Ir}$) to produce **4.7** and **4.8**, respectively. Since $^{\text{Mes}}[\text{CP}]\text{Ir}(\text{COD})$ (**4.8**) was found to be very similar to its $^{\text{Mes}}[\text{CN}]\text{Ir}(\text{COD})$ congener (**2.11**), hydrogenation reactions that were unproductive with **2.11** were performed with **4.8** to evaluate its activity with the NHC-phosphide ligand. The results showed an improvement in overall activity, but still low compared to other known Ir-NHC hydrogenation catalysts. The complications associated with precursor **4.6**, as well as only a marginal improvement in catalytic activity of **4.8** relative to **2.11**, encouraged further ligand modifications to be made to the amino substituent of **2.2** instead of proceeding to synthesize derivatives of **4.6**.

A similar approach to the synthesis of **2.1** was successfully applied to the construction of an ammonium functionalized dicationic ligand precursor, $^{\text{Mes}}[\text{HCNH}_3] \cdot 2\text{Cl}$ (**4.9**). However, **4.9** was dicationic and required an additional deprotonation step with KOH in 2-propanol to yield precursor **4.10**, $^{\text{Mes}}[\text{HCNH}_2]\text{Cl}$, that incorporated a primary amino tether. The deprotonation of **4.10** with K^tOBu resulted in the production of the free NHC species $^{\text{Mes}}[\text{CNH}_2]$ (**4.11**), but was found to be a low-yielding process. While it is common to scale up reactions to alleviate a low-yielding synthesis, the poor solubility of **4.9** in non-alcoholic solvents, in addition to the H_2O byproduct produced during the synthesis of **4.10**, limited the efficiency of a large scale reaction. Alternative techniques such as the conversion of the imidazolium salt into a transmetallation

agent using Ag_2O or $n\text{-BuLi}$ were not useful as solvating **4.9** was problematic. Despite the lack of efficiency of the synthesis of **4.11**, sufficient product can be recovered for further reactivity. Compound **4.11** was designed for the application of byfunctional transfer hydrogenation operating as an auxiliary ligand in a Ru catalytic system. However, the synthesis of a $^{\text{Mes}}[\text{CNH}_2]\text{-Ru}$ based catalyst precursor was not straightforward.

While the formation of a transmetallating agent incorporating $^{\text{Mes}}[\text{CNH}_2]$ or $^{\text{Mes}}[\text{CPH}]$ was not possible, the addition of free NHC **2.2** to AgOTf generated complex **4.1**, ($^{\text{Mes}}[\text{CNH}]_2\text{Ag}$)OTf. Compound **4.1** was intended for the synthesis of a cationic Pd-based catalyst precursor, which are often overlooked in the literature. However, the synthesis of a cationic $^{\text{Mes}}[\text{CNH}]\text{-Pd}$ complex that contained a coordinated amino tether was found to be difficult as the reactions performed were unsuccessful in determining an appropriate combination of ligands to stabilize the $^{\text{Mes}}[\text{CNH}]\text{-Pd}$ system.

An alternative synthesis to prepare a $^{\text{Mes}}[\text{CNH}]\text{-Ag}$ transmetallating agent was to introduce **2.1** to a solution of Ag_2O , which resulted in the formation of $^{\text{Mes}}[\text{CNH}]\text{AgCl}$ (**4.2**). Complex **4.2** was added to $\text{Pd}(\text{COD})\text{MeCl}$ with the aim of generating $^{\text{Mes}}[\text{CNH}]_2\text{PdMeCl}$, a potentially active catalyst precursor for C—C coupling reactions. However, a mixture of products were obtained from the reaction with one species being identified as $^{\text{Mes}}[\text{CNH}]_2\text{PdCl}_2$ by single crystal X-ray diffraction analysis. Direct synthesis of $^{\text{Mes}}[\text{CNH}]_2\text{PdCl}_2$ by the addition of **4.2** to $\text{Pd}(\text{COD})\text{Cl}_2$ was unfortunately more complicated than expected.

To showcase the versatile coordinative ability of the $^{\text{Mes}}[\text{CNH}]$ ligand, a dimeric lithiated NHC-amido variant was isolated when $n\text{-BuLi}$ was added to a solution of **2.2** to generate $^{\text{Mes}}[\text{CNLi}]_2$ (**4.3**). Complex **4.3** was fully characterized and identified as a rare dimeric Li-NHC complex that bridged through the tethered amido groups. Regrettably, **4.3** was found to be

ineffective as a transmetallating agent. The reaction of **4.3** with halogenated transition metal complexes of Zr and Rh resulted in a mixture of unidentifiable products.

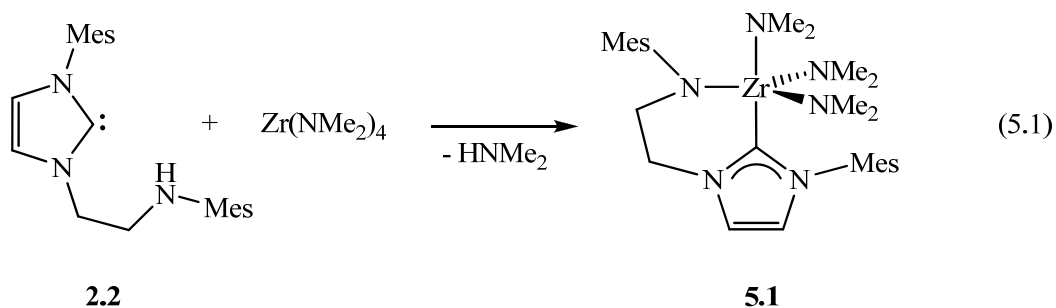
It has been demonstrated throughout this thesis that the bidentate NHC ligand set designed herein is versatile for the synthesis of various late metal complexes. The hemilabile nature of the ligands give flexibility to the coordination mode of the compounds prepared. However, the complexes synthesized have unfortunately not been efficient catalyst precursors. Although the ligands have, thus far, not behaved effectively as auxiliary ligands for catalysts, the coordinative properties of the ligand set have been studied in detail. The following section aims to explore other possible applications of this versatile ligand set with hopes of yielding more positive results and improved functionality of chemical transformations.

5.2 *Future Work*

Small molecule activation is an area of active research in the Fryzuk group. With nitrogen fixation being one particular focus in the group, it would be interesting to evaluate whether NHCs can function as useful auxiliary ligands in transition metal complexes to induce dinitrogen activation. With the success and expertise in early metal chelating amido-phosphine systems achieved by the Fryzuk group, it was intriguing to implement similar strategies to synthesize early metal NHC complexes for the purpose of fixing dinitrogen. Earlier work within the group has shown that a tridentate diamido NHC ligand forms complexes with Group 4 and 5 metals and have shown interesting insertion reactivity with small molecules.^{1, 2} It was hoped that a bidentate ligand variation would also have success in binding small molecules.

A useful entry to early metal NHC complexes would be through salt metathesis of a metal complex with a transmetallation agent. In Chapter 4, the synthesis of ^{Mes}[CNLi]₂ (**4.4**) was described, which would seemingly be ideal for salt metathesis with early metal halide

complexes. However, it was found that the reactivity of **4.4** with Zr and Ti halide complexes was not straightforward and yielded a mixture of unidentifiable products. While metathesis was unsuccessful for syntheses of a Zr- or Ti-NHC complex, aminolysis was found to be productive for the preparation of $^{\text{Mes}}[\text{CN}]\text{Zr}(\text{NMe}_2)_3$ (**5.1** in eq 5.1). Compound **5.1** can be synthesized by the facile addition of **2.2** to $\text{Zr}(\text{NMe}_2)_4$ at ambient temperature. Complex **5.1** is best identified by its diagnostic carbene resonance at δ 195.2 in the ^{13}C NMR spectrum that indicates coordination due to its upfield shift from δ 215.6 in the free NHC state of **2.2**. Crystals suitable for single crystal X-ray diffraction analysis were grown by slowly evaporating a concentrated solution of **5.1** in toluene. Figure 5.1 depicts the solid-state molecular structure of **5.1**.



The geometry of **5.1** is trigonal bipyramidal and exhibits a $\text{Zr1}-\text{C02}$ bond length of 2.500(2) Å, which is significantly longer than the expected range for Zr—NHC complexes. Typically, Zr-NHC complexes display $\text{Zr}-\text{C}_{\text{carbene}}$ bond lengths between 2.423 – 2.456 Å.³ Thus, the elongated $\text{Zr}-\text{C}_{\text{carbene}}$ bond of **5.1** could indicate a weakly bound NHC unit, which was not observed in similar diamido NHC-Zr systems.¹

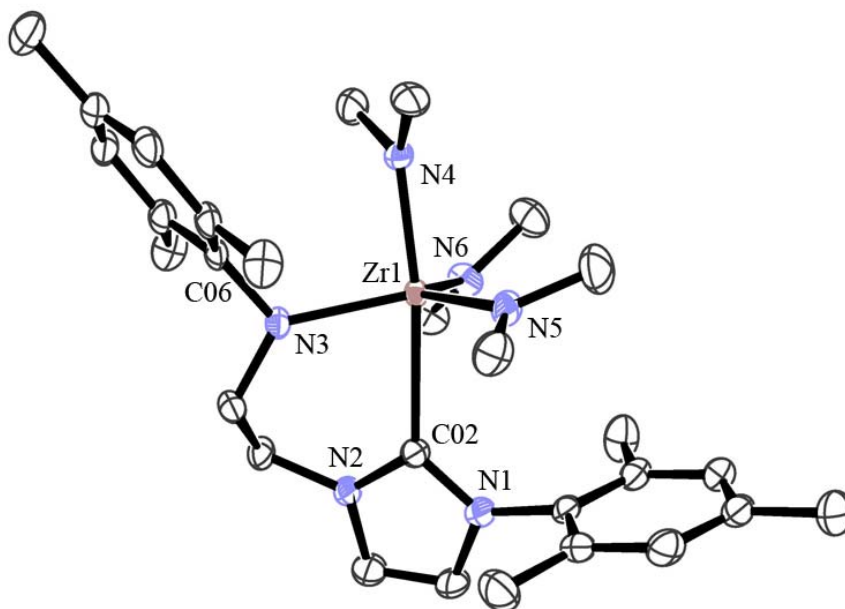
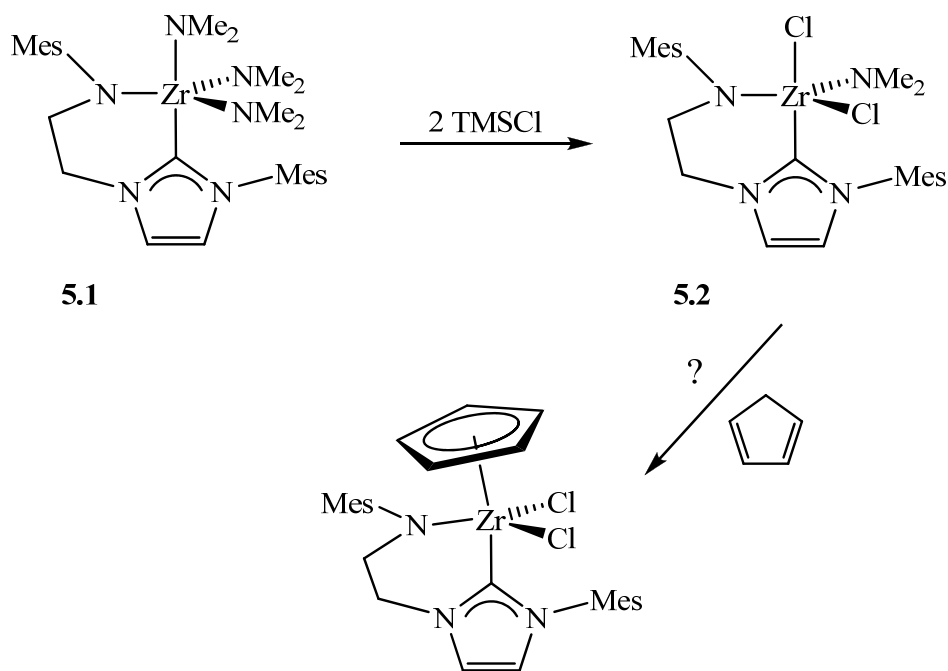


Figure 5.1. An ORTEP drawing of $^{\text{Mes}}[\text{CN}]\text{Zr}(\text{NMe}_2)_3$, **5.1**, with thermal ellipsoids drawn at 50 % probability. All hydrogens atoms were removed for clarity.

To accommodate small molecules more selectively, complex **5.1** would need to increase its steric bulk around the metal center to form a pocket that would only accept specific molecules. One possibility could be the addition of a cyclopentadienyl (Cp) ligand via salt metathesis with NaCp. However, to use salt metathesis as an entry to add the Cp ligand, the amido ligands of **5.1** needed to be replaced by halides first. Three equivalents of trimethylsilyl chloride (TMSCl) were added to **5.1**, but yielded a product characterized as $^{\text{Mes}}[\text{CN}]\text{Zr}(\text{NMe}_2)\text{Cl}_2$ (**5.2**) by ^1H NMR spectroscopy. The addition of an excess of TMSCl also produced a similar result. Despite only a double chlorination, NaCp was added to **5.2**, but resulted in a mixture of products that were not identifiable by NMR spectroscopy. However, it would be interesting to add cyclopentadiene to **5.2** and use aminolysis to stoichiometrically incorporate the Cp ligand (Scheme 5.1) as the pK_a of cyclopentadiene is 15 and considerably more acidic than that of dimethylamine with a pK_a of approximately 36 – 38.⁴ Should this method be successful for the

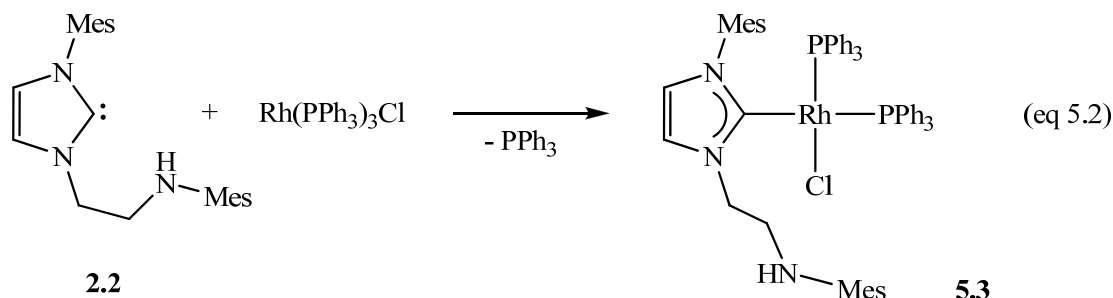
addition of the Cp ligand, the resultant compound could bind small molecules as its structure would be similar to that of Zr-Cp systems that have been shown to be effective for small molecule activation.⁵

Scheme 5.1



Late transition metal complexes have also shown ability in binding and transforming small molecules. Palladium(II) complexes have been found to be useful for their ability to catalyze oxidation reactions.⁶ More recently, NHC-Pd complexes have been explored and have shown promising results where Pd-peroxo complexes can be formed when exposed to O₂.⁷ While these Pd-O₂ compounds have shown some intriguing reactivity and can be useful for oxidation applications, less is known about Rh-peroxo analogues, especially those that incorporate NHC ligands.^{8,9} Moreover, there have been no reports of Rh complexes containing chelating NHC ligands that are able to coordinate dioxygen.

It was previously reported that Rh-NHC complexes such as Rh(IMes)(PPh₃)₂Cl and Rh(IPr)₂Cl were effective for binding O₂.⁸ Our approach to synthesize a similar complex was to introduce **2.2** to Rh(PPh₃)₃Cl to coordinate the NHC unit. This reaction can be performed without complications to produce the expected ^{Mes}[CNH]Rh(PPh₃)₂Cl compound (denoted **5.3**) as described by eq 5.2. Complex **5.3** can be easily detected by its ³¹P NMR spectrum as two sets of doublet of doublets are observed at δ 35.6 ($J_{\text{PRh}} = 120$ Hz, $^2J_{\text{PP}} = 39$ Hz) and δ 51.4 ($J_{\text{PRh}} = 211$ Hz, $^2J_{\text{PP}} = 39$ Hz) to account for coupling of the two ³¹P atoms to one another and to ¹⁰³Rh. Compound **5.3** also forms crystals suitable for X-ray crystallography when a concentrated solution of **5.3** in toluene is slowly evaporated. Figure 5.2 depicts the solid-state molecular structure of **5.3**.



Crystallographic analysis of **5.3** shows two molecules in the asymmetric unit that exhibit the expected square planar geometry about the Rh centers. Compound **5.3** displays Rh—C_{carbene} bond lengths in the region of 2.022 – 2.041 Å, which is within the range observed for similar Rh-NHC complexes.¹⁰ The PPh₃ ligands *trans*-disposed to the NHC show noticeable Rh—P_{*trans*} bond elongation as expected from the strong NHC *trans*-influence with an average distance of 2.319 Å compared to PPh₃ ligands positioned *cis* to the NHC with Rh—P_{*cis*} bond lengths averaging 2.204 Å. Although the amino tether was non-coordinating in solution, in the solid-state it positions the amino hydrogen in close contact with the chlorine atom with an NH...Cl distance in the range of 2.637 – 2.742 Å, which is within the sum of the van der Waals radii at 2.84 Å.

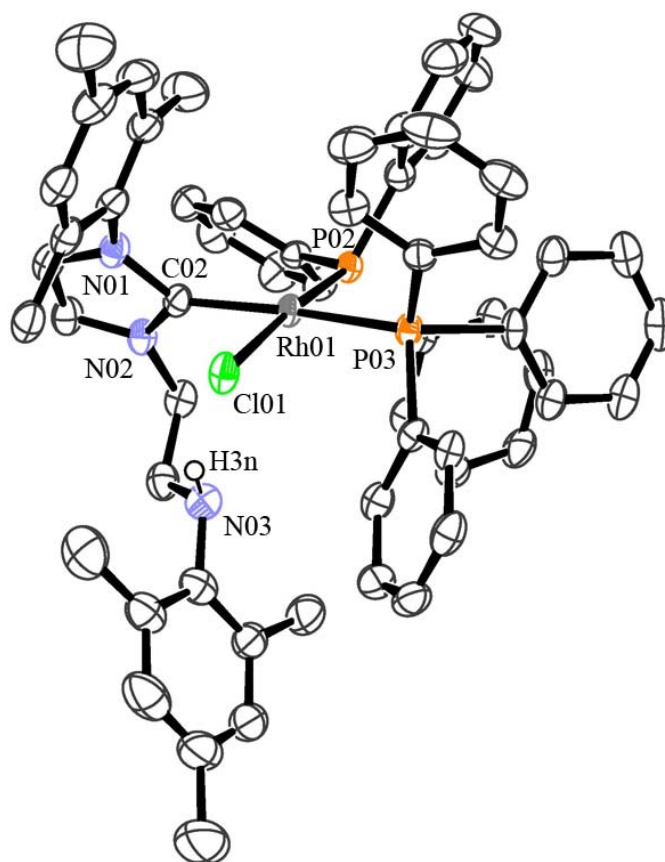
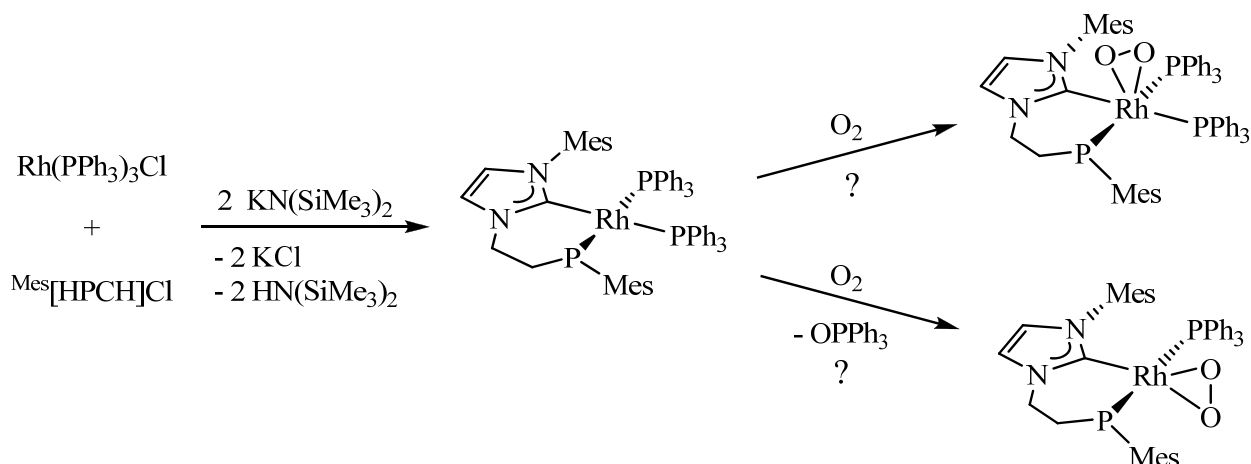


Figure 5.2. An ORTEP drawing of one molecule of $^{\text{Mes}}[\text{CNH}]\text{Rh}(\text{PPh}_3)_2\text{Cl}$, **5.3**, in the asymmetric unit with thermal ellipsoids drawn at 50 % probability. All hydrogens atoms were removed for clarity, except for H3n that was located in a difference map and refined isotropically.

While **5.3** does not feature a coordinated amino tether, it was important to test if it would bind dioxygen. Neither exposing **5.3** to air nor applying 1.5 atm of O_2 pressure for an extended period of time resulted in the detection of a bound dioxygen species by NMR spectroscopy. Typically a color change is also observed to indicate O_2 has coordinated, which was not observed with **5.3**. This inability to bind dioxygen may be steric in nature. Thus, $\text{KN}(\text{SiMe}_3)_2$ was added to a solution of **5.3** to deprotonate the amino tether, which was shown in Chapter 2 to be an effective technique to induce coordination. However, the reaction did not proceed as expected and yielded a mixture of products.

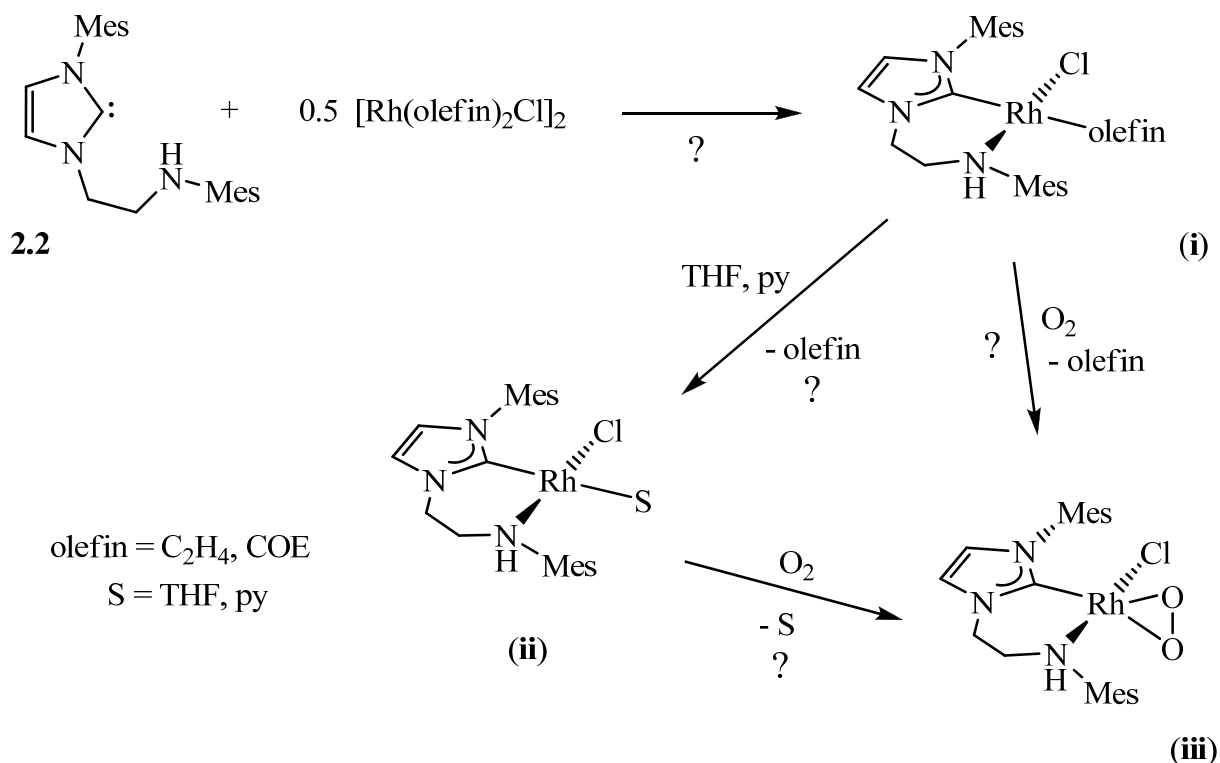
Scheme 5.2



It was anticipated that having a stronger donating auxiliary ligand may assist in the stabilization of a bound peroxo species. Thus, efforts to synthesize a $^{\text{Mes}}[\text{CP}]\text{Rh}(\text{PPh}_3)_2$ analogue, by reacting $^{\text{Mes}}[\text{HCPH}]\text{Cl}$ with $\text{Rh}(\text{PPh}_3)_3\text{Cl}$ and two equivalents of $\text{KN}(\text{SiMe}_3)_2$, may provide the appropriate balance of steric and electronic properties to bind O_2 , which could occur via different routes (Scheme 5.2). It has been reported that one of the PPh_3 ligands of $\text{Rh}(\text{IMes})(\text{PPh}_3)_2\text{Cl}$ dissociates before O_2 binds.⁸ However, ligand dissociation is not a prerequisite to O_2 coordination as it has also been demonstrated that dioxygen can be incorporated into square-planar Rh complexes without the need to dissociate a ligand.⁹

An alternative strategy could be the incorporation of $^{\text{Mes}}[\text{CNH}] \kappa^2$ to Rh by the reaction of **2.2** with $[\text{Rh}(\text{olefin})\text{Cl}]_2$ (olefin = ethylene, cyclooctene (COE)) (**i**) followed by exposure to O_2 to yield a $^{\text{Mes}}[\text{CNH}]\text{Rh}-\text{O}_2$ complex (**iii**) (Scheme 5.3). Another route to generate (**iii**) could be the addition of THF or pyridine to (**i**) to generate a solvent stabilized species (**ii**) that may be reactive towards oxygen to yield (**iii**). Substitution of Rh centers with Ir for the reactivity outlined in Scheme 5.3 could also yield promising results.

Scheme 5.3



An alternative approach to the coordination and activation of small molecules could be through the use of iron complexes, which have also been found to be effective for binding dinitrogen.^{11, 12} With the primary research focus of the Fryzuk group being small molecule activation, it was intriguing to investigate iron complexes that incorporated an NHC ligand motif that could potentially yield Fe systems that bind small molecules. It has been shown by Danopoulos *et al.* that upon reduction, their (L)FeBr₂ (L = tridentate NHC pincer) complex has the capacity to bind N₂.¹³ It was desirable to investigate the uniqueness of their Fe compound and test if other chelating NHC ligands could also serve as useful auxiliary ligands in Fe-N₂ systems.

The facile addition of **2.2** to FeBr₂ yielded a product that was not characterizable by NMR spectroscopy due to paramagnetism in the resultant ^{Mes}[CNH]FeBr₂ complex (**5.4**). Fortunately, crystals of **5.4** that were suitable for single crystal X-ray diffraction analysis could

be grown from a solution of methylene chloride. Figure 5.3 depicts the solid-state molecular structure of **5.4**. Complex **5.4** features tetrahedral geometry and a Fe01—C02 bond length of 2.060(3) Å, which is in the range expected for Fe—C_{carbene} bonds lengths of Fe-NHC compounds.¹⁴ Similarly, the Fe01—N03 bond length is also typical of Fe—NR₂ bonds.¹⁵

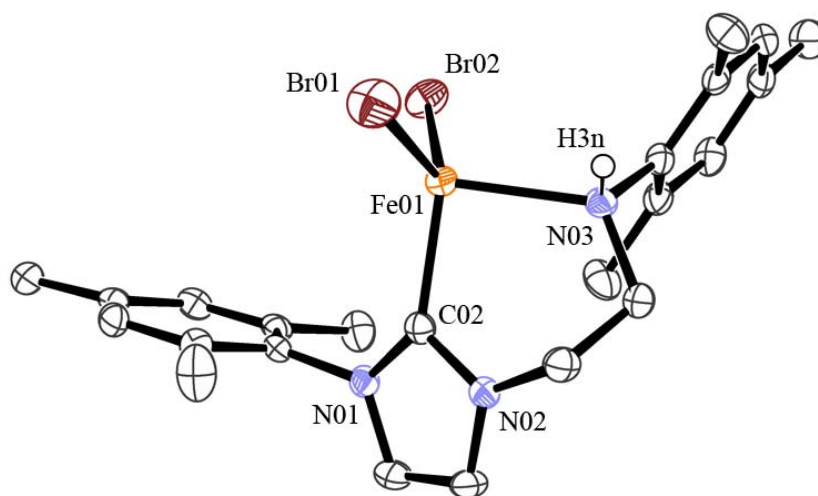
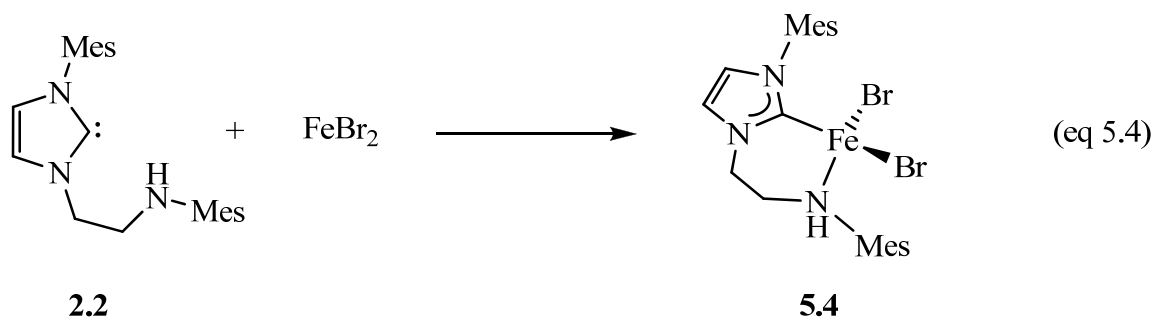
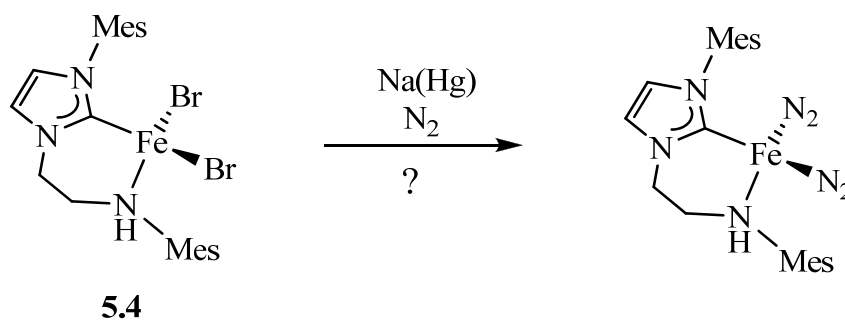


Figure 5.3. An ORTEP drawing of ^{Mes}[CNH]FeBr₂, **5.4**, with thermal ellipsoids drawn at 50 % probability. All hydrogens atoms were removed for clarity, except for H3n that was located in a difference map and refined isotropically.

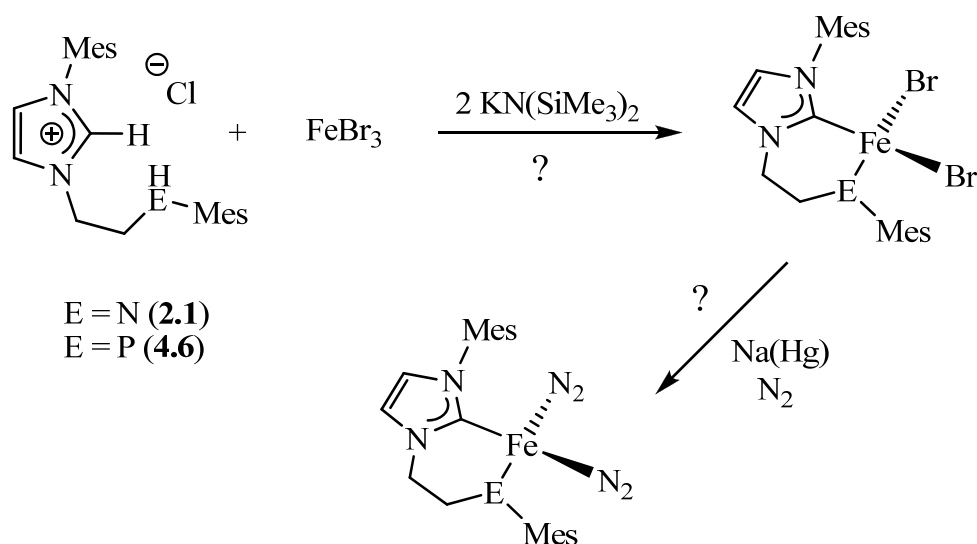
The synthesis of **5.4** provides a promising starting point for the reduction with sodium amalgam that has been successfully used with other Fe precursors to coordinate dinitrogen (Scheme 5.4).^{12, 13} However, if the reduction process is found to be reactive with the tethering amine, the synthesis of Fe(III) analogues could be an alternative. The Fe(III) analogues would

incorporate a bound amido tether to reinforce ligand coordination and eliminate the hemilabile property. Moreover, the anchoring of the tether to Fe(III) could also be used with the phosphido-NHC ligand analogue (Scheme 5.5).

Scheme 5.4



Scheme 5.5



Currently, there is still relatively little emphasis on investigating the properties of first-row transition metals that contain chelating NHC ligands. For example, nickel compounds that incorporate chelating NHC ligands are significantly less popular than those of palladium.

However, chelating Ni-NHC complexes have recently been found useful in C—C coupling^{16, 17}

and transfer hydrogenation reactions.¹⁸ Thus, employing the ligand set developed in this thesis to select first row transition metals would be of interest to broaden the scope of the field.

Our initial attempt to synthesize a chelating NHC-Ni complex began with the addition of **2.2** to Ni(DME)Cl₂ to displace the dimethoxyethane ligand to incorporate the ^{Mes}[CNH] unit. However, the synthesis of expected bidentate Ni complex was not obvious by NMR spectroscopy. Fortunately, the mixture precipitated crystals that were sufficient for analysis by X-ray crystallography. The single crystal X-ray analysis had shown that instead of the bidentate coordinating motif of **2.2** to NiCl₂, two equivalents of **2.2** had been incorporated into NiCl₂ and bound in a monodentate fashion through the carbene. Figure 5.4 depicts the solid-state molecular structure of ^{Mes}[CNH]₂NiCl₂ (**5.5**).

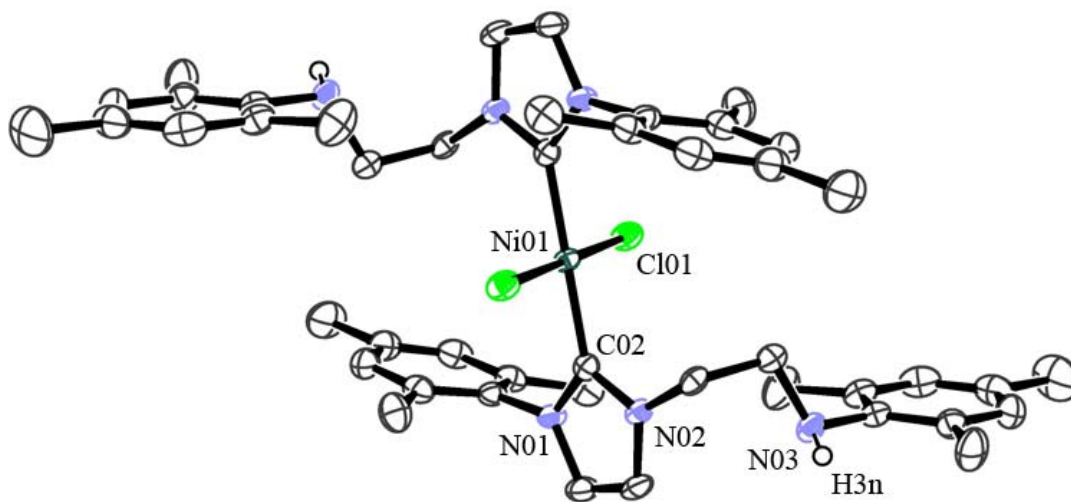
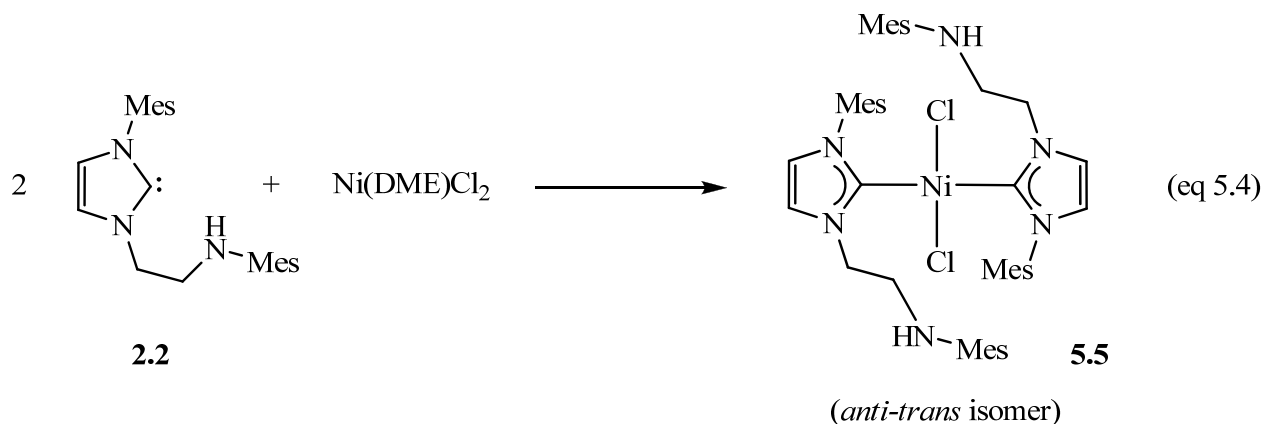


Figure 5.4. An ORTEP drawing of ^{Mes}[CNH]₂NiCl₂, **5.5**, with thermal ellipsoids drawn at 50 % probability. All hydrogens atoms were removed for clarity, except for H3n that was located in a difference map and refined isotropically. The molecular structure was solved as a half unit and the full molecule was generated by inversion symmetry.

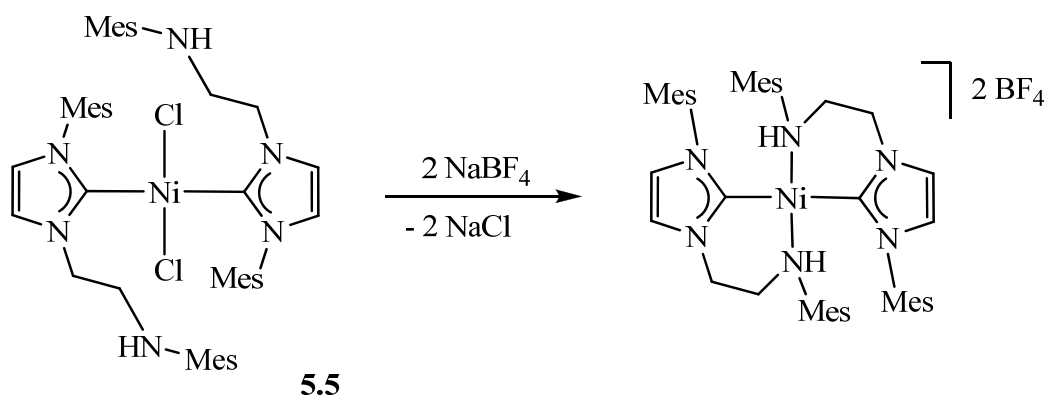
Compound **5.5** exhibits the expected square planar geometry and has a C02—N01 bond length of 1.902(4) Å that is in the range expected for similar biscarbene Ni compounds.¹⁹ Synthesis of **5.5** can be performed by the addition of two equivalents of **2.2** to Ni(DME)Cl₂ (eq 5.4). While the ¹H NMR spectrum of **5.5** was complicated, it did resemble the spectrum produced by the reaction of one equivalent of **2.2** with Ni(DME)Cl₂, which indicates that the donor strength of the amino tether was not strong enough to encourage the bidentate coordination mode. The complicated ¹H NMR spectrum can be rationalized by the existence of multiple isomers of **5.5** in solution, such as those observed in other biscarbene Ni complexes that have asymmetric NHC ligands.¹⁹



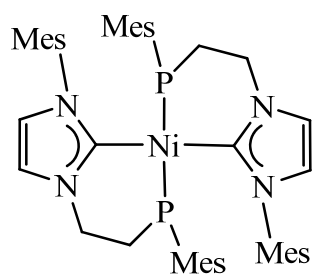
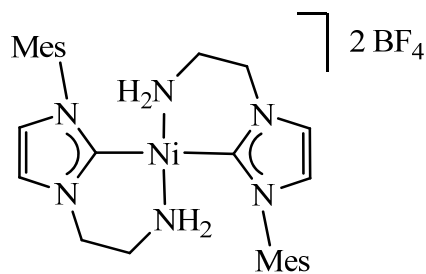
The possible isomers that are observed could be the *anti-trans* conformation of **5.5** as shown by the solid-state molecular structure. The other possibility would be the *syn-trans* conformation what would have the pendant amino tether on the same side of one another in the Ni square plane. Alternatively, a *cis* isomer could also be possible as *cis*-disposed NHC systems have been previously observed.²⁰ However, none of the other isomers could be identified except for the *anti-trans* species of **5.5**, which could only be obtained by crystallization. ¹H/¹H NMR correlation (COSY) analysis implies that there are two noticeable species in solution in approximately 2:1 ratio as indicated by the discrete resonance pairs representing the diagnostic proton signals of the ethylene tether. However, the resonances of the major species are broad and

difficult to assign, while the minor species had much better signal resolution. While the identity of the other isomer is unknown at this point, it seems more likely that the *syn-trans* isomer would be present rather than a *cis* isomer. However, the initial purpose was to synthesize the coordinated tether derivative of **5.5**. Thus, the employment of a halide abstracting agent such as NaBF_4 could be used to synthesize a dicationic version of **5.5** (Scheme 5.6), which may be useful for C—C coupling reactions as demonstrated by other cationic biscarbene Ni examples.^{16, 21}

Scheme 5.6



There could also be an opportunity to explore the reactivity of $^{\text{Mes}}[\text{HCPH}]$ (**4.6**) with Ni complexes. The synthesis of a compound such as **I** could be useful for C—C coupling reactions since it has been shown that tethering NHC-phosphine chelates are capable of performing such transformations.²² Complex **4.11** could also be more fortunate with Ni as recently, it has been shown by Morris *et al.* that their primary amino tethered NHC ligand is effective for transfer hydrogenation when used as an auxiliary ligand in a Ni(II) cationic precursor.¹⁸ The synthesis of **II** would provide access to a compound with similar characteristics to the complex prepared by Morris and co-workers, which could produce interesting results when used for transfer hydrogenation applications.

**I****II**

5.3 Concluding Remarks

The work of this thesis has been conducted with the intent to broaden the scope of research of organometallic complexes containing hemilabile mixed-donor NHC ligands. The ligand set developed has demonstrated versatility and flexibility in the syntheses for incorporating different functionalized tethers into the NHC motif. While complexes with this ligand set did not perform well as catalysts for some known organic transformations, the complexes synthesized outlined the coordinative potential of the ligand set and showed some interesting implications of incorporating hemilabile tethers into select catalyst precursors. The experience gained from the work of this thesis can be used to improve the applicability of hemilabile mixed-donor ligands and assist in the design of useful precursors in the future.

5.4 Experimental Section

General Considerations. Unless otherwise specified, all experimental procedures were performed in a dry, oxygen-free nitrogen or argon atmosphere by Schlenk or glovebox techniques. Synthesis of compound **2.2** was prepared as described in Chapter 2. SiMe_3Cl (TMSCl) was purified by treatment with 4 Å molecular sieves and distilled under N_2 into a Teflon sealed glass vessel. All other reagents were purchased commercially and used as received. Anhydrous toluene, hexanes and pentane were purchased from Aldrich, sparged with nitrogen, and passed through columns containing activated alumina and Radox catalyst. Methylene chloride and tetrahydrofuran were purified similarly, except without treatment from Radox catalyst. Deuterated benzene (C_6D_6), methylene chloride (CD_2Cl_2) and pyridine ($\text{C}_5\text{D}_5\text{N}$) were purified via refluxing under nitrogen with CaH_2 then vacuum transferred in to a Kontes sealed glass vessel containing 4 Å molecular sieves. Gases were removed by three freeze-pump-thaw cycles. Deuterated chloroform (CDCl_3) was distilled under N_2 and collected over activated 4 Å molecular sieves into a Kontes sealed glass vessel followed by three freeze-pump-thaw degassing cycles. ^1H , ^{13}C and ^{31}P NMR spectra were obtained by a Bruker AVANCE 300, 400 MHz spectrometer.

Mes[CN]Zr(NMe₂)₃ (5.1). To 86 mg (0.3215 mmol) of $\text{Zr}(\text{NMe}_2)_4$ in 5 mL of THF was added dropwise 123 mg (0.3540 mmol) of **2.2** in 5 mL of THF at room temperature. The brown mixture was stirred overnight then the solvent was removed under vacuum. Hexanes was added to the brown solid, cooled to $-30\text{ }^\circ\text{C}$ and the resulting precipitate was collected by filtration. The beige product was then washed with cold hexanes and dried under vacuum. Crystals suitable for single crystal X-ray analysis was grown by slowly concentrating a solution of **5.1** in toluene. Yield: 170 mg (30 %). ^1H NMR (C_6D_6 , 400 MHz) δ : 1.94 (s, 6H, *-o*-ArCH₃), 2.10 (s, 3H, *-p*-ArCH₃), 2.28 (s, 3H, *-p*-ArCH₃), 2.54 (s, 6H, *-o*-ArCH₃), 2.79 (s, 18, -NCH₃), 3.35 (m, 2H, -N_{Ar}CH₂), 3.81 (m,

2H, -N_{imid}CH₂), 5.99 (d, 1H, *J* = 1.5 Hz, -imid*H*), 6.14 (d, 1H, *J* = 1.5 Hz, -imid*H*), 6.75 (s, 2H, -Ar*H*), 7.08 (s, 2H, -Ar*H*). ¹³C NMR (C₆D₆, 100 MHz) δ: 17.7, 20.7, 21.3, 21.4 (-ArCH₃), 44.0 (-NCH₃), 55.8 (-N_{Ar}CH₂), 57.9 (-N_{imid}CH₂), 121.0, 121.8 (-imidC), 129.3, 129.4 (-ArC), 130.5, 133.8, 135.8, 138.1, 138.3, 156.0 (-ArC_{ipso}), 195.2 (-ZrC_NCN).

Mes₂[CN]Zr(NMe₂)Cl₂ (5.2). To 450 mg (0.7896 mmol) of **5.1** in 30 mL of toluene was added 0.2 mL of TMSCl via syringe at room temperature and stirred overnight. The resulting beige suspension was concentrated to 1/4 volume under vacuum. An equal volume of hexanes was then added and the pale beige solid was collected by filtration. The powder was washed with one aliquot (10 mL) of a 50:50 mixture of toluene/hexanes followed by two aliquots (5 mL) of hexanes. The solid was then dried under vacuum. Yield: 220 mg (50 %). ¹H NMR (C₅D₅N, 400 MHz) δ: 2.15 (s, 3H, -ArCH₃), 2.18 (s, 3H, -ArCH₃), 2.21 (s, 6H, -ArCH₃), 2.30 (s, 6H, -ArCH₃), 2.75 (s, 6H, -NCH₃), 3.46 (m, 1H, -N_{Ar}CH₂), 3.67 (m, 1H, -N_{Ar}CH₂), 3.95 (m, 2H, -N_{imid}CH₂), 6.51 (s, 2H, -Ar*H*), 6.97 (s, 2H, -Ar*H*), 7.14 (d, 1H, *J* = 1.2 Hz, -imid*H*), 7.61 (d, 1H, *J* = 1.2 Hz, -imid*H*).

Mes₂[CNH]Rh(PPh₃)₂Cl (5.3). To 100 mg (0.2878 mmol) of **2.2** dissolved in 5 mL of THF was added a 5 mL THF solution containing 240 mg (0.2595 mmol) of Rh(PPh₃)₃Cl. The brown solution was stirred overnight at room temperature and then concentrated to 1 mL under vacuum. 10 mL of Et₂O was added to precipitate a mustard yellow solid that was collected by filtration, washed with Et₂O and dried under vacuum. Crystals suitable for single crystal X-ray analysis was grown by slowly evaporating a concentrated solution of **5.3** in C₆H₆. Yield: 160 mg (61 %). ¹H NMR (C₆D₆, 400 MHz) δ: 1.63 (s, 3H, -ArCH₃), 2.22 (s, 3H, -ArCH₃), 2.40 (s, 3H, -ArCH₃), 2.42 (s, 6H, -ArCH₃), 2.46 (s, 3H, -ArCH₃), 3.13 (m, 1H, -N_{Ar}HCH₂), 3.44 (m, 1H, -N_{Ar}CH₂), 4.30 (t, 1H, *J* = 7.3 Hz, -N_{Ar}HCH₂), 5.73 (m, 1H, -N_{imid}CH₂), 6.16 (d, 1H, *J* = 1.2 Hz, -imid*H*), 6.39 (d, 1H, *J* = 1.2 Hz, -imid*H*), 6.79 – 7.01 (br, -PPh₃, -Ar*H*), 7.10 (s, 1H, -Ar*H*), 7.59 (t, 6H, *J*

= 7.4 Hz, -PPh₃). ³¹P NMR (C₆D₆, 121 MHz) δ : 35.6 (dd, $J_{\text{PRh}} = 120$ Hz, $J_{\text{PP}} = 39$ Hz, -RhP), 51.4 (dd, $J_{\text{PRh}} = 211$ Hz, $J_{\text{PP}} = 39$ Hz, -RhP).

Mes₃[CNH]FeBr₂ (5.4). To 312 mg (0.8978 mmol) of **2.2** dissolved in 5 mL of THF was added a 5 mL solution containing 176 mg (0.8161 mmol) of FeBr₂ at room temperature. The mixture was stirred overnight then concentrated to 1 mL under reduced pressure. The addition of hexanes afforded a grey-brown solid that was collected by filtration, washed with 3 x 5 mL of hexanes, and dried under vacuum. Crystals suitable for single crystal X-ray analysis were grown by slowly concentrating a solution of **5.4** in CH₂Cl₂. Yield: 142 mg (31 %).

Mes₃[CNH]₂NiCl₂ (5.5). To 30 mg (0.1365 mmol) of Ni(DME)Cl₂ suspended in 5 mL of THF was added 100 mg (0.2878 mmol) of **2.2** dissolved in 5 mL of THF. The mixture was stirred overnight at room temperature and then concentrated under vacuum. Et₂O was then added to precipitate a pink powder that was collected by filtration, washed with 3 x 5 mL of Et₂O, and dried under vacuum. Crystals suitable for X-ray diffraction analysis were grown by slow evaporation of a concentrated solution of **5.5** in CH₂Cl₂. Yield: 75 mg (67 %). ¹H NMR of the minor product (CD₂Cl₂, 400 MHz) δ : 1.89 (s, 3H, -ArCH₃), 2.15 (s, 6H, -ArCH₃), 2.21 (s, 6H, -ArCH₃), 2.55 (s, 3H, -ArCH₃), 3.85 (m, 2H, -NCH₂), 5.34 (m, 2H, -NCH₂), 6.59 (d, 1H, $J = 1.7$ Hz, -imidH), 6.93 (d, 1H, $J = 1.7$ Hz, -imidH), 6.95 (s, 2H, -ArH), 7.04 (s, 2H, -ArH).

5.5 *References*

1. Spencer, L. P.; Winston, S.; Fryzuk, M. D., *Organometallics* **2004**, *23*, 3372.
2. Spencer, L. P.; Fryzuk, M. D., *J. Organomet. Chem.* **2005**, *690*, 5788.; Spencer, L. P.; Beddie, C.; Hall, M. B.; Fryzuk, M. D., *J. Am. Chem. Soc.* **2006**, *128*, 12531.
3. Niehues, M.; Kehr, G.; Erker, G.; Wibbeling, B.; Frohlich, R.; Blacque, O.; Berke, H., *J. Organomet. Chem.* **2002**, *663*, 192.
4. Inoue, S.; Furukawa, K., *J. Organomet. Chem.* **1972**, *37*, 25.; Li, J.-N.; Liu, L.; Fu, Y.; Guo, Q.-X., *Tetrahedron* **2006**, *62*, 4453.
5. Chen, Y.-X.; Marks, T. J., *Organometallics* **1997**, *16*, 3649.; Pool, J. A.; Lobkovsky, E.; Chirik, P. J., *Nature* **2004**, *427*, 527.
6. Stahl, S. S., *Angew. Chem., Int. Ed.* **2004**, *43*, 3400.
7. Konnick, M. M.; Guzei, I. A.; Stahl, S. S., *J. Am. Chem. Soc.* **2004**, *126*, 10212.; Sigman, M. S.; Jensen, D. R., *Acc. Chem. Res.* **2006**, *39*, 221.
8. Praetorius, J. M.; Allen, D. P.; Wang, R.; Webb, J. D.; Grein, F.; Kennepohl, P.; Crudden, C., *J. Am. Chem. Soc.* **2008**, *130*, 3724.
9. Yu, X.-Y.; Patrick, B. O.; James, B. R., *Organometallics* **2006**, *25*, 4870.
10. Allen, D. P.; Crudden, C. M.; Calhoun, L. A.; Wang, R.; Decken, A., *J. Organomet. Chem.* **2005**, *690*, 5736.
11. MacKay, B. A.; Fryzuk, M. D., *Chem. Rev.* **2004**, *104*, 385.; Field, L. D.; Guest, R. W.; Vuong, K. Q.; Dalgarno, S. J.; Jensen, P., *Inorg. Chem.* **2009**, *48*, 2246.
12. Bart, S. C.; Lobkovsky, E.; Chirik, P. J., *J. Am. Chem. Soc.* **2004**, *126*, 13794.
13. Danopoulos, A. A.; Wright, J. A.; Motherwell, W. B., *Chem. Commun.* **2005**, 784.
14. Chen, M.-Z.; Sun, H.-M.; Li, W.-F.; Wang, Z.-G.; Shen, Q.; Zhang, Y., *J. Organomet. Chem.* **2006**, *691*, 2489.

15. Small, B. L.; Brookhart, M.; Bennett, A. M. A., *J. Am. Chem. Soc.* **1998**, *120*, 4049.; McGowan, P. C.; Temple, C. N., *Inorg. Chim. Acta* **2009**, *362*, 3165.
16. Xi, Z.; Liu, B.; Chen, W., *J. Org. Chem.* **2008**, *73*, 3954.
17. Liao, C.-Y.; Chan, K.-T.; Zeng, J.-Y.; Hu, C.-H.; Tu, C.-Y.; Lee, H. M., *Organometallics* **2007**, *26*, 1692.; Berding, J.; van Dijkman, T. F.; Lutz, M.; Spek, A. L.; Bouwman, E., *Dalton Trans.* **2009**, 6948.
18. O, W. W. N.; Lough, A. J.; Morris, R. H., *Organometallics* **2009**, *28*, 6755.
19. Huang, Y.-P.; Tsai, C.-C.; Shih, W.-C.; Chang, Y.-C.; Lin, S.-T.; Yap, G. P. A.; Chao, I.; Ong, T.-G., *Organometallics* **2009**, *28*, 4316.
20. Herrmann, W. A.; Elison, M.; Fischer, J.; Kocher, C.; Artus, G. R. J., *Angew. Chem., Int. Ed.* **1995**, *34*, 2371.; McGuinness, D. S.; Cavell, K. J., *Organometallics* **2000**, *19*, 741.
21. Zhou, Y.; Xi, Z.; Chen, W.; Wang, D., *Organometallics* **2008**, *27*, 5911.
22. Wolf, J.; Labande, A.; Natella, M.; Daran, J.-C.; Poli, R., *J. Mol. Catal. A: Chem.* **2006**, *259*, 205.

APPENDIX A

Supplementary Information

A.1 *X-Ray Crystallographic Data*

General Considerations. All crystals were mounted on a glass fiber and measured on a Bruker X8 diffractometer with graphite monochromated Mo-K α radiation. The data was collected at a temperature of $-100.0 \pm 0.1^\circ\text{C}$ with the Bruker APEX II CCD area-detector set at distance of 36.00 mm. Data was collected and integrated using the Bruker SAINT¹ software package and corrected for absorption effects using the multi-scan technique (SADABS).² The data was corrected for Lorentz and polarization effects and the structure was solved by direct methods.³ Neutral atom scattering factors for all non-hydrogen atoms were taken from Cromer and Waber.⁴ Anomalous dispersion effects were included in F_{calc} .⁵ The values for $\Delta f'$ and $\Delta f''$ were those of Creagh and McAuley.⁶ The values for mass attenuation coefficients are those of Creagh and Hubbell.⁷ All non-hydrogen atoms were refined anisotropically, while all hydrogen atoms except those coordinated to the amino tether were placed in calculated positions but were not refined. Amino protons were located in a difference map and refined isotropically. All refinements were performed using the SHELXTL⁸ crystallographic software package of Bruker-AXS.

Table A.1. Crystallographic structural refinement information for $^{\text{Mes}}[\text{CNH}]$ (**2.2**), $^{\text{Mes}}[\text{CNH}]\text{Rh}(\text{COD})\text{Cl}$ (**2.3**) and $^{\text{Mes}}[\text{CN}]\text{Rh}(\text{COD})$ (**2.5**).

Compound	2.2	2.3	2.5
Dataset ID	mf594	mf638	mf653
Empirical formula	C23 H29 N3	C34 H44 Cl N3 Rh	C31 H40 N3 Rh
Formula weight (g/mol)	347.49	633.08	557.57
$\lambda/\text{\AA}$	0.71073	0.71073	0.71073
Crystal system	Monoclinic	Triclinic	Monoclinic
Space group	P2(1)/c	P-1	P2(1)/n
a/ \AA	5.7858(4)	10.1543(6)	15.836(2)
b/ \AA	24.499(2)	12.0573(7)	8.7280(9)
c/ \AA	14.433(1)	13.9204(7)	20.572(2)
$\alpha/^\circ$	90	86.436(2)	90
$\beta/^\circ$	99.982(2)	70.448(2)	105.789(6)
$\gamma/^\circ$	90	87.218(2)	90
$V/\text{\AA}^3$	2014.9(2)	1602.3(2)	2736.1(5)
Z	4	2	4
$D_c/\text{g cm}^{-3}$	1.146	1.312	1.354
μ/mm^{-1}	0.068	0.642	0.648
$F(000)$	752	662	1168
Crystal size/ mm^3	0.30 x 0.10 x 0.10	0.25 x 0.25 x 0.1	0.31 x 0.23 x 0.11
$\theta_{\min} - \theta_{\max}/^\circ$	1.66 to 26.74	1.55 to 27.97	2.55 to 22.53
Reflections collected	32003	31972	3490
Independent reflections [R(int)]	4263 [0.0604]	7531 [0.0407]	3490 [0.0472]
Completeness to θ_{\max}	99.50%	97.60%	97.30%
Max. and min. transmission	0.9933 and 0.9800	0.9378 and 0.8110	0.9312 and 0.8923
Data / restraints / parameters	4263 / 0 / 245	7531 / 7 / 362	3490 / 0 / 330
Goodness-of-fit on F^2	1.025	1.077	0.977
R [$I > 2\sigma(I)$]	R1 = 0.0491, wR2 = 0.1275	R1 = 0.0312, wR2 = 0.0727	R1 = 0.0268, wR2 = 0.0663
R (all data)	R1 = 0.0839, wR2 = 0.1476	R1 = 0.0439, wR2 = 0.0756	R1 = 0.0386, wR2 = 0.0683
Largest diff. peak and hole ($\text{e}/\text{\AA}^3$)	0.234 and -0.190	0.459 and -0.452	0.849 and -0.350

Table A.2. Crystallographic structural refinement information for [^{Mes}[CNH]Rh(NBD)]BF₄ (**2.8**), ^{Mes}[CNH]Ir(COD)Cl (**2.10**) and ^{Mes}[CN]Ir(COD) (**2.11**).

Compound	2.8	2.1	2.11
Dataset ID	mf690	mf691	mf710
Empirical formula	C30 H37 B F4 N3 Rh	C34 H44 Cl Ir N3	C37 H54 Ir N3
Formula weight (g/mol)	629.35	722.37	733.03
$\lambda/\text{\AA}$	0.71073	0.71073	0.71073
Crystal system	Triclinic	Triclinic	Triclinic
Space group	P-1	P-1	P-1
$a/\text{\AA}$	10.857(1)	10.116(1)	9.3371(6)
$b/\text{\AA}$	11.144(1)	11.983(1)	11.6985(7)
$c/\text{\AA}$	13.344(1)	13.850(2)	16.363(1)
$\alpha/^\circ$	71.425(4)	86.366(6)	104.157(3)
$\beta/^\circ$	84.597(4)	70.434(6)	90.470(3)
$\gamma/^\circ$	66.204(4)	87.242(6)	106.511(4)
$V/\text{\AA}^3$	1399.1(2)	1578.2(3)	1655.8(2)
Z	2	2	2
$D_c/\text{g cm}^{-3}$	1.494	1.52	1.47
μ/mm^{-1}	0.662	4.341	4.061
$F(000)$	648	726	748
Crystal size/ mm^3	0.35 x 0.15 x 0.04	0.36 x 0.24 x 0.09	0.27 x 0.21 x 0.11
$\theta_{\min} - \theta_{\max}/^\circ$	1.61 to 23.15	1.56 to 28.16	1.88 to 27.91
Reflections collected	16270	32002	32844
Independent reflections [R(int)]	3926 [0.0591]	7430 [0.0470]	7748 [0.0288]
Completeness to θ_{\max}	99.20%	96.00%	97.70%
Max. and min. transmission	0.9739 and 0.7916	0.6766 and 0.3882	0.6397 and 0.5443
Data / restraints / parameters	3926 / 0 / 378	7430 / 2 / 386	7748 / 0 / 402
Goodness-of-fit on F^2	0.95	1.013	1.123
R [$I > 2\sigma(I)$]	R1 = 0.0342, wR2 = 0.0658	R1 = 0.0264, wR2 = 0.0485	R1 = 0.0268, wR2 = 0.0638
R (all data)	R1 = 0.0487, wR2 = 0.0712	R1 = 0.0343, wR2 = 0.0505	R1 = 0.0323, wR2 = 0.0657
Largest diff. peak and hole ($e/\text{\AA}^3$)	0.353 and -0.372	0.834 and -1.062	2.211 and -0.788

Table A.3. Crystallographic structural refinement information for ^{Mes}[CNH]Ru(=CHPh)(PCy₃)Cl₂ (**3.1**), ^{Mes}[CNH]Ru(=CHPh)(py)Cl₂ (**3.5**) and ^{Mes}[CNH]Ru(=CHPh)(PMe₃)Cl₂ (**3.7**).

Compound	3.1	3.5	3.7
Dataset ID	mf713	mf753	mf769
Empirical formula	C ₄₉ H ₇₀ Cl ₄ N ₃ P Ru	C ₃₅ H ₃₉ Cl ₂ N ₄ Ru	C ₃₃ H ₄₄ Cl ₂ N ₃ P Ru
Formula weight (g/mol)	974.92	687.67	685.65
$\lambda/\text{\AA}$	0.71073	0.71073	0.71073
Crystal system	Monoclinic	Monoclinic	Monoclinic
Space group	P2(1)/c	P2(1)/n	P2(1)/c
$a/\text{\AA}$	15.643(1)	14.348(2)	14.3005(3)
$b/\text{\AA}$	20.613(2)	11.915(1)	17.1993(4)
$c/\text{\AA}$	16.062(1)	19.481(2)	13.4452(3)
$\alpha/^\circ$	90	90	90
$\beta/^\circ$	107.075(2)	105.065(5)	104.821(1)
$\gamma/^\circ$	90	90	90
$V/\text{\AA}^3$	4950.7(6)	3216.0(6)	3196.9(1)
Z	4	4	4
$D_c/\text{g cm}^{-3}$	1.308	1.42	1.425
μ/mm^{-1}	0.6	0.684	0.735
$F(000)$	2048	1420	1424
Crystal size/ mm^3	0.22 x 0.17 x 0.11	0.22 x 0.11 x 0.07	0.18 x 0.18 x 0.09
$\theta_{\min} - \theta_{\max}/^\circ$	1.65 to 27.79	1.58 to 23.88	1.89 to 27.49
Reflections collected	52300	35237	51433
Independent reflections [R(int)]	11449 [0.0389]	4966 [0.0394]	7323 [0.0510]
Completeness to θ_{\max}	97.90%	99.80%	99.90%
Max. and min. transmission	0.9361 and 0.8449	0.9532 and 0.8596	1.0000 and 0.8814
Data / restraints / parameters	11449 / 0 / 545	4966 / 5 / 410	7323 / 0 / 386
Goodness-of-fit on F^2	1.035	1.036	1.027
R [$I > 2\sigma(I)$]	R1 = 0.0359, wR2 = 0.0780	R1 = 0.0239, wR2 = 0.0534	R1 = 0.0246, wR2 = 0.0558
R (all data)	R1 = 0.0592, wR2 = 0.0880	R1 = 0.0367, wR2 = 0.0587	R1 = 0.0330, wR2 = 0.0589
Largest diff. peak and hole ($\text{e}/\text{\AA}^3$)	1.399 and -1.261	0.315 and -0.298	0.342 and -0.572

Table A.4. Crystallographic structural refinement information for ^{Mes}[CNH]AgCl (**4.2**), ^{Mes}[CNH]₂PdCl₂ (**4.3**) and ^{Mes}[CNLi]₂ (**4.4**).

Compound	4.2	4.3	4.4
Dataset ID	mf787	mf785	mf580
Empirical formula	C46 H58 Ag2 Cl2 N6	C23 H29 Cl N3 Pd0.50	C46 H56 Li2 N6
Formula weight (g/mol)	981.62	436.14	706.85
$\lambda/\text{\AA}$	0.71073	0.71073	0.71073
Crystal system	Triclinic	Monoclinic	Monoclinic
Space group	P-1	P2(1)/n	P21/n
$a/\text{\AA}$	7.860(3)	7.9055(3)	13.823(4)
$b/\text{\AA}$	9.581(4)	24.639(1)	19.978(5)
$c/\text{\AA}$	14.815(6)	11.8683(5)	16.141(4)
$\alpha/^\circ$	86.50(2)	90	90
$\beta/^\circ$	88.12(2)	109.144(2)	109.983(6)
$\gamma/^\circ$	84.45(2)	90	90
$V/\text{\AA}^3$	1107.9(8)	2183.9(2)	4189.2(2)
Z	1	4	4
$D_c/\text{g cm}^{-3}$	1.471	1.326	1.121
μ/mm^{-1}	1.043	0.586	0.066
$F(000)$	504	912	1520
Crystal size/ mm^3	0.18 x 0.10 x 0.07	0.15 x 0.12 x 0.05	0.50 x 0.50 x 0.40
$\theta_{\min} - \theta_{\max}/^\circ$	2.14 to 26.06	1.65 to 26.11	2.39 to 27.88
Reflections collected	15328	15988	34162
Independent reflections [R(int)]	4327 [0.0349]	4317 [0.0554]	9347 [0.0770]
Completeness to θ_{\max}	98.60%	99.30%	93.60%
Max. and min. transmission	0.9269 and 0.8303	0.9711 and 0.8391	1.0000 and 0.7332
Data / restraints / parameters	4327 / 0 / 263	4317 / 0 / 260	9347 / 0 / 510
Goodness-of-fit on F^2	1.028	1.02	1.113
R [$I > 2\sigma(I)$]	R1 = 0.0254, wR2 = 0.0573	R1 = 0.0408, wR2 = 0.0858	R1 = 0.0897, wR2 = 0.1994
R (all data)	R1 = 0.0318, wR2 = 0.0595	R1 = 0.0673, wR2 = 0.0948	R1 = 0.1235, wR2 = 0.2225
Largest diff. peak and hole ($\text{e}/\text{\AA}^3$)	0.420 and -0.342	1.187 and -0.494	0.277 and -0.267

Table A.5. Crystallographic structural refinement information for ^{Mes}[CP]Rh(COD) (**4.7**), ^{Mes}[CP]Rh(COD) (**4.8**) and **4.8a**.

Compound	4.7	4.8	4.8a
Dataset ID	mf777	mf775	mf774
Empirical formula	C31 H40 N2 P Rh	C31 H40 Ir N2 P	C21.25 H28 Cl0.50 Ir N P0.50
Formula weight (g/mol)	574.53	663.82	522.86
$\lambda/\text{\AA}$	0.71073	0.71073	0.71073
Crystal system	Monoclinic	Monoclinic	Triclinic
Space group	C2/c	C2/c	P-1
$a/\text{\AA}$	23.5038(7)	23.4285(9)	15.4768(8)
$b/\text{\AA}$	12.9623(4)	12.9602(5)	16.6020(9)
$c/\text{\AA}$	18.0620(6)	18.0646(7)	16.8536(9)
$\alpha/^\circ$	90	90	67.119(3)
$\beta/^\circ$	90.379(1)	90.234(2)	87.644(3)
$\gamma/^\circ$	90	90	80.676(3)
$V/\text{\AA}^3$	5502.7(3)	5485.1(4)	3935.9(4)
Z	8	8	8
$D_c/\text{g cm}^{-3}$	1.387	1.608	1.765
μ/mm^{-1}	0.701	4.949	6.896
$F(000)$	2400	2656	2044
Crystal size/ mm^3	0.12 x 0.10 x 0.05	0.15 x 0.05 x 0.05	0.24 x 0.15 x 0.06
$\theta_{\min} - \theta_{\max}/^\circ$	1.73 to 22.97	1.74 to 22.23	1.47 to 27.60
Reflections collected	14586	18703	82104
Independent reflections [R(int)]	3818 [0.0322]	3458 [0.0453]	17993 [0.0443]
Completeness to θ_{\max}	99.80%	99.80%	98.50%
Max. and min. transmission	0.9656 and 0.6462	0.7808 and 0.4842	0.6611 and 0.3901
Data / restraints / parameters	3818 / 0 / 322	3458 / 0 / 322	17993 / 2 / 893
Goodness-of-fit on F^2	1.055	1.029	1.039
R [$I > 2\sigma(I)$]	R1 = 0.0245, wR2 = 0.0533	R1 = 0.0217, wR2 = 0.0461	R1 = 0.0283, wR2 = 0.0760
R (all data)	R1 = 0.0374, wR2 = 0.0582	R1 = 0.0322, wR2 = 0.0493	R1 = 0.0458, wR2 = 0.0834
Largest diff. peak and hole ($\text{e}/\text{\AA}^3$)	0.413 and -0.374	0.761 and -0.485	2.364 and -0.994

Table A.6. Crystallographic structural refinement information for ^{Mes}[CN]Zr(NMe₂)₃ (**5.1**), ^{Mes}[CNH]Rh(PPh₃)₂Cl (**5.3**) and ^{Mes}[CNH]FeBr₂ (**5.4**).

Compound	5.1	5.3	5.4
Dataset ID	mf574	mf749	mf740
Empirical formula	C ₂₉ H ₄₆ N ₆ Zr	C ₆₅ H ₆₅ Cl N ₃ P ₂ Rh	C ₂₃ H ₂₉ Br ₂ Fe N ₃
Formula weight (g/mol)	569.94	1088.5	563.16
$\lambda/\text{\AA}$	0.71073	0.71073	0.71073
Crystal system	Monoclinic	Monoclinic	Monoclinic
Space group	P2(1)/c	P2(1)/n	P2(1)/c
$a/\text{\AA}$	18.696(1)	18.705(2)	17.158(3)
$b/\text{\AA}$	8.8066(4)	22.405(3)	7.798(1)
$c/\text{\AA}$	19.900(1)	26.876(3)	17.852(4)
$\alpha/^\circ$	90	90	90
$\beta/^\circ$	110.709(2)	100.288(4)	101.769(7)
$\gamma/^\circ$	90	90	90
$V/\text{\AA}^3$	3064.9(3)	11082(2)	2338.4(7)
Z	4	8	4
$D_c/\text{g cm}^{-3}$	1.235	1.305	1.6
μ/mm^{-1}	0.385	0.457	4.077
$F(000)$	1208	4544	1136
Crystal size/ mm^3	0.3 x 0.3 x 0.3	0.35 x 0.15 x 0.11	0.28 x 0.22 x 0.07
$\theta_{\min} - \theta_{\max}/^\circ$	2.56 to 27.87	1.53 to 22.49	2.33 to 25.43
Reflections collected	27262	89404	16559
Independent reflections [R(int)]	6814 [0.0505]	14355 [0.0441]	4295 [0.0487]
Completeness to θ_{\max}	93.10%	99.20%	99.30%
Max. and min. transmission	1.0000 and 0.8519	0.9510 and 0.8702	0.7517 and 0.5363
Data / restraints / parameters	6814 / 0 / 337	14355 / 6 / 1258	4295 / 0 / 272
Goodness-of-fit on F^2	1.175	1.061	1.023
R [$I > 2\sigma(I)$]	R1 = 0.0403, wR2 = 0.0957	R1 = 0.0968, wR2 = 0.2135	R1 = 0.0326, wR2 = 0.0649
R (all data)	R1 = 0.0498, wR2 = 0.1079	R1 = 0.1178, wR2 = 0.2297	R1 = 0.0641, wR2 = 0.0729
Largest diff. peak and hole ($\text{e}/\text{\AA}^3$)	1.163 and -0.582	6.775 and -7.011	0.706 and -0.539

Table A.7. Crystallographic structural refinement information for ^{Mes}[CNH]₂NiCl₂ (**5.5**).

Compound	5.5
Dataset ID	mf731
Empirical formula	C ₂₄ H ₃₀ Cl ₄ N ₃ Ni _{0.50}
Formula weight (g/mol)	531.66
$\lambda/\text{\AA}$	0.71073
Crystal system	Monoclinic
Space group	P2(1)/c
$a/\text{\AA}$	7.800(1)
$b/\text{\AA}$	28.776(4)
$c/\text{\AA}$	12.352(2)
$\alpha/^\circ$	90
$\beta/^\circ$	108.372(5)
$\gamma/^\circ$	90
$V/\text{\AA}^3$	2631.1(6)
Z	4
$D/\text{g cm}^{-3}$	1.342
μ/mm^{-1}	0.813
$F(000)$	1108
Crystal size/ mm^3	0.34 x 0.11 x 0.09
$\theta_{\min} - \theta_{\max}/^\circ$	1.42 to 25.16
Reflections collected	19759
Independent reflections [R(int)]	4617 [0.0429]
Completeness to θ_{\max}	97.70%
Max. and min. transmission	0.9294 and 0.6925
Data / restraints / parameters	4617 / 0 / 308
Goodness-of-fit on F^2	1.084
R [$I > 2\sigma(I)$]	R1 = 0.0599, wR2 = 0.1365
R (all data)	R1 = 0.0800, wR2 = 0.1460
Largest diff. peak and hole ($\text{e}/\text{\AA}^3$)	1.088 and -1.092

A.2 Details from the Magnetization Transfer Experiments

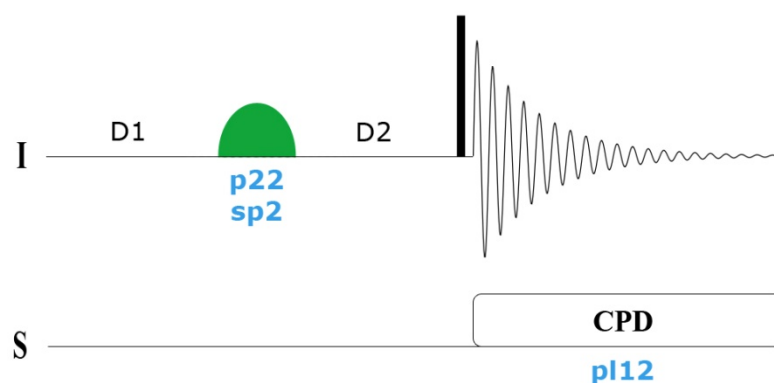


Figure A.1. A pulse sequence diagram of the magnetization transfer experiment used to measure the phosphine exchange rate of **3.1** and PCy₃.

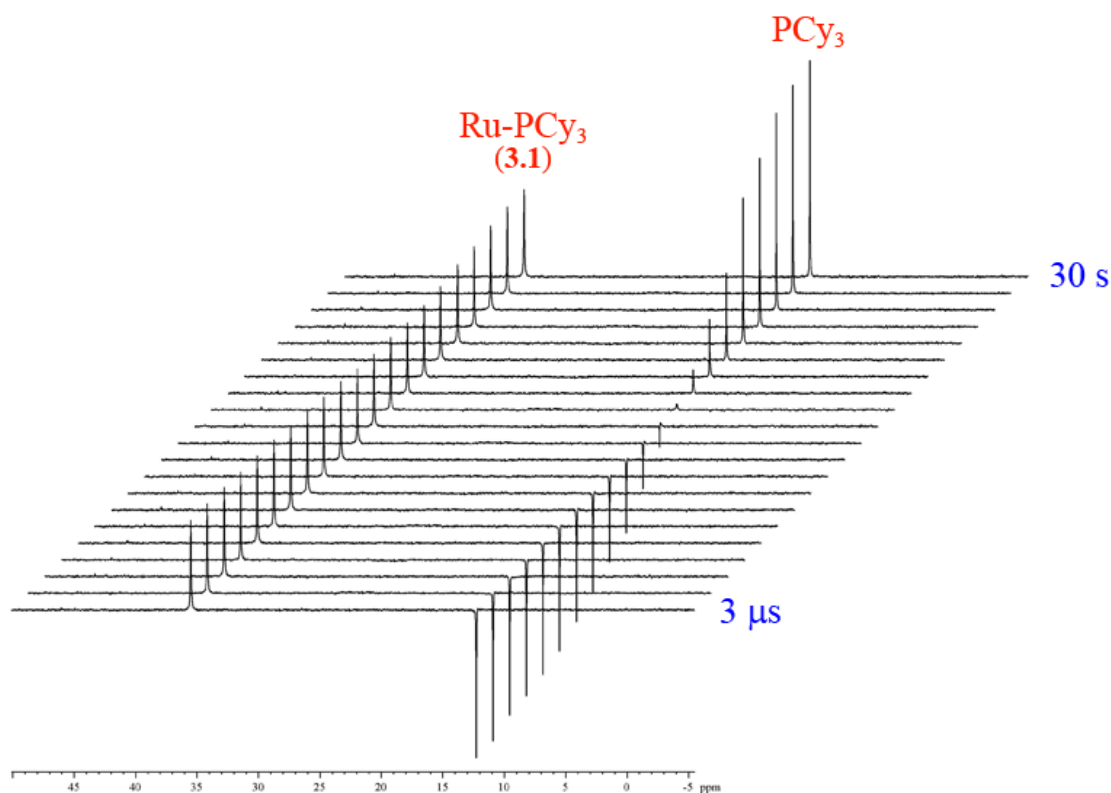


Figure A.2. A stacked 162 MHz ³¹P NMR spectrum of the magnetization transfer experiment used to measure the phosphine exchange rate of **3.1** and PCy₃ in d₁₀-o-xylene at 80 °C.

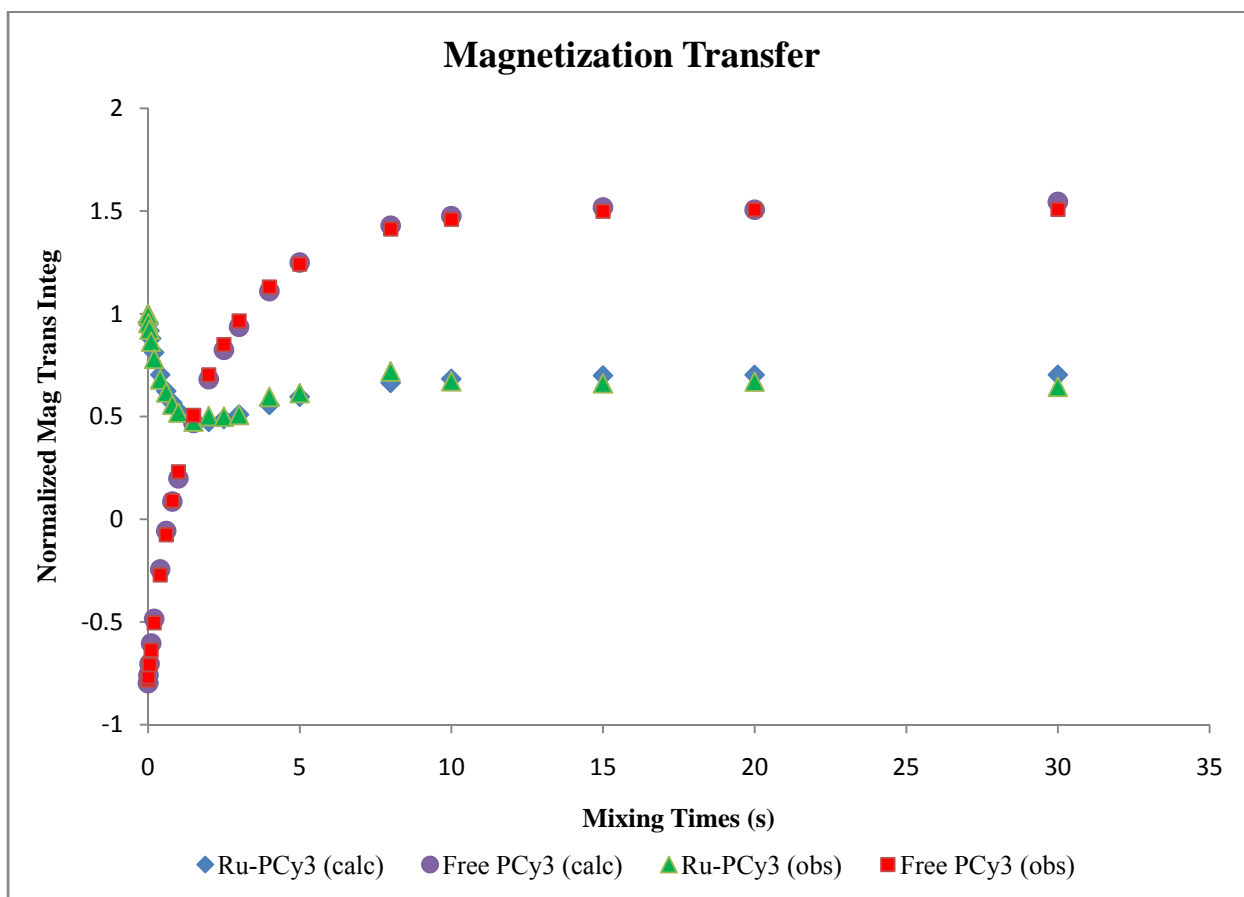


Figure A.3. A plot of the observed normalized integrals of the Ru-PCy₃ (**3.1**) and free PCy₃ resonances measured by the ³¹P NMR magnetization transfer experiment at 95 °C. The observed data is fitted and overlaid with the calculated values generated by the CIFIT software.

Table A.8. The tabulated rate constants and T₁ values obtained from the variable temperature magnetization transfer experiments of **3.1** used for the Eyring plot.

k_{obs} (s ⁻¹)	T (K)	T ₁ (3.1) (s)	T ₁ (PCy ₃) (s)
0.083 ± 0.004	353	2.7	6.3
0.32 ± 0.01	363	2.9	3.6
0.63 ± 0.03	368	2.9	3.0
1.09 ± 0.05	373	3.6	3.0

A.3 References

1. Bruker AXS Inc. *SAINT*, Version 7.03A; Madison, Wisconsin, USA, 1997 - 2003.
2. Bruker AXS Inc. *SADABS*, V2.10; Madison, Wisconsin, USA, 2003.
3. Altomare, A.; Burla, M. C.; Camalli, M.; Cascarano, G. L.; Giacovazzo, C.; Guagliardi, A.; Moliterni, A. G. G.; Polidori, G.; Spagna, R., *J. Appl. Cryst.* **1999**, 32, 115
4. Cromer, D. T.; Waber, J. T., *International Tables for X-Ray Crystallography*. The Kynoch Press: Birmingham, England, 1974; Vol. IV.
5. Ibers, J. A.; C., H. W., *Acta Crystallogr.* **1964**, 17, 781.
6. Creagh, D. C.; McAuley, W. J., *International Tables for Crystallography*. A.J.C. Wilson ed.; Kluwer Academic Publishers: Boston, 1992; Vol. C.
7. Creagh, D. C.; Hubbell, J. H., *International Tables for Crystallography*. A.J.C. Wilson ed.; Kluwer Academic Publishers: Boston, 1992; Vol. C.
8. Bruker AXS Inc. *SHELXTL*, Version 5.1; Madison, Wisconsin, USA, 1997.